STRUCTURE-FUNCTION STUDY OF AN IMP-SPECIFIC 5'-NUCLEOTIDASE FROM *PLASMODIUM FALCIPARUM*

A Thesis Submitted for the Award of the Degree of

Doctor of Philosophy

By

Shukla Arpit Prakashkumar

Molecular Biology and Genetics Unit,

Jawaharlal Nehru Centre for Advanced Scientific Research

(Deemed University)

Bangalore-560064, India

March, 2018

DECLARATION

I hereby declare that this thesis entitled **" Structure-function study of an IMP-specific 5'-nucleotidase from *Plasmodium falciparum"*** is an authentic record of the research work carried out by me under the supervision of Prof. Hemalatha Balaram at the Molecular Biology and Genetics Unit (MBGU), Jawaharlal Nehru Centre for Advanced Scientific Research (JNCASR), Bangalore, India and that this work has not been submitted elsewhere for the award of any other degree.

In keeping with the general practice of reporting scientific observations, due acknowledgements have been made wherever the work described has been based on findings of other investigators. Any omission, which might have occurred by oversight or misjudgement, is regretted.

(Shukla Arpit Prakashkumar)

Place :

Date :

Molecular Biology and Genetics Unit
JAWAHARLAL NEHRU CENTRE FOR ADVANCED SCIENTIFIC RESEARCH
Jakkur, Bangalore – 560 064, India.

Hemalatha Balaram, Ph. D.
Professor

CERTIFICATE

This is to certify that the work described in this thesis entitled **"Structure-function study of an IMP-specific 5'-nucleotidase from *Plasmodium falciparum*"** is the result of investigations carried out by Mr. Shukla Arpit Prakashkumar in the Molecular Biology and Genetics Unit (MBGU), Jawaharlal Nehru Centre for Advanced Scientific Research (JNCASR), Bangalore, India, under my supervision, and that the results presented in this thesis have not previously formed the basis for the award of any other diploma, degree or fellowship.

(Hemalatha Balaram)

Place:

Date:

♦ Telephone: 91-80-22082812 ♦ Telefax: 91-80-22082766 ♦ email: hb@jncasr.ac.in

ACKNOWLEDGEMENTS

A work spanning six years of one's career, involving rigorous training and research, attempting to solve the intriguing mysteries of our world, would not have been possible without the help and support of several people involved at various levels in bringing it to fruition. First and foremost, I would like to thank my supersivor and mentor, Prof. Hemalatha Balaram, for providing me with the opportunity to work on the project. Her vast knowlwdge and immense experience in the field of plasmodium biochemistry has guided me through the process of negotiating the unpredictable terrain of carrying out a scientific investigation. I faltered many times, found myself incapable of deliverance and struggled for confidence, yet she patiently bore with all my shortcomings and guided me throughout this journey. I am extremely thankful to her for creating a positive scientific environment in the workplace. I will always be grateful for her various lessons as they continue to inspire me in my scientific journey forward.

The interdisciplinary atmosphere permeating the campus and the positive energy one derives by being able to communicate across diverse specialties is one feature that I enjoyed immensely during my stay at the Jawaharlal Nehru Centre for Advanced Scientific Research (JNCASR), one of the finest world-class institute with a strong foundation for interdisciplanary scientific research. The Molecular Biology and Genetics Unit (MBGU), with its thrust on biomedical research, is a wonderful place to exercise one's scientific curiosity, with state-of-the-art facilities and diverse research groups addressing the critical challenges relevant in the current biological research arena. The culture of departmental presentations, journal club, and the ensuing exchange of ideas and constructive criticisms, helped in shaping the work as it progressed. I would like to thank Prof. Anuranjan Anand and Prof. Udaykumar Ranga, the preceding and current chairmen of the unit, for their vision, support and encouragement. I would also like to thank the various faculty members, Prof. Tapas Kumar Kundu, Prof. Maneesha Inamdar, Prof. Kaustuv Sanyal, Prof. Namita Surolia, Prof. Ravi Manjithaya, and Prof. James Chelliah for their critical comments and suggestions on several aspects of my work. I would like to thank Prof. H. Balaram, Prof. K. Sanyal, Prof. M. Inamdar, Prof. A. Joshi and Prof. V. K. Sharma (EOBU), for their course works during my first academic year. I am immensely grateful to Prof. M.R.N.Murthy for his insightful course on 'protein bioinformatics and evolution' through a special arrangement at MBU, IISc. I also thank Prof. Sidhartha Sarma and Prof. D. N. Rao for their valuable suggestions and critical evaluation during my comprehensive examination. I would like to thank Prof. Eswaramoorthy (CPMU) and his student Dr. Piyush for allowing us to use the Malvern Zetasizer instrument for DLS measurements, and Prof. R. Vardharajan (MBU, IISc) and his students Aparna and Deva for allowing us to use the Microcal ITC instrument. I would also like to thank Ansuman (IISc) for our fruitful collaborative project on thymidylate kinase.

My research would not be complete without the help, encouragement and resourceful insights from my fellow members at JNCASR. I would like to thank my senior lab members Dr. Javaid, Dr. Vinay and Dr. Vasudeva for their valuable guidance through my initial years, and a special thanks to Dr. Vijay, Dr. Sanjeev and Dr. Sourav as well as Dr. Moumita, Dr. Vidhi and Dr. Debarati for their immense support in and out of the lab. I am immensely grateful to Dr. Bharath for his constant guidance throughout the various phases of my work, and to Sonia from whom I learnt the techniques of protein purification and enzyme kinetics. I would also like to thank my past and present labmates Umesh, Manu, Jyothi, Prasoona, Santosh, Asutosh, Arpitha, Malini, Aparna, Pavitra, Anusha, Dr. Ruchika, Dr. Darshan and Dr. Dhanlaxmi, summer interns Sandhya, Lakshmi Krupa, Rohini, Elizabeth, Raju, Akshay, Avishek and Rahul, integrated Ph.D rotation students Suresh, Meenakshi, Sarika, Veena, Rashi, Satya and Irene for creating a warm, friendly and lively work environment. A special thanks to Lakshmeesha for his immense support in and out of the lab. I am grateful to Neelakshi and Resmi for their immense help on the PfISN1 project and wish them the best for the future. I would also like to thank Bala, our lab assistant, for his help.

My MBGU-JNC seniors Dr. Ronak, Dr. Vijay Akhade, Dr. Rohan, Dr. Pavitra, Dr. Manpreet, Dr. Nikhil, batchmates Dr. Amrutha, Dr. Malini and Vaijayanthi, integrated Ph.D batchmates Vikas, Suresh, Lakshmi Sreekumar, Surabhi, Shveta, juniors Shalini, Simi, Sundar, Prabhu, Aditya, Arnab, Neha, Piyush, Gaurav, Shashank, Arun, hostel mates Anshuman, Monojit, Dhananjay, Mohit, Avinash, Piyush, Vybhav, Gopal, Anirudh, Nishit, Soumik, Raagesh, Subhojit Das, Abhiroop, Manoj, Nisha, Nikita, and many others have provided me immense support throughout my journey. My M.Sc. batch of 2008-10 deserves a special mention for their invaluable support, well-wishes and love.

I would like to thank the complab, library, academic, administration, security, dining hall, hostel and other JNCASR staff for making my stay at JNCASR a memorable experience. I would like to thank Dr. Prakash at the Animal Facility, Anitha madam at the sequencing facility and Suma madam at the confocal facility for their help. Financial support from CSIR-JRF/SRF and JNCASR is duly acknowledged.

This journey would have been impossible to begin, without the constant love and enduring support of my family. My father and mother have been the backbone of this support, with their endearing words of wisdom and unconditional love, guiding me through my darkest hours. My grandfather has always been a source of intellectual wisdom for me. I am immensely grateful to my dear wife, Trusha, for her constant love and support. This thesis is dedicated to the two most important women in my family, my two dearest grandmothers, who have nourished me through my growing years and have taught me the two most significant virtues of life – patience and humility.

Synopsis of the thesis entitled

"Structure-function study of an IMP-specific 5'-nucleotidase from *Plasmodium falciparum*"

Submitted by

Shukla Arpit Prakashkumar.

Molecular Biology & Genetics Unit (MBGU), Jawaharlal Nehru Centre for Advanced Scientific Research (JNCASR), Bangalore, India.

Thesis supervisor: Prof. Hemalatha Balaram

In living systems, phosphate esters form an important class of metabolites that are involved in energy, nucleotide and lipid metabolism and serve as intermediary metabolites in several biochemical pathways. They are hydrolyzed by phosphatases, a family of enzymes that regulate phosphate metabolism along with kinases. Phosphatases can be classified according to their optimum pH, substrate specificity or cellular localization

Nucleotidases are a sub-class of phosphatases that catalyze the dephosphorylation of nucleotide phosphate esters. Some nucleotidases also act as phosphotransferases by transferring the phosphate group from one substrate to another. Over a span of more than five decades, several nucleotidases from various kingdoms of life have been studied, revealing important information about their function, structure, evolution and physiological role (*1–3*). Nucleotidases have been broadly classified based on their substrate specificity and cellular localization. They act primarily on purine and pyrimidine nucleotides, including nucleoside 5' and 3' mono-, di- and tri-phosphates. Some nucleotidases also act on non-canonical nucleotides like 5-fluoro-2'-deoxyuridine monophosphate (5-FdUMP) (*4*). They are localized in the cytosol, mitochondria and the extracellular side of the cell membrane (*5–10*). The 5'-nucleotidases belong to the Haloacid Dehalogenase (HAD) superfamily of proteins which is one of the largest protein superfamilies. A Rossmann fold core architecture is a common feature of HAD members along with a variable cap domain. HAD members also share four invariant motifs that are known to play a critical role in catalysis (*11*). Except for the four motif sequences, the proteins show a high degree of variability in their amino acid sequence and consequently in their biochemical features like substrate specificity, kinetic parameters, mode of regulation and physiological role (*12*).

Malaria is an infectious disease caused by the protozoan parasite of the genus *Plasmodium* and spread by mosquitoes. It has been a global challenge with its high mortality rate and its impact on the economy of developing countries. Efforts to eradicate malaria have failed so far. Moreover, several plasmodial strains have developed resistance against commonly used anti-malarial drugs, pushing the need for new drugs (*13, 14*). Of all the plasmodial species, *Plasmodium falciparum* is the most lethal as it causes cerebral malaria, a severe complication responsible for high mortality rate amongst infected patients.

Understanding parasite metabolism can aid in the discovery of new drug targets. During the intraerythrocytic stages, the parasite exhibits increased purine and pyrimidine nucleotide metabolism. Genes encoding enzymes of the de-novo pathway for purine nucleotide biosynthesis are absent in Plasmodia and hence the parasite is dependent on the salvage pathway for its purine nucleotide requirements (*15, 16*). It salvages purine nucleosides and nucleobase precursors from the host through membrane transporters (*17*) which act as precursors for the purine salvage pathway enzymes to form purine mono-, di- and triphosphates. Enzymes of the purine salvage pathway are thus considered as potential drug targets.

5'-nucleotidases play an important role in regulating cellular nucleotide pools (*18, 19*) and are critical for cell survival (*20, 21*). The nucleotidases studied so far from various organisms have no known homologs in *P. falciparum*. A 5'-nucleotidase, expressed by the gene *YOR155c* and hydrolyzing inosine 5'-monophosphate (IMP) to inosine and inorganic phosphate, was recently discovered in yeast. It had no sequence homology to other 5'-nucleotidases and was thus classified as a separate family of 5'-nucleotidases, called as IMP-specific 5'-nucleotidases (ISN1) (*22*). Although ISN1 homologs are widespread in fungi, they are also present in a small number of apicomplexans, stramenopiles, viridiplantae and cryptophytes. ISN1 homologs are absent in prokaryotes, archaea and higher eukaryotes. This study comprises of the biochemical characterization of an IMP-specific 5'-nucleotidase from *Plasmodium falciparum* (PfISN1). The results from this study have put forth some novel biochemical features that set this protein apart from other 5'-nucleotidases. This study is divided into five chapters.

Chapter one is an introduction to phosphatases, the HAD superfamily of enzymes and 5'-nucleotidases, which are members of the HAD superfamily. It explains the role of 5'-nucleotidases as enzymes of physiological significance. It also introduces the ISN1 family of 5'-nucleotidases and highlights the differences in its features as compared to the conventional cytosolic nucleotidases. ISN1 sequences also contain the four invariant HAD motifs and have been previously shown, through *in silico* studies, to belong to the HAD superfamily (*23*). The homolog of *YOR155c* in *P. falciparum* is a 444 amino acid protein encoded by the gene *PF3D7_1206100*. It is intriguing that this gene is present in the plasmodial species like *P. falciparum, P. vivax and P. knowlesi* that infect primates, but absent in the species like *P. berghei, P. yoelii and P. chabaudi* that infect rodents (*24*).

Chapter two describes the cloning, expression, purification and preliminary biochemical characterization of the recombinant PfISN1 protein. The gene *PF3D7_1206100* was cloned into pET21b with an N-terminal 6X His tag, recombinantly expressed in *E. coli*, and further purified by Ni-NTA™ affinity chromatography and size-exclusion chromatography. Analytical size-exclusion chromatography revealed that the protein was a tetramer in solution. A large set of phosphorylated substrates were screened for phosphatase activity with the enzyme. Of these, only IMP and AMP

were found to be hydrolyzed of which IMP was hydrolyzed with a significantly higher catalytic efficiency than AMP. The enzyme also hydrolyzed p-nitrophenyl phosphate (pNPP), a non-physiological substrate used commonly for assaying phosphatase activity (*25*) with a catalytic efficiency at least 1000 fold lower than IMP. pH-dependant kinetics revealed that the enzyme showed optimum activity at pH 4.0-5.0. A screen set up with various compounds as potential modulators of enzyme activity yielded ATP as a potent activator of the enzyme. However, ATP activated enzyme activity only at pH 8.0 and had no significant activation of enzyme activity at pH 5.0. The enzyme was also tested for phosphotransferase activity but no such activity was detected.

Chapter three describes the role of motif I asparates in catalysis. All HAD members contain the four invariant motifs that contain residues which are critical for catalysis and Motif I (D_1 X D_2 X T/V) is the most important as it contains the two invariant aspartates D_1 (D170 in PfISN1) and D_2 (D172 in PfISN1) which have been shown to be critical for catalysis (*26*). To probe their role in the catalytic activity of PfISN1, the mutants D170N, D172N and D170N-D172N were generated. All the three mutants showed no IMP hydrolyzing activity. Interestingly, D172N showed about a 100-fold higher pNPP hydrolyzing activity. D172A also showed no IMP hydrolyzing activity but about 10-fold higher pNPP hydrolyzing activity. pNPP hydrolysis by D172N and D172A was inhibited by IMP with an IC_{50} value that was at least 1000-fold lower than the K_m of the wild-type enzyme for IMP, suggesting a strong affinity for IMP for the mutants. Overall, the mutations pertaining to the two aspartates in motif I perturbed the catalytic activity of the enzyme, affirming their critical role in catalysis and validating that ISN1 enzymes belong to the HAD superfamily.

Chapter four describes the crystal structure of the PfISN1 protein. Crystal structures of the PfISN1 protein under various conditions were solved in collaboration with Prof. Nushin Aghajari (IBCP, Lyon Cedex, France). Initial attempts to crystallize the protein were unsuccessful due to low stability of the protein at high concentration. Removal of disordered regions has been previously shown to aid in protein crystallization (*27*). Using PrDOS (*28*), a tool for predicting residue disorder probability from amino acid sequence, segments at the N-terminus and C-terminus were found to contain residues with high disorder probability. These were removed to generate three deletion variants, namely ΔN30, a 30-residue deletion from the N-terminus, ΔC10, a 10-residue deletion from the C-terminus and ΔN30_C10, a 30-residue and 10-residue deletion from the N-terminal and C-terminal ends of the protein, respectively. Crystal structures were obtained for the apo protein, IMP-Mg^{2+} bound and ATP-bound protein. These are the first structures obtained for an ISN1 family protein till date. The overall protein structure has several distinguishable features that are different from the structure of other 5'-nucleotidases. The tertiary structure can be divided into four distinct domains, namely the core domain, the cap domain, the oligomerization domain (OD) and the N-terminal regulatory domain (NTRD). Analysis of the

IMP-Mg^{2+}-bound structure revealed residues interacting with IMP-Mg^{2+} at the active site. These residues were mutated to validate their role. The mutants either displayed poor or no catalytic activity with IMP. Analysis of the ATP-bound structure revealed the allosteric site, containing H150, a poorly conserved residue which interacted with ATP. The mutant H150V showed no activation by ATP, validating the location of the allosteric site. A total of 15 non-conservative mutations for 15 residues and 2 conservative mutations for 1 residue were made. Overall, these mutants had a significant impact on enzyme function.

Chapter five describes the localization of the protein in the intraerythrocytic asexual and sexual stages of the parasite. Polyclonal antibodies against the recombinant PfISN1 protein were raised in rabbits, purified by antigen-affinity chromatography and used for indirect immunofluorescence microscopy, which revealed cytosolic localization of the protein in asexual as well as sexual intraerythrocytic stages of the parasite.

This study describes the first detailed biochemical characterization and crystal structure of an ISN1 member till date. Apart from the implications of this study on the nucleotide metabolism of the parasite, it also serves as a model for understanding the structure-function properties of other ISN1 members.

References

1. S. A. Hunsucker, J. Spychala, B. S. Mitchell, *J. Biol. Chem.* **276**, 10498–504 (2001).
2. F. Bontemps, G. Van den Berghe, H. G. Hers, *Biochem J.* **250**, 687–696 (1988).
3. A. Singh R., *Phytochemistry*. **25**, doi:10.1016/S0031-9422(00)81676-3.
4. B. Titz, R. Häuser, A. Engelbrecher, P. Uetz, *FEMS Microbiol. Lett.* **270**, 49–57 (2007).
5. E. P. Garvey, G. T. Lowen, M. R. Almond, *Biochemistry*. **37**, 9043–51 (1998).
6. R. Itoh, *Comp. Biochem. Physiol. B.* **105**, 13–9 (1993).
7. D. C. Rees, J. A. Duley, A. M. Marinaki, *Br. J. Haematol.* **120**, 375–383 (2003).
8. T. Monecke, J. Buschmann, P. Neumann, E. Wahle, R. Ficner, *PLoS One*. **9**, e90915 (2014).
9. N. Kochanowski *et al.*, *Anal Biochem*. **348**, 243–251 (2006).
10. H. Zimmermann, *Biochem J.* **285 (Pt 2**, 345–365 (1992).
11. A. M. Burroughs, K. N. Allen, D. Dunaway-Mariano, L. Aravind, *J Mol Biol*. **361**, 1003–1034 (2006).
12. E. Kuznetsova *et al.*, *J. Biol. Chem.* **290**, 18678–18698 (2015).
13. S. Thaithong, *Bull. World Health Organ.* **61**, 709–12 (1983).
14. R. N. Price *et al.*, *Lancet*. **364**, 438–447 (2004).
15. T. Booden, R. W. Hull, *Exp. Parasitol.* **34**, 220–228 (1973).
16. K. Chaudhary *et al.*, *J. Biol. Chem.* **279**, 31221–31227 (2004).
17. I. J. Frame, E. F. Merino, V. L. Schramm, M. B. Cassera, M. H. Akabas, *Biochem. J.* **446**, 179–90 (2012).
18. S. A. Hunsucker, B. S. Mitchell, J. Spychala, *Pharmacol Ther*. **107**, 1–30 (2005).
19. C. Federico *et al.*, *Biochim. Biophys. Acta* (2015), doi:10.1016/j.bbagen.2015.03.017.
20. F. Cividini *et al.*, *Int. J. Biochem. Cell Biol.* **65** (2015), doi:10.1016/j.biocel.2015.06.011.
21. S. Kviklyte *et al.*, *Am. J. Physiol. - Endocrinol. Metab.* (2017).
22. R. Itoh *et al.*, The yeast ISN1 (YOR155c) gene encodes a new type of IMP-specific 5'-nucleotidase. *BMC Biochem.* **4** (2003), , doi:10.1186/1471-2091-4-4.
23. B. Srinivasan, H. Balaram, *Silico Biol.* **7**, 187–193 (2007).
24. C. Frech, N. Chen, *PLoS Comput Biol*. **7**, e1002320 (2011).
25. O. A. Bessey, O. H. Lowry, M. J. Brock, *J Biol Chem*. **164** (1946).
26. S. Allegrini *et al.*, *Eur J Biochem*. **271**, 4881–4891 (2004).
27. K. Wallden, P. Nordlund, *J Mol Biol*. **408**, 684–696 (2011).
28. T. Ishida, K. Kinoshita, *Nucleic Acids Res.* **35**, W460-4 (2007).

LIST OF PUBLICATIONS

Publications from the thesis

1. **Shukla A.**, Balaram H. *et. al.* (2018): Structural basis of inter-domain communication in *Plasmodium falciparum* IMP-specific 5'-nucleotidase. (**manuscript under preparation**).

Other publications

1. Srinivasan B, Forouhar F, **Shukla A**, Sampangi C, Kulkarni S, Abashidze M, Seetharaman J, Lew S, Mao L, Acton TB, Xiao R, Everett JK, Montelione GT, Tong L. and Balaram H. (2014): Allosteric regulation and substrate activation in cytosolic nucleotidase II from Legionella pneumophila. *FEBS J.* 281: p1613-28.

2. Srinivasan B, Kempaiah Nagappa L, **Shukla A** and Balaram H. (2015): Prediction of substrate specificity and preliminary kinetic characterization of the hypothetical protein PVX_123945 from Plasmodium vivax. *Exp Parasitol.* 151: p56-63.

3. Biswas A, **Shukla A**, Vijayan R S, Jeyakanthan J and Sekar K. (2017): Crystal structures of an archaeal thymidylate kinase from Sulfolobus tokodaii provide insights into the role of a conserved active site Arginine residue. *J Struct Biol.* 197: p236-249.

4. Biswas A, **Shukla A**, Chaudhary S, R Santhosh, Jeyakanthan J and Sekar K (2017): Characterizing active site dynamics from structural studies on the Intermediates along the reaction coordinate of a hyperthermophilic Thymidylate Kinase. *FEBS J.* 284: p2527-2544.

(This page is intentionally left blank)

List of abbreviations

2,3-BPG	2,3-Bisphosphoglyceric acid
A.U.	Arbitary units
ADP	Adenosine diphosphate
AEC	3-amino-9-ethylcarbazole
AMP	Adenosine monophosphate
AQUA	Advanced quick assembly
AraGMP	9-β-D-arabinofuranosylguanine monophosphate
ATP	Adenosine triphosphate
AZTMP	Zidovdine 5'-monophosphate
BSD	Blasticidin
CDC	Centers for disease control and prevention
cdN	Cytosolic deoxynucleotidase
CMP	Cytidine monophosphate
cN	Cytosolic nucleotidase
CoA	Coenzyme A
CRT	Chloroquine resistance transporter
dATP	Deoxyadenosine triphosphate
dCTP	Deoxycytidine monophosphate
dGMP	Deoxyguanosine monophosphate
dGTP	Deoxyguanosine triphosphate
DHAP	Dihydroxyacetone phosphate
DIC	Differential interference contrast
dIMP	Deoxyinosine monophosphate
DLS	Dynamic light scattering
DNA	Deoxyribonucleic acid
dTTP	Deoxythymidine triphosphate
dUTP	Deoxyuridine triphosphate
ecDHFR	*E. coli* dihydrofolate reductase
EDTA	Ethylenediaminetetraacetic acid
eN	Ecto nucleotidase
ER	Endoplasmic reticulum

FAD	Falvin adenine dinucleotide
FdUMP	5-fluorodeoxyuridine monophosphate
FMN	Flavin mononucleotide
FP-2	Falcipain-2
GDP	Guanosine diphosphate
GFP	Green fluorescent protein
GMP	Guanosine monophosphate
GPI	Glycosylphosphatidylinositol
GTP	Guanosine triphosphate
HA	Human influenza hemagglutinin
HAD	Haloacid dehalogenase
HEPES	4-(2-hydroxyethyl)-1-piperazineethanesulfonic acid
HGPRT	Hypoxanthine-guanine phosphoribosyltransferase
HRP	Horseradish peroxidase
IMP	Inosine monophosphate
IP-RP-HPLC	Ion-pair reversed phase high-performance liquid chromatography
IPTG	Isopropyl β-D-1-thiogalactopyranoside
ISN1	IMP-specific 5'-nucleotidase
ITC	Isothermal titration calorimetry
ITP	Inosine triphosphate
LB	Luria broth
LC-MS	Liquid chromatography-mass spectrometry
LPC	Lysophosphatidylcholine
mdN	Mitochondrial nucleotidase
MES	2-(N-morpholino)ethanesulfonic acid
NAD	Nicotinamide adenine dinucleotide
NADP	Nicotinamide adenine dinucleotide phosphate
NAG	N-Acetylglucosamine
NAM	Nicotinamide mononucleotide
NaMN	Nicotinic acid mononucleotide
NaR	Nicotinic acid ribonucleotide
NMN	Nicotinamide mononucleotide

NR	Nicotinamide ribonucleotide
NTA	Nitrilotriacetic acid
NTD	N-terminal domain
OD	Oligomerization domain
PAGE	Polyacrylamide gel electrophoresis
PBS	Phosphate-buffered saline
PCR	Polymerase chain reaction
PfISN1	*P. falciparum* IMP-specific 5'-nucleotidase
PLP	Pyridoxal phosphate
PNC	Purine nucleoside cycle
pNP	Para-nitrophenol
pNPP	para-nitrophenyl phosphate
PVDF	Polyvinylidene fluoride
RFA	Regulatable fluorescent affinity
Rib-1-P	D-Ribose 1-phosphate
RNA	Ribonucleic acid
RPMI	Roswell Park Memorial Institute
ScISN1	*Saccharomyces cerevisiae* IMP-specific 5'-nucleotidase
SDS	Sodium dodecyl sulfate
SFLD	Structure function linkage database
TB	Terrific broth
TBAHS	Tetrabutylammonium hydrogen sulfate
TCA	Trichloroacetic acid
TCEP	Tris(2-carboxyethyl)phosphine
TMP	Trimethoprim
UMP	Uridine monophosphate
vWA	Von willebrand A
XMP	Xanthosine monophosphate

(This page is intentionally left blank)

TABLE OF CONTENTS

Chapter One

Structural and functional properties of 5'-nucleotidases

Table of Contents

1.1 Abstract

This chapter provides an introduction to 5'-nucleotidases and briefly highlights upon their biochemical features including their classification, substrate specificity, catalytic mechanism, structural features and physiological role. Malaria is an infectious disease casued by the protozoan parasite *Plasmodium*, claiming several lives every year. Due to widespread drug resistance developing in several species of the parasite, there is an ever-growing need to develop new anti-malarial drugs. Understanding nucleotide metabolism in the parasite can aid in the discovery of new drug targets. IMP-specific 5'-nucleotidase in *P. falciparum* (PfISN1) is a protein from a recently discovered family of IMP-specific 5'-nucleotidases (ISN1). The introduction is concluded by stating the objectives of this study involving biochemical characterization of PfISN1, which will provide a better understanding of the structural and functional aspects of this novel enzyme.

1.2 5'-nucleotidases

1.2.1 Overview

Nucleotides are important biomolecules necessary for several biochemical processes in living organisms. Nucleic acids DNA and RNA are long chain polymers formed from nucleoside triphosphate precursors. Nucleoside triphosphates ATP and GTP are high-energy phosphate compounds serving as important components of energy metabolism. The hydrolysis of these high-energy compounds when coupled to enzymatic reactions provides the energy needed to drive them. Nucleotides are components of coenzymes like NAD, FAD, FMN and coenzyme A which are necessary for the function of several enzymes. Improper functioning of nucleotide metabolic pathways can lead to several abnormalities. Lesch–Nyhan syndrome is one such condition in which the absence of a functional hypoxanthine-guanine phosphoribosyltransferase (HGPRT) enzyme in the purine salvage pathway, leading to hyperuricemia and hyperuricosuria, associated with severe gout and kidney problems (Seegmiller et al., 1967). Both purine and pyrimidine forms of nucleotides can be obtained either by the *de novo* biosynthetic pathway or the salvage pathway. In the *de novo* biosynthetic pathway, the nitrogen base of the nucleotide is built from the metabolites aspartate, glycine, formate and glutamine. In the salvage pathway, nucleoside and nucleotide precursors obtained from catabolic processes or extracellular environment are salvaged to form nucleotides. Several enzymes involved in these pathways are essential for cell growth and are highly regulated to maintain homeostasis of nucleotide pools in the cell (Becker and Kim, 1987; Serina et al., 1995; Yamaoka et al., 2001).

5'-nucleotidases (EC 3.1.3.5) are one of the key enzymes involved in nucleotide metabolism, catalyzing the hydrolysis of nucleoside monophosphates to nucleosides and inorganic phosphate. 5'-nucleotidase was first discovered in 1934 by Reis (Reis, 1934) in heart muscle. It was named 5'-nucleotidase because it specifically acted only on 5'-AMP and 5'-IMP but not 3'-AMP. It was later found in other human tissues as well (Reis, 1937a, 1937b, 1940). It had a varied distribution amongst various tissues in the body with the thyroid, aorta walls and testicles having the highest levels (Reis, 1950a, 1950b). Since then, 5'-nucleotidases from many different sources were extracted and studied extensively to elucidate their biochemical properties.

1.2.2 Classification

5'-nucleotidases have been characterized from many organisms. Mammalian 5'-nucleotidases have been extensively studied. There are seven different mammalian 5'-nucleotidases identified in humans, namely cN-Ia, cN-Ib, cN-II, cN-III, cdN, mdN and edN (Bianchi and Spychala, 2003). They are differentiated on the basis of their cellular localization and substrate specificity (Table 1.1). Recently, a new member, cN-IIIb, has been identified in human and drosophila (Buschmann et al., 2013). Many of these 5'-nucleotidases have overlapping substrate specificities and even act on 5'- and 2'(3')-(deoxy)ribonucleoside monophosphates. Some 5'-nucleotidases show ubiquitous expression (eN, cN-II, cdN, and mdN) while others show tissue-specific expression (cN-I and cN-III).

Ecto 5'-nucleotidase (eN) – This is a membrane-bound enzyme, also called as CD73 due to its property of being a lymphocyte surface antigen. It is attached to the outer side of the plasma membrane via a glycosylphosphatidylinositol (GPI) anchor. Despite its broad substrate specificity, AMP is considered as the preferred substrate for eN. Enzyme activity is not dependant on divalent cations but addition of Mg^{2+} increases activity (Ong et al., 1990). Zn^{2+} is presumably the natural metal ligand associated with the enzyme since the enzyme purified from chicken gizzard contains Zn^{2+} tightly associated with the enzyme (Fini et al., 1990).

Table 1.1. List of various mammalian 5'-nucleotidases classified according to their cellular localization and substrate specificity[*].

S. No.	Name	Localization	Preferred physiological substrate(s)
1.	cN-Ia	cytosolic	TMP[a]
2.	cN-Ib	cytosolic	AMP[b]
3.	cN-II	cytosolic	GMP, AMP, IMP, dIMP[c]
4.	cN-IIIa	cytosolic	UMP, CMP and dCMP[d]
5.	cN-IIIb	cytosolic	7-methyl GMP, CMP, UMP[e]
6.	cdN	cytosolic	dIMP, dGMP, 2'- and 3'-monophosphates[f]
7.	mdN	mitochondrial	5'- and 2'(3')-dUMP, 5'- and 2'(3')-dTMP[g]
8.	eN	extracellular, anchored to plasma membrane	AMP

[*]FOOTNOTE: [a](Garvey et al., 1998); [b](Sala-Newby et al., 2003); [c](Itoh, 1993); [d](Rees et al., 2003); [e](Buschmann et al., 2013); [f](Rampazzo et al., 2000b); [g](Rampazzo et al., 2000a); [h](Zimmermann, 1992).

Apart from 5'-nucleotidase activity, eNs isolated from some sources display FAD pyrophosphatase activity (Lee and Ford, 1988) and UDP-glucose hydrolase activity (VOLKNANDT et al., 1991). eN is a homodimer with interchain disulphide bonds (DIECKHOFF et al., 1985; Grondal and Zimmermann, 1987), which are essential for enzyme activity (Worku et al., 1984; Fini et al., 1985). Conversion of extracellular AMP to adenosine is the major physiological role of eNs. The extracellular adenosine formed can be taken up by the cell via nucleoside transporters and used in the purine salvage pathway for nucleotide synthesis. Adenosine is also involved in purinergic signalling through G protein-coupled receptors that regulate several process including cell proliferation, migration and death, inflammation and neuromodulation (Burnstock, 2006).

Cytosolic nucleotidase-1 (cN-Ia & cN-Ib) – cN-Ia preferentially hydrolyzes deoxypyrimidine monophosphates (Garvey et al., 1998) and AMP. It is highly expressed in heart and skeletal muscle tissues where its physiological function is to generate adenosine during ischemic conditions (Sala-Newby et al., 1999, 2000). Its homolog, related to human autoimmune infertility gene (AIRP) is highly expressed in testis and designated as cN-Ib (Sala-Newby and Newby, 2001).

Cytosolic nucleotidase-II (cN-II) – This enzyme preferentially hydrolyzes GMP and IMP. It is a tetramer in solution and activated by ATP, dATP, GTP 2,3-bisphosphoglycerate, polyphosphates and decavanadate in a complex manner (Bontemps et al., 1988, 1989; Van Den Berghe et al., 1989; Bretonnet et al., 2005; Srinivasan et al., 2014). Apart from 5'-nucleotidase activity, it also displays phosphotransferase activity, transferring a phosphate group from nucleoside monophosphate to inosine or guanosine (Pesi et al., 1994).

Cytosolic nucleotidase-III (cN-IIIa & b) – cN-IIIa shows preferential activity on pyrimidine oxy- and deoxy-nucleoside monophosphates and has no activity on purine nucleoside monophosphates. It is highly expressed in erythrocytes where it degrades RNA during erythrocyte maturation (Rees et al., 2003). It also displays phosphotransferase activity (Amici et al., 1997), but with lesser efficiency than cN-II. cN-IIIb shows greater preference for CMP and UMP, with a lower preference for GMP and AMP. However, it shows highest preference for hydrolysis of 7-methyl GMP (m^7GMP) formed during degradation of mRNA, thus preventing its undesirable salvage and subsequent incorporation into nucleic acids (Buschmann et al., 2013).

Cytosolic 5'(3')-deoxynucleotidase (cdN) – First isolated from human placenta, cdN is ubiquitously expressed in human tissues with highest expression in pancreas, skeletal muscles and heart. It acts primarily on pyrimidine 5'-, 3'- and 2'-deoxynucleoside monophosphates. Purine nucleoside monophosphates dIMP and dGMP are also hydrolyzed by this enzyme. Unlike cN-II and cN-III, cdN does not display phosphotransferase activity (Höglund and Reichard, 1990).

Mitochondrial 5'(3')-deoxynucleotidase (mdN) – Sharing a high level of sequence homology with cdN, mdN shows a narrow substrate specificity limited to hydrolysis of dUMP and dTMP . It is expressed ubiquitously in all human tissues with the highest expression in heart, brain and skeletal muscles (Rampazzo et al., 2000a; Mazzon et al., 2003).

1.2.3 Catalytic mechanism

All intracellular nucleotidases have an absolute requirement for Mg^{2+} as a cofactor for catalytic activity (Tozzi et al., 1991; Pesi et al., 1994). Hydrolysis of nucleoside monophosphates by 5'-nucleotidases is a bi-substrate reaction. The first step involves the breakage of the phosphoester bond with the concomitant formation of a phosphoenzyme intermediate and release of the nucleoside. The phosphoenzyme intermediate is then hydrolyzed by a water molecule. In case of phosphotransferase

activity, the phosphoenzyme intermediate is dephosphorylated by an acceptor nucleoside instead of a water molecule (Fig. 1.1). The formation of a phosphoenzyme intermediate was first demonstrated in cN-II by trapping the covalent enzyme-phosphate intermediate formed during the reaction (Baiocchi et al., 1996). Earlier, the formation of a covalent enzyme-substrate intermediate had been demonstrated for phosphotransferases like phosphoglucomutase (Joshi and Handler, 1969) and phosphoglyceromutase (Fersht, 1985) and hydrolases like alkaline phosphatase (Stinson et al., 1987) and phosphotyrosine protein phosphatase (Cirri et al., 1993), which also display phosphotransferase activity.

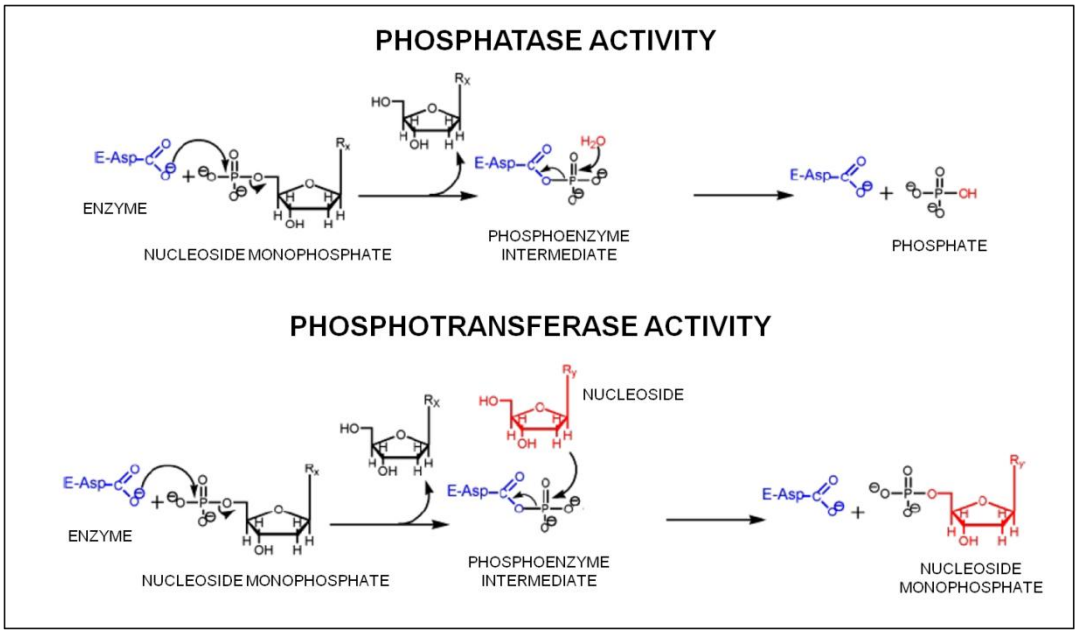

Figure 1.1. Reaction scheme describing phosphatase and phosphotransferase activity of 5'-nucleotidases. Only nucleoside 5'-monophosphates are shown in the scheme. However, the same is applicable for nucleoside 2'- and 3'-(deoxy)monophosphates.

During catalysis, the first step of phosphoester hydrolysis occurs through nucleophilic attack on the phosphoester bond by the first aspartate residue of a highly conserved, DXDXT/V, motif sequence (Allegrini et al., 2001), which is also present in several other phosphohydrolases including phosphomannomutases and L-3-phosphoserine phosphatases (Collet et al., 1998) as well as the Haloacid Dehalogenase (HAD) superfamily of proteins.

1.2.4 Structure-function relationship

Crystal structures of nucleotidases and other phosphohydrolases helped in identifying conserved structural elements and key amino acid residues associated with the catalytic process. Crystal structure of human mitochondrial deoxyribonucleotidase was the first structure obtained for a cytosolic nucleotidase (Rinaldo-Matthis et al., 2002). The structural fold was similar to the HAD superfamily of proteins. The first structural evidence of a covalent phosphoenzyme intermediate was obtained from the crystal structure of β-phosphoglucomutase which showed a stable pentavalent phosphorane intermediate formed during the phorphoryl transfer from C1(O) of glucose-1,6-bisphosphate to the nucleophilic aspartate residue (Lahiri et al., 2003).

From crystallographic and site-directed mutagenesis studies, it was demonstrated that apart from the first motif described above, three other conserved motifs are also present at the active site that play an important role in catalysis (Aravind et al., 1998; Collet et al., 1998, 1999; Rinaldo-Matthis et al., 2002). The first is a conserved serine/threonine residue included in a hydrophobic region, the second is a conserved lysine residue and the third is a pair of conserved aspartic acid residues (Fig. 1.2).

Kinetic and structural evidence has demonstrated that all cytosolic 5'-nucleotidases are members of the HAD superfamily of proteins, which is one of the largest superfamily of proteins with 79,778 entries in the Structure Function Linkage Database (SFLD) spanning the entire living kingdom, with only 22,547 entries assigned to a sub-family (www.sfld.rbvi.ucsf.edu/django/superfamily/3).

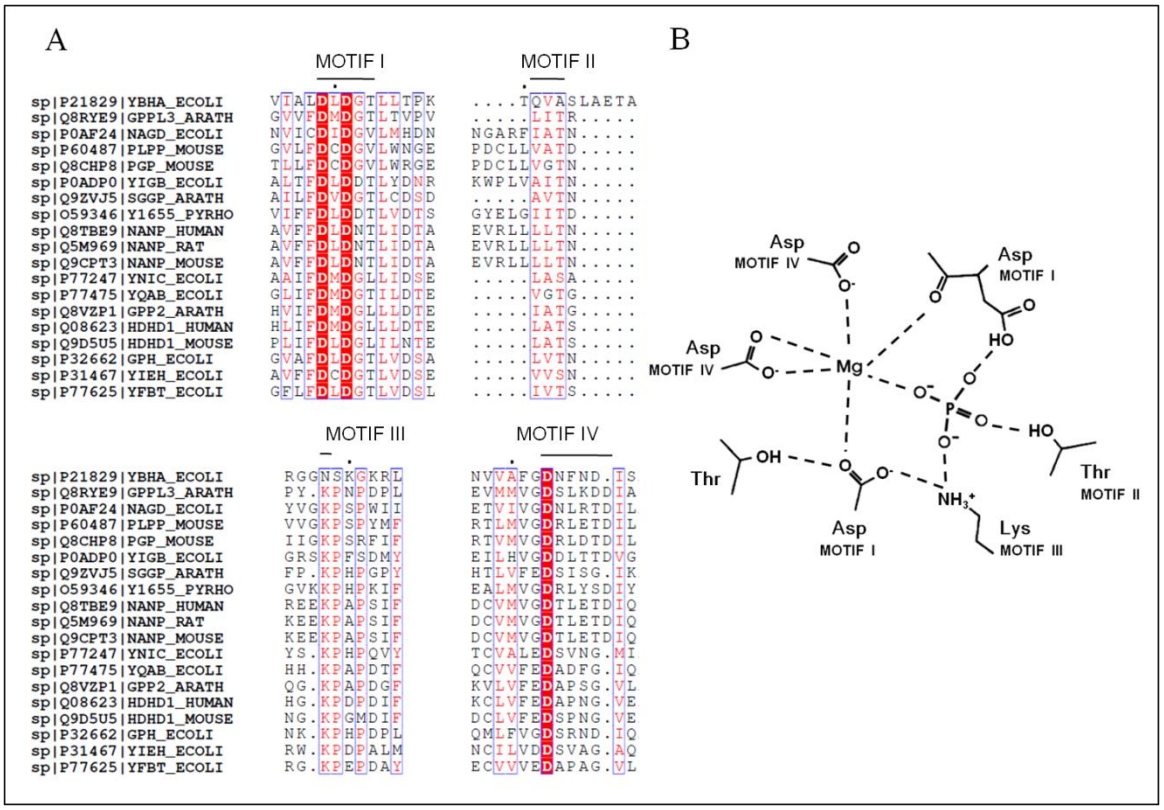

Figure 1.2. (A) Multiple sequence alignment highlighting conserved motif stretches in selected HAD members. (B) Schematic representation of motif residues in the catalytic site in cN-II (Allegrini et al., 2004).

Several sub-families including acid phosphatase, HAD-like hydrolase, 5'-nucleotidase, P-type ATPase and phosphoserine phosphatase are part of this superfamily. HAD superfamily proteins share little sequence homology (10% overall sequence identity) but unequivocally contain the four motif stretches. HAD superfamily structures are sub-divided into the core and the cap domain (Fig. 1.3A). HAD superfamily shares structural features with the 'DHH' motif family of phosphoesterases, the Receiver (CheY) domain in histidine protein kinase superfamily, the von Willebrand A (vWA) domain in extracellular matrix proteins and integrin receptors, the Toprim domain in topoisomerases type-Ia and II, histone deacetylases and PIN/FLAP nuclease domains containing a specific form of the Rossmann fold, which is distinguished from the others by the presence of equivalently placed acidic catalytic residues including one at the end of the first core β-strand of the central sheet and two key structural features, a 'squiggle' (a single helical turn) and a 'flap' (a β-hairpin motif) located immediately downstream of the first β-strand of the core Rossmanoid fold. The 'squiggle' and the 'flap' provide the necessary mobility to these enzymes to adopt 'open' and 'closed' conformations (Fig. 1.3B). The cap domains are inserted into either one of the two positions shown in Figure 1.3B. Structurally HADs can be classified into 3 major types

based on their cap structure. Type I (C1) has insertions occurring in the middle of the β-hairpin of the 'flap' motif. Type II (C2) has insertions occurring in the linker immediately after strand S3. Type III (C0) has only short insertions in either of the two positions of cap insertion (Burroughs et al., 2006). Variability in cap structure is a major factor for the vast substrate diversity found in HAD members. Members of type I subfamily hydrolyze small substrates like phosphoserine, hexose phosphates and ATP, type II subfamily members hydrolyze intermediate substrates like nucleoside phosphates and sucrose-6-phosphate while type III subfamily members hydrolyze tRNAs and phosphoproteins (Fig. 1.3C) (Allen and Dunaway-Mariano, 2004).

1.2.5 Physiological role and clinical significance

Intracellular 5'-nucleotidases are catabolic enzymes that hydrolyze ribo- and deoxyribonucleotides. Along with kinases, they are involved in substrate cycles that regulate the ribo- and deoxyribonucleotide pools in the cell (Reichard, 1988; Gazziola et al., 2001; Bianchi and Spychala, 2003). Due to overlapping substrate specificities, a particular 5'-nucleotidase might be involved in more than one substrate cycle. Intracellular 5'-nucleotidases have relatively high K_m values and operate on substrates generally present at low concentrations (Piec and Le Hir, 1991; Gazziola et al., 2001). cN-I is the primary producer of adenosine in heart and skeletal muscle tissues during ischemic and hypoxic conditions (Garvey and Prus, 1999). cN-II is primarily involved in the regulation of inosine and guanosine nucleotide pools.

However, it also participates in more complex substrate cycles like the purine nucleoside cycle (see section 1.3.2 for details), utilizing phosphoribosyl pyrophosphate (PRPP) and generating D-ribose 1-phosphate (Rib-1-P) during the cycle which in turn regulates purine salvage and pyrimidine salvage pathways, respectively (Barsotti et al., 2003). cN-III is primarily involved in the degradation of uridine and cytidine deoxyribonucleotides produced by RNA degradation during erythrocyte maturation (Rees et al., 2003). Its selective activity towards pyrimidine nucleotides ensures that purine nucleotide pools are not depleted (Paglia and Valentine, 1975). cdN forms substrate cycles along with nucleoside kinases to regulate deoxynucleotide levels in cells. Its substrate specificity and expression profile suggests that it is involved in protecting cells from expansion of pyrimidine nucleotide pools, particularly dUTP and dTTP (Gazziola et al., 2001).

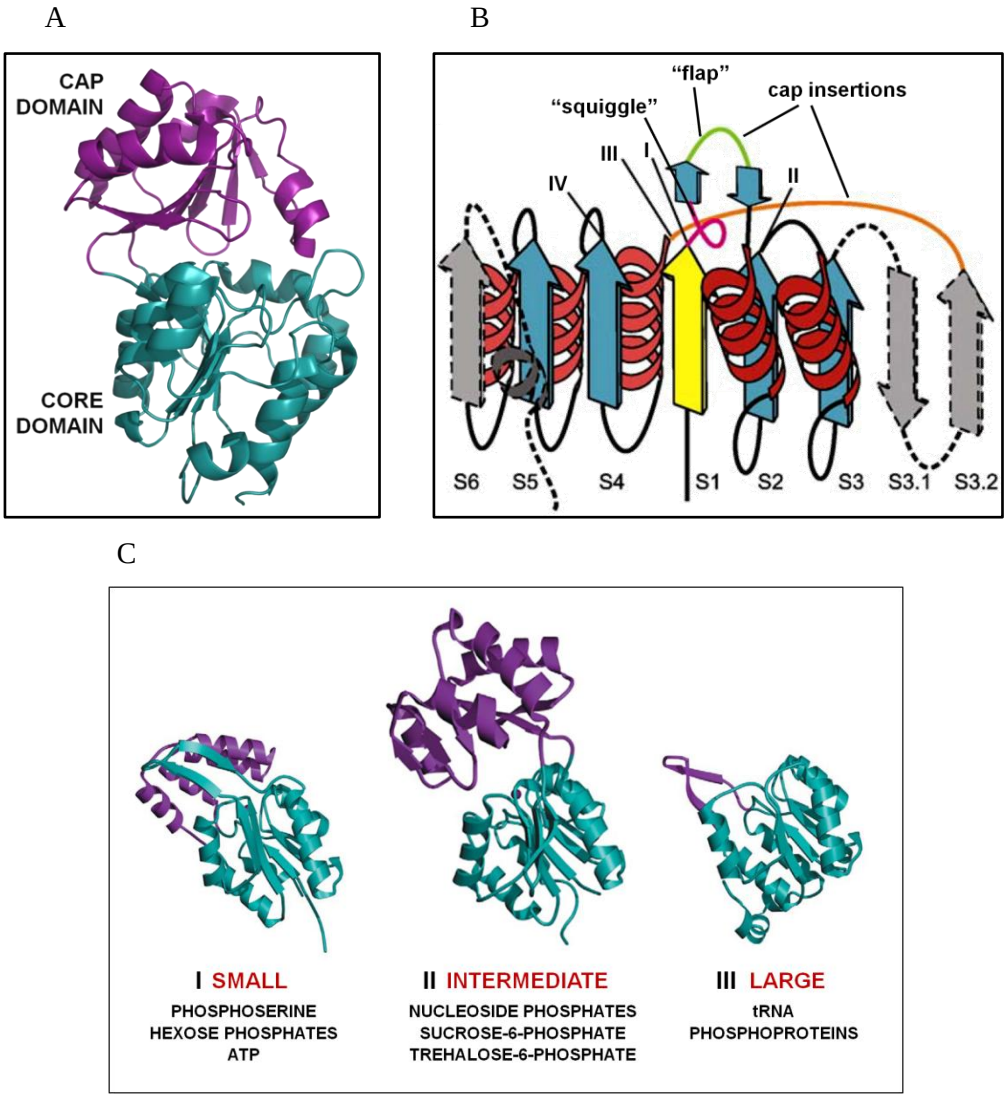

Figure 1.3. Common structural features of HAD superfamily proteins. (A) Domain architecture in a broad specificity HAD phosphatase from *P. vivax* (PDB ID 2B30) with the core and cap domains colored in cyan and purple, respectively. (B) Topological diagram of secondary structural elements in a HAD superfamily protein. The figure is reprinted from *J. Mol. Biol.*, 361, Burroughs A. M., Allen K. N., Debra Dunaway-Mariano D. and Aravind L., Evolutionary Genomics of the HAD Superfamily: Understanding the Structural Adaptations and Catalytic Diversity in a Superfamily of Phosphoesterases and Allied Enzymes, 1003-1034, Copyright (2006), with permission from Elsevier. (C) Classification of HAD sub-families based on cap domain architecture (purple) with the core domain highlighted in cyan. (I) Subfamily I, phosphoserine phosphatase (1F5S). (II) Subfamily II, phosphatase TM0651 from Thermotoga maritime (1NF2). (III) Subfamily III, 8-KDO phosphatase (1J8D). Substrates catalysed by each sub-family are mentioned below each class. The figure is reprinted from TiBS, 29, Allen, K. N. and Dunaway-Mariano, D., Phosphoryl group transfer: evolution of a catalytic scaffold, 495-503, Copyright (2004), with permission from Elsevier. See Appendix A for Rights & Permissions.

Its 3'-nucleotidase activity might play a role in recycling nucleotides produced by nucleases in dying cells (Fritzson, 1977). mdN is primarily involved in protecting mitochondria against excess dTTP levels which can be mutagenic for mitochondrial DNA replication (Rampazzo et al., 2000a). Ecto-nucleotidases act on the extracellular side of the cell membrane, generating adenosine, salvaging extracellular nucleotides, mediating cell adhesion and possibly acting as co-receptor for T-cell activation. Along with extracellular kinases, they provide a regulatory switch between P1 and P2 purinergic signaling pathways (Yegutkin et al., 2002).

Nucleoside analogs are vital components of anti-cancer and antiviral therapies. They enter the cell through nucleoside transporters and are incorporated into DNA after being phosphorylated into the triphosphate form, leading to chain termination. Mechanisms of resistance to nucleoside analogs are only partially understood. Extensive clinical studies have suggested that 5'-nucleotidases, specially cN-II, may play a role in nucleoside analog resistance by dephosphorylating the analogs and deactivating them (Hunsucker et al., 2005). Purified recombinant cN-II has shown activity against several nucleoside monophosphate analogs including 5-fluorodeoxyuridine monophosphate (FdUMP), zidovudine 5'-monophosphate (AZTMP) and 9-β-D-arabinofuranosylguanine monophosphate (araGMP) (Mazzon et al., 2003). The extent of clinical drug resistance to these analogs will depend on the expression levels of 5'-nucleotidases as well as their relative ratio to kinases in the cell.

1.2.6 A novel class of IMP-specific 5'-nucleotidases (ISN1)

Amongst the three kingdoms of life, ISN1 sequences are present only in eukaryotes with 83% of the selected sequences found in fungi. This apart, a small number of organisms belonging to the Alveolata, Viridiplantae, Stramenopiles and Cryptophyta also possess ISN1 (Fig. 1.4). An *in silico* study conducted earlier showed through motif and fold conservation that ISN1s also belong to the HAD superfamily of proteins (Srinivasan and Balaram, 2007) and contain the characteristic motifs present in all HAD members (Fig. 1.5).

ISN1 from *S. cerevisiae* (ScISN1) was the first protein from the ISN1 family to be biochemically characterized. Assays with the enzyme purified from yeast extract showed that it selectively hydrolyzed IMP. It had a pH optimum of 6.0-6.5 and was dependant on divalent metal ions for its activity. The velocity *vs* IMP concentration plot was sigmoidal. The enzyme was activated by ATP, which reduced the K_m value and sigmoidicity (Itoh, 1994).

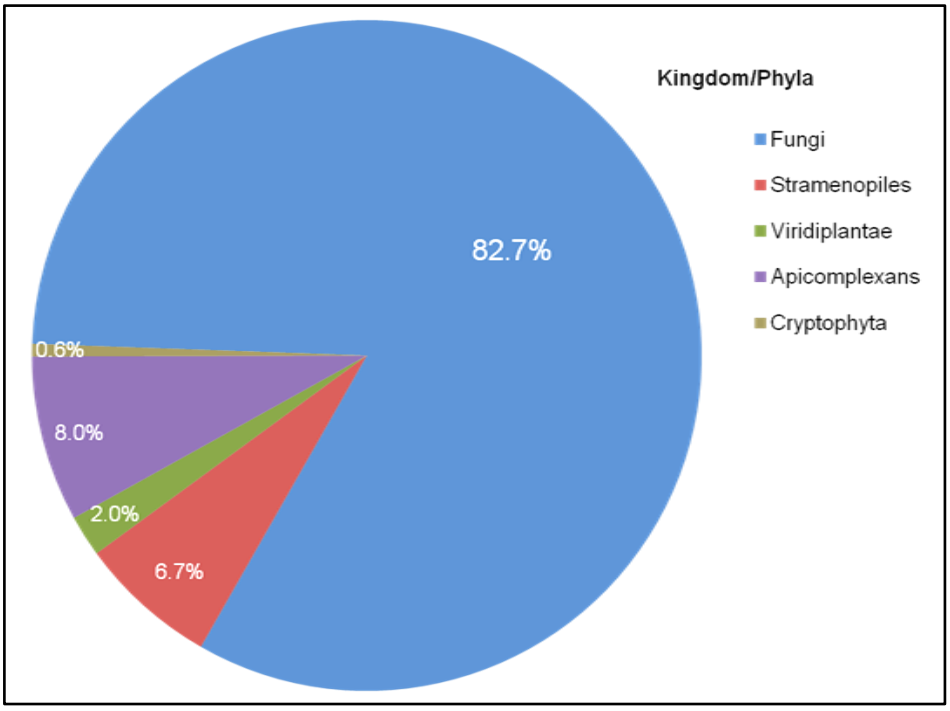

Figure 1.4. Distribution of ISN1 sequences amongst various kingdoms/phyla of life.

It was reported to be encoded by the gene *YOR155c* with homologs present in *N. crassa*, *P. falciparum* and several yeast species. Dominant mutations or overexpression of the *ADE4* gene in the IMP biosynthetic pathway resulted in increased IMP biosynthesis and subsequently increased inosine and hypoxanthine secretion in the medium (Rebora et al., 2001). A plasmid overexpressing a dominant mutant form of *ADE4* when transformed into wild-type and *isn1* mutant strains resulted in decreased inosine and hypoxanthine secretion in the medium in the *isn1* mutant as compared to wild-type, indicating its role in the *in vivo* degradation of IMP (Itoh et al., 2003). Apart from being an IMP 5'-nucletidase, ScISN1 was also found to act as a pyridine 5'-nucleotidase, hydrolyzing nicotinamide mononucleotide (NMN) and nicotinic acid mononucleotide (NaMN) to nicotinamide ribonucleotide (NR) and nicotinic acid ribonucleotide (NaR), respectively, as inferred from the decreased levels of NR and NaR in the *isn1* deletion strain. Both NR and NaR are biosynthetic precursors of NAD^+, suggesting the role of ScISN1 in NAD^+ metabolism. Levels of ScISN1 protein were found to be upregulated by glucose (Bogan et al., 2009). In a study that attempted to understand glucose induced activation of purine salvage pathway, as indicated by a transient drop in ATP and ADP levels with a concomitant rise in IMP and inosine, glucose was implicated as an activator of ScISN1 activity (Loret et al., 2007). In another study that analyzed changes in the levels of 24 intracellular metabolite pools by LC-MS during the respiro-fermentative growth transitions in wild-type, AMP deaminase (*amd1)* and *isn1* deletion yeast strains revealed that ISN1, in conjugation with *amd1*, was responsible for pronounced drop in adenine nucleotide content (ATP+ADP+AMP=AXP) in respiring *S. cerevisiae* cells responding to a sudden

increase in glucose concentration (Walther et al., 2010). Despite the various studies, the physiological role of ISN1 remains yet unclear.

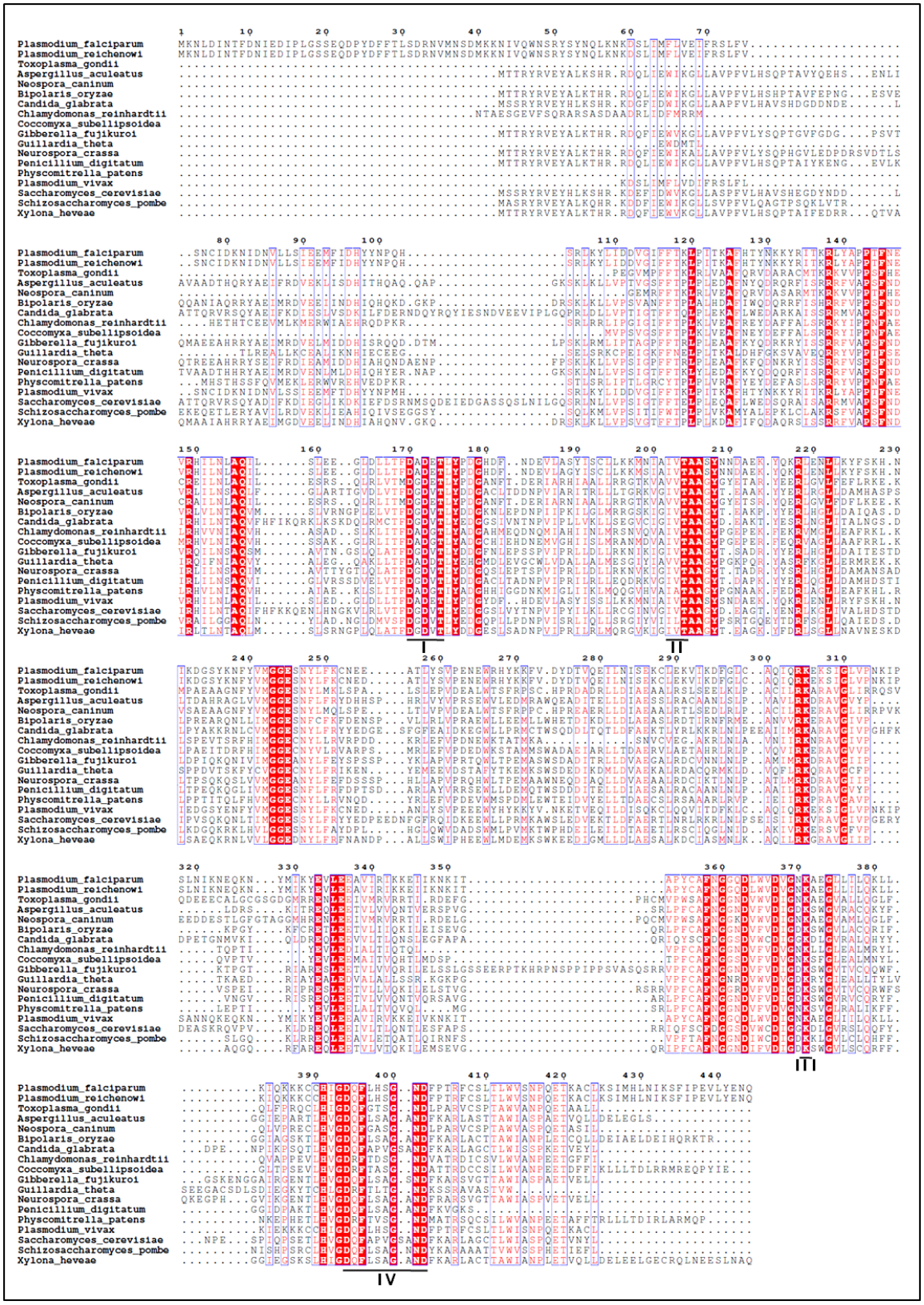

Figure 1.5. Multiple sequence alignment of selected ISN1 sequences representing all taxa/phyla that contain ISN1 sequences with the motifs I, II, III and IV underlined.

1.3 Nucleotide metabolism in *Plasmodia*

1.3.1 Malaria : an overview.

Malaria is an infectious disease caused by the protozoan parasite of the genus *Plasmodium* and spread by mosquitoes. It has been a global challenge with its high mortality rate and its impact on the economy of developing countries. *P. vivax, P. falciparum, P. ovale* and *P. malariae* are the four major species that infect humans. Although *P. knowlesi* primarily infects primates other than humans, it has also been found to infect humans in some cases (Singh et al., 2004). *P. vivax and P. falciparum* account for most of the infected cases of which *Plasmodium falciparum* is the most lethal as it causes cerebral malaria, a severe complication responsible for high mortality rate amongst infected patients. Efforts to eradicate malaria globally have not been successful. Moreover, several plasmodial strains have developed resistance against commonly used anti-malarial drugs, pushing the need for new drugs (Thaithong, 1983; Price et al., 2004). Over the past five decades, efforts towards understanding the metabolism of the parasite and the host-parasite relationship has helped in the discovery of potential drug targets leading to the development of various anti-malarial drugs (Parker et al., 2000; Gardiner et al., 2009). Nucleotide metabolism in the parasite, particularly of purines, has gained significant attention (Cassera et al., 2011). Genes encoding enzymes for the *de novo* biosynthesis of purine nucleotides are absent in the protozoan genome (Chaudhary et al., 2004). Hence, the parasite is dependent on the salvage of purines from the host through the purine salvage pathway. Uptake of purines from the host occurs through nucleoside transporters (Frame et al., 2012). Thus, enzymes of this pathway are considered as potential drug targets (Hyde, 2007; Cassera et al., 2011; Ducati et al., 2013).

1.3.2 Purine salvage pathway in *P. falciparum*.

Purine nucleotides are essential for various cellular processes, including synthesis of nucleic acids DNA and RNA, energy metabolites ATP and GTP, co-factors NAD, FAD, FMN and CoA. During the intraerythrocytic stages when the parasite resides in the erythrocytes, hypoxanthine is salvaged from the infected erythrocytes and phosphoribosylated to inosine 5'-monophosphate (IMP) by the enzyme HGPRT. IMP is utilized downstream for the synthesis of AMP and GMP. An alternative fate of IMP is its hydrolysis into inosine with the release of inorganic phosphate by a 5'-nucleotidase. Phosphorolysis of inosine to hypoxanthine is carried out by the enzyme purine nucleoside phosphorylase (PNP) with the release of Rib-1-P. HGPRT, 5'-nucleotidase

and PNP together constitute the purine nucleoside cycle (PNC) (Fig. 1.6) (Barsotti et al., 2003, 2005).

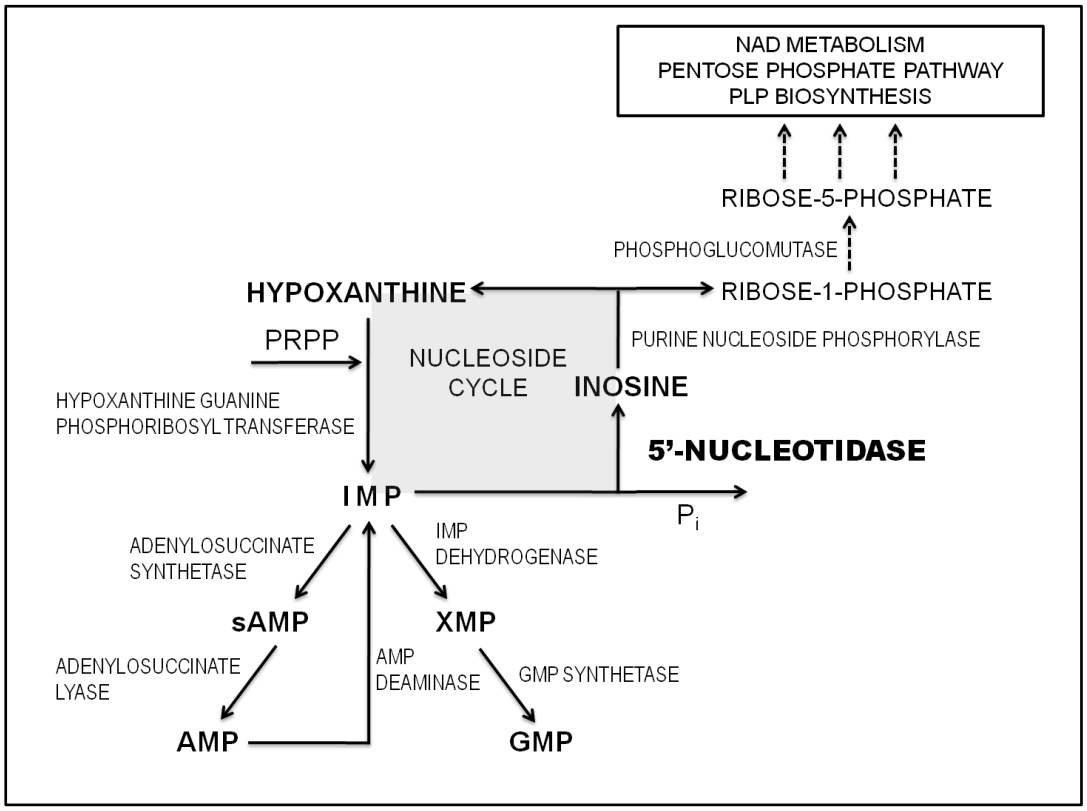

Figure 1.6. Schematic representation of purine salvage pathway in *P. falciparum.* Channeling of ribose-5-phosphate into other pathways is represented by broken arrows.

Substrate cycles like these may seem futile but they serve an important role in regulatory metabolism. PNC has been proposed to serve a role in the regulation of intracellular PRPP levels while R-1-P is utilized in pyrimidine salvage (Cappiello et al., 1998) and nucleoside interconversion pathways (Giorgelli et al., 1997). However, since the pyrimidine salvage pathway is not active in *P. falciparum*, R-1-P would primarily be involved in nucleoside interconversion. However, it could also be channeled into the pentose phosphate pathway, after its conversion to ribose-5-phosphate (R-5-P) by the enzyme phosphoglucomutase or utilized in PLP biosynthesis and NAD metabolism.

While HGPRT and PNP from *P. falciparum* have been extensively characterized (Kicska et al., 2002; Schnick et al., 2005; Roy et al., 2015), 5'-nucleotidase remains yet uncharacterized as no homologs of mammalian 5'-nucleotidases were found in the genome of apicomplexans, including Plasmodium and Toxoplasma. However, a study on a 5'-nucleotidase from *S. cerevisiae* identified a gene (*YOR155c)* encoding an IMP-specific 5'-nucleotidase (ISN1) that shared no significant homology with mammalian

5'-nucleotidases (Itoh et al., 2003). Homologs of this gene were found primarily in fungi, lower plants and plasmodia including *P. falciparum* (gene *PF3D7_1206100*).

1.3.3 IMP-specific 5'-nucleotidase from *P. falciparum* (PfISN1)

The gene *PF3D7_1206100* in *P. falciparum* was identified as a homolog of *YOR155c* gene in *S. cerevisiae* which codes for the IMP-specific 5'-nucleotidase protein. Present on chromosome 12, it is 1335 bp in length, coding for a single transcript containing 9 exons (Fig. 1.7). The translated product is a 444 amino acid protein with no predicted splice variants.

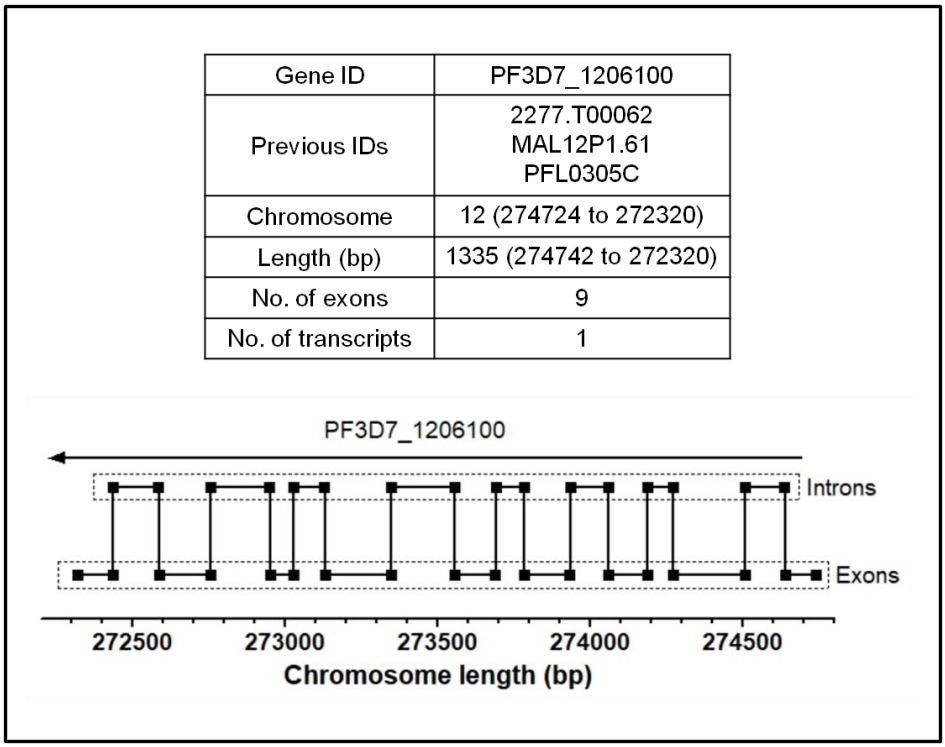

Figure 1.7. *PF3D7_1206100* gene coding for IMP-specific 5'-nucleotidase in *P. falciparum.* Gene map shown in the figure is to scale. Arrow indicates transcriptional direction. Information obtained from PlasmoDB (www.plasmodb.org, (Aurrecoechea et al., 2009)).

All 17 species of Plasmodia whose whole genomes have been sequenced do not have ISN1 gene (Table 1.2). Interestingly, ISN1 is one amongst few other genes, including a phosphoethanolamine N-methyltransferase, acid phosphatase and thiamine-phosphate pyrophosphorylase that are only present in species that have a primate host (Frech and Chen, 2011). In *P. falciparum*, the gene upstream to *PF3D7_1206100* encodes a shewanella-like protein phosphatase 2 protein while the gene downstream it encodes a eukaryotic translation initiation factor 3 subunit C protein.

Table 1.2. List of Plasmodium species, their host, geographical distribution and presence/absence of ISN1 gene.

No.	Species	Host	Distribution	ISN1 gene	Gene ID
1	*Plasmodium falciparum*	Human	Africa, Asia South/Central America	YES	PF3D7_1206100
2	*Plasmodium vivax*	Human	Africa, Asia, South/Central America	YES	PVX_084340
3	*Plasmodium knowlesi*	Macaque, Human	Southeast Asia	YES	PKNA1_C2_1305800
4	*Plasmodium reichenowi*	Chimpanzee	Africa	YES	PRCDC_1205400
5	*Plasmodium coatneyi*	Macaque	Southeast Asia	YES	PCOAH_00006900
6	*Plasmodium inui*	Macaque	Southeast Asia	YES	C922_04475
7	*Plasmodium malariae*	Human	Africa, Asia, South/Central America	YES	PMUG01_13016100
8	*Plasmodium fieldi**	Macaque	Southeast Asia	NO	
9	*Plasmodium ovale*	Human	Africa	YES	POWCR01_130012600
10	*Plasmodium simiovale**	Macaque	Southeast Asia	NO	
11	*Plasmodium hylobati**	Macaque	Southeast Asia	NO	
12	*Plasmodium gonderi**	Mandrill	Africa	NO	
13	*Plasmodium cynomolgi*	Macaque	Southeast Asia	YES	PCYB_131470
14	*Plasmodium berghei*	Rodent	Africa	NO	
15	*Plasmodium yoelii*	Rodent	Africa	NO	
16	*Plasmodium chabaudi*	Rodent	Africa	NO	
17	*Plasmodium brasilianum**	Spider monkey	South America	NO	
18	*Plasmodium atheruri**	Rodent	Africa	NO	
19	*Plasmodium mexicanum**	Lizard	North America	NO	
20	*Plasmodium elongatum**	Bird	Worldwide	NO	
21	*Plasmodium chiricahuae**	Lizard	North America	NO	
22	*Plasmodium vinckei*	Rodent	Africa	NO	
23	*Plasmodium gallinaceum*	Bird	Southeast Asia	YES	PGAL8A_00315900
24	*Plasmodium relictum*	Bird	Worldwide	YES	PRELSG_1304900
25	*Plasmodium floridense**	Lizard	Carribbean/Central America	NO	
26	*Plasmodium azurophilum**	Lizard	Carribbean/Central America	NO	
27	*Plasmodium faircihildi**	Lizard	Central America	NO	
28	*Plasmodium agamae**	Lizard	Africa	NO	
29	*Plasmodium giganteum**	Lizard	Africa	NO	
30	*Plasmodium mackerassae**	Lizard	Australia	NO	
31	*Plasmodium simium**	Spider Monkey	South America	NO	
32	*Plasmodium gaboni*	Hominids	-	YES	PGSY75_1206100
33	*Plasmodium fragile*	Simian	-	YES	AK88_02036
34	*Plasmodium lophurae**	Bird	Southeast Asia	NO	

*Whole genome sequence data not available in PlasmoDB database.

Both the genes were conserved across all the 17 species of Plasmodia, including those where ISN1 gene was absent, suggesting that in the syntenic chromosome regions

across Plasmodia, loss of ISN1 gene in certain Plasmodium species was restricted only to the ISN1 gene loci (Fig. 1.8).

Multiple sequence alignment of ISN1 protein sequences from all Plasmodium species shows >95% identity (Fig. 1.9). Studies on the cellular proteome of *P. falciparum* parasites in the asexual trophozoite and sexual gametocyte stages by tandem mass spectrometry reported that PfISN1 protein was enriched in the mature (stage V) female gametocytes (Silvestrini et al., 2010; Tao et al., 2014). Proteome analysis of male and female gametocytes conducted in another study also reported PfISN1 protein to be differentially expressed in female gametocytes. Interestingly, PNP and HGPRT enzymes which complete the PNC were not differently expressed, suggesting that in mature female gametocytes, PfISN1 might have a significant physiological role that extends beyond the purine nucleoside cycle (Lasonder et al., 2016). PfISN1 was also reported to be one amongst a set of host-specific lysophosphatidylcholine (LPC) – responsive genes that were found to be transcriptionally upregulated in response to depletion of host LPC levels, initiating sexual commitment and gametocytogenesis in *P. falciparum.* Its absence in the rodent malaria parasite *P. berghei* and the absence of LPC mediated regulation of sexual commitment in *P. berghei* suggest a possible role of PfISN1 in sexual commitment in *P. falciparum* (Brancucci et al., 2017).

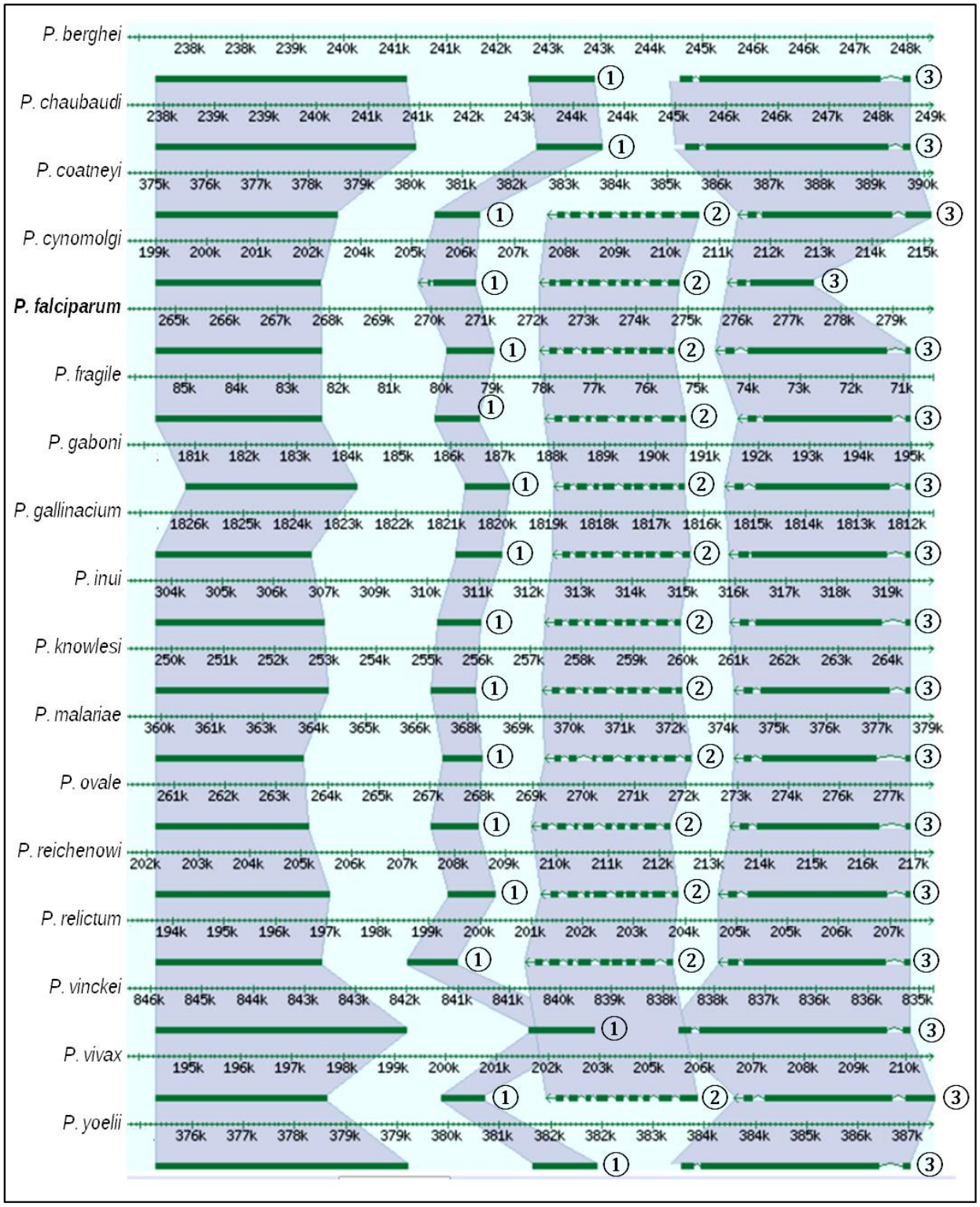

Figure 1.8. Syntenic region on chromosome 12 in various Plasmodium species within ~8 kbp upstream and downstream of *PF3D7_1206100* gene in *P. falciparum* (highlighted in bold). Syntenic regions and shading is based on OrthoMCL orthology. In each of the contigs, ISN1 gene (②) is flanked upstream by gene encoding shewanella-like protein phosphatase 2 (①) and downstream by gene encoding eukaryotic translation initiation factor 3 subunit C/8 (③). Image adapted from www.plasmodb.org, (Aurrecoechea et al., 2009)).

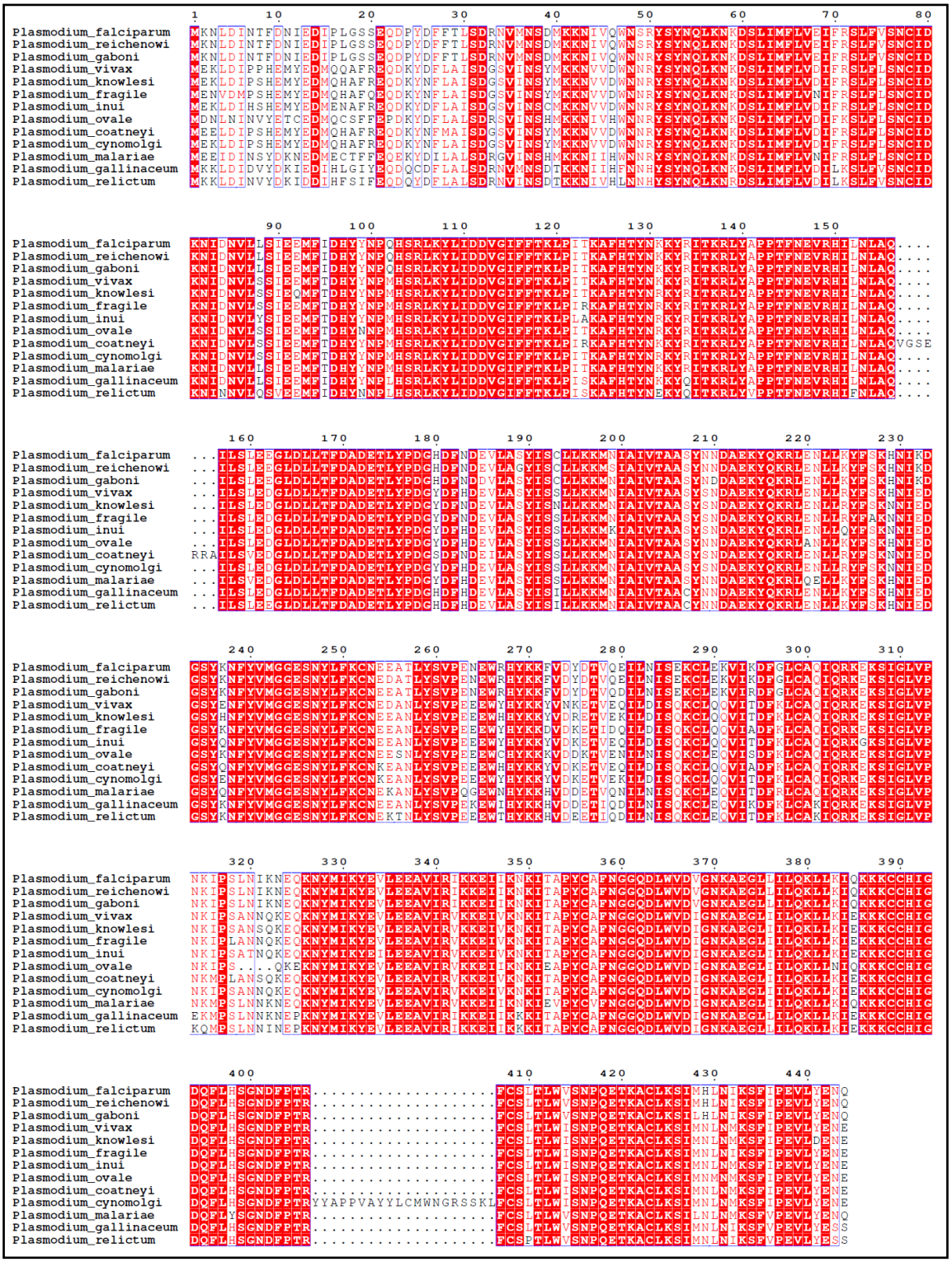

Figure 1.9. Multiple sequence alignment of ISN1 protein sequences from all Plasmodium species.

1.4 Summary

5'-nucleotidases play a crucial role in intracellular and extracellular nucleotide metabolism. Several mammalian 5'-nucleotidases have been characterized in the past five decades. In the context of purine metabolism in *P. falciparum*, 5'-nucleotidases have not been previously characterized. The ISN1 family of 5'-nucleotidases is a recently discovered class of enzymes, with only one member from *S. cerevisiae* being biochemically characterized so far. PfISN1 protein could play an important role in purine metabolism. Biochemical characterization of this protein would provide valuable information in the context of parasite biology and host-parasite relationship.

1.5 Objectives of the study

The primary objective of this study is the biochemical characterization of IMP-specific 5'-nucleotidase from *P. falciparum* (PfISN1). In order to determine its substrate and co-factor specificity, a comprehensive substrate and cofactor screen will be carried out. A modulator screen will also be carried out to search for potential modulator compounds of the enzyme. A detailed kinetic characterization of the enzyme will include determination of its catalytic efficiency with its substrate(s) and the effect of modulators, if any, on the catalytic efficiency of the enzyme. In HAD members, motif I aspartates play a critical role in catalysis. In various studies, non-conservative mutations in these residues have lead to a complete loss of enzyme activity. Hence, in PfISN1, non-conservative mutations in these aspartates and their subsequence impact on enzyme function will provide biochemical evidence that ISN1s belong to the HAD superfamily.

In order to understand the structure-function relationship in the protein, a crystal structure will be obtained. As seen in Figure 1.5, there are several conserved residues apart from the motifs, which might play an important role in enzyme function. Analysis of the structure will reveal the role of these and other key residues involved in processes like substrate binding, catalysis and regulation. Based on their conservation pattern, these residues will be mutated to observe their impact on enzyme function.

Using anti-PfISN1 antibodies, indirect immunofluorescence microscopy will be performed to obtain localization of the protein in various asexual and sexual intraerythrocytic stages of the parasite.

Chapter Two

Biochemical characterization of recombinant PfISN1 protein

Table of Contents

2.1 Abstract

Biochemical characterization of PfISN1 was performed with the recombinant enzyme, expressed and purified from *E. coli*. Apart from ScISN1, no other ISN1 family protein has been biochemically characterized till date. PfISN1 protein is a putative IMP-specific 5'-nucleotidase with its physiological function yet to be established. A detailed biochemical characterization of recombinant PfISN1 protein was carried out *in vitro* to identify important biochemical properties like oligomeric state, substrate preference, cofactor preference, conditions for optimum activity, regulators, etc. Values of kinetic parameters for its substrates IMP and AMP were determined. Since a few 5'-nucleotidases have phosphotransferase activity, PfISN1 was also checked for phosphotransferase activity. From these studies, several biochemical features common with the ScISN1 protein as well as unique to the protein have been elucidated.

2.2 Enzyme catalysis, kinetics and regulation

Enzymes and catalytic RNA molecules act as biocatalysts to accelerate the rate of biochemical reactions without affecting the equilibrium constant of the reaction or getting consumed in the process. The rate enhancement brought about by enzymes is remarkably high, ranging from 10^7 to 10^{19} fold (Wolfenden and Snider, 2001). The non-enzymatic rates of several biochemical reactions like glycine decarboxylation, phosphate monoester hydrolysis and fumarate hydration are in the order of 10^5-10^9 years, making enzymes critical for performing biochemical reactions as they enhance the rate to the order of 10^1-10^3 seconds. Enzyme catalysis proceeds through a series of steps from binding of the substrate(s) to release of the product(s), during which the substrate forms a transient high-energy low-stability intermediate. Pauling had proposed that rate enhancement could be achieved by the preferential binding of a transition-state intermediate to the enzyme rather than the substrate (Pauling, 1946) which was later supported by the use of transition-state analogues that had higher affinity than the substrate for the enzyme (Wolfenden, 1972, 1976).

Specificity of enzymes for their substrates is either to a particular substrate, functional group or a stereoisomer, governed by the chemical interactions between the enzyme and the substrate. According to the 'induced-fit' hypothesis, enzymes are flexible macromolecules that undergo structural changes upon substrate binding which are important for catalysis (Koshland and Jr., 1958). As discussed in section 1.2.4 of chapter 1, the enormous substrate diversity in HAD superfamily members is primarily due to the diverse structure of their cap domains. Members with small cap domains (C0)

have a highly accessible catalytic site, catalysing macromolecular substrates while those with large cap domains (C1/C2) have a restricted access to the catalytic site, catalysing small/intermediate molecular substrates. In several HADs, substrate binding motifs in the cap domain contribute to their specificity. For example, in a HAD phosphatase from *T. onnurineus* NA1, the substrate interacts with two Trp residues that are a part of substrate binding motif, WxxW (Ngo et al., 2015). A tight beta-turn in the helix-loop-helix motif of the cap domain in HADs contains a stringently conserved Gly, flanked by residues whose side chains contribute to the catalytic site. The flexibility provided by Gly is critical for enzyme function (Lahiri et al., 2004). In *P. Falciparum* HAD1, a sugar phosphatase, distinct conserved residues from the cap domain mediate substrate recognition (Park et al., 2015).

Enzymes exhibit rate-saturation kinetics, wherein the reaction rate increases linearly with the substrate concentration up to a particular value, beyond which the rate becomes non-linear and finally achieves saturation. The Michaelis-Menten model (Fig. 2.1) explains the relationship between initial rate and substrate concentration in enzyme-catalysed reactions (Michaelis and Menten, 1913). The model assumes that the catalytic rate is measured during the initial stage of the reaction, termed as initial rate when substrate depletion and product inhibition are negligible. The Michaelis-Menten equation $v = V_{max}\cdot[S]/(K_m+[S])$ has two parameters V_{max} and K_m (Michaelis constant) which represent maximum initial rate of the enzyme and substrate concentration at $0.5\cdot V_{max}$, respectively. These parameters are constant for a particular enzyme-substrate pair. The plot of the equation is a rectangular hyperbola (Fig. 2.1).

In several multimeric enzymes, regulation of activity is achieved by cooperativity in which the binding of the substrate to one subunit affects its binding to the other subunits. The mechanism was coined as ‘allostery’ by Jacob and Monod, derived from the Greek *allos* meaning “other” and *stereos* meaning “structure” (MONOD and JACOB, 1961). If the binding of the substrate to one subunit increased the affinity of the other subunits, it is called positive homotropic cooperativity/allostery, while the reverse is called negative homotropic cooperativity/allostery (Bardsley and Wyman, 1978; Neet, 1995).

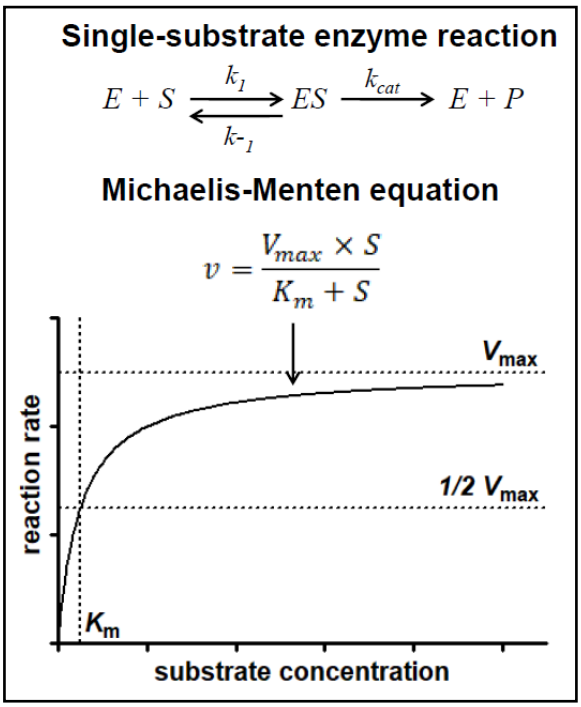

Figure 2.1. Michaelis-Menten model for steady-state initial rate enzyme kinetics. Reaction scheme for a single-substrate enzyme reaction and Michaelis-Menten equation describing the reaction rate *vs* substrate concentration curve with parameters V_{max} *and* K_m highlighted. E – enzyme, S – subsrate, k_1, k_{-1} and k_{cat} are rate constants of their respective reactions.

If a molecule other than the substrate regulates activity through another distinct binding site, it is called heterotropic allostery. The binding of allosteric modulators induces conformational changes in the protein, which in several cases involves reorganization of the catalytic site. Several HAD members display allosteric modulation of enzyme activity (Table 2.1).

Table 2.1. Allosteric modulators of HAD members[*].

Enzyme	Organism	Modulator(s)
cytosolic nucleotidase-II[1]	*H. sapiens*	ATP, 2,3-BPG, diadenosine polyphosphate
cytosolic nucleotidase-II[2]	*L. pneumophila*	GTP, dGTP, GDP, GMP
phosphatidylinositol-4-phosphate phosphatase[3]	*S. cerevisiae*	phosphatidylinositol, phosphatidylserine
Phosphonoacetaldehyde hydrolase[4]	*P. aeruginosa*	n-butylphosphonic acid

[*]References: [1](Wallden and Nordlund, 2011), [2](Srinivasan et al., 2014a), [3](Zhong et al., 2012), [4](Dumora et al., 1991)

The structural basis of allosteric activation in human cytosolic nucleotidase-II was found to be a disorder-to-order transition in a helix that contained motif IV residues (Wallden and Nordlund, 2011), whereas in its *L. pneumophila* counterpart, subunit reorganization upon modulator binding was the probable mechanism of allosteric

activation (Srinivasan et al., 2014b). The above example presents a case of diversity in regulatory mechanisms amongst even close members of the HAD superfamily.

Regulatory enzymes display non-Michaelis-Menten kinetic behaviour with sigmoidal ('S' shaped) initial rate *vs* substrate concentration plots (MONOD et al., 1963). The Hill model (Hill, 1910), originally derived to account for the sigmoidal nature of oxygen binding to haemoglobin, explains cooperative binding in regulatory enzymes. Apart from the parameters V_{max} and $K_{0.5}$, the equation has the parameter h (Hill coefficient), which indicates the nature and strength of cooperativity (Fig. 2.2). Value of $h>1$ and $h<1$ indicate positive and negative cooperativity, respectively. When $h=1$, the equation is equivalent to the Michalis-Menten equation.

However, the Hill model has its limitations. It does not consider the conformational changes induced upon binding of the regulator. It also assumes that the binding of substrate to one site would induce binding of substrate to all n sites and intermediate binding of (n-1) sites is not considered. In spite of its limitations, is still widely used as an empirical measure of the strength of cooperativity in enzymes.

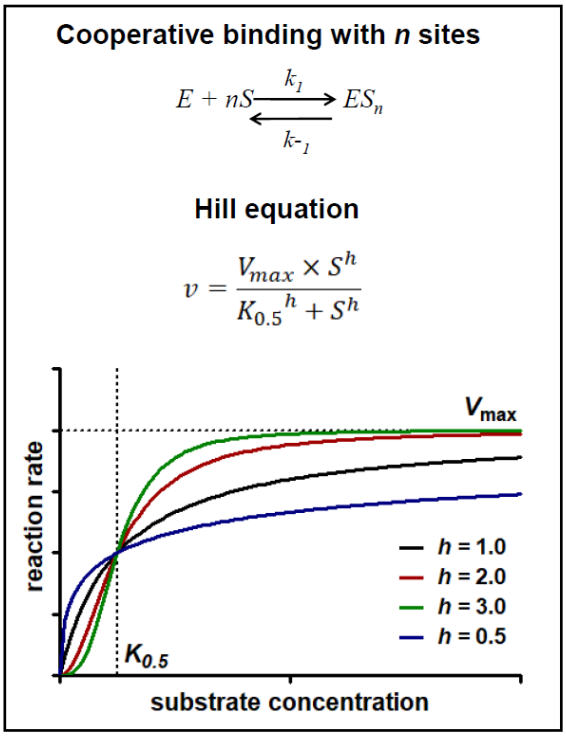

Figure 2.2. Cooperative substrate binding model with Hill equation. Shape of initial rate *vs* substrate concentration plots with various h values. E – enzyme, S – subsrate, n – number of binding sites, k_1 and k_{-1} and are rate constants of their respective reactions.

2.3 Earlier studies done in the laboratory

During earlier studies in the laboratory, the gene *PF3D7_1206100* was cloned into pET21b expression vector modified with a hexahistidine tag at the N-terminus. The expression conditions were optimized to obtain high amount of soluble protein suitable for further purification by Ni-NTA™ chromatography (Srinivasan, 2011).

2.4 Materials and Methods

2.4.1 Purification of recombinant PfISN1 protein

For protein expression, a seed culture of E. coli BL21 (DE3) strain containing the pET21b-PfISN1 plasmid that expressed the wild-type PfISN1 protein was grown overnight in Luria Broth (LB) medium that contained 100 µg ml^{-1} ampicillin. This seed culture was then used to inoculate 800 ml of Terrific Broth (TB) medium. Upon reaching an absorbance of 0.6 at 600 nm, the medium was induced with 0.3 mM Isopropyl β-D-1-thiogalactopyranoside (IPTG) and incubated at 18 °C for 16 hrs after which the cells were harvested by centrifugation at 4000 x g for 10 min at 4 °C. The cell pellet was re-suspended in 30 ml lysis buffer and lysed using French© pressure cell press (Thermo IEC Inc., USA) over 6 cycles at 1000 psi. The components of the lysis buffer were 50 mM Tris HCl, pH 8.0, 100 mM NaCl, 10% w/v glycerol, 0.1 mM PMSF and 0.5 mM TCEP (tris-(2-carboxyethyl) phosphine). The lysate was centrifuged at 14000 x g for 45 min at 5 °C and the supernatant bound to Ni-NTA™ beads (NI-NTA His-Bind® Resin, Qiagen, USA) for 3 hrs at 5 °C. Post binding, the beads were loaded onto a glass column and washed with at least 10 equivalent of bead volume of lysis buffer containing increasing concentrations of 0, 20 and 40 mM imidazole. The protein was eluted in 5 ml of lysis buffer containing 500 mM imidazole. 1 mM of ethylenediaminetetraacetic acid (EDTA) was added to chelate Ni^{2+} ions eluted along with the protein. The eluted protein was concentrated using Amicon® Ultra Centrifugal filter with a 30,000 Da molecular weight cut-off (Millipore™ Corporation, USA) and loaded onto a 16 mm x 60 cm column packed with Sephacryl™ S-200 HR beads. The eluted fractions were examined by SDS-PAGE for purity. Pure fractions were pooled, concentrated, flash-frozen and stored at -80 °C. Protein concentration was estimated by Bradford assay (Bradford, 1976) using bovine serum albumin as the standard protein.

2.4.2 Analytical size-exclusion chromatography

The oligomeric status of the protein was determined by size-exclusion chromatography using an AKTA® Basic HPLC system (Amersham Biosciences Ltd., U.K.). The protein was loaded onto an analytical Superdex™ S-200 HR 1 cm x 30 cm

column pre-equilibrated with 50 mM Tris HCl, pH 8.0, 100 mM NaCl, 10% (w/v) glycerol and 0.5mM tris(2-carboxyethyl)phosphine TCEP and calibrated using molecular weight standards, β-amylase (200 kDa); alcohol dehydrogenase (150 kDa); bovine serum albumin (66 kDa); carbonic anhydrase (29 kDa) and cytochrome c (12.4 kDa). V_o (void volume) of the column was taken as V_e (elution volume) of Blue Dextran (2000 kDa). The mass of the protein was calculated using a plot of V_e/V_o. *vs* Log (molecular weight in Da).

2.4.3 Measurement of PfISN1 enzyme activity

a) Measurement of phosphatase activity - Phosphatase activity assays were performed in a reaction mixture containing 50 mM Tris HCl, pH 8.0 or 50 mM 2-(N-morpholino)ethanesulfonic acid (MES), pH 5.0 and 30 mM $MgCl_2$. The reaction mixture containing the substrate was mixed with 0.4-0.9 µM enzyme and incubated for a fixed time after which the reaction was quenched with 10% trichloroacetic acid (TCA). The amount of inorganic phosphate formed during the reaction was estimated by Chen's assay (Chen et al., 1956). Chen's reagent (prepared fresh by mixing deionized water, 6N sulfuric acid, 2.5% ammonium molybdate, 10% ascorbic acid in a 2:1:1:1 ratio) was added to the quenched reaction mixture and incubated for 2 hrs at 37 °C. The absorbance was recorded at 820 nm using a Hitachi U-2010 spectrophotometer (Hitachi High Technologies America, Inc., San Jose, CA, USA) and the amount of inorganic phosphate was calculated using a molar extinction coefficient of 25000 M^{-1} cm^{-1}. Specific activity (SA) was reported as µmol or nmol of product formed per minute per mg of protein. All phosphatase activity assays were performed at 25 °C, unless mentioned otherwise.

b) Measurement of p-nitrophenyl phosphate (pNPP) hydrolysis activity - Continuous measurement of pNPP hydrolysis was performed by monitoring the change in absorbance due to p-nitrophenol (pNP) formation at 405 nm. Reaction mixture contained 50 mM Tris HCl, pH 8.0 and 30 mM $MgCl_2$. The amount of pNP formed was calculated using molar extinction coefficient of 18000 M^{-1} cm^{-1} at pH 8.0. All pNPP hydrolysis activity assays were performed at 25 °C, unless mentioned otherwise.

c) Units of enzyme activity - Specific Activity (SA) of the enzyme was represented as the amount of product (nmol or µmol) formed per minute per unit quantity of protein (µg or mg). Assuming that there is one catalytic site per monomer, k_{cat} or turnover number was represented as the number of molecules of product formed (nmol or µmol) per second, per molecule of monomer.

2.4.4 pH-dependent enzyme activity and stability assays

For pH-dependent activity measurements, a buffer containing a mixture of 50 mM Tris HCl, 50 mM MES and 50 mM glycine, adjusted to different pH values was used in the assay. To examine the stability of PfISN1 at various pH, the enzyme was pre-incubated with the mixed buffer at a particular pH for 15 min, followed by incubation in the reaction mixture containing 50 mM Tris HCl, pH 8.0 and 30 mM $MgCl_2$ for 3 min. Reaction was initiated with the addition of 10 mM IMP to the reaction mixture. % activity represents the enzyme activity at various pH with reference to pH 8.0. Subsequently, all activity assays at low pH were performed with 50 mM MES, pH 5.0 buffer.

2.4.5 Non-linear regression analysis of initial rate *vs* substrate concentration plots

The initial rate *vs* substrate concentration plots were generated using GraphPad Prism® version 5.0 (GraphPad Software Inc., SanDiego, CA). Non-linear regression method was used to fit the data using the Michaelis-Menten equation (eq. 2.1) for hyperbolic plots and the Hill equation (eq. 2.2) (Hill, 1910) for sigmoidal plots.

$$v = \frac{V_{max} \times S}{K_m + S} \qquad \text{(eq. 2.1)}$$

$$v = \frac{V_{max} \times S^h}{K_m^h + S^h} \qquad \text{(eq. 2.2)}$$

where v is initial rate, $V_{\max}$ is maximum rate; K_m is the apparent affinity constant, S is substrate concentration and h is Hill coefficient.

2.4.6 Enzyme activity assays in the presence of ATP

For assays containing ATP in the reaction mixture, additional $MgCl_2$ was added to account for depletion in free Mg^{2+} due to the formation of the ATP·Mg^{2+} complex.

2.4.7 Ion-pair reversed-phase HPLC.

The separation of nucleotides was achieved by ion-pair reversed-phase HPLC (IP-RP-HPLC), performed on a Genesis® C18 column (4µm pore size, 150 mm × 4.6 mm, Grace Davison Discovery Science, IL, USA), at 25 °C using an AKTA® Basic HPLC system (GE AMERSHAM, U.K.). The mobile phase consisted of two eluants; buffer A containing 20 mM Tris HCl, pH 7.4, 4 mM tetrabutylammonium hydrogen sulfate (TBAHS) and buffer B containing 20mM Tris HCl, pH 7.4, 4 mM TBAHS and 50 % (v/v) acetonitrile. Prior to sample injection, the column was pre-equilibrated with

several column volumes of buffer A. Post injection, the column was washed with 8.0 ml of buffer A, followed by elution of the analytes with an increasing linear gradient of buffer B in the following steps: 0-8 % B in 12.0 ml; 8-15 % B in 4.0 ml; 15-100 % B in 8.0 ml and continued at 100 % B for further 8.0 ml. The flow rate was 0.45 ml min^{-1} and the analytes were detected at 254 nm. Additionally, the peak fractions were analyzed by UV spectroscopy to distinguish between inosine (λ_{max} – 249 nm) and adenosine (λ_{max} – 259 nm) moieties. The column was washed with 70 % (v/v) acetonitrile after completion of the run. Peak intensities were determined using UNICORN® v3.00 software (Amersham Pharmacia Biotech AB, U.K.).

Phosphotransferase activity assay – In 5'-nucleotidases, phosphotransferase reaction involves the transfer of a phosphate group from a donor nucleoside 5'-monophosphate to an acceptor nucleoside. PfISN1 utilizes 5'-IMP and 5'-AMP as substrates and can transfer the phosphate group to adenosine and inosine, respectively. Hence, to detect any phosphotransferase activity in PfISN1, 5'-IMP-adenosine and 5'-AMP-inosine were used as donor-acceptor pairs. The reaction was quenched after 5 min with 10 % TCA, neutralized with NaOH and filtered through a 0.2 µM polyvinylidene fluoride (PVDF) membrane filter before injection. Individual peaks were assigned to metabolites by running several combinations of the standard metabolites IMP, AMP, adenosine and inosine at varying concentrations under assay conditions. Additionally, the peak fractions were analyzed by UV spectroscopy to distinguish between inosine (λ_{max} – 249 nm) and adenosine (λ_{max} – 259 nm) moieties.

2.4.8 Product inhibition assays

Product inhibition was tested with pNPP as the substrate since the product orthophosphate was incompatible with Chen's assay. Only up to 2 mM of orthophosphate (KPO_4, pH 7.0) and 4 mM of inosine and adenosine could be used in the assay due to low solubility of the products under the specific assay conditions. Sub-saturating pNPP (4 mM) was used in the assay in order to detect competitive inhibition by the products.

2.5 Results

Large scale purification of the protein was carried out to obtain pure protein in amounts sufficient to perform biochemical assays. Phosphatase activity of the protein was estimated by an assay that measures the amount of orthophosphate released upon the hydrolysis of the phosphorylated substrate. Foremost, a large comprehensive screen of compounds was performed to identify substrates of PfISN1, followed by a screen to

identify divalent metal ions that can serve as cofactors for the enzyme. Optimum pH for enzyme activity was also determined. Once the substrates were identified, the catalytic efficiency of the enzyme for its substrates was determined by steady-state kinetic measurements under various conditions. A screen to identify modulators of enzyme activity was also performed. In order to understand the mechanism of modulation, catalytic efficiency of the enzyme was determined in the presence of the modulators.

2.5.1 Purification of recombinant PfISN1 protein and determination of oligomeric state

800 ml of the bacterial culture containing the over-expressed protein was harvested. The protein was purified by Ni-NTA™ chromatography and followed by size-exclusion chromatography (Fig. 2.3). The protein was predominantly a tetramer in solution with a minor proportion of soluble higher-order aggregates, as determined by analytical size-exclusion chromatography (Fig. 2.4).

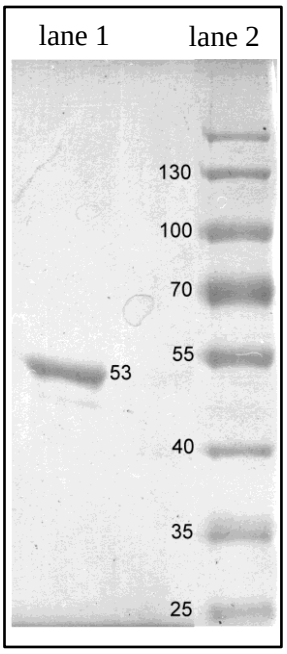

Figure 2.3. SDS-PAGE showing the purified recombinant PfISN1 protein fraction after Ni-NTA™ chromatography and size-exclusion chromatography (lane 1) and standard protein ladder (lane 2) with band sizes (kDa) marked alongside. Molecular weight of recombinant PfISN1 protein is 53031.8 Da.

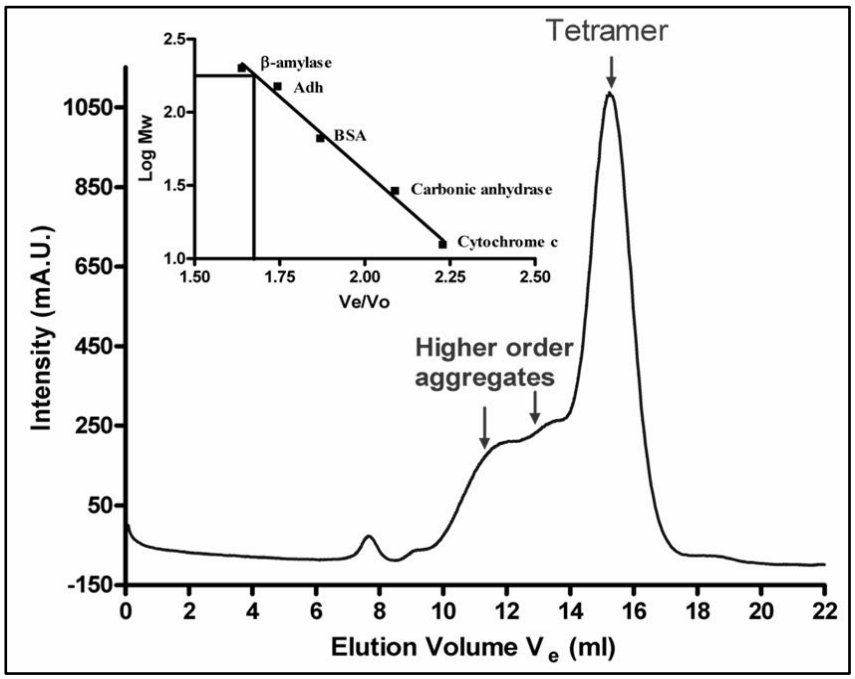

Figure 2.4. Analytical size-exclusion chromatogram representing the oligomeric state of the recombinant PfISN1 protein. Inset shows V_e/V_0 *vs* log(molecular weight in Da) plot of the protein standards (see 'Materials and Methods' for details).

2.5.2 Measurement of PfISN1 enzyme activity

The orthophosphate released during the catalytic reaction of 5'-nucleotidases was estimated by Chen's assay (Chen et al., 1956), an end-point assay described in detail in the 'Materials and Methods' section. The method was optimized in order to ensure reliable and accurate estimation of PfISN1 enzyme activity. A phosphate standard curve was obtained and the observed molar extinction coefficient value of 24,000 M^{-1} cm^{-1} was close to the reported value of 25,000 M^{-1} cm^{-1} suggesting that the assay reported an accurate measurement of orthophosphate (Fig. 2.5A).

The ratio of observed to expected orthophosphate (O/E) was used to determine the maximum limit of accurate determination of orthophosphate. A value closer to 1 indicates accurate measurement of orthophosphate. The O/E ratio was >0.85 for upto 1000 µM orthophosphate beyond which the ratio gradually declined (Fig. 2.5B). Hence, if an assay reported >1000 µM orthophosphate, the original reaction mixture was diluted in Chen's assay to obtain a lower absorbance value with the dilution factor incorporated later into the specific activity calculation. An optimized incubation time of 90-120 mins with Chen's reagent was chosen to allow saturation of the formation of colorimetric complex phosphomolybdenum blue (Fig. 2.5C). The quencher TCA had no effect on the assay (Fig. 2.5D).

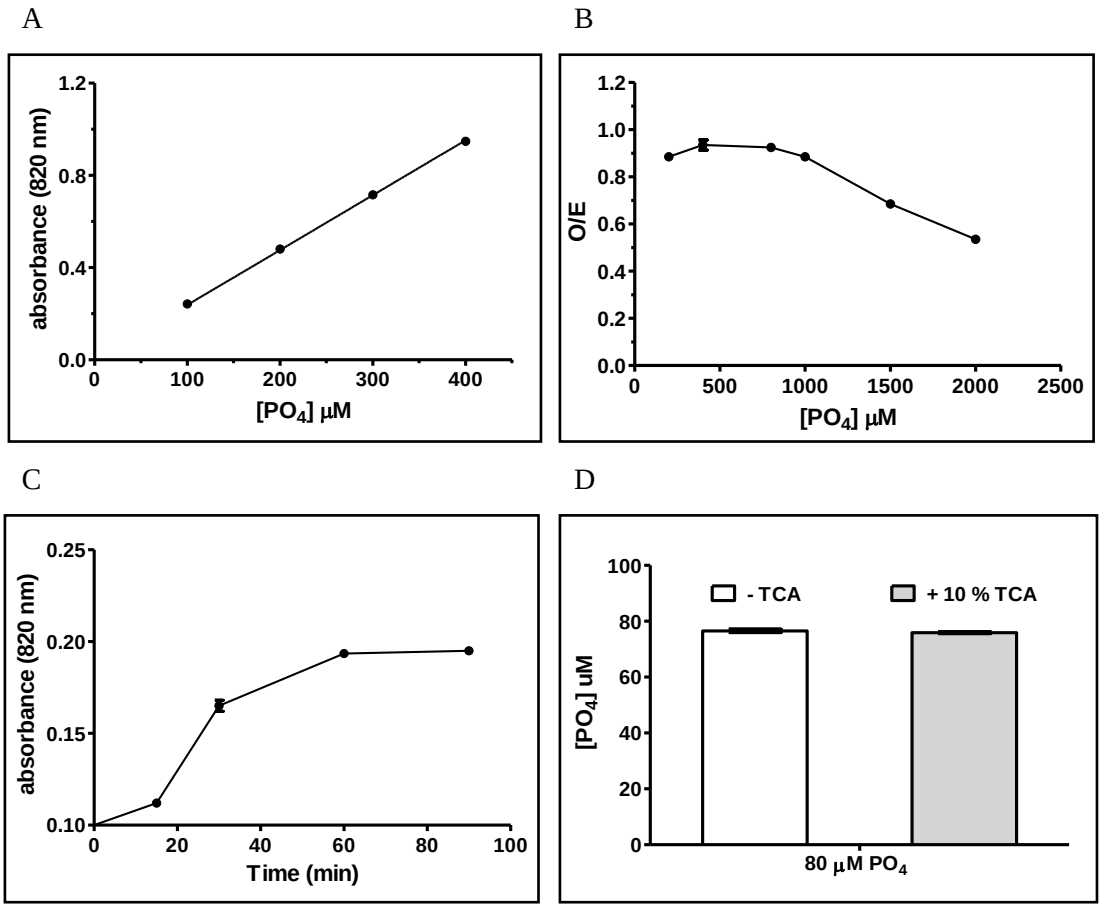

Figure 2.5. Optimization of Chen's assay. (A) Orthophosphate concentration *vs* absorbance (820 nm) standard plot. (B) Ratio of observed/actual orthophosphate concentration (O/E) *vs* actual orthophosphate concentration plot. (C) Absorbance (820 nm) *vs* time plot for 100 µM orthophosphate. (D) Effect of TCA on Chen's assay.

2.5.3 Substrate screen for PfISN1

Since several HAD members are known to exhibit broad substrate specificity (Daughtry et al., 2013; Huang et al., 2015), a comprehensive substrate screen was designed to detect substrates hydrolyzed by PfISN1 (Table 2.2). This screen contained a broad range of chemically diverse compounds including nucleoside 5'-monophosphates, diphosphates and triphosphates, nucleoside 3'-monophosphates, 3',5'-cyclic monophosphates, sugar phosphates, phosphoglycerates, amino acid phosphates and small molecule phosphates.

Table 2.2. List of phosphorylated compounds screened for as potential substrates of PfISN1[*].

Substrate	Specific Activity (µmol min^{-1} mg^{-1})		Substrate	Specific Activity (µmol min^{-1} mg^{-1})
Purine 5'-monophosphates			Aldohexose sugar phosphates	
IMP	2.85 ± 0.22		glucose-1-phosphate	N.D.
AMP	0.08 ± 0.03		glucose-6-phosphate	N.D.
GMP	N.D.[$]		mannose-6-phosphate	N.D.
XMP	N.D.		Aldopentose sugar phosphates	
Purine deoxy 5'-monophosphates			ribose-1-phosphate	N.D.
dAMP	N.D.		Ketopentose sugar phosphates	
dIMP	N.D.		ribulose-5-phosphate	N.D.
Pyrimidine 5'-monophosphates			Aldotetrose sugar phosphates	
UMP	N.D.		erythrose-4-phosphate	N.D.
TMP	N.D.		Glycolytic intermediates	
CMP	N.D.		phosphoenol pyruvate	N.D.
Nucleoside diphosphates			DHAP	N.D.
ADP	N.D.		2,3-BPG	N.D.
GDP	N.D.		Amino acid phosphates	
Adenosine 3',5'-diphosphate	N.D.		o-phospho-L-tyrosine	N.D.
Nucleoside triphosphates			o-phospho-L-serine	
ATP	N.D.		Other phosphates	
GTP	N.D.		p-nitrophenyl phosphate	N.D.
CTP	N.D.		p-nitrophenyl sulfate	N.D.
ITP	N.D.		p-aminophenyl phosphate	N.D.
Cyclic nucleotides			2-phosphoglycolic acid	N.D.
cAMP	N.D.		phosphonoacetic acid	N.D.
Purine 3'-monophosphates			3-deoxy-2-keto 6-phosphogluconic acid	N.D.
3'-AMP	N.D.		phenyl phosphate	N.D.
Other nucleotides			Vitamin precursors and cofactors	
succinyl-AMP	N.D.		NAD	N.D.
PRPP	N.D.		NADP	N.D.
Glycerol phosphates			NAM	N.D.
2-phosphoglycerate	N.D.		NMN	N.D.
3-phosphoglycerate	N.D.		NaMN	N.D.
α-glycerophosphate	N.D.		FMN	N.D.
β-glycerophosphate	N.D.		PLP	N.D.
Ketohexose sugar diphosphates				
fructose-1,6-bisphosphate	N.D.			

[*]FOOTNOTE: 10 mM substrate and 30 mM Mg^{2+} were used in all the assays. Specific activity values represent mean ± standard deviation (SD) of 3 independent measurements. [$]N.D. indicates Not Detectable.

Of all the compounds tested, the PfISN1 enzyme acted only on IMP and AMP. One of the screened compounds, pNPP which is a commonly used chromogenic phosphorylated substrate (Bessey et al., 1946) was not detected as a substrate but its hydrolysis by PfISN1 was detected by a different assay which detects the formation of pNP in a continuous manner. The assay is described in detail in the 'Materials and Methods' section. The progress curve of the reaction shows a positive slope due to an increase in pNP concentration with time, suggesting that pNPP was hydrolyzed by the enzyme (Fig. 2.6). However, the specific activity (~3.0 nmol min^{-1} mg^{-1}) was 1000-fold lower than that for IMP (~3.0 µmol min^{-1} mg^{-1}) and hence not detected by Chen's method.

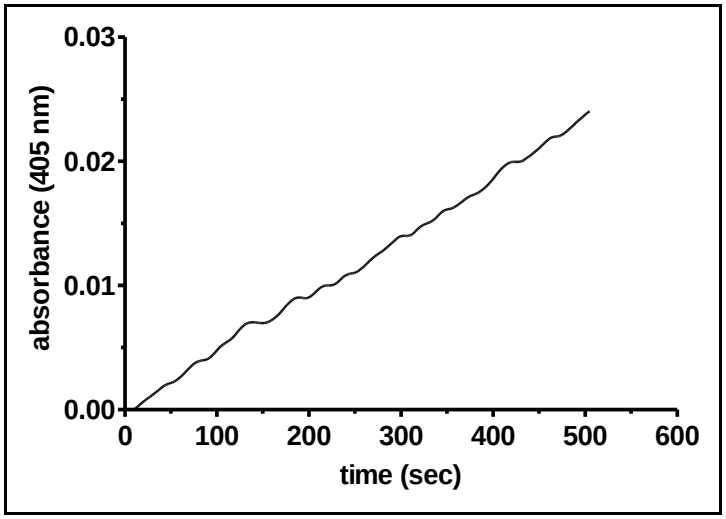

Figure 2.6. pNPP hydrolysis activity of PfISN1. A positive slope in the progress curve shows an increase in pNP concentration with time.

2.5.4 Cofactor screen

5'-nucleotidases have an obligatory requirement for divalent metal ions as a cofactor (Hunsucker et al., 2005). Although Mg^{2+} is the preferred co-factor for 5'-nucleotidases, Mn^{2+}, Fe^{2+}, Ni^{2+}, Co^{2+}, etc. are also preferred by some 5'-nucleotidases (Table 2.3). Several divalent metal ions were screened as co-factors for PfISN1 (Table 2.4). Although Mg^{2+} was the most preferred cofactor, significant IMP hydrolysis activity was also observed in the presence of Mn^{2+} and Fe^{2+}.

Table 2.3. List of divalent metal ions utilized as cofactors by 5'-nucleotidases from various organisms.

S. No.	Cofactor	Organism	Reference
1.	Mg^{2+}	*Bos Taurus*	(Smith et al., 1978)
		Homo sapiens	(Sylvestre et al., 1978)
		Rattus norvegicus	(Hinder and Bremner, 1978)
		Sus scrofa	(Honrubia et al., 1979)
		Vibrio parahaemolyticus	(Braude and De Clercq, 1979)
2.	Co^{2+}	*Escherichia coli*	(Proudfoot et al., 2004)
3.	Ni^{2+}	*Escherichia coli*	
4.	Mn^{2+}	*Escherichia coli*	
		Legionella pneumophila	(Srinivasan et al., 2014a)
		Xylella fastidiosa	(Santos et al., 2013)
5.	Fe^{2+}	*Clostridium propionicum*	(Stadtman et al., 1960)

Table 2.4. List of divalent metal ions screened as co-factors for PfISN1[*].

S. No.	Divalent metal ion	Specific Activity (µmol min^{-1} mg^{-1})
1.	Mg^{2+}	0.4 ± 0.01
2.	Mn^{2+}	0.11 ± 0.01
3.	Co^{2+}	0.07 ± 0.01
4.	Fe^{2+}	0.16 ± 0.01
5.	Ni^{2+}	0.02 ± 0.01
6.	Zn^{2+}	N.D.[$]
7.	Ca^{2+}	N.D.
8.	Cu^{2+}	N.D.

[*]FOOTNOTE: The assay was performed at pH 8.0 with 0.9 µM enzyme, 30 mM IMP and 0.2 mM MCl_2 where M is the divalent metal ion. Specific activity values represent mean ± SD of 3 independent measurements. [$]N.D. indicates Not Detectable.

2.5.5 Effect of pH on PfISN1 activity

The optimal pH for enzyme activity of PfISN1 was determined by measuring the enzyme activity in the pH range 2.0-9.0 with the substrates IMP (Fig. 2.7A) and AMP (Fig. 2.7B). Extremely high or low pH values could affect enzyme stability, resulting in an irreversible loss of enzyme activity. A pH-dependant enzyme stability assay was performed wherein the enzyme was pre-incubated in solution of different pH and the activity was then checked at pH 8.0. Enzyme activity at pH 8.0 was taken as reference value (100%). In the pH range 4.0-9.0, there was no significant change in activity as

compared to pH 8.0. However, the 5-fold lower activity at pH 2.0 and 3.0 suggested irreversible loss of enzyme stability below pH 4.0 (Fig. 2.7C).

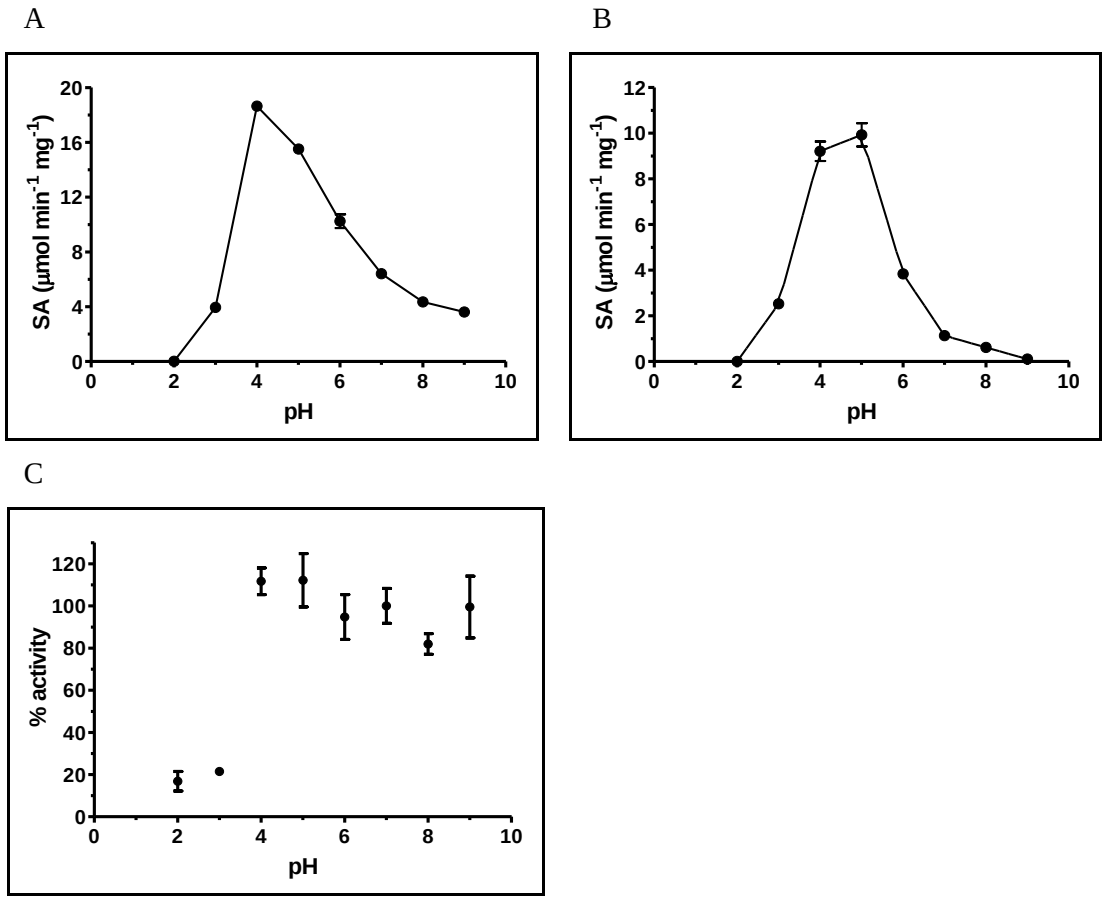

Figure 2.7. pH-dependant activity of PfISN1 with substrates (A) IMP and (B) AMP. The assay contained 0.9 µM enzyme, 30 mM substrate and 30 mM $MgCl_2$. (C) Enzyme stability assay was performed at pH 8.0 with 0.4 µM enzyme, 10 mM IMP and 30 mM $MgCl_2$ after pre-incubation for 15 min at room temperature. Activity at pH 8.0 was considered as 100 %. See 'Materials and Methods' section for more details.

2.5.6 Steady-steady kinetics with substrates IMP and AMP

Initial rate *vs* substrate concentration plots for IMP at pH 8.0 (Fig. 2.8A) and pH 5.0 (Fig. 2.8B) were hyperbolic, indicating absence of cooperativity. At pH 8.0, enzyme activity did not saturate even with 140 mM IMP which could not be further increased due to limited solubility. Steady-state kinetic parameters V_{max} and K_m, were obtained by non-linear regression analysis (see 'Materials and Methods' section for details) of the data. The increase in enzyme activity at low pH was due a significant decrease in the K_m value (Fig. 2.8C) and a mild increase in V_{max} value (Fig. 2.8D) for IMP.

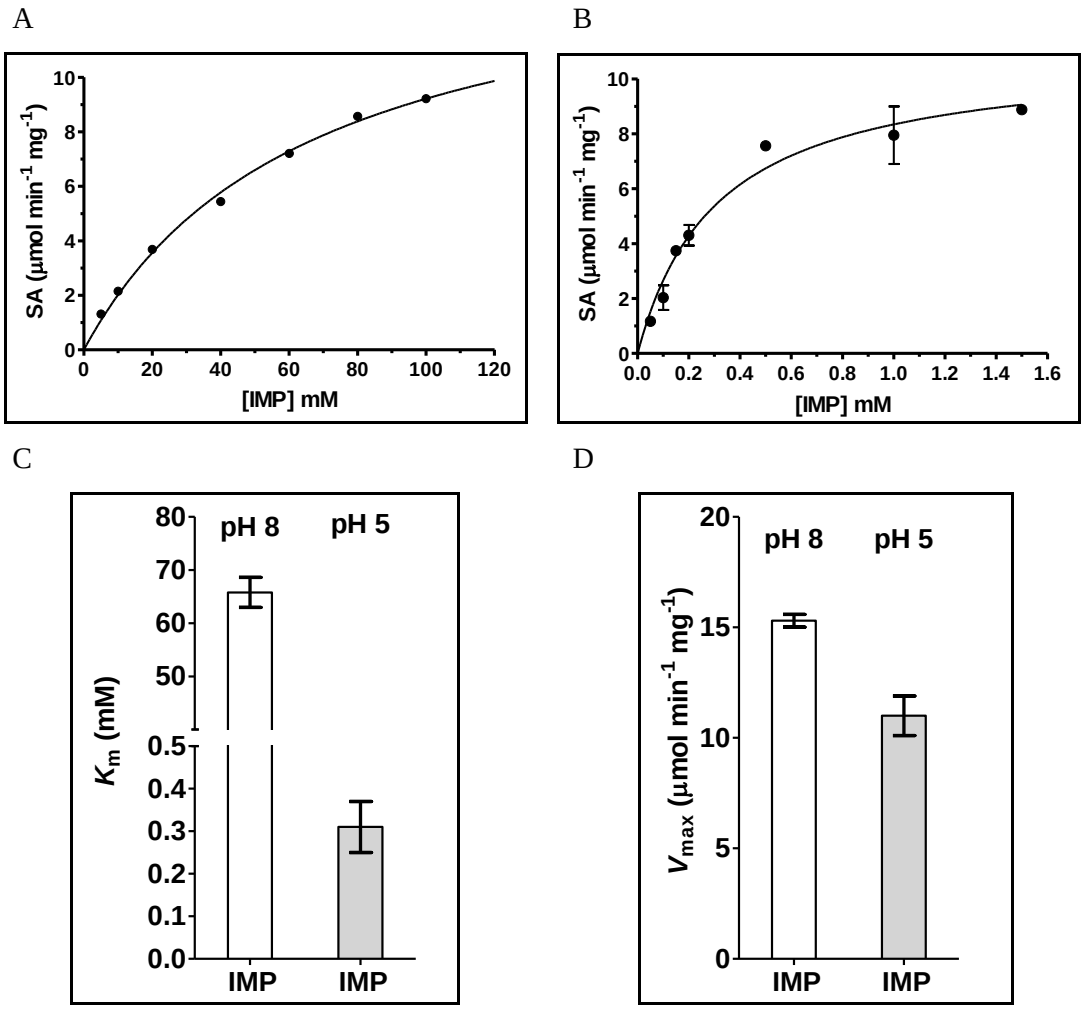

Figure 2.8. Initial rate *vs* substrate concentration plot for IMP at (A) pH 8.0 and (B) pH 5.0. Steady-state kinetic parameters (C) K_m (y-axis is segmented for ease of visualization) and (D) V_{max} derived from the plots A and B. Data points represent mean ± SD of 3 independent measurements.

Initial rate *vs* substrate concentration plots were obtained for AMP at pH 8.0 (Fig. 2.9A) and pH 5.0 (Fig. 2.9B). The shape of the plot at pH 8.0 was sigmoidal while at pH 5.0 it was hyperbolic. A sigmoidal shape indicates cooperativity. Steady-state kinetic parameters V_{max} and K_m, were obtained by non-linear regression analysis (see 'Materials and Methods' section for details) of the plots. At low pH, K_m (Fig. 2.9C) and V_{max} (Fig. 2.9D) values were not significantly altered when compared to values at pH 8.0. The degree of cooperativity for AMP at pH 8.0 was high, with an *h* value of 5.3 ± 0.3.

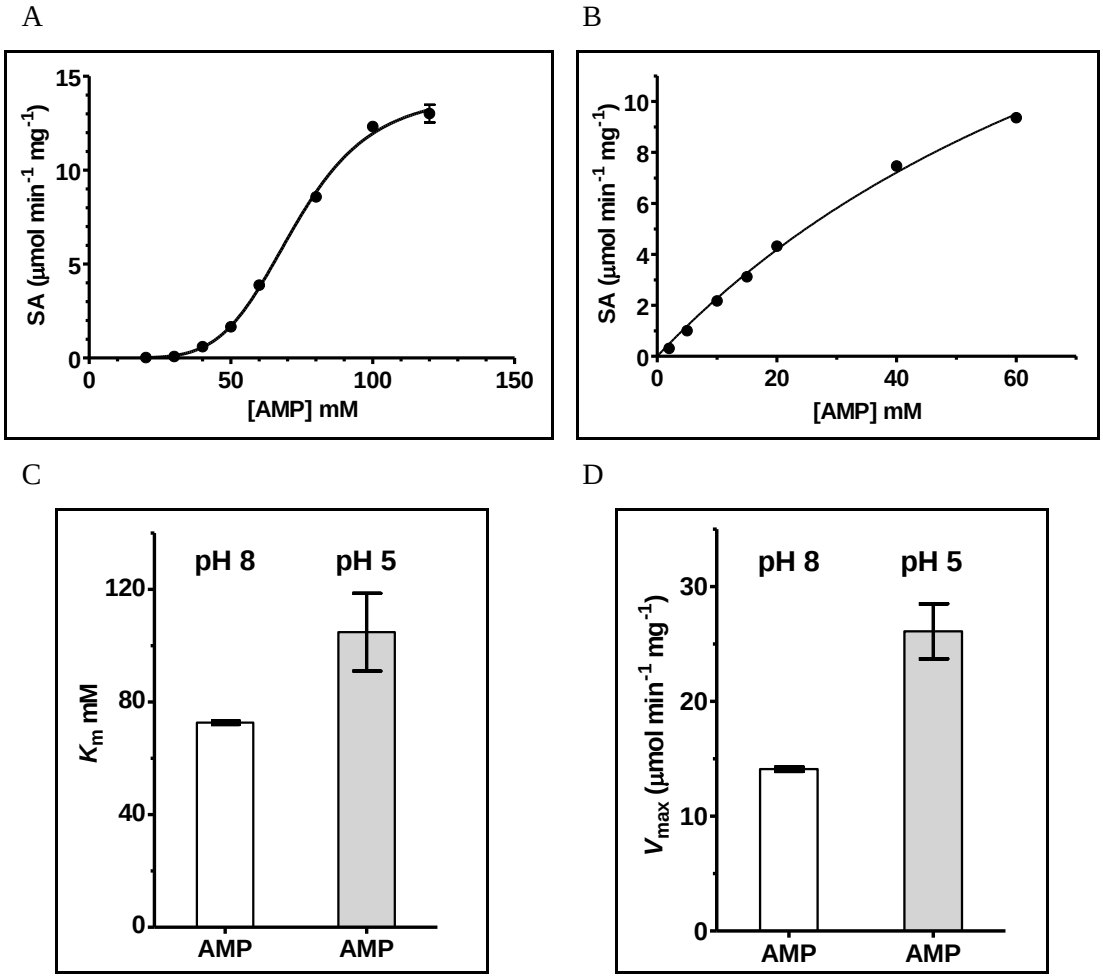

Figure 2.9. Initial rate *vs* substrate concentration plot for AMP at (A) pH 8.0 and (B) pH 5.0. Steady-state kinetic parameters (C) K_m and (D) V_{max} derived from the plots. Data points represent mean ± SD of 3 independent measurements.

A comparative representation of the catalytic efficiency of PfISN1 for both the substrates IMP and AMP at high and low pH is shown in Table 2.5. However, during the pH-dependent assay with AMP (Fig. 2.7B), the enzyme showed optimum activity at low pH due to loss of sigmoidicity (Fig. 2.9B), leading to increased enzyme activity at 30 mM AMP used in the assay.

Table 2.5. Catalytic efficiency for IMP and AMP at pH 5.0 and 8.0.

Substrate	pH	Catalytic efficiency (k_{cat}/K_m) (sec^{-1} mM^{-1})
IMP	5.0	31.4 ± 6.6
	8.0	0.21 ± 0.22
AMP	5.0	0.22 ± 0.04
	8.0	0.171 ± 0.005

2.5.7 Effect of cofactor Mg^{2+} on PfISN1 activity

Initial rate *vs* total Mg^{2+} concentration plots were obtained with IMP as the substrate. At pH 8.0, the plot was sigmoidal in nature (Fig. 2.10A), with an *h* value of (1.7 ± 0.2) while the plot at pH 5.0 was hyperbolic (Fig. 2.10B). The K_m value for free Mg^{2+} (26.6 ± 1.9 mM) was much higher at pH 8.0 than that at pH 5.0 (2.0 ± 0.3 mM), suggesting that like IMP, Mg^{2+} also bound to the enzyme with a stronger affinity at low pH. It should be noted that due to the dissociation constant (K_d) of IMP·Mg^{2+} complex being very high in solution (O'Sullivan and Smithers, 1979), the concentration of total Mg^{2+} will be equivalent to free Mg^{2+}.

2.5.8 Modulator screen

Modulators are compounds that can either activate or inhibit enzyme activity. A comprehensive list of compounds was chosen to screen for modulation of enzyme activity (Table 2.6). Amongst these were also compounds that are activators of cytosolic nucleotidases (cN-II). ATP and 2,3-bisphosphoglycerate (2,3-BPG) activate human cN-II (Wallden and Nordlund, 2011) while GTP activates *L. pneumophila* cN-II (Srinivasan et al., 2014a). Of all the compounds, only ATP and dATP activated the PfISN1 enzyme. ATP also activates ScISN1 (Itoh et al., 2003). It should be noted that ATP was included in the substrate screen (Table 2.1) but was not hydrolyzed by PfISN1.

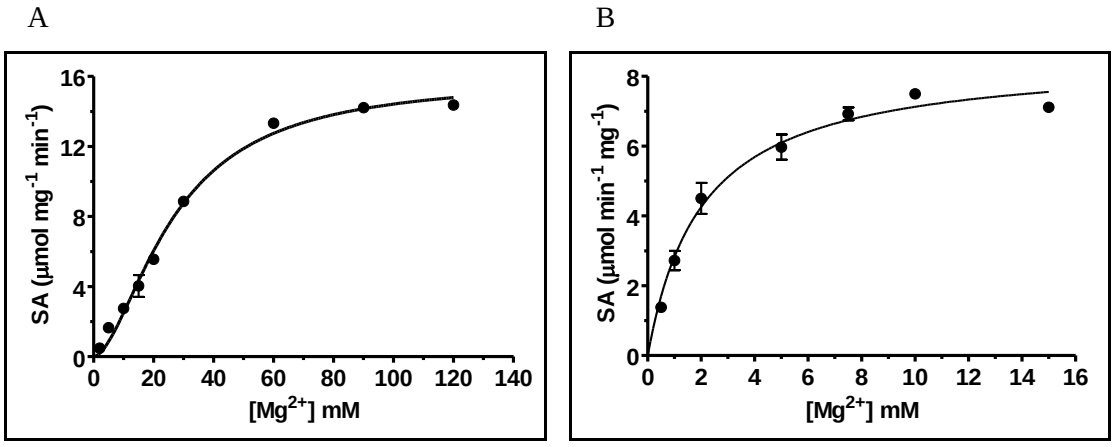

Figure 2.10. Initial rate *vs* total Mg^{2+} concentration plots with IMP at (A) pH 8.0 and (B) pH 5.0. For details see 'Materials and Methods' section.

Table 2.6. List of putative compounds screened for modulation of PfISN1 activity*.

Compound	Specific Activity (µmol min^{-1} mg^{-1})	Fold change		Compound	Specific Activity (µmol min^{-1} mg^{-1})	Fold change
Control	2.85 ± 0.22	1.0		Nucleoside monophosphates		
Nucleoside triphosphates				TMP	2.32 ± 0.32	0.8
ATP	7.31 ± 0.97	2.6		UMP	3.06 ± 0.01	1.1
dATP	8.83 ± 0.53	3.1		CMP	3.12 ± 0.02	1.1
dGTP	2.42 ± 0.34	0.8		GMP	2.05 ± 0.33	0.7
dTTP	3.94 ± 1.43	1.4		Sugar phosphates		
dCTP	2.78 ± 1.42	1.0		Glucose-6-phosphate	3.08 ± 0.27	1.1
ITP	1.74 ± 0.14	0.6		Mannose-6-phosphate	2.90 ± 0.25	1.0
GTP	1.97 ± 0.24	0.7		Vitamin precursors		
Glycolytic intermediates				NMN	3.25 ± 0.25	1.1
2,3-BPG	3.23 ± 0.19	1.1				

*FOOTNOTE: Fold change is calculated as specific activity for the given compound divided against the Specific Activity for the Control assay. 10 mM IMP, 30 mM $MgCl_2$ and 2 mM activator were used in the assay.

In order to confirm that ATP activated the enzyme by increasing the rate of IMP hydrolysis, the amount of inosine formed during the reaction in the presence and absence of ATP was detected and quantified by ion-pair reversed-phase HPLC (IP-RP-HPLC), a technique used to analyze nucleotide, nucleoside and nucleobase levels in a sample (Stocchi et al., 1987). The amount of inosine formed was higher in the presence of ATP when compared to its absence (Fig. 2.11A). Standard elution profile of inosine, IMP and ATP is shown in Fig. 2.11B.

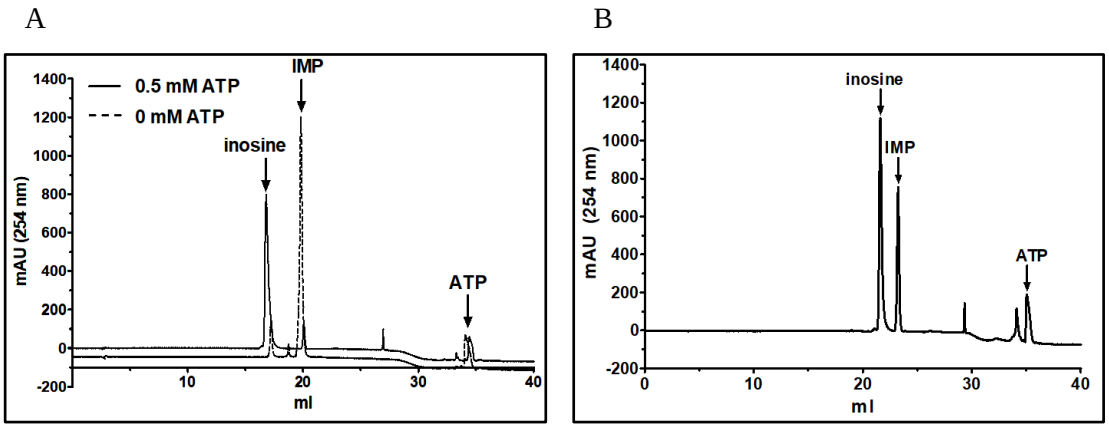

Figure 2.11. Chromatogram of IP-RP-HPLC performed in the (A) presence and absence of ATP. Peak intensities of inosine were 141 mAU (0 mM ATP) and 798 mAU (0.5 mM ATP). (B) Standard elution profile of 1 mM inosine, 0.5 mM IMP and 0.5 mM ATP. See 'Materials and Methods' section for details. mAU is milli-Absorbance Units.

2.5.9 Steady-state kinetics with modulator ATP

Initial rate *vs* substrate concentration plots for IMP (Fig.2.12A) and AMP (Fig. 2.12B) were obtained in the presence of ATP at pH 8.0. For IMP, there was a significant reduction in K_m (Fig. 2.12C) and a moderate increase in V_{max} (Fig. 2.12D). For AMP, while there was no significant change in K_m value (Fig. 2.12C), a moderate increase in V_{max} value was observed (Fig. 12D). Additionally, the plot for AMP was sigmoidal in nature (Fig. 2.12B), similar to the plot without ATP (Fig. 2.9A). At pH 5.0, there was no significant change in the K_m or V_{max} value for IMP. In conclusion, ATP activated enzyme activity by reducing the K_m value only for substrate IMP and only at pH 8.0. Overall, the catalytic efficiency of PfISN1 for IMP increased by about 15-fold in the presence of 4 mM ATP. For AMP, the catalytic efficiency did not increase significantly in the presence of ATP (Table 2.7).

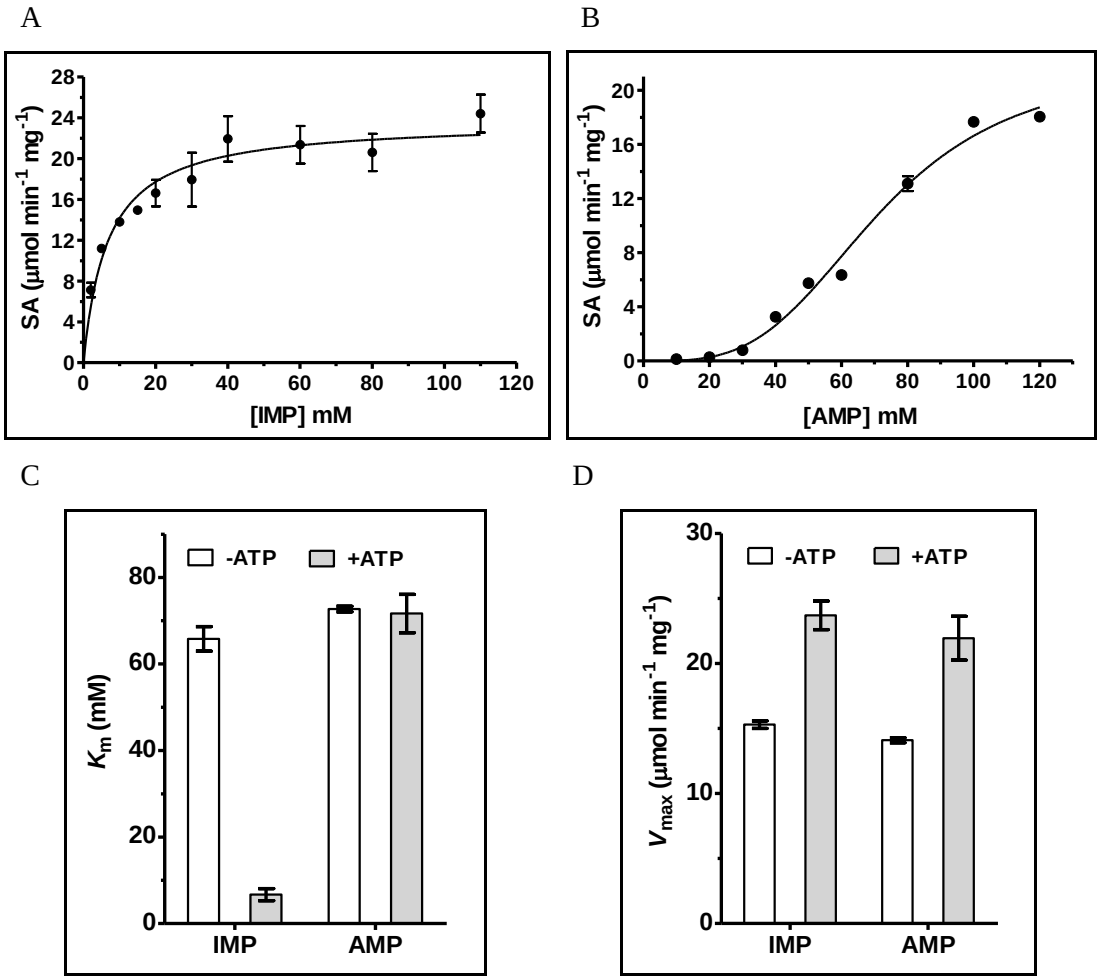

Fig. 2.12. Initial rate *vs* substrate concentration plots for (A) IMP and (B) AMP, obtained in the presence of 4 mM ATP. Steady-state kinetic parameters (C) K_m and (D) V_{max} derived from the plots for IMP and AMP. Data points represent mean ± SD of 3 independent measurements.

Table 2.7. Catalytic efficiency of PfISN1 for IMP and AMP with modulator ATP at pH 8.0.

Substrate	Activator	Catalytic efficiency (k_{cat}/K_m) (sec^{-1} mM^{-1})
IMP	- ATP	0.21 ± 0.22
	+ ATP	3.13 ± 0.67
AMP	- ATP	0.171 ± 0.005
	+ ATP	0.271 ± 0.027

2.5.10 Steady-state kinetics with pNPP

Although pNPP is not a physiological substrate, it was hydrolyzed by PfISN1 with a 1000-fold lower specific activity than IMP. At pH 8.0, initial rate *vs* pNPP concentration plot was sigmoidal (Fig. 2.13A), with an *h* value of 2.95 ± 0.28. In the presence of ATP, the plot continued to be sigmoidal (Fig. 2.13B), with an *h* value of 2.56 ± 0.2 and no significant change in K_m value (Fig. 2.13C) and V_{max} (Fig. 2.13D). Assays were not performed at pH 5.0 due to the low absorbance of the chromogenic product, pNP.

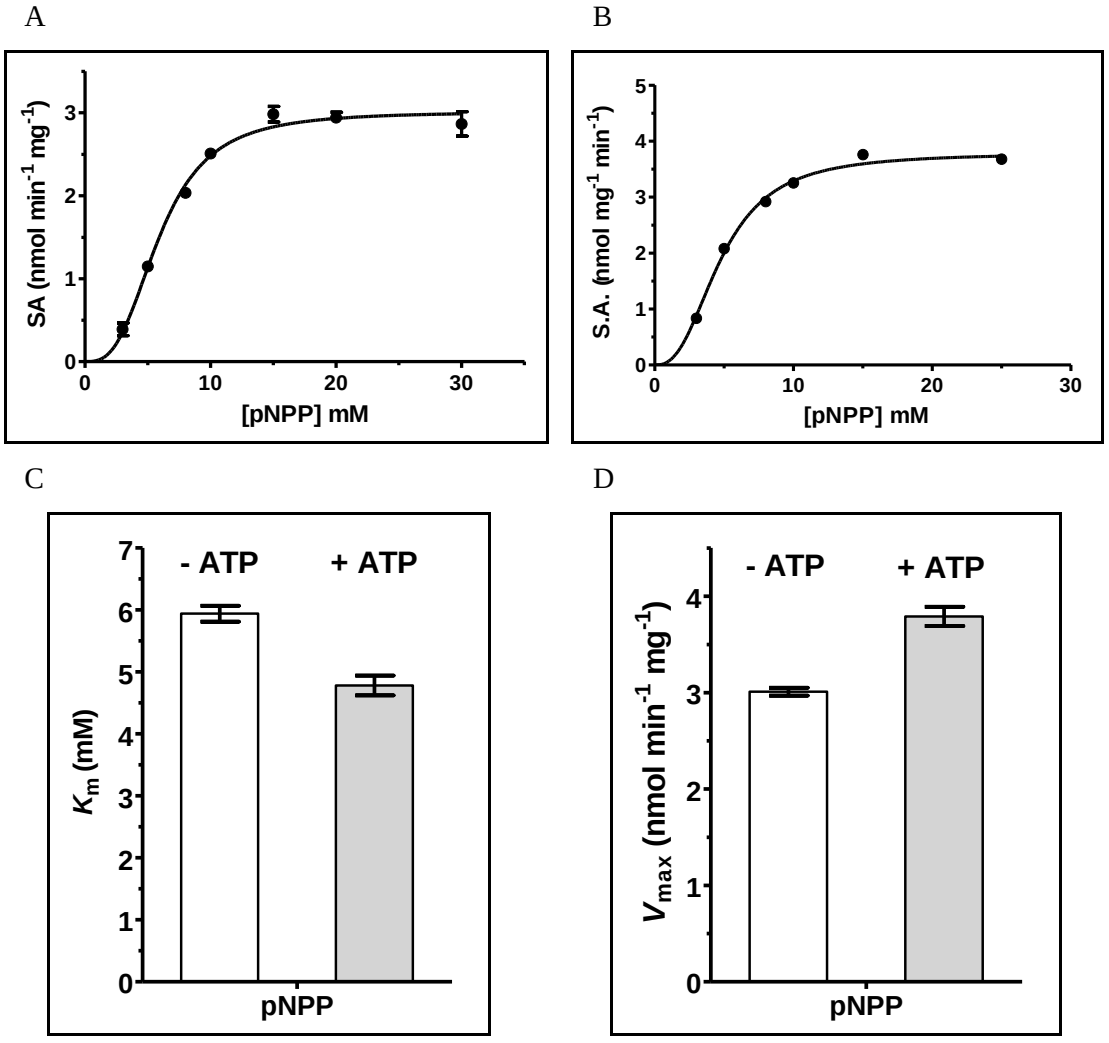

Figure 2.13. Initial rate *vs* substrate concentration plots for pNPP in the (A) absence and (B) presence of ATP at pH 8.0. Steady-state kinetic parameters (C) K_m and (D) V_{max} derived from the plots. Data points represent mean ± SD of 3 independent measurements.

2.5.11 Phosphotransferase activity of PfISN1

Certain 5'-nucleotidases act as bifunctional enzymes, exhibiting phosphotransferase and phosphatase activity (Pesi et al., 1994). PfISN1 was tested for phosphotransferase activity with IMP-adenosine and AMP-inosine as phosphate donor-acceptor pairs by IP-RP-HPLC (see 'Materials and Methods' section for details). No significant phosphotransferase activity was detected by the assay (Fig. 2.14).

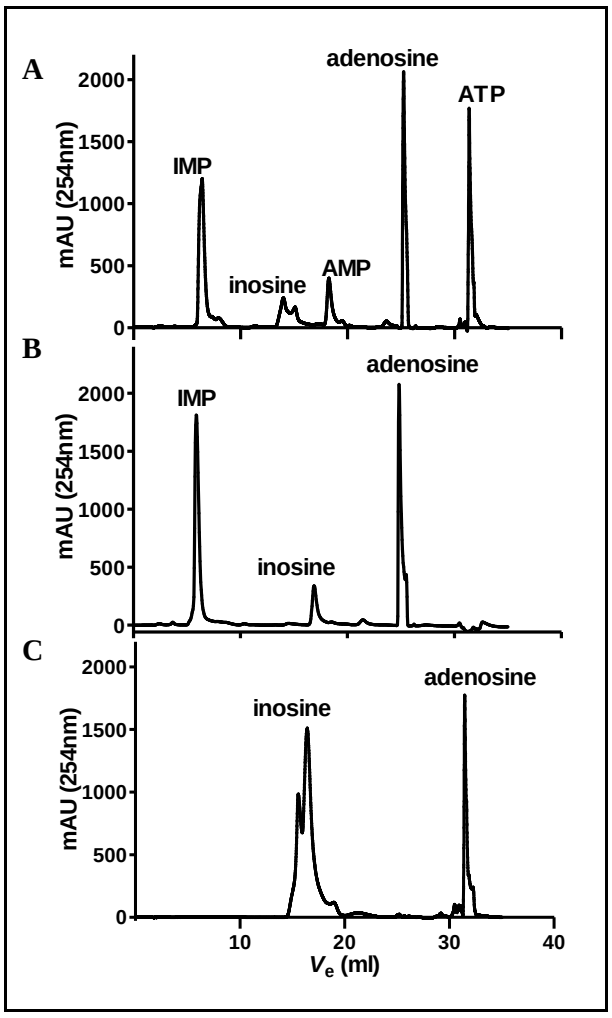

Figure 2.14. Chromatogram of IP-RP-HPLC to detect phosphotransferase activity in PfISN1. (A) Elution profile of standard metabolites IMP, AMP, inosine, adenosine and ATP. Phosphotransferase activity was checked with (B) 5 mM IMP and 5 mM adenosine, (C) 0.5 mM AMP and 0.5 mM inosine.

2.5.12 Product inhibition of PfISN1

Product inhibition is a characteristic feature of several enzymes and a mechanism of regulation. The products of PfISN1 hydrolysis with substrate IMP are inosine and orthophosphate. Since orthophosphate at high concentration was incompatible with Chen's assay, pNPP hydrolysis activity was used to detect inhibition. Weak inhibition was observed with up to 4 mM inosine (Fig. 2.15A) and up to 2 mM orthophosphate (Fig. 2.15B) beyond which inhibition could not be checked due to low solubility of the compounds.

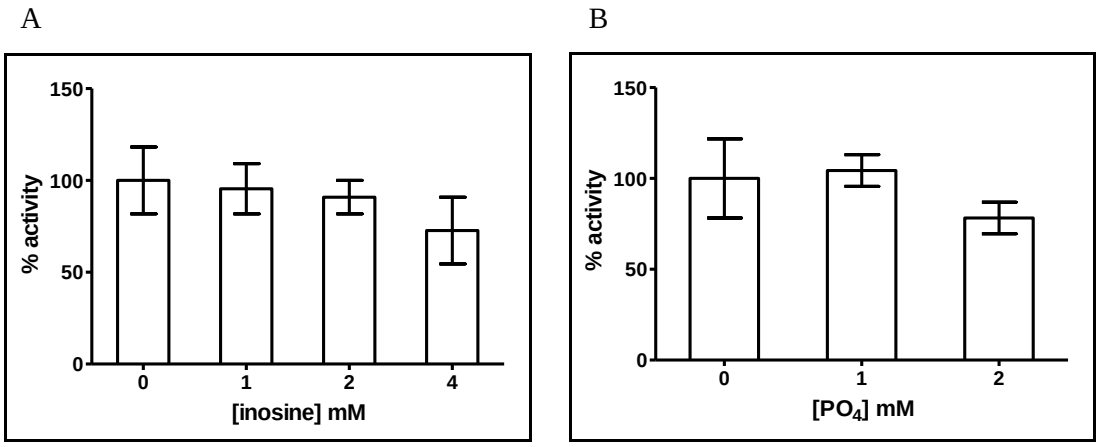

Figure 2.15. Product inhibition of PfISN1 enzyme activity with substrate pNPP and products (A) inosine and (B) orthophosphate.

2.6 Conclusion

The recombinant PfISN1 protein was purified and characterized biochemically, leading to several important features of the protein. The protein existed as a tetramer in solution, along with the presence of higher order aggregates. IMP and AMP were its most preferred substrates and Mg^{2+} its most preferred cofactor. Optimum enzyme activity was at pH 4.0-5.0, at which IMP was hydrolyzed with a much higher catalytic efficiency than AMP. ATP activated the enzyme at pH 8.0 by reducing the K_m for the substrate IMP. However, at pH 5.0, no significant ATP activation was observed. The enzyme did not display any phosphotransferase activity. Products inosine and orthophosphate did not inhibit the enzyme significantly.

Chapter Three

Biochemical validation of PfISN1 as a HAD superfamily member

Table of Contents

3.1 Abstract

HAD superfamily proteins contain four characteristic motif sequences that are important for catalysis. While it was earlier shown through an *in silico* study from our laboratory (Srinivasan and Balaram, 2007) that ISN1 family of 5'-nucleotidases belong to the HAD superfamily, there was no biochemical evidence to validate the role of motif residues in catalysis in ISN1. Comparison of motif position with other HAD members and amongst ISN1 sequences as well as phylogentic relationship amongst ISN1 sequences revealed important features contributing to sequence diversity. Of the four motifs present in HAD superfamily proteins, the first motif is the most important as it contains the two aspartate residues involved in nucleophilic attack on the phosphate group and coordination with Mg^{2+} respectively. In PfISN1, the conserved motif I (DXDXT/V) stretches from residue 170 to 175 and contains the invariant aspartyl residues D170 and D172. In order to probe their role in catalysis, both the aspartates were mutated individually to asparagines to generate mutants PfISN1_D170N and PfISN1_D172N as well as together to generate the mutant PfISN1_D170N-D172N. All the three mutants showed no catalytic activity with IMP. Interestingly, PfISN1_D172N showed increased pNPP-hydrolyzing activity compared to wild-type enzyme. Another mutant PfISN1_D172A also showed increased pNPP-hydrolyzing activity compared to wild-type enzyme but significantly lower than PfISN1_D172N. The mutants PfISN1_D172N and D172A also showed a change in their intrinsic protein fluorescence spectra and inhibition of pNPP-hydrolyzing activity in the presence of IMP, suggesting binding of IMP to the mutant proteins.

3.2 Introduction

5'-nucleotidases belong to the HAD superfamily of enzymes, containing 4 characteristic motif sequences that are critical for enzyme function (Burroughs et al., 2006). The role of these motifs has been discussed in detail in Chapter 1. Briefly, motif I has the sequence DX_1DX_2T/V wherein the first aspartate is the nucleophile attacking the phosphate moiety while the second aspartate coordinates with Mg^{2+} and X is any amino acid residue. Motif II has the sequence $X_hX_hX_hT/S$ where wherein a conserved serine/threonine interacts with the substrate and X_h is a hydrophobic residue. Motif III has a conserved lysine which interacts with the substrate while motif IV contains two aspartates that are separated by 1-4 or more residues and coordinate with Mg^{2+}. Various studies through site-directed mutagenesis have confirmed the critical role of these residues in catalysis (Allegrini et al., 2004). Motif I plays a central role in catalysis

since mutation of its aspartates resulted in total abolishment of catalytic activity in HAD proteins (Table 3.1).

Table 3.1. Mutations of motif residues and their impact on enzyme function[*].

Enzyme	Motif	Mutant	Relative activity (%)[$]	Motif	Mutant	Relative activity (%)[$]
Bovine cN-II[$]	I	D52E	0	III	K292R	0.1
		D52A	0		K292M	0.1
		D54E	0	IV	D351E	0.7
		D54A	0		D351N	0.1
	II	T249S	20		D356E	2.3
		T249V	1.6		D356N	0.6
Phosphoserine phosphatase[*]	I	D20E	0	III	K158R	1
		D20N	0		K158A	0.4
		D22E	50	IV	D179E	78
		D22N	0		D179N	0.6
	II	S109T	115		D183E	63
		S109A	6		D183N	0.4
Ca^{2+}-ATPase[#]	I	D351E	0	III	-	-
		D351N	0	IV	D703E	31
		T353S	20		D703N	5
		T353A	0		D707E	5
	II	T625S	79		D707N	5

[*]FOOTNOTE: [$](Allegrini et al., 2001, 2004), [*](Collet et al., 1998, 1999), [#](Maruyama and MacLennan, 1988; Maruyama et al., 1989; Clarke et al., 1990). [$]Activity relative to wild-type enzyme.

In motif I (DX_1DX_2T/V), X_1 and X_2 are not invariant but remain highly conserved amongst sub-classes of HAD members and are critical for proper orientation of the aspartates (Allegrini et al., 2004). Amongst ISN1s, X_1 is conserved but not invariant while X_2 is poorly conserved (Table 3.2).

Table 3.2. Conservation of motif I residues amongst ISN1 sequences.

Position in motif I	**Conservation**
D (first aspartate)	D (invariant)
X_1	G (85%), A (15%)
D (second aspartate)	D (invariant)
X_2	V (79%), E (8%), D (7%), I (3%), G (2%), L (1%)
T/V	T (invariant)

3.3 Materials and Methods

3.3.1 Phylogenetic analysis of ISN1 sequences

The Pfam protein family database lists 375 sequences (up to Jan 31, 2018 and including redundant sequences) under the ISN1 family (family id: PF06437). To generate an exhaustive list of ISN1 sequences, the list of Pfam ISN1 sequences (family id: PF06437) was combined with non-redundant sequences obtained by performing a BLAST® search in the NCBI database using the BLASTp program (Altschul et al., 1997) and with an e-value below 0.001 and query coverage >60%. This combined set of non-redundant sequences totaling 262 were aligned. Sequences lacking any of the four HAD superfamily motifs and those with large insertions or deletions were eliminated. After multiple rounds of alignment and elimination, the final list contained 150 sequences. This dataset was used to generate a maximum likelihood tree to derive phylogenetic relationships. Phylogenetic and molecular evolutionary analyses were conducted using MEGA version 7 (Kumar et al., 2016). The evolutionary history was inferred by using the Maximum Likelihood method based on the Le_Gascuel_2008 model (Le and Gascuel, 2008). The bootstrap consensus tree inferred from 500 replicates was taken to represent the evolutionary history of the taxa analyzed (Felsenstein, 1985). Branches corresponding to partitions reproduced in less than 50% bootstrap replicates were collapsed. Initial tree(s) for the heuristic search were obtained automatically by applying Neighbor-Join and BioNJ algorithms to a matrix of pairwise distances estimated using a JTT model, and then selecting the topology with superior log likelihood value. A discrete Gamma distribution was used to model evolutionary rate differences among sites (5 categories (+G, parameter = 0.8644)). The rate variation model allowed for some sites to be evolutionarily invariable ([+I], 8.68% sites). The analysis involved 150 amino acid sequences. All positions containing gaps and missing data were eliminated. There were a total of 167 positions in the final dataset.

3.3.2 Multiple sequence alignment

Multiple sequence alignment was done using MUSCLE (Edgar, 2004), integrated into Seaview software (Version 4.6.1) (Galtier et al., 1996). The alignment image was generated using ESPript 3.0 (Gouet et al., 1999).

3.3.3 Generation of PfISN1 mutants by site-directed mutagenesis

The mutants PfISN1_D170N and D172N were generated by quick change PCR method using a single mutagenic oligonucleotide primer (Shenoy and Visweswariah, 2003). List of primers is given in Table 3.3. Stage I primers were used to insert an

EcoRV restriction endonuclease cleavage site (bold letters) at the mutation site while Stage II primers were used to knock-out the restriction site and introduce the desired mutation (underlined letters) at the same site. Mutated PCR product could be selected by a distinct restriction digestion pattern with EcoRV at each stage. The PCR product was further digested with DpnI to reduce the background of parental DNA and transformed into XL-1 blue strain of *E. coli*. The mutation was further confirmed by DNA sequencing. The plasmid was then extracted and transformed into *E. coli* BL21 (DE3) strain for expression.

Table 3.3. Primers for site-directed mutagenesis of D170N and D172N.

PfISN1 mutant	PCR stage	Primer sequence (5' to 3')
D170N	I	GATTTATTAACA**GATATC**GCTGACGAAACG
	II	GATTTATTAACATTT<u>A</u>ATGCTGACGAAACG
D172N	I	ACATTTGAT**GATATC**GAAACGCTATATCCG
	II	ACATTTGATGCT<u>A</u>ACGAAACGCTATATCCG

The mutants D172A and D170N-D172N were generated by a ligation-free cloning method also called as Advanced Quick Assembly (AQUA) cloning (Beyer et al., 2015). A schematic is described in Figure 3.1. Two mutated overlapping gene fragments were generated from the parental wild-type plasmid (pET21b-PfISN1) by PCR using mutagenic primers and T7 site primers (Table 3.4) in step I-II and further extended in step III by PCR-driven overlap extension (Heckman and Pease, 2007). The overlapping fragments were combined into a single fragment by T7-promoter (forward) and T7-terminator (reverse) site primers. The ends of this mutagenic insert fragment shared homology with pET21b plasmid (backbone vector), both of which were co-transformed into *E. coli* XL-1 Blue strain where both the fragments would recombine to form a single circular plasmid (pET21b-PfISN1_mutant) by two single site-specific recombination events at the homologous ends. Prior to co-transformation, the pET21b plasmid was double-digested between the homologous ends in order to prevent selection of transformants containing pET21b plasmid. Positive clones were identified by PCR using gene-specific primers (Table 3.4) and the mutation was confirmed by DNA sequencing.

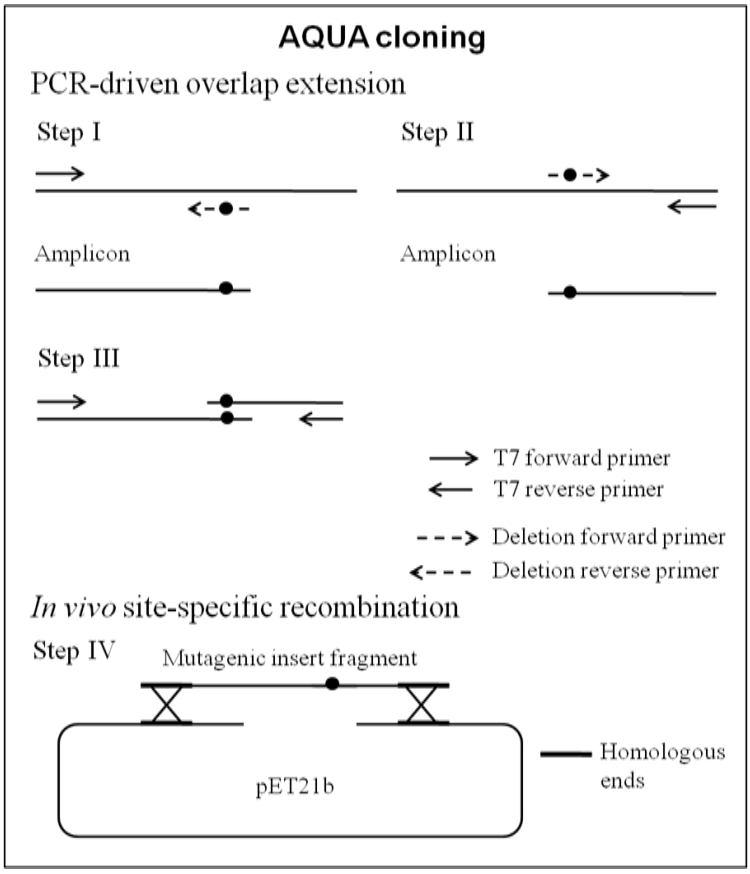

Figure 3.1. Schematic representation of AQUA cloning procedure.

Table 3.4. Primers for site-directed mutagenesis of mutants D172A and D170N-D172N*.

Primer	Primer sequence (5' to 3')
D172A forward	GATTTATTAACATTTGATGCTGCCGAAACGCTATATCCGGATG
D172A reverse	CATCCGGATATAGCGTTTCGGCAGCATCAAATGTTAATAAATC
D170N-D172N forward	GTTTAGATTTATTAACATTTAATGCTAACGAAACGCTATATCCGGATG
D170N-D172N reverse	CATCCGGATATAGCGTTTCGTTAGCATTAAATGTTAATAAATCTAAAC
T7 forward	TAATACGACTCACTATAGGG
T7 reverse	TAATACGACTCACTATAGGG
gene-specific forward	CGGGATCCAAGAATTTGGACATAAATACATTCGATAATATTGAAGATATTCC
gene-specific reverse	GGAAGCTTTTATTGATTTTCATATAAAACTTCCGGAATAAATGATTTTATG

*FOOTNOTE: Base pair changes at the mutation site are underlined.

3.3.4 Expression, purification and kinetic characterization of PfISN1 mutants

All the mutant proteins were expressed and purified by the same methods and conditions as followed for the wild-type protein. For the mutants, phosphatase activity was measured similar to wild-type enzyme, either by estimation of inorganic phosphate by Chen's method for all substrates except pNPP or by continuous measurement of pNP formation for pNPP hydrolysis activity (see 'Materials and methods' section of Chapter 2 for details).

3.3.5 Intrinsic protein fluorescence

Fluorescence spectroscopy was performed using a Hitachi F-2500 fluorescence spectrophotometer (Hitachi Ltd., Japan). The samples were excited at 295 nm which selectively excites tryptophan residues and the emission spectra were recorded between 298-500 nm. 5μM protein and 0.5 mM IMP in 50 mM Tris HCl, pH 8.0 and 30 mM $MgCl_2$ were used. Ligand absorption at the excitation and emission wavelengths leads to quenching of sample fluorescence, termed as inner-filter effect. The observed fluorescence intensity values (F_{obs}) at the emission maxima (λ_{max}) wavelength (nm) were corrected for inner-filter effect using eq. 3.1 (Lakowicz, 1999).

$$F_{corr} = F_{obs} \times antilog\left(\frac{O.D._{em} + O.D._{ex}}{2}\right) \qquad \text{(eq. 3.1)}$$

where $O.D._{em}$ and $O.D._{ex}$ are the absorbance of the substrate IMP at the excitation and emission maxima (λ_{max}) wavelength, respectively.

3.3.6 Determination of binding constant (K_d) of IMP for PfISN1 mutants D172N and D172A.

For mutants PfISN1_D172N and D172A, percent inhibition of pNPP-hydrolyzing activity (v), determined using eq. 3.2, was plotted against IMP concentration for a fixed concentration of pNPP.

$$\%\ inhibition\ of\ v = 100 - \frac{v_i}{v_0} \qquad \text{(eq. 3.2)}$$

where v_i is the enzyme activity at various IMP concentrations and v_0 is the enzyme activity at 0 mM IMP.

The plot was fitted to a one-site specific binding model (eq. 3.3)

$$\%\ inhibition\ of\ v = \frac{B_{max} \times I}{K_d + I} \qquad \text{(eq. 3.3)}$$

where I is the inhibitor concentration, B_{max} is the maximum % inhibition of v, and binding constant K_d is the inhibitor concentration at which half-maximum inhibition is achieved. This equation is related to the Michaelis-Menten equation (eq. 2.1 in chapter 2) wherein B_{max} is related to $V_{\max}$, the maximum enzyme activity, and K_d is related to the Michaelis constant K_{m}.

3.4 Results

3.4.1 Motif position and phylogenetic relationship amongst ISN1 sequences.

The sequential position of the HAD motifs differs in ISN1s as compared to other HAD members (Fig. 3.2A). The differences are summarized below.

1. Amongst other HADs, the N-terminal segment leading up to motif I is about 20-50 residues. It is much longer in ISN1s, in the range of about 170-400 residues.
2. Amongst other HADs, the segment between motifs I and II is about 100-200 residues. It is much shorter in ISN1s, in the range of about 30-40 residues.
3. The segment between motifs II and III in HADs is about 30-50 residues. It is longer in ISN1s, in the range of about 150-180 residues.

The sequential position of the HAD motifs amongst ISN1s is largely conserved (Fig. 3.2B), with the exception of ISN1s from *T. gondii* and *N. caninum*, which have a longer than average N-terminal segment of about 350-400 residues.

The phylogenetic relationship amongst ISN1 sequences reveals that in spite of the N-terminal insertion, *T. gondii* and *N. caninum* ISN1s are closer to PfISN1 than *S. cerevisiae* and other fungal ISN1s. ISN1s from Stramenopiles, Cryptophytes, and Viridiplantae are also closer to PfISN1 than to fungal ISN1s (Fig. 3.3).

A

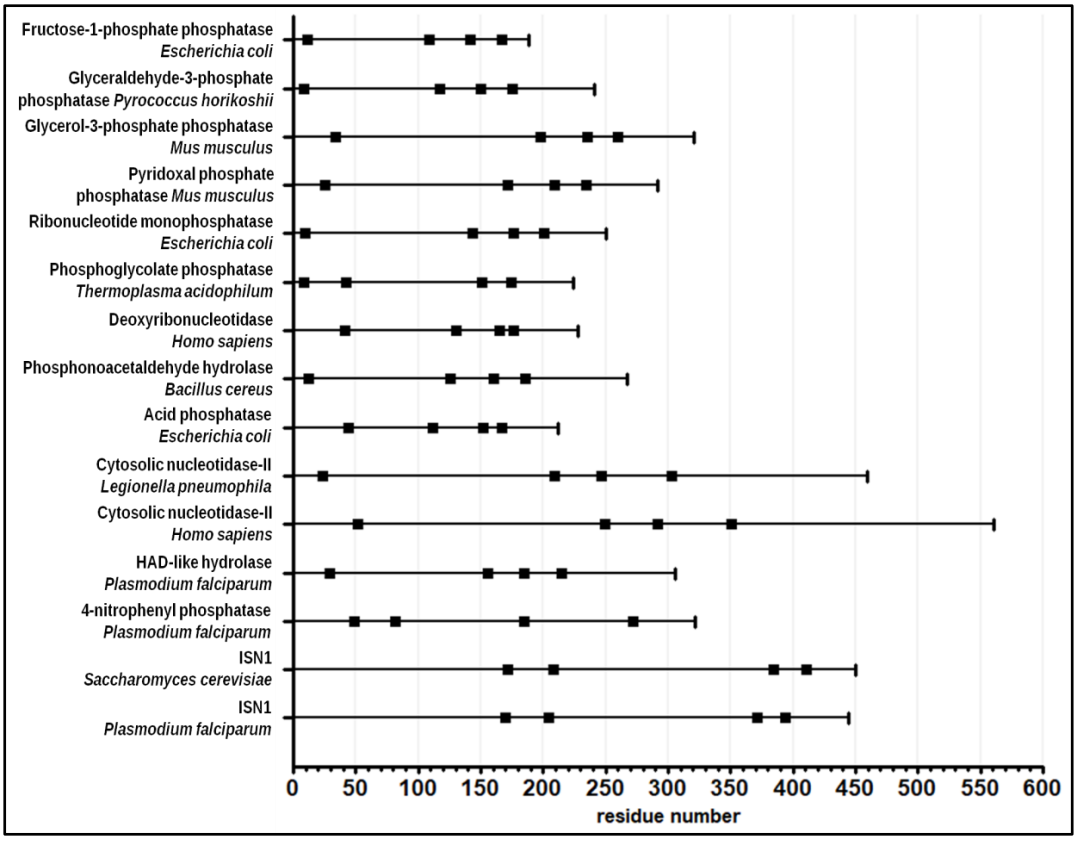

B

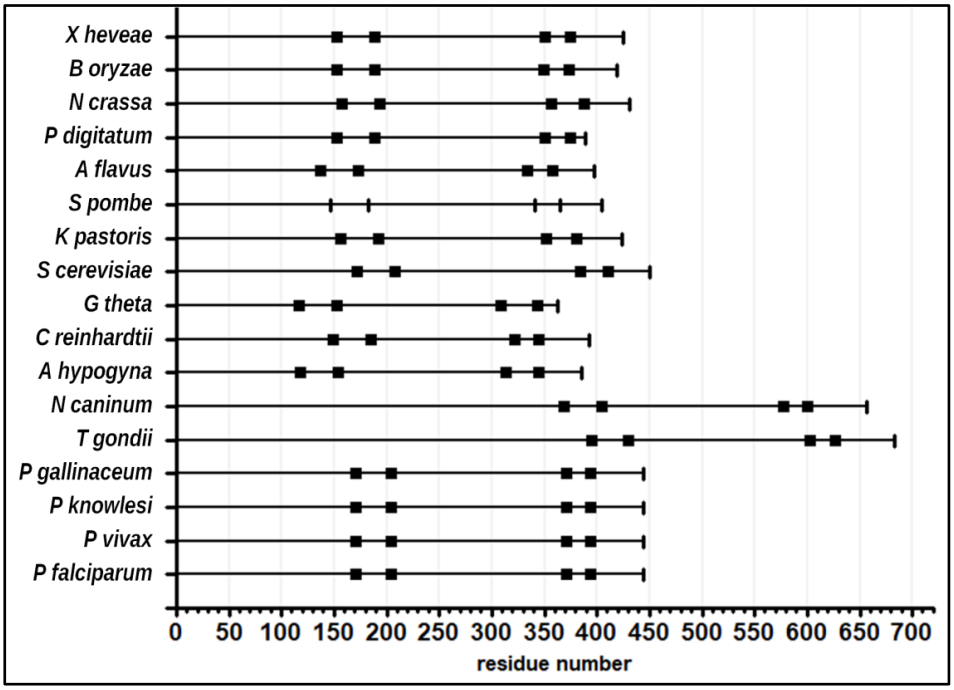

Figure 3.2. Position of motifs stretches I, II, III and IV in sequential order, represented by a black square (■) in (A) various HAD members and (B) amongst ISN1 sequences. Protein sequences were obtained from www.uniprot.org and www.plasmodb.org.

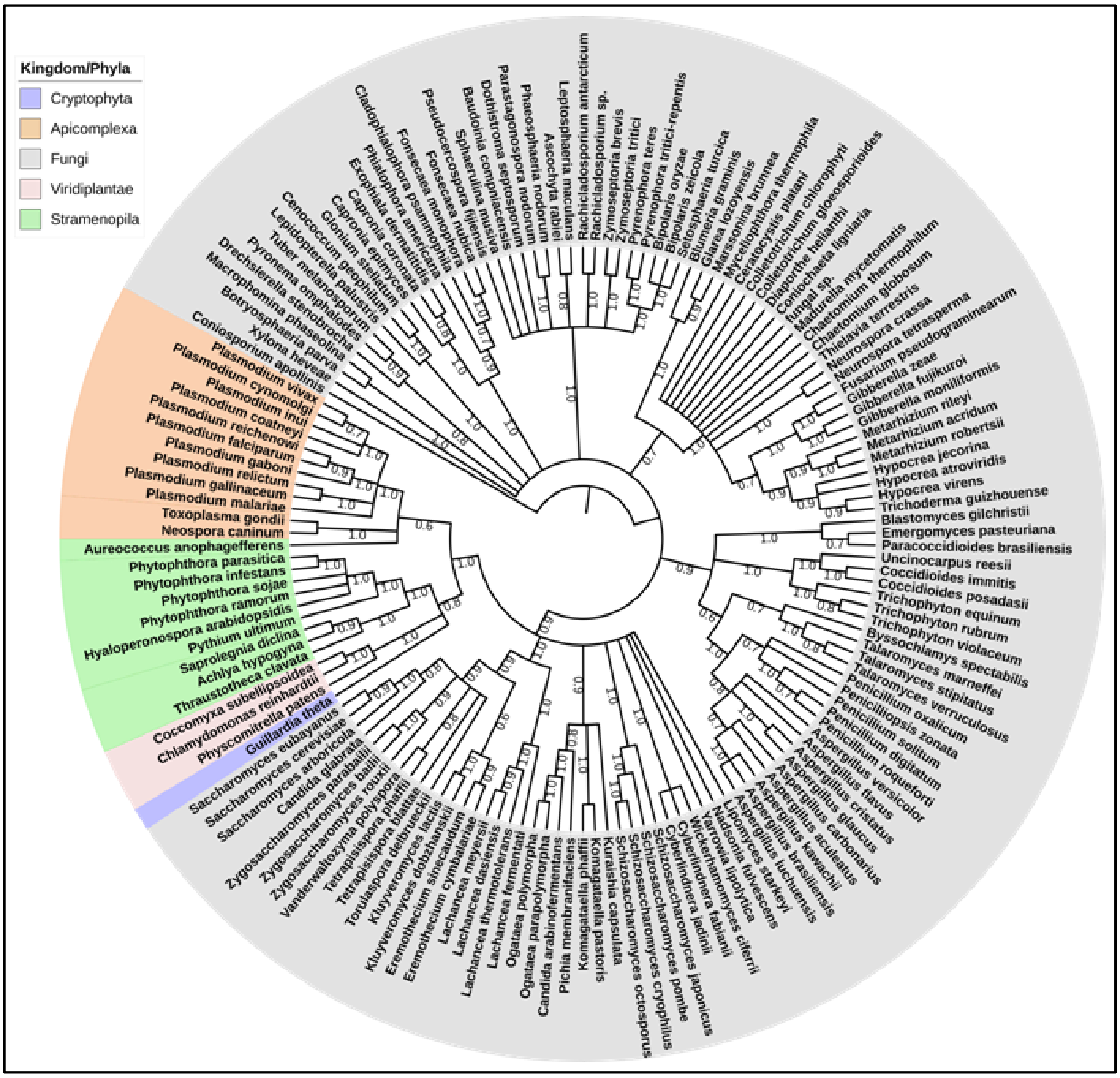

Figure 3.3. Maximum likelihood tree representing phylogenetic relationship amongst ISN1 sequences. Bootstrap support values for internal nodes are shown with values <0.6 eliminated. Clades corresponding to major kingdoms/phyla are distinctively colored. See 'materials and methods' section for details.

3.4.2 Biochemical characterization of PfISN1 mutants D170N, D172N and D170N-D172N.

While it was earlier shown through *in silico* studies that ISN1 belongs to the HAD superfamily of proteins (Srinivasan and Balaram, 2007), biochemical validation was needed to establish the critical role of the motif residues in catalysis. Aspartates of motif I have been shown to play a central role in catalysis in other HAD members. Hence, they were mutated to asparagine to generate two single mutants, PfISN1_D170N and PfISN1_D172N and a double-mutant PfISN1_D170N-D172N.

3.4.2.1 Cloning, expression and purification of the mutants.

All the three mutants were generated through site-directed mutagenesis using a single mutagenic primer (see 'Materials and Methods' section for details). The mutation at the target site was confirmed by Sanger sequencing. Expression and purification of the mutants was carried out under the same conditions as that followed for wild-type PfISN1 (see Appendix B, Figure B1).

3.4.2.2 Kinetic characterization of the mutants.

All the three mutants did not show any IMP-hydrolyzing activity at pH 8.0 in the absence or presence of ATP, or at pH 5.0 (Fig. 3.4A). No phosphatase activity was detected even with AMP (Fig. 3.4B).

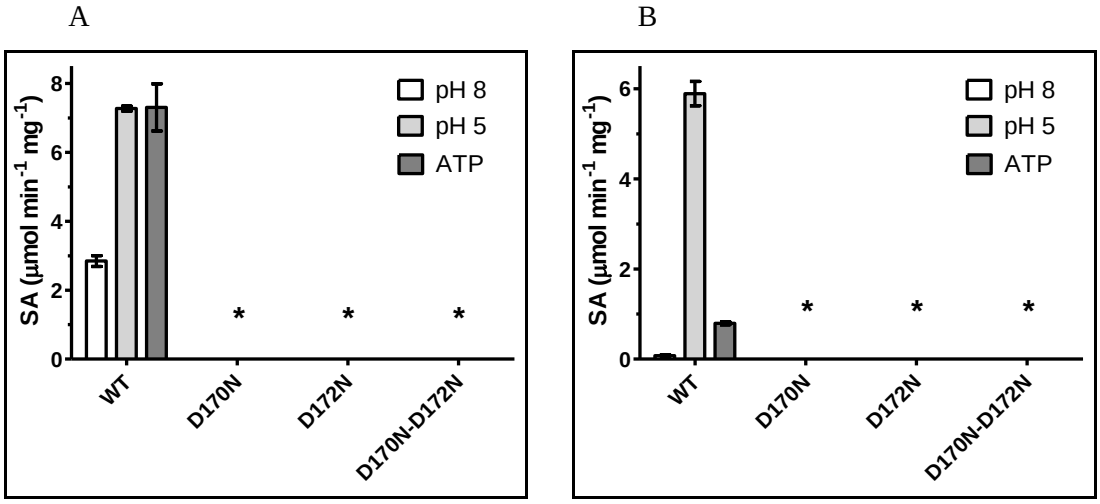

Figure 3.4. Phosphatase activity of mutants D170N, D172N and D170N-D172N with (A) IMP and (B) AMP at pH 8.0, in the presence of 2 mM ATP and at pH 5.0. Wild-type PfISN1 (WT) activity is shown for reference. *No detectable activity.

While the mutants PfISN1_D170N and D170N-D172N showed pNPP-hydrolyzing activity comparable to wild-type enzyme, D172N showed about 51-fold higher pNPP-hydrolyzing activity than wild-type enzyme (Fig. 3.5A). Since D170 in motif I is critical for catalysis, it was surprising that the PfISN1 mutants D170N and D170N-D172N showed pNPP-hydrolyzing activity comparable to the wild-type enzyme. However, the significant increase in pNPP-hydrolyzing activity of PfISN1_D172N was even more surprising. Initial rate *vs* pNPP concentration plot was hyperbolic in nature. Its V_{max} value for pNPP was 106-fold higher while its K_m value was 4-fold lower than wild-type enzyme (Fig. 3.5B). The catalytic efficiency (k_{cat}/K_m) of PfISN1_D172N mutant for pNPP was 420-fold higher than wild-type enzyme.

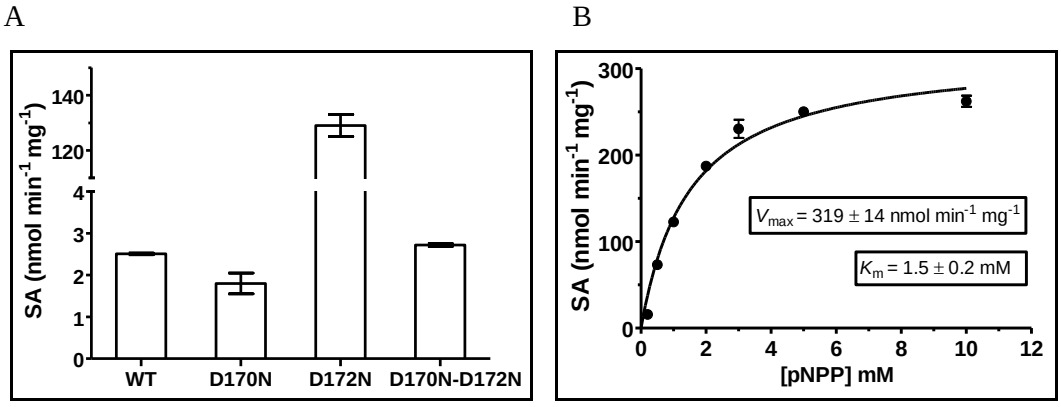

Figure 3.5. (A) pNPP-hydrolyzing activity of wild-type PfISN1 (WT) and mutants D170N, D172N and D170N-D172N of PfISN1, with 10 mM pNPP and 30 mM $MgCl_2$. Y-axis has been segmented for ease of visualization. (B) Initial rate *vs* substrate concentration plot for mutant PfISN1_D172N with pNPP. Wild-type PfISN1 (WT) activity is shown for reference.

3.4.3. Effect of IMP on pNPP-hydrolyzing activity of the mutants.

In the presence of 0.5 mM IMP, the pNPP-hydrolyzing activity of PfISN1_D172N was inhibited by about 100-fold, but PfISN1_D170N and D170N-D172N were not significantly inhibited (Fig.3.6A), suggesting that D170 has a role in the binding of IMP as well as its hydrolysis while D172 has a role only in catalysis. Products of IMP-hydrolysis reaction inosine and orthophosphate, and substrate AMP did not inhibit the enzyme (Fig. 3.6B).

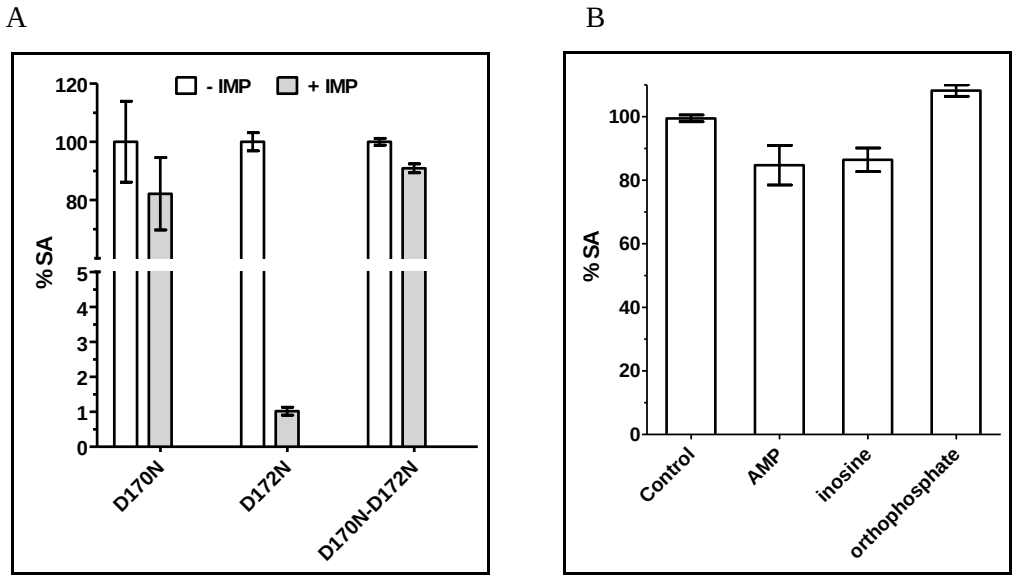

Figure 3.6. Inhibition of pNPP-hydrolysis activity of mutants PfISN1_D170N, D172N and D170N-D172N in the presence of IMP. (A) % pNPP-hydrolyzing activity of the mutants (%SA) in the presence of 0.5 mM IMP with activity in the absence of IMP regarded as 100%. 10 mM pNPP and 30 mM $MgCl_2$ were used in the assay. Y-axis has been segmented for ease of visualization. (B) % pNPP-hydrolyzing activity of PfISN1_D172N (%SA) in the presence of 0.1 mM of AMP, inosine and orthophosphate with activity of control regarded as 100%.

A change in the intrinsic fluorescence spectrum of the mutants was also observed in the presence of IMP. PfISN1_D170N did not show a change in its intrinsic fluorescence spectrum while PfISN1_D172N and D170N-D172N showed quenching of intensity. PfISN1_D172N also showed a blue-shift in emission maxima (λ_{max}) value (Fig. 3.7A-C). PfISN1_D170N-D172N showed 20% drop in fluorescence intensity while PfISN1_D172N showed 50% drop in fluorescence intensity (Fig. 3.7D) and a blue-shift of 5.5 ± 1.5 nm (Fig. 3.7E). Changes in the intrinsic tryptophan fluorescence spectra of these mutants in the presence of IMP suggested a perturbation in the micro environment of one or more tryptophan residues that might be involved in IMP binding.

3.4.4 Probing the role of D172 in pNPP-hydrolyzing activity of PfISN1.

In order to further probe the role of D172 in the increased pNPP-hydrolyzing activity of PfISN1_D172N, it was mutated to alanine. The mutant PfISN1_D172A was cloned, expressed and purified by methods and conditions as followed for PfISN1_D170N-D172N (see Appendix B, figure B1 for SDS-PAGE of the purified protein).

3.4.4.1 Biochemical characterization of PfISN1 mutant D172A.

PfISN1_D172A did not show any IMP-hydrolyzing activity. It showed about 6-fold higher and 52-fold lower pNPP-hydrolyzing activity compared to the wild-type and PfISN1_D172N enzyme, respectively (Fig. 3.8A). In the presence of IMP, its pNPP-hydrolyzing activity was significantly inhibited by about 4-fold (Fig. 3.8B). Its V_{max} value for pNPP was 7-fold higher than wild-type enzyme but 14-fold lower than PfISN1_D172N, while K_m value was comparable to wild-type enzyme but 3-fold higher than PfISN1_D172N (Fig. 3.8C). Overall, the catalytic efficiency (k_{cat}/K_m) of PfISN1_D172A for pNPP was 9-fold higher than wild-type enzyme but 45-fold lower than PfISN1_D172N.

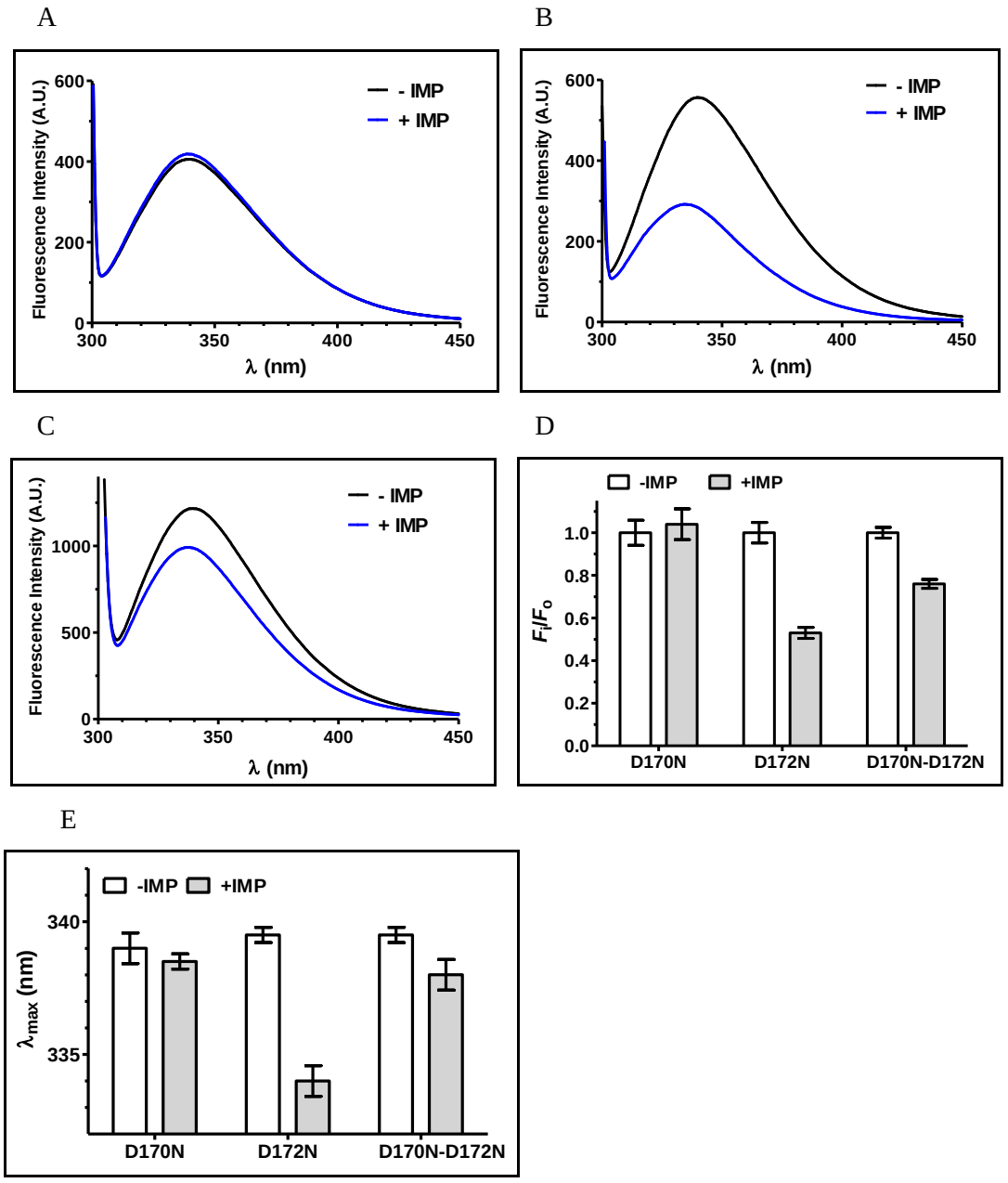

Figure 3.7. Fluorescence emission spectra of mutants (A) PfISN1_D170N, (B) PfISN1_D172N and (C) PfISN1_D170N-D172N in the absence and presence of 0.5 mM IMP. Fluorescence intensity is represented in arbitrary units (A.U.). (D) Ratio of fluorescence intensities (F_i/F_o) where F_i and F_0 are fluorescence intensities at emission maxima (λ_{max}) wavelength, in the presence and absence of 0.5 mM IMP, respectively. The values have been corrected for inner filter effect (see 'materials and methods' section for details). (E) Emission maxima (λ_{max}) wavelength values of the fluorescence spectra.

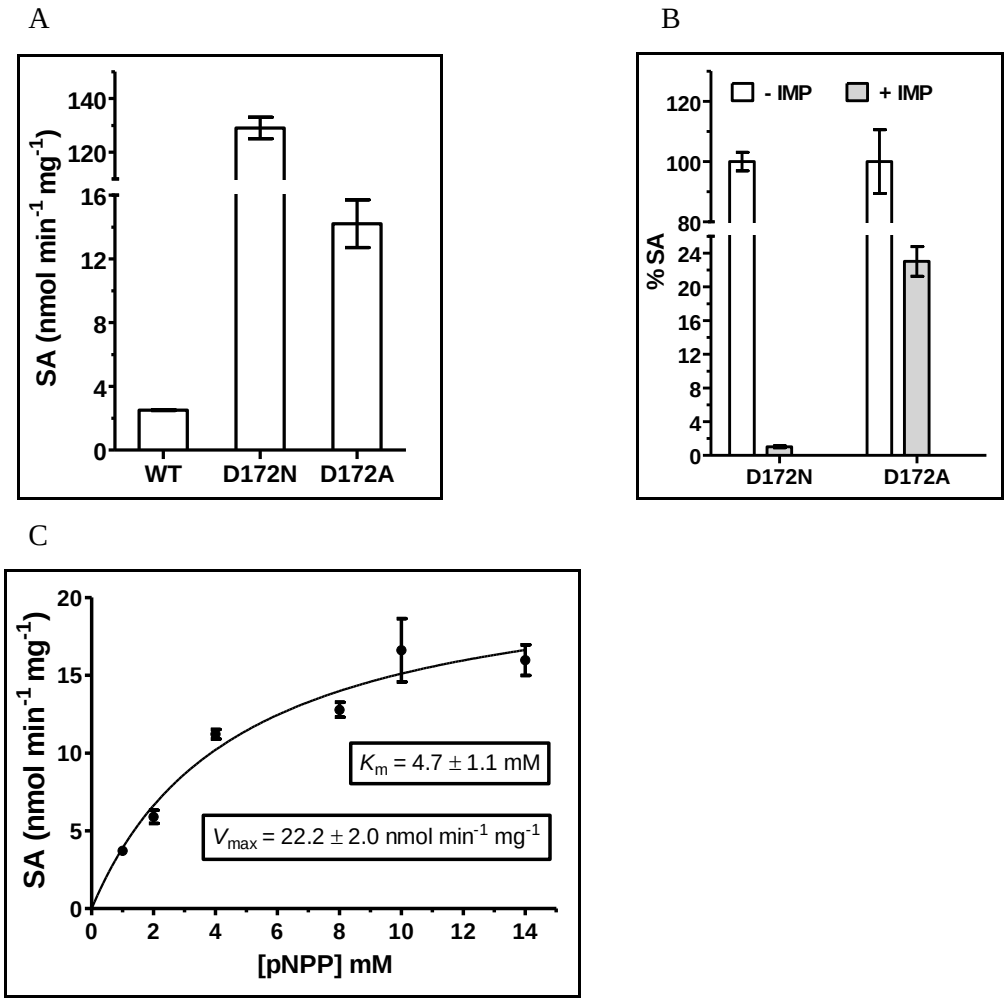

Figure 3.8. Biochemical characterization of PfISN1_D172A. (A) pNPP-hydrolyzing activity of wild-type PfISN1 (WT) and mutants D170N, D172N, D170N-D172N of PfISN1, with 10 mM pNPP and 30 mM $MgCl_2$. Y-axis has been segmented for ease of visualization. (B) Inhibition of pNPP-hydrolysis activity of mutants PfISN1_D172N and PfISN1_D172A in the presence of 0.5 mM IMP. (C) Initial rate *vs* substrate concentration plot for mutant PfISN1_D172A with pNPP.

PfISN1_D172A also showed quenching of fluorescence intensity and blue-shift in the λ_{max} value in the presence of IMP (Fig. 3.9A). However, compared to PfISN1_D172N, it showed only a 22% drop in fluorescence intensity (Fig. 3.9B) and a blue-shift in the λ_{max} value of 3.5 nm (Fig. 3.9C). Overall, the changes in its intrinsic fluorescence spectra were similar to that observed for PfISN1_D172N but to a lesser magnitude.

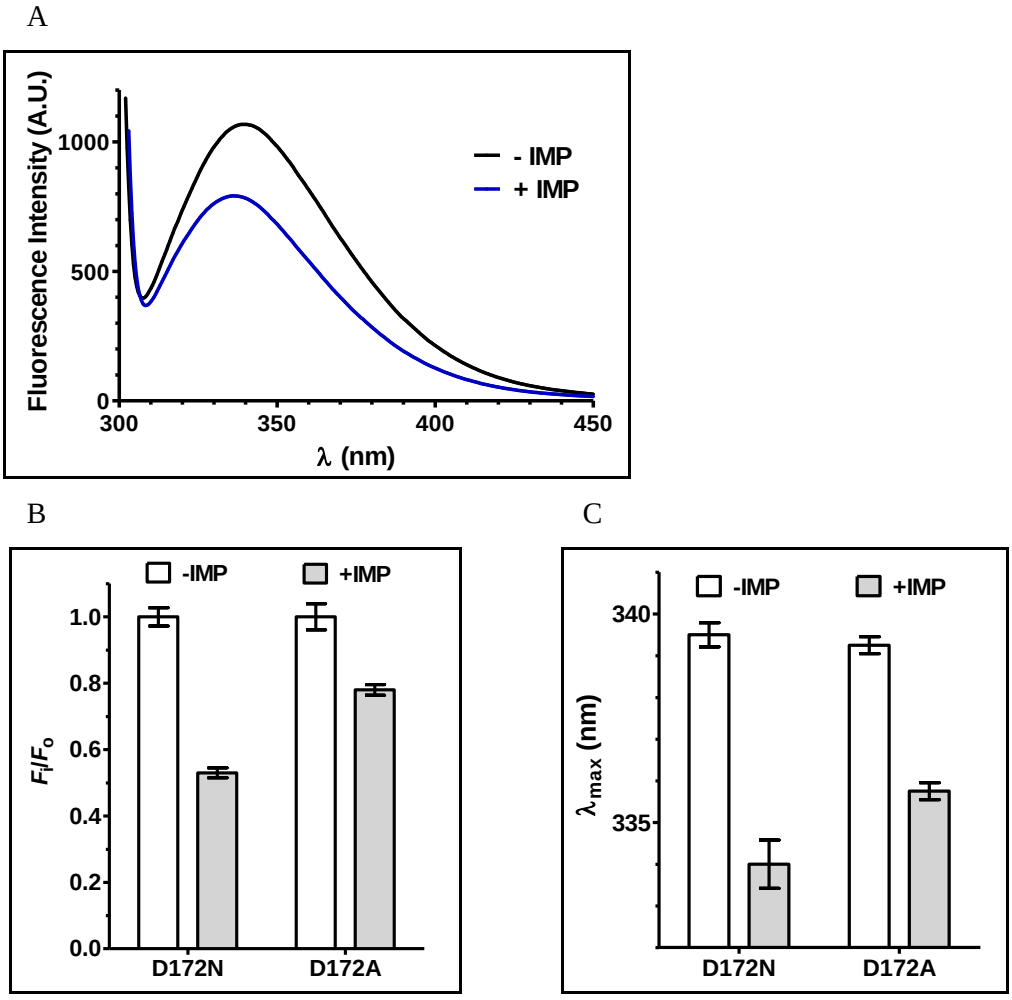

Figure 3.9. Intrinsic fluorescence spectrum of PfISN1_D172A. (A) Fluorescence emission spectra of PfISN1_D172A in the absence and presence of 0.5 mM IMP. Fluorescence intensity is represented in arbitrary units (A.U.). (B) Ratio of fluorescence (F_i/F_o) where F_i and F_0 are fluorescence intensities at emission maxima (λ_{max}) wavelength, in the presence and absence of 0.5 mM IMP, respectively. The values have been corrected for inner filter effect (see 'materials and methods' section for details). (C) Emission maxima (λ_{max}) wavelength values of the fluorescence spectra.

3.4.4.2 Comparative biochemical properties of PfISN1 mutants D172N and D172A.

For substrate pNPP, the catalytic efficiencies of PfISN1_D172N and D172A were 418-fold and 9-fold higher than wild-type enzyme, respectively (see Appendix B, Table B1 for kinetic parameters). Both the mutants showed inhibition of pNPP-hydrolysis activity in the presence of IMP, with PfISN1_D172N being inhibited to a significantly greater extent. Their affinity for IMP was quantified by using a one-site binding model to estimate the binding constant (K_d) value, which was 23-fold lower for PfISN1_D172N (Fig. 3.10A) than that for PfISN1_D172A (Fig. 3.10B).

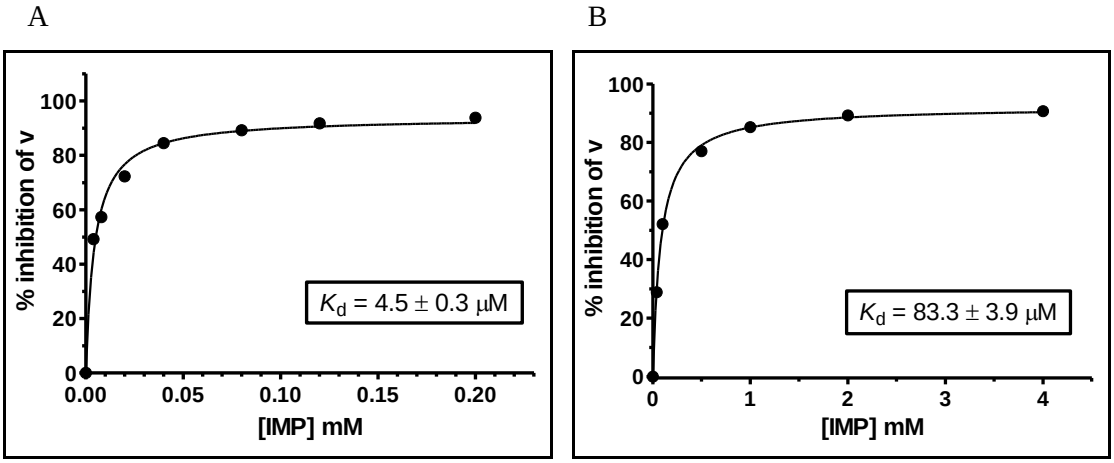

Figure 3.10. Inhibition *vs* IMP concentration plots for mutants (A) PfISN1_D172N and (B) PfISN1_D172A with their K_d values. 10 mM pNPP and 30 mM $MgCl_2$ were used in the assay. See 'materials and methods' section for details.

D172 is the second aspartate of motif I and plays a crucial role in catalysis in HAD proteins. The mutant PfISN1_D172N was inactive with IMP but showed increased pNPP-hydrolyzing activity compared to wild-type enzyme. Although pNPP is not a physiological substrate, it is widely used as a generic substrate to detect phosphatase activity. Although alkaline and phosphatases have primarily been reported to hydrolyze pNPP with a high turnover (k_{cat}), other phosphoesterases including 5'-nucleotidases, sugar phosphatases and protein arginine phosphatases have also been reported to hydrolyze pNPP with a k_{cat} value comparable to or greater than PfISN1 enzyme (Table 3.5). Enzymatic studies on various HAD members had demonstrated that mutation of the second aspartate in motif I resulted in a complete loss of enzyme activity (Table 3.1). However, the impact of the mutation on pNPP-hydrolyzing activity was not reported in these studies except for one on an alkaline phosphatase from *Anabaena sp.* wherein mutation of an Asp25 residue, involved in Mg^{2+} coordination, to alanine led to a 30% increase in pNPP-hydrolyzing activity of the enzyme (Luo et al., 2010).

Table 3.5. Phosphatase activity of various HAD members with pNPP*.

Enzyme	Organism	k_{cat} (sec^{-1})	Assay conditions
alkaline phosphatase[a]	*E. coli*	12	25°C, pH 8.0, wild-type enzyme
alkaline phosphatase[b]	*H. sapiens*	971	pH 10.5, wild-type enzyme
acid phosphatase[c]	*A. thaliana*	162	37°C, pH 4.5, wild-type enzyme
5'-nucleotidase[d]	*E. coli*	41	22°C, pH 7.0, wild-type enzyme
ISN1[e]	*P. falciparum*	0.002	25°C, pH 8.0, wild-type enzyme
ISN1[e]	*P. falciparum*	0.28	25°C, pH 8.0, D172N mutant enzyme
pyrimidine nucleotidase[f]	*P. falciparum*	2.5	37°C, pH 8.0, wild-type enzyme
PNPPase[f]	*P. berghei*	18.5	37°C, pH 8.0, wild-type enzyme
broad specificity phosphatase[g]	*P. vivax*	0.002	27°C, pH 8.0, wild-type enzyme
cN-II[h]	*L. pneumophila*	0.001	27°C, pH 8.0, wild-type enzyme
sugar phosphatase[i]	*B. subtilis*	0.012	37°C, pH 7.0
glycerol 3-phosphate phosphatase[j]	*M. tuberculosis*	1	22°C, pH 7.0
5'-deoxynucleotidase[k]	*E. coli*	0.56	37°C, pH 8.0, presence of Co^{2+}
protein arginine phosphatase[l]	*G. stearothermophilus*	1.12	25°C, pH 7.6, wild-type enzyme

*FOOTNOTE: [a](O'Brien et al., 2008), [b](Numa et al., 2008), [c](Kuang et al., 2009), [d](Krug et al., 2013) [e](this study), [f](Nagappa and Balaram), [g](Srinivasan et al., 2015), [h](Srinivasan et al., 2014), [i](Godinho and de Sá-Nogueira, 2011), [j](Larrouy-Maumus et al., 2013), [k](Proudfoot et al., 2004), [l](Fuhrmann et al., 2013).

3.5 Conclusion

An *in silico* study had reported that ISN1s belong to the HAD superfamily of proteins and contain the four conserved HAD motifs. The position of these motifs in ISN1 sequences differs significantly from other HADs but is largely conserved within ISN1s. Motif I (DX_1DX_2T/V) plays a central role in catalysis wherein the first aspartate is involved in nucleophilic attack on the phosphate group while the second aspartate is involved in coordinating Mg^{2+} ion. In PfISN1, mutating these two aspartates (D170 and D172) to asparagine led to a complete loss of IMP-hydrolyzing activity in the enzyme. This is the first biochemical evidence of an ISN1 family protein belonging to the HAD superfamily. Interestingly, both PfISN1_D172N and PfISN1_D172A showed a significant increase in pNPP-hydrolyzing activity compared to the wild-type enzyme with PfISN1_D172N showing higher activity than the latter. However, neither PfISN1_D170N nor PfISN1_D170N-D172N showed any change in pNPP-hydrolyzing activity compared to the wild-type enzyme. Both PfISN1_D172N and PfISN1_D172A showed inhibition of pNPP hydrolysis activity by IMP with PfISN1_D172N showing a

stronger affinity for IMP than the latter. However, neither PfISN1_D170N nor PfISN1_D170N-D172N showed inhibition by IMP. This observation is also supported by fluorescence studies wherein there was a quenching of fluorescence intensity and a blue-shift in emission maxima of the intrinsic tryptophan fluorescence of PfISN1_D172N and PfISN1_D172A in the presence of IMP, while that of PfISN1_D170N and PfISN1_D170N-D172N did not change significantly.

The above results suggest that D170 is involved in binding of IMP as well as its catalysis while D172 is involved only in its catalysis. Mutating D172 had an impact on pNPP-hydrolyzing activity as well as the affinity for IMP, both of which are positively correlated, suggesting a critical and previously uncharacterized role of D172 in pNPP hydrolysis. Since the impact of this mutation on pNPP-hydrolyzing activity has not been reported in studies on other HAD members, it is possible that this novel role might exist in other HAD members as well. Due to its strong affinity and no detectable activity with IMP, PfISN1_D172N was also used to obtain crystal structure of IMP-bound protein, as described in chapter 4.

Chapter Four

Structure-function studies on PfISN1: analysis of crystal structure and the role of key residues

Table of Contents

4.1 Abstract

In order to understand the structure-function relationship of the protein, a structural solution of PfISN1 protein was obtained by x-ray diffraction. In collaboration with Prof. Nushin Aghajari (Lyon, France), crystal structures of PfISN1 protein were solved in apo and liganded (IMP-Mg^{2+}, ATP) forms. In order to reduce intrinsic disorder in the protein, terminal deletion constructs were generated which showed interesting functional properties. The overall quaternary structure of the protein, its various domains, conformational changes induced upon ligand binding and the role of several key residues are discussed in this chapter. The primary objective was to generate mutants of these residues by site-directed mutagenesis and analyze their role in enzyme function through kinetic assays.

4.2 Introduction

ISN1 family of proteins is a unique subset of HAD superfamily proteins, limited to the eukaryotic kingdom. It is present predominantly in several species of fungi and a few species of apicomplexans and lower plants. The yeast ISN1 protein was the first of the family to be biochemically characterized. However, no crystal structure of an ISN1 protein is currently available. Apart from the 4 conserved motif stretches, ISN1 sequences do not share sequence homology with cytosolic nucleotidases (cN) or other HAD members. However, there is significant sequence homology within the ISN1 family members. Apart from motif residues, there are several other invariant and highly conserved residues present whose role is yet unknown (Table 4.1).

Table 4.1. List of invariant and highly conserved residues present in ISN1 sequences*.

Residue	Conservation	Residue variety		Residue	Conservation	Residue variety
before motif I						
E91	highly conserved	E (94%), S (4%), Q (2%)		L152	highly conserved	L (96%), F (1%), M (1%), N (1%)
L106	highly conserved	L (99%), I (1%)		N153	highly conserved	N (97%), G (3%)
L120	highly conserved	L (99%), M (1%)		A155	invariant	A
A125	highly conserved	A (99%), G (1%)		Q156	highly conserved	Q (94%), T (6%)
R138	invariant	R		L166	highly conserved	L (92%), M (7%), F (1%), A (1%)
P143	invariant	P		T168	highly conserved	T (97%), S (3%)
F145	invariant	F		F169	highly conserved	F (98%), L (1%), M (1%)
R149	invariant	R				
(table continued on next page)						

motif I						
D170	invariant	D		T174	invariant	T
D172	invariant	D				
after motif I						
L175	highly conserved	L (97%), I (7%)		D178	highly conserved	D (99%), H (1%)
Y176	invariant	Y		G179	invariant	G
motif II						
V203	highly conserved	V (95%), L (3%), C (1%), A (1%)		T204	invariant	T
after motif II						
A205	invariant	A		R304	invariant	R
A206	invariant	A		K305	invariant	K
Y208	invariant	Y		G310	invariant	G
Y215	invariant	Y (98%), F (2%)		E333	invariant	E
R218	invariant	R		L335	highly conserved	L (99%), W (1%)
R245	invariant	R		E336	highly conserved	E (99%), D (1%)
L219	highly conserved	L (95%), V (1%), F (3%), M (1%)		E337	highly conserved	E (99%), D (1%)
L222	highly conserved	L (92%), I (7%), F (1%)		V339	highly conserved	V (91%), A (5%), S (3%), C (1%)
G243	invariant	G		F358	invariant	F
G244	invariant	G		G360	invariant	G
E245	invariant	E		G361	highly conserved	G (99%), N (1%)
N247	highly conserved	N (93%), S (7%)		D363	invariant	D
W266	highly conserved	W (99%), F (1%)		D367	invariant	D
L282	invariant	L		G369	highly conserved	G (98%), A (2%)
L289	highly conserved	L (91%), F (8%), I (1%), C (1%)				
motif III						
K371	invariant	K				
after motif III						
G374	invariant	G		H391	after motif III	invariant
Q379	highly conserved	Q (97%), M (1%), I (1%), L (1%)		G393	invariant	G
motif IV						
D394	invariant	D		G400	highly conserved	G (98%), I (1%), S (1%)
Q395	highly conserved	Q (91%), R (9%)		N401	invariant	N
F396	invariant	F		D402	invariant	D

(table continued on next page)

after motif IV						
R406	highly conserved	R (99%), G (1%)		P417	invariant	P
T411	highly conserved	T (92%), C (5%), I (1%), V (1%)		E419	highly conserved	E (98%), N (1%), A (1%)
W413	highly conserved	W (98%), Y (1%), M (1%)		T420	highly conserved	T (98%), V (1%), Y (1%)

*FOOTNOTE: Residue numbering is based on PfISN1 sequence. Position is relative to motif (I-IV) stretches. Only residues at each position with >90% conservation (total 150 sequences) are included in the table.

X-ray crystallography is the most widely used technique available for the visualization of macromolecular structures at atomic resolution. Crystal structures provide information about the overall fold and domain architecture as well as a map of residue interactions in the protein. Ligand-bound structures provide information about residues interacting with the ligand. Comparative analysis of the apo and liganded structures provides information about conformational changes induced upon ligand binding. Residues interacting with the substrate in the ligand–bound crystal structure could play an important role in substrate binding and catalysis, whose significance can be examined by site-directed mutagenesis, in which the DNA sequence coding for the protein in the plasmid vector is mutated by PCR using synthetic oligodeoxynucleotide primers, leading to the expression of mutated protein. The technique was first used about 3 decades ago by M. Smith et. al. for mutating a cysteine residue in tyrosyl tRNA synthetase (Winter et al., 1982; Wilkinson et al., 1983). In recent times, with the easy availability of custom-synthesised oligodeoxynucleotides, it has become increasingly convenient to use this approach to study the structural and functional impact of a specific amino acid residue in the protein. Wild-type and various mutant constructs of PfISN1 were sent to our collaborative group lead by Prof. Nushin Aghajari (CNRS-University of Lyon, France) for solving the crystal structures of PfISN1 in apo and liganded forms. Of all the mutants inactive on the substrate IMP, PfISN1_D172N was selected for obtaining IMP-bound crystals due to its high affinity for IMP (Chapter 3).

4.3 Materials and methods

4.3.1 Dynamic light scattering (DLS) measurements.

The experiments were performed on a Nano Zetasizer (Malvern Instruments Ltd., Worcestershire, UK) with a He–Ne laser, operating at 532 nm. The scattering signal for size analysis was measured at 90°. All measurements were carried out at 25 ºC in protein size measurement mode. Each measurement was an average of 10 different scans between 0.5 and 10^7 μs. Refractive index of water and solvent viscosity were set

to 1.33 and 0.8872, respectively. An exponential decay function was generated from the scattering data and the rate of decay of this function was used to calculate translational diffusion coefficient, Dτ. The hydrodynamic radius of a spherical particle is then calculated from Dτ using Stokes-Einstein equation.

4.3.2 Homology modeling

PfISN1 protein model was predicted by homology modeling using I-TASSER server (Roy et al., 2010). Details of the threading templates used and their homology with PfISN1 sequence is given in Table 4.2.

Table 4.2. Threading templates used by I-TASSER modelling server for PfISN1.

Template Rank	Template PDB ID	% Identity with PfISN1	Normalized Z-score	Annotated Protein Function
1	4bnd	15	1.82	α-phosphoglucomutase
2	4ofz	17	1.64	trehalose-6-phosphate phosphatase
3	3l7y	13	2.00	putative uncharacterized protein
4	2vgl	23	1.34	AP2 clathrin adaptor core
5	4bnd	15	1.26	α-phosphoglucomutase
6	1jdh	16	1.31	β-catenin and HTCF-4
7	4bnd	15	1.24	α-phosphoglucomutase
8	1ejlI	15	1.31	Importin α-SV40 large T antigen NLS peptide complex
9	4bnd	15	2.00	α-phosphoglucomutase
10	4bnd	15	0.97	α-phosphoglucomutase

4.3.3 Generation of mutants and deletion constructs by site-directed mutagenesis.

The various mutants described in this chapter were generated by a ligation-free cloning method also called as Advanced Quick Assembly (AQUA) cloning (Beyer et al., 2015). A schematic of the scheme has already been described (Materials and methods section, Chapter 3). The deletion mutants PfISN1_ΔN30, ΔN30-D172N, ΔN60, ΔN102, ΔC10, ΔC10-H150V and ΔN30-ΔC10 were generated by a ligation-dependant cloning procedure. A schematic is described in Figure 4.2. A step-wise procedure is briefly described here. Through PCR-driven overlap extension in step-I, the insert fragment with an N-terminal or C-terminal deleted region was generated from the parental wild-type plasmid (D172N mutant plasmid and H150V mutant plasmid were used as templates for ΔN30-D172N and ΔC10-H150V, respectively) and by PCR using one primer downstream of the deletion region and another being the forward/reverse

cloning primer which was used originally to clone the gene into pET21b plasmid from the cDNA. Both the primers contained restriction sites at their 5' ends. In step II, the deletion fragment was digested with the restriction enzymes and ligated with pET21b plasmid (backbone vector) which was also digested with the same restriction enzymes. The ligated product was now transformed into *E. coli* XL-1 Blue strain. Positive clones were identified by PCR using gene-specific primers and the deletion was further confirmed by DNA sequencing. The list of primers used for generation of mutants as well as deletion constructs is given in Table 4.4.

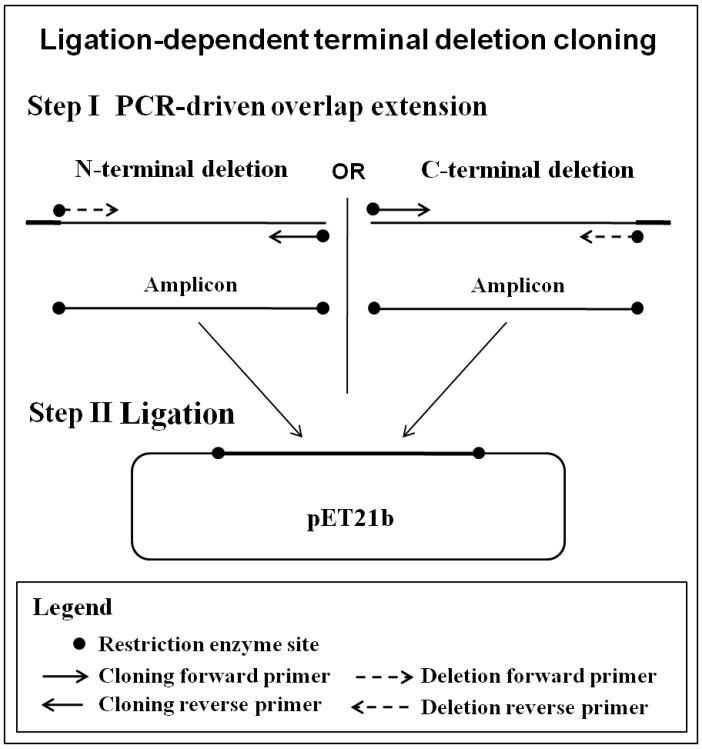

Figure 4.2. Schematic representation of cloning procedure for terminal deletion constructs.

Table 4.4. Mutagenic primers for site-directed mutagenesis of various mutants and deletion constructs.

K41L	
Forward primer	5'-GATAGAAATGTTATGAATTCAGATATGTTAAAAAATATTGTTCAGTGGAATAG-3'
Reverse primer	5'-CTATTCCACTGAACAATATTTTTTAACATATCTGAATTCATAACATTTCTATC-3'
H150V	
Forward primer	5'-CAACATTCAATGAAGTTAGGGTTATACTTAATCTTGCTCAAATTTTG-3'
Reverse primer	5'-CAAAATTTGAGCAAGATTAAGTATAACCCTAACTTCATTGAATGTTG-3'
(table continued on next page)	

Y176L	
Forward primer	5'-GATGCTGACGAAACGCTATTACCGGATGGTCATGATTTTAATG-3'
Reverse primer	5'-CATTAAAATCATGACCATCCGGTAATAGCGTTTCGTCAGCATC-3'
D178V	
Forward primer	5’-GACGAAACGCTATATCCGGTTGGTCATGATTTTAATG-3’
Reverse primer	5’-CATTAAAATCATGACCAACCGGATATAGCGTTTCGTC-3’
R218L	
Forward primer	5'-GCAGAAAAATACCAAAAACTATTAGAGAATTTGTTAAAATATTTTTC-3'
Reverse primer	5'-GAAAAATATTTTAACAAATTCTCTAATAGTTTTTGGTATTTTTCTGC-3'
D363V	
Forward primer	5’-CATTTAATGGAGGACAGGTTTTATGGGTAGACGTTG-3’
Reverse primer	5’-CAACGTCTACCCATAAAACCTGTCCTCCATTAAATG-3’
W365L	
Forward primer	5'- GGATTTATTGGTAGACGTTGGTAATAAAGCGG -3'
Reverse primer	5'- CGTCTACCAATAAATCCTGTCCTCCATTAAATG -3'
W365Y	
Forward primer	5'-GGAGGACAGGATTTATATGTAGACGTTGGTAATAAAG-3'
Reverse primer	5'-CTTTATTACCAACGTCTACATATAAATCCTGTCCTCC-3'
W365F	
Forward primer	5'-GGAGGACAGGATTTATTCGTAGACGTTGGTAATAAAG-3'
Reverse primer	5'-CTTTATTACCAACGTCTACGAATAAATCCTGTCCTCC-3'
D367V	
Forward primer	5’-GACAGGATTTATGGGTAGTCGTTGGTAATAAAGCG-3’
Reverse primer	5’-CGCTTTATTACCAACGACTACCCATAAATCCTGTC-3’
D394V	
Forward primer	5’-GAAATGTTGTCATATCGGTGTTCAGTTCTTACACTCAG-3’
Reverse primer	5’-CTGAGTGTAAGAACTGAACACCGATATGACAACATTTC-3’
Q395L	
Forward primer	5’-GTCATATCGGTGATCTGTTCTTACACTCAGGAAATG-3’
Reverse primer	5’-CATTTCCTGAGTGTAAGAACAGATCACCGATATGAC-3’
F396L	
Forward primer	5’-CATATCGGTGATCAGTTATTACACTCAGGAAATGATTTTC-3’
Reverse primer	5’-GAAAATCATTTCCTGAGTGTAATAACTGATCACCGATATG-3’
H398V	
Forward primer	5’-CATATCGGTGATCAGTTCTTAGTCTCAGGAAATGATTTTCC-3’
Reverse primer	5’-GGAAAATCATTTCCTGAGACTAAGAACTGATCACCGATATG-3’

(table continued on next page)

D402V	
Forward primer	5’-GTTCTTACACTCAGGAAATGTTTTTCCAACAAGATTTTGTAG-3’
Reverse primer	5’-CTACAAAATCTTGTTGGAAAAACATTTCCTGAGTGTAAGAAC-3’
R406L	
Forward primer	5'-CAGGAAATGATTTTCCAACATTATTTTGTAGTTTAACATTATG-3'
Reverse primer	5'-CATAATGTTAAACTACAAAATAATGTTGGAAAATCATTTCCTG-3'
W413L	
Forward primer	5'-GTAGTTTAACATTATTGGTTAGCAACCCTCAAG-3'
Reverse primer	5'-CTTGAGGGTTGCTAACCAATAATGTTAAACTAC-3'
ΔN30	
Forward primer	5'-CGGGATCCGATAGAAATGTTATGAATTCAGATATGAAAAAAAATATTGTTC-3'
ΔN60	
Forward primer	5’-CGGGATCCAGTTTGATCATGTTTCTTGTAGAAATATTTAGATCTCTTTTTGTATCC-3’
ΔN102	
Forward primer	5’-CGGGATCCCATAGTCGACTGAAATATTTGATAGATGATG-3’
ΔC10	
Reverse primer	5’-GGAAGCTTTTATGATTTTATGTTTAAATGCATTATACTCTTTAAGCATGCTTTAG-3'
Other primers	
Forward Cloning primer	5'-CGGGATCCAAGAATTTGGACATAAATACATTCGATAATATTGAAGATATTCC-3'
Reverse Cloning primer	5'-GGAAGCTTTTATTGATTTTCATATAAAACTTCCGGAATAAATGATTTTATG-3'
T7 promoter primer	5'-TAATACGACTCACTATAGGG-3'
T7 terminator primer	5'-GCTAGTTATTGCTCAGCGG-3'

4.3.4 Purification of mutants and deletion constructs.

All mutants and deletion constructs were purified under conditions similar to wild-type protein.

Denaturing Ni-NTA™ chromatography – For PfISN1_ΔN102, Ni-NTA™ chromatography was also performed under denaturing conditions. Briefly, the harvested culture was lysed by mechanical shearing using French Press® with buffer conditions similar to wild-type and centrifuged at 16,000 × g for 45 min. The pellet obtained was solubilised in the same buffer containing 6 M guanidinium hydrochloride and centrifuged at 13,000 × g for 30 min. PfISN1_ΔN102 in the supernatant was purified using Ni-NTA™ chromatography. The protein was then eluted with 500 mM imidazole containing 6 M guanidinium hydrochloride and dialysed with buffer containing guanidinium hydrochloride. To allow refolding, the concentration of guanidinium hydrochloride was reduced in successive decrements of 4, 3, 2, 1.3, 0.8, 0.5, 0.3, and 0

M, respectively. Finally, the dialysed sample was centrifuged at 13,000 × g for 30 min after which the supernatant and pellet were examined by SDS-PAGE.

4.3.5 Rendering of three-dimensional structure figures.

Structure figures were rendered using PyMoL (DeLano Scientific LLC, http://pymol.sourceforge.net/) and Chimera.

4.3.6 Isothermal titration calorimetry.

Binding constant, stoichiometry and associated thermodynamic parameters were determined for the *Pf*ISN1_D172N-IMP complex using a VP-isothermal titration calorimeter (ITC) (Microcal, Inc., Northampton, MA, USA). The protein was extensively dialyzed against buffer containing 50 mM Tris-HCl, pH 8.0, 100 mM NaCl and 10% w/v glycerol prior to use. Stock solution of ligand IMP was made in the same buffer. IMP additions were done at 25 °C by step-wise addition of small volumes (10 µl) of ligand stock (IMP at a concentration of 2 mM) to *Pf*ISN1 (80 µM) in the sample cell. A control experiment was performed in which the ligand at the same concentration was diluted against buffer alone in the sample cell in order to obtain the heat of dilution. The raw calorimetric signals were integrated and corrected for the heat of dilution of IMP. The resulting corrected binding isotherms were subjected to nonlinear least squares analysis using ORIGIN® software (Malvern Instruments, Malvern, U.K.) and fit to a single-site model to obtain the association constant K, binding enthalpy ΔH, binding stoichiometry N and entropy ΔS.

4.3 Results and Discussion

Expression constructs of PfISN1 wild-type full-length and truncated forms, and various mutants inactive on substrate IMP were provided to our collaborative group in France, lead by Prof. Nushin Aghajari (CNRS-University of Lyon, France). As mentioned in Chapter 2, higher order aggregates were observed during analytical size-exclusion chromatography, supported by dynamic light scattering (DLS) experiment, wherein polydispersivity indicated non-homogeneity in size of the protein in solution (Fig. 4.1).

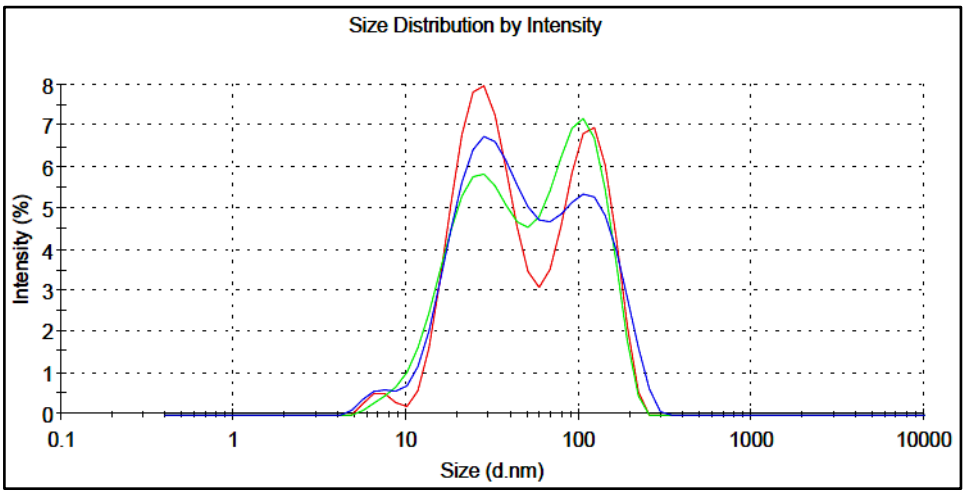

Figure 4.1. Particle size distribution profile of 3 independent PfISN1 wild-type protein samples (red, green and blue curves) by DLS measurement. Presence of more than one peak indicates polydispersed sample.

4.3.1 Removal of N- and C-terminal disordered regions.

Several proteins have regions with high flexibility even in their native state. Such regions, called as intrinsically disordered regions, could lead to protein aggregation and precipitation, leading to difficulties in crystallization. Disordered regions in PfISN1 were predicted based on the protein sequence using PrDOS server (Ishida and Kinoshita, 2007). In the residue-wise disorder profile, the N-terminal region of ~30 residues and the C-terminal region of ~10 residues showed a higher disorder probability (Fig. 4.2).

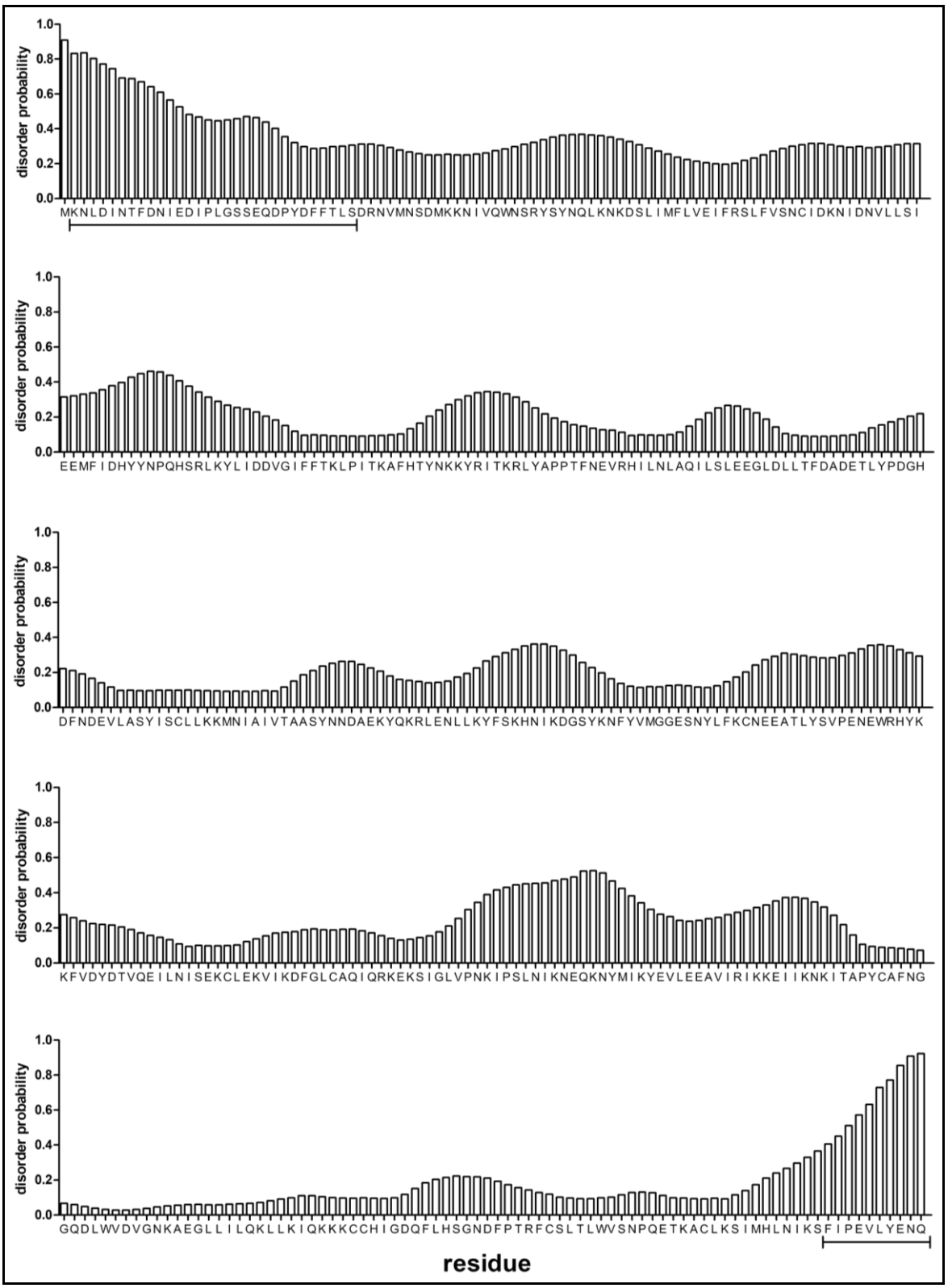

Figure 4.2. Residue disorder profile of PfISN1 protein obtained by plotting disorder probability *vs* residue. 30 residues from the N-terminal and 10 residues from the C-terminal are underlined.

Truncation of disordered terminal regions in proteins is a common practice adopted in order to improve upon the solubility, stability and homogeneity of the protein in solution (Yeh et al., 1996; Chen et al., 1998; Martin et al., 2000). Based on the predicted disordered regions, a set of three terminal truncated protein constructs were designed: PfISN1_ΔN30 with a truncation of 30 residues from N-terminus, PfISN1_ΔC10 with a truncation of 10 residues from C-terminus and PfISN1_ΔN30-ΔC10 with a combined truncation of ΔN30 and ΔC10. Cloning procedure is described in Materials and Methods section 4.4.3. All the deletion constructs were expressed and purified under conditions identical to the wild-type protein (Fig. 4.3A) and utilized for biochemical studies and crystallization. Preliminary kinetic assays were carried out for all the 3 deletion constructs.

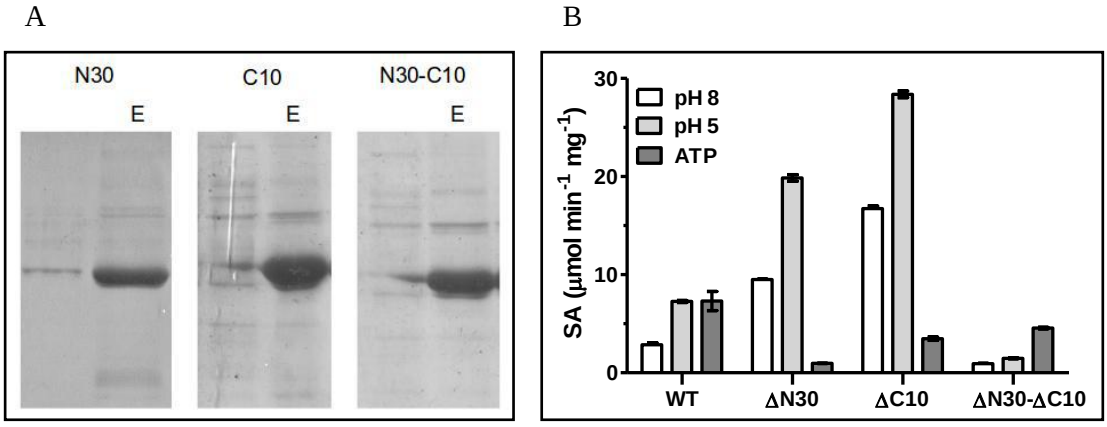

Figure 4.3. (A) SDS-PAGE showing the eluted fraction (labeled as E) of the deletion constructs PfISN1_ΔN30, ΔC10 and ΔN30-ΔC10 after Ni-NTA™ chromatography. Histogram of (B) IMP-hydrolyzing activity with 10 mM IMP at pH 8.0 with and without 2 mM ATP and with 0.5 mM IMP at pH 5.0. SA indicates specific activity.

At pH 8.0, PfISN1_ΔN30 and ΔC10 showed 3-fold and 6-fold higher IMP hydrolyzing activity as compared to wild-type enzyme, respectively. PfISN1_ΔN30-ΔC10 however showed 3-fold lower IMP hydrolyzing activity as compared to wild-type enzyme. At pH 5.0, PfISN1_ΔN30 and ΔC10 showed 3-fold and 4-fold higher IMP hydrolyzing activity as compared wild-type enzyme, respectively. However, PfISN1_ΔN30-ΔC10 showed 5-fold lower IMP hydrolyzing activity compared to the wild-type enzyme. At pH 8.0, PfISN1_ΔN30 and ΔC10 showed inhibition by ATP. PfISN1_ΔN30 and ΔC10 showed 10-fold and 5-fold lower IMP hydrolyzing activity in the presence of ATP, respectively. However, PfISN1_ΔN30-ΔC10 was activated by ATP and showed 5-fold higher IMP hydrolyzing activity in the presence of ATP (Fig. 4.3B).

Removal of N-terminal segment – From homology-based modeling studies, an N-terminal segment of ~100 residues was found to be highly flexible and disordered (Fig. 4.4A) and lacked significant conservation (Fig. 4.4B). Removing this segment could improve protein solubility and stability. A deletion construct PfISN1_ΔN102 was generated in this regard. Under wild-type conditions, the protein was expressed but found in insoluble fraction after cell lysis. The theoretically calculated isoelectric point (pI) of the ΔN102 deletion construct is 8.5 as compared to 6.9 for wild-type protein. Hence, attempts to purify the protein at pH 7.4, 7.0 and 6.5 were also made. However, the protein was found in insoluble fraction under all these conditions (Fig. 4.5A). During denaturing Ni-NTA™ chromatography, the protein precipitated during refolding by dialysis (Fig. 4.5B). Removal of the 102-residue segment at the N-terminus, leading to loss of protein solubility suggests that although the N-terminal segment has no significant conserved residues, it is important for structural integrity of the protein.

A

B

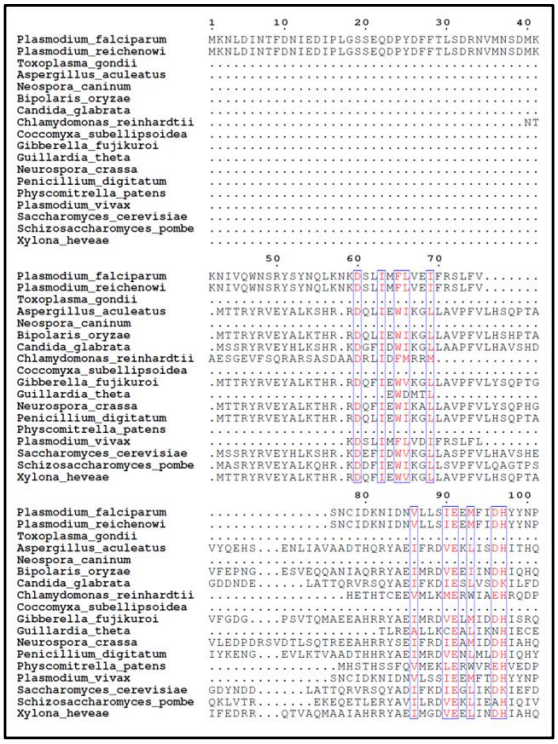

Figure 4.4. (A) PfISN1 protein model predicted from PfISN1 sequence by homology modeling using i-TASSER server. The different domains highlighted are N-terminus (blue), core (green) and cap (orange) domain. Motif I loop is highlighted in magenta. (B) Multiple sequence alignment of N-terminal segment in ISN1 up to 100 residues (PfISN1 numbering).

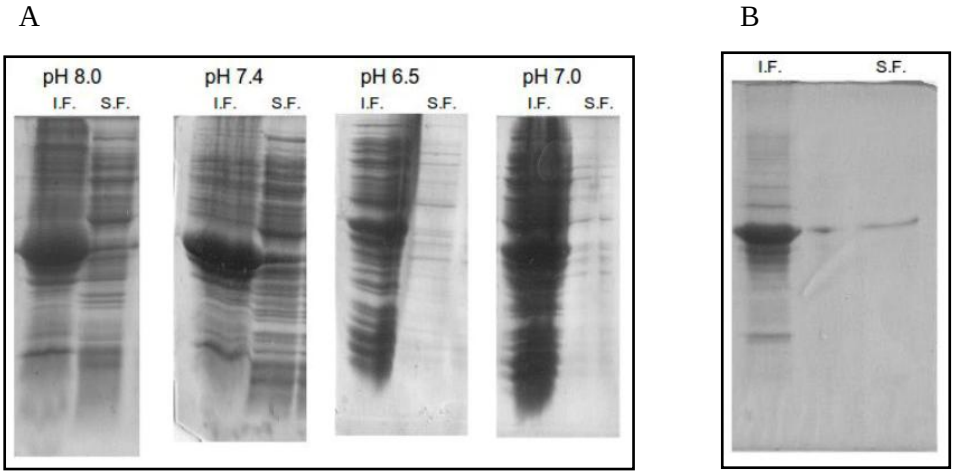

Figure 4.5. SDS-PAGE of PfISN1_ΔN102 protein. (A) Pellet (I.F.) and supernatant (S.F.) after cell lysis at various pH. (B) Pellet (I.F.) and supertanant (S.F.) of dialyzed sample after denaturating Ni-NTA™ chromatography. See Materials and methods section for details. I.F., insoluble fraction; S.F., soluble fraction.

4.3.2 Quaternary structure and domain architecture in PfISN1.

Crystal structures were solved for the wild-type full-length active enzyme in apo- and ATP-bound forms, and for the inactive mutant PfISN1_D172N (full-length) bound with IMP-Mg^{2+}, to 2.6 Å, 2.5 Å and 3.1 Å resolution, respectively. These are the first crystal structures to be obtained for an ISN1 family protein. All the solved structures adopted a tetrameric assembly which is in agreement with the oligomeric state of the protein determined in solution in Chapter 2. In a tetramer, each subunit consists of four domains, viz., N-Terminal Domain (NTD) from M1 to D60, oligomerization Domain (OD) from S61 to T143, core (catalytic) domain from F144 to K270 and from K371 to Q444, and the cap domain from K271 to N370 (Fig. 4.6A). The core domain contains the catalytic/active site pocket that possesses the four highly conserved motifs characteristic to the HAD superfamily. It displays an α/β Rossmann-like fold with a seven parallel β-strands surrounded by eight α-helices. The cap domain is composed of four anti-parallel β-strands and two α-helices. From the top-view, the tetrameric assembly is 'X' shaped (Fig. 4.6B) and from the side-view, it has a central cavity (Fig. 4.6C). Two different dimeric interfaces are formed in the tetrameric assembly. 'Dimer interface 1' is formed by the interaction of the OD of one subunit with the cap domain of another subunit. 'Dimer interface 2' is formed by the ODs of two subunits (Fig. 4.7).

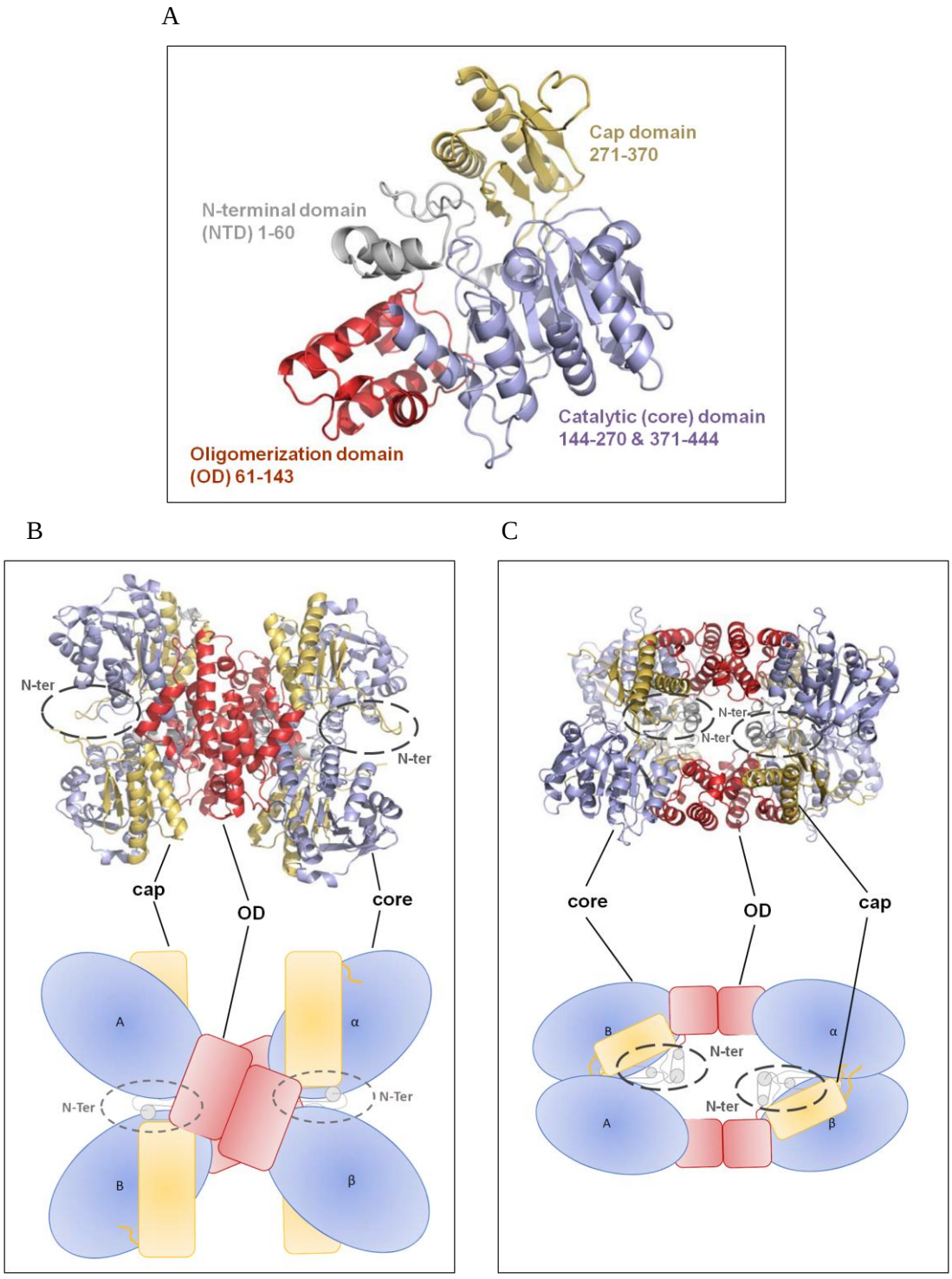

Figure 4.6. Crystal structure of PfISN1-apo protein. (A) Monomeric subunit structure with various domains highlighted in different colors. Tetrameric assembly of PfISN1-apo protein with (B) top view and (C) side view. Schematic representation of domain architecture is shown below in panels B and C. NTD is encircled and labeled as 'N-Ter'.

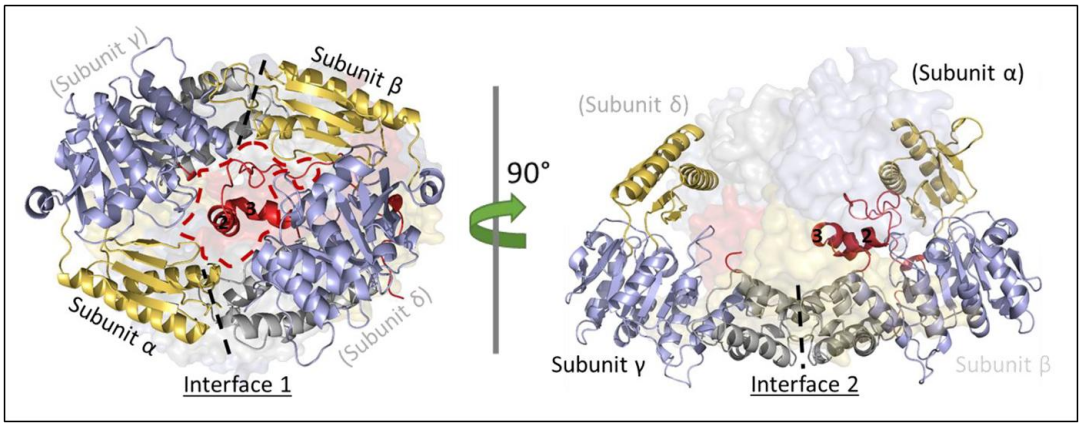

Figure 4.7. Dimer interfaces in the tetrameric assembly of PfISN1-apo structure. Black-dashed lines in the left panel represent dimer interface 1 formed by the interaction between the OD of subunit β and the cap domain of subunit α. Subunits γ and δ reside behind subunits α and β, respectively. The red-dashed area defines the cavity accommodating an NTRD from subunit β. Black-dashed lines in the right panel represent the dimer interface 2 formed by the interaction between the ODs of subunits β and γ.

In the PfISN1-apo structure, the cavity in the dimeric assembly shown in Figure 4.7A has space for only one NTD from one of the subunits to be accommodated, forcing the other NTD of the other subunit to be located elsewhere. Therefore, in the tetrameric assembly, two of the NTDs are structured while the other two are unstructured. The two unstructured NTDs are situated on the same side in the tetramer (for e.g., subunits α and γ in Fig. 4.7, left panel). This unusual asymmetry in the NTD led to the further investigation of its role in enzyme function. A deletion construct PfISN1_ΔN60 was generated wherein the entire NTD was removed. This truncated enzyme showed no detectable activity with IMP at pH 8.0 in the presence or absence of ATP. At pH 5.0, it showed 5-fold lower activity than the wild-type enzyme (Fig. 4.8). A detailed kinetic characterization of the PfISN1_ΔN30 enzyme (see section 4.3.1) revealed that at pH 8.0, the enzyme had a 2-fold higher V_{max} and 2-fold lower K_m than the wild-type enzyme, increasing its catalytic efficiency 5-fold higher than the wild-type enzyme. At pH 5.0, the enzyme had a 6-fold increase in V_{max} and a 9-fold increase in K_m, having no significant change in catalytic efficiency as compared to the wild-type enzyme (Fig. 4.9). These functional properties of PfISN1_ΔN30 and ΔN60 suggest a significant regulatory role of NTD in enzyme function.

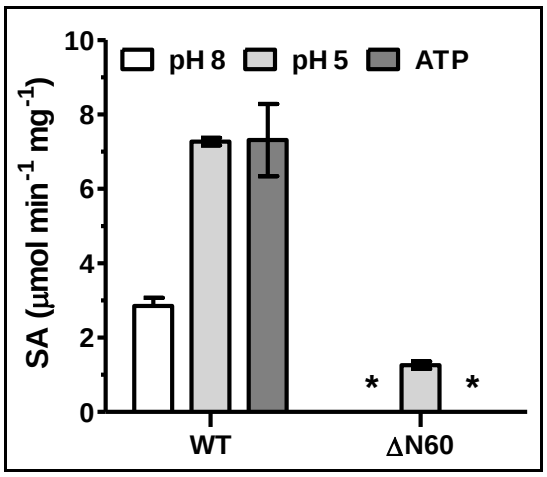

Figure 4.8. IMP hydrolyzing activity of ΔN60 at pH 8.0, pH 5.0 and at pH 8.0 in the presence of ATP. 10 mM IMP at pH 8.0, 0.5 mM IMP at pH 5.0 and 2 mM ATP were used in the assay. SA indicates specific activity. *No detectable activity.

4.3.3 Active site architecture in PfISN1

In the PfISN1_D172N-IMP-Mg^{2+} structure, the active site is mainly composed of conserved residues from the four HAD motifs, and by W365 which is situated on β-strand H in the cap domain. Examination of ISN1 sequence alignments indicated two residues, Y176 and D178, at the C-terminus of motif I and R218 at the C-terminus of motif II that are invariant. Y176L and R218L interact with D172 (motif I aspartate) while D178 coordinates the sugar moiety of IMP. The base moiety of the nucleotide is mainly stabilized by a π-stacking interaction with W365 and by three hydrogen bonds to A205, S207 and D367 (Fig. 4.10).

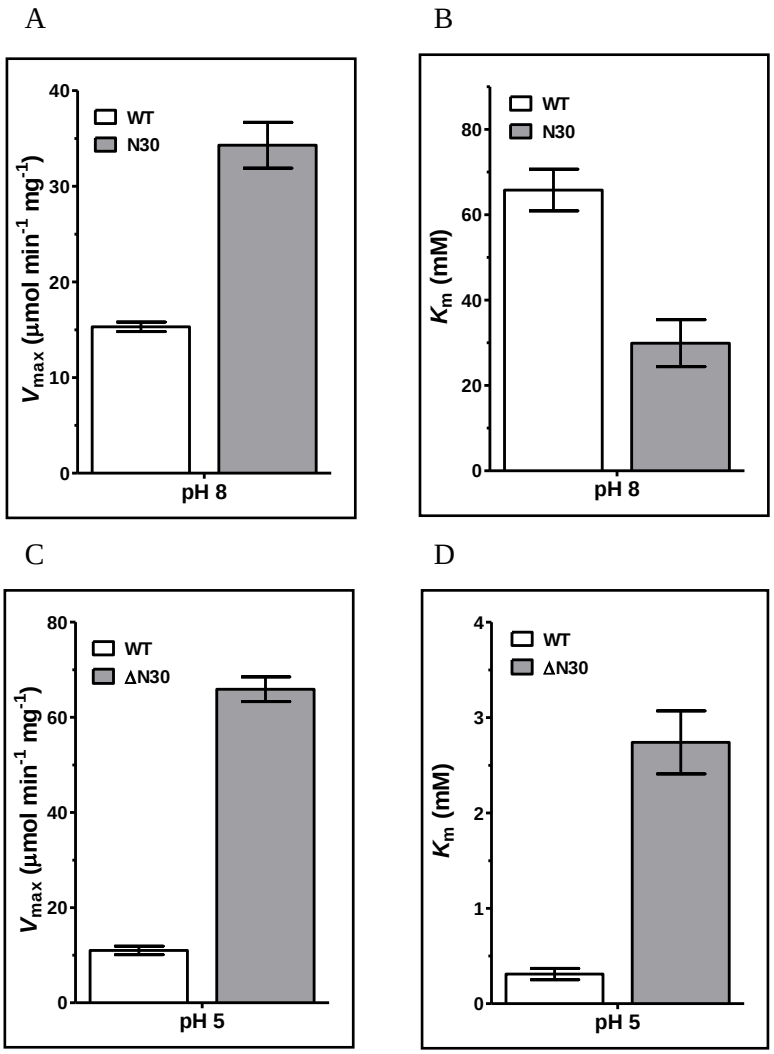

Figure 4.9. Kinetic parameters (V_{max} and K_m) of PfISN1_ΔN30 at (A-B) pH 8.0 and (C-D) pH 5.0. See appendix C for initial rate *vs* IMP concentration plots and kinetic parameter values.

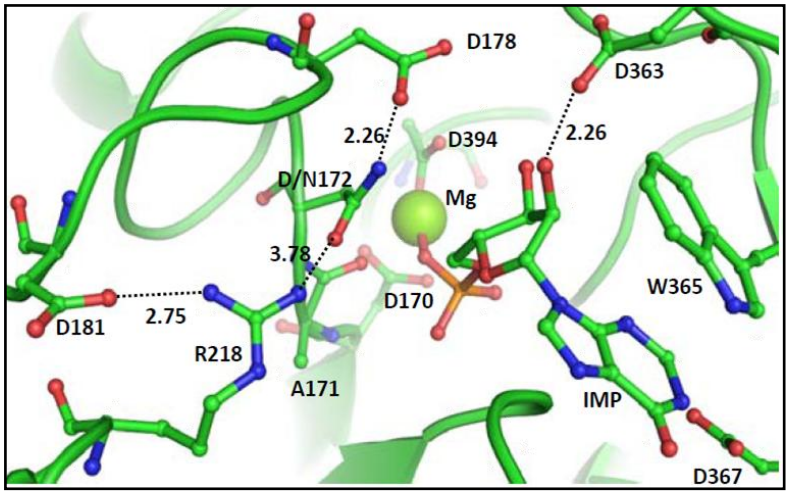

Figure 4.10. Active site pocket in PfISN1_D172N IMP-Mg^{2+} bound structure showing residues interacting with IMP.

The 2' and 3' hydroxyl groups of the sugar moiety form hydrogen bonds with D178, D363 and W365 (Fig. 4.10). At pH 8.0, mutants PfISN1_Y176L and D178V showed 12-fold and 6-fold lower IMP-hydrolyzing activity, respectively, while PfISN1_R218L was inactive on IMP. At pH 5.0, PfISN1_Y176L and R218L showed 10-fold and 23-fold lower activity, respectively, while PfISN1_D178V showed activity comparable to wild-type enzyme. PfISN1_D363V showed 10-fold lower IMP-hydrolyzing activity at pH 8.0 while PfISN1_D367V was inactive on IMP (Fig. 4.11).

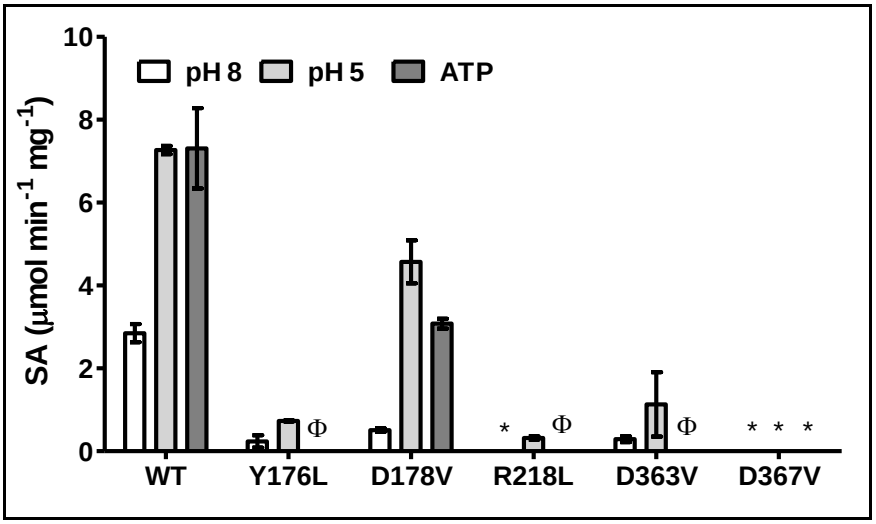

Figure 4.11. IMP hydrolysis activity of mutants PfISN1_Y176L, D178V, R218L, D363V and D367V at pH 8.0 in the presence and absence of ATP and at pH 5.0. 10 mM IMP at pH 8.0, 0.5 mM IMP at pH 5.0 and 2 mM ATP were used in the assay. *No detectable activity; ΦAssay with ATP not performed due to poor activity at pH 8.0.

The possible role of W365 in π-stacking interaction with the base moiety of IMP was envisaged before the availability of the IMP-bound crystal structure. In the homology-modeled structure, W365 from the cap domain was positioned towards the active site cavity, marked by motif I residues D170 and D172 (Fig. 12A). W365 is not a highly conserved residue. However, the aromaticity is conserved at that position, with some ISN1 sequences containing phenylalanine instead of tryptophan (Fig. 12B). Trp365 was mutated to a non-aromatic hydrophobic residue leucine as well as to aromatic residues phenylalanine and tyrosine. While PfISN1_W365L was inactive with IMP, both PfISN1_W365Y and W365F showed IMP-hydrolyzing activity comparable to the wild-type enzyme, suggesting that an aromatic nature of the residue was critical for IMP binding (Fig. 4.12C). The π-stacking interaction of W365 with IMP in the IMP-bound crystal structure has been described in Figure 4.10.

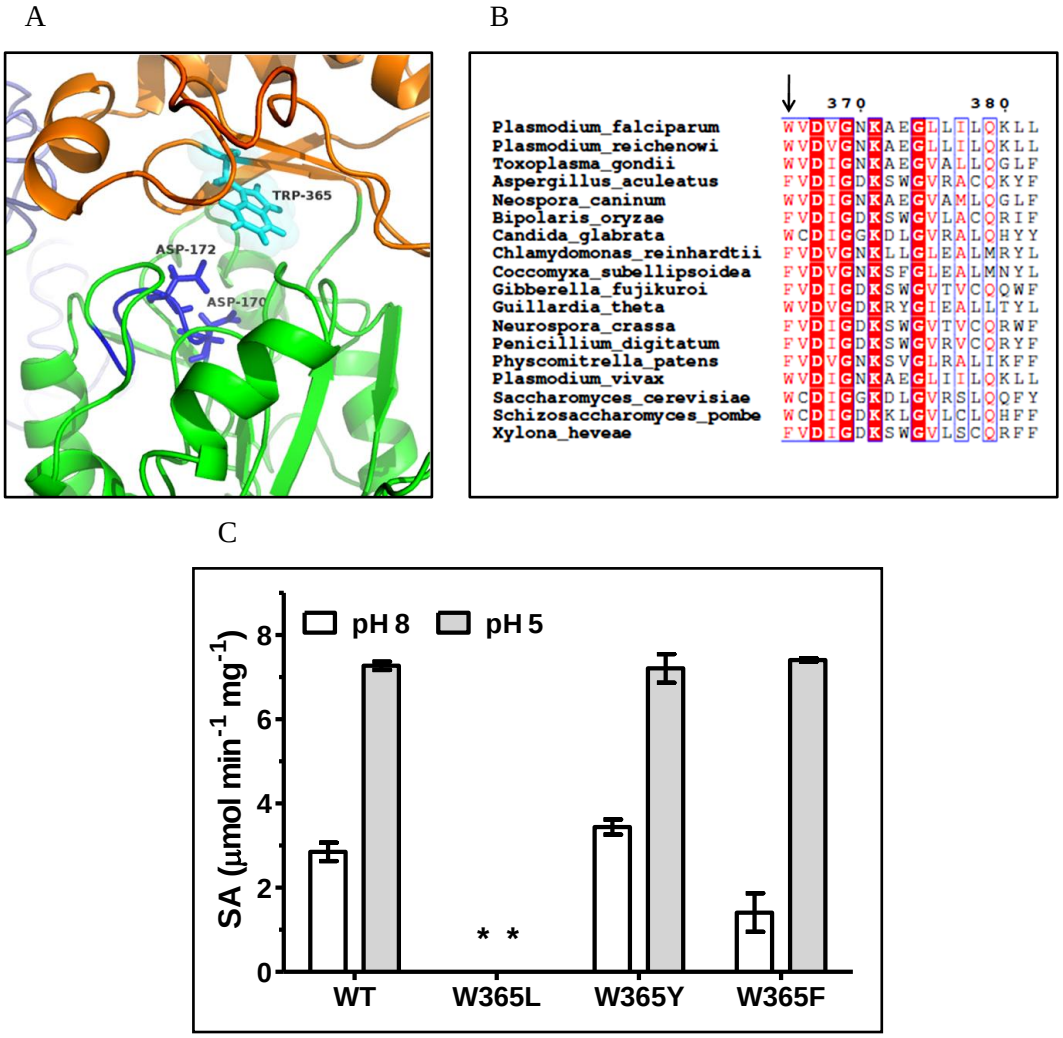

Figure 4.12. (A) Position of W365 in homology-modeled structure, along with motif I residues D170 and D172. The core domain, cap domain and N-terminal segment are highlighted as green, orange and blue respectively. (B) Multiple sequence alignment (PfISN1 numbering) highlighting conservation of residues at W365 position (black arrow). (C) IMP hydrolyzing activity of mutants PfISN1_W365L, W365Y and W365F at pH 8.0 (10 mM IMP) and 5.0 (0.5 mM IMP). * No detectable activity.

The phosphate moiety of IMP interacts with the main chain of A171 and D/N172, and the side chains of D170, T204, K371, D394, N401 and two water molecules. These same water molecules are involved in coordination of Mg^{2+} ion together with the phosphate moiety, side chains of D170, D394 and Q395, and the main chain carbonyl of D/N172 (Fig. 4.13). Mutants PfISN1_D394V, Q395L and D402V were inactive on IMP at pH 8.0 in the presence and absence of ATP, and at pH 5.0 (Fig. 4.14).

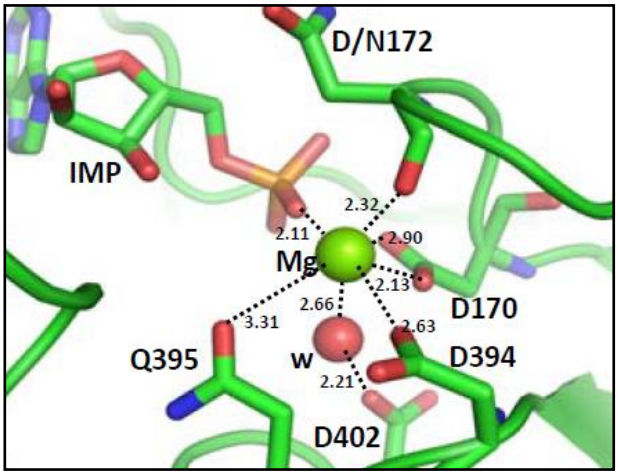

Figure 4.13. Active site pocket in PfISN1_D172N IMP-Mg^{2+} bound structure showing residues coordinating with Mg^{2+}. 'w' indicates water molecule.

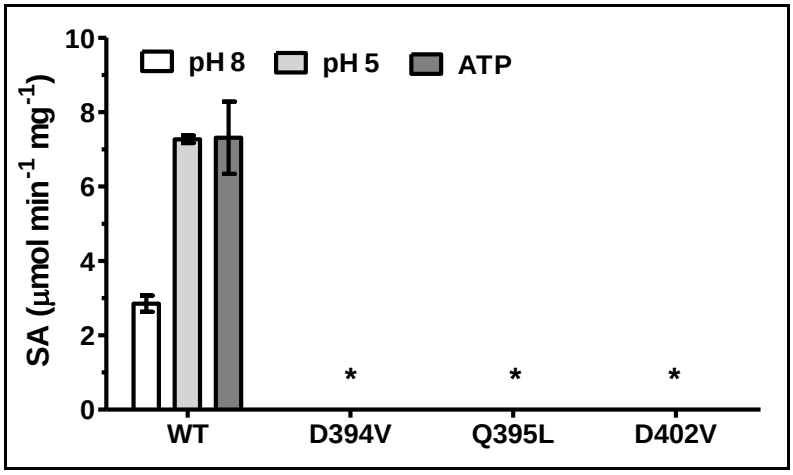

Figure 4.14. IMP hydrolysis activity of mutants PfISN1_D394V, Q395L, H398V and D402V at pH 8.0 in the presence and absence of ATP and at pH 5.0. 10 mM IMP at pH 8.0, 0.5 mM IMP at pH 5.0 and 2 mM ATP were used in the assay. *No detectable activity.

4.3.4 Conformational changes induced upon IMP-Mg^{2+} binding in PfISN1

Significant conformational changes occur in the structure upon IMP-Mg^{2+} binding, amongst which the closure of the cap domain and reorganization of the NTD are the most prominent in the quaternary structure (Fig. 4.15).

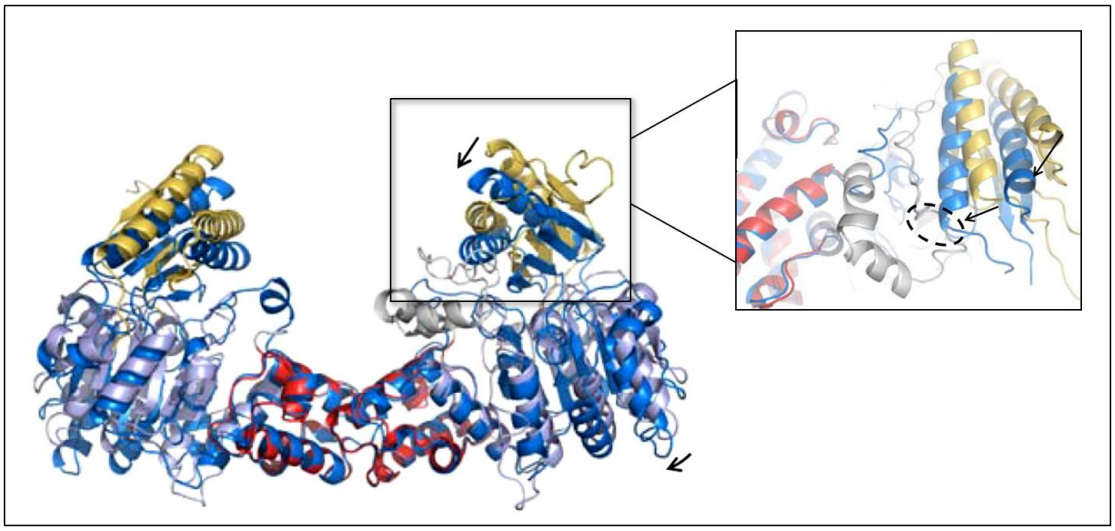

Figure 4.15. Dimers of PfISN1-apo (grey-gold-red) and PfISN1_D172N-IMP-Mg^{2+} (blue) structures showing global conformational changes induced upon IMP-Mg^{2+} binding. Direction of cap domain closure is shown by solid black arrow. Inset highlights cap domain closure and steric clash with NTD (encircled) upon IMP-Mg^{2+} binding.

During cap closure, its steric clash with the NTD causes the latter to be re-organized wherein it adopts a conformation very different from either of the two conformations observed in the PfISN1-apo structure. During its re-organization, two important salt bridges between NTD and motif IV loop (D60-R406 and K41-D394) are broken, contributing to the reorganization of the motif IV loop (Fig. 4.16A and C) which orients residues D394, Q395 and D402 that interact with IMP-Mg^{2+} towards the active site. Moreover, helix 8 containing motif I residues D170 and D172 also restructures into a loop and orients the side chain of E173 to accommodate the substrate while side chains of D178 and D394 flip into the catalytic pocket to coordinate the substrate (Fig. 4.16C).

The significance of the salt bridges was supported by the observation that the PfISN1_R406L mutant has highly compromised IMP-hydrolyzing activity while PfISN1_K41L had 3-fold higher IMP-hydrolyzing activity at pH 8.0 and 5.0 with only a marginal activation by ATP (Fig. 4.16B and D).

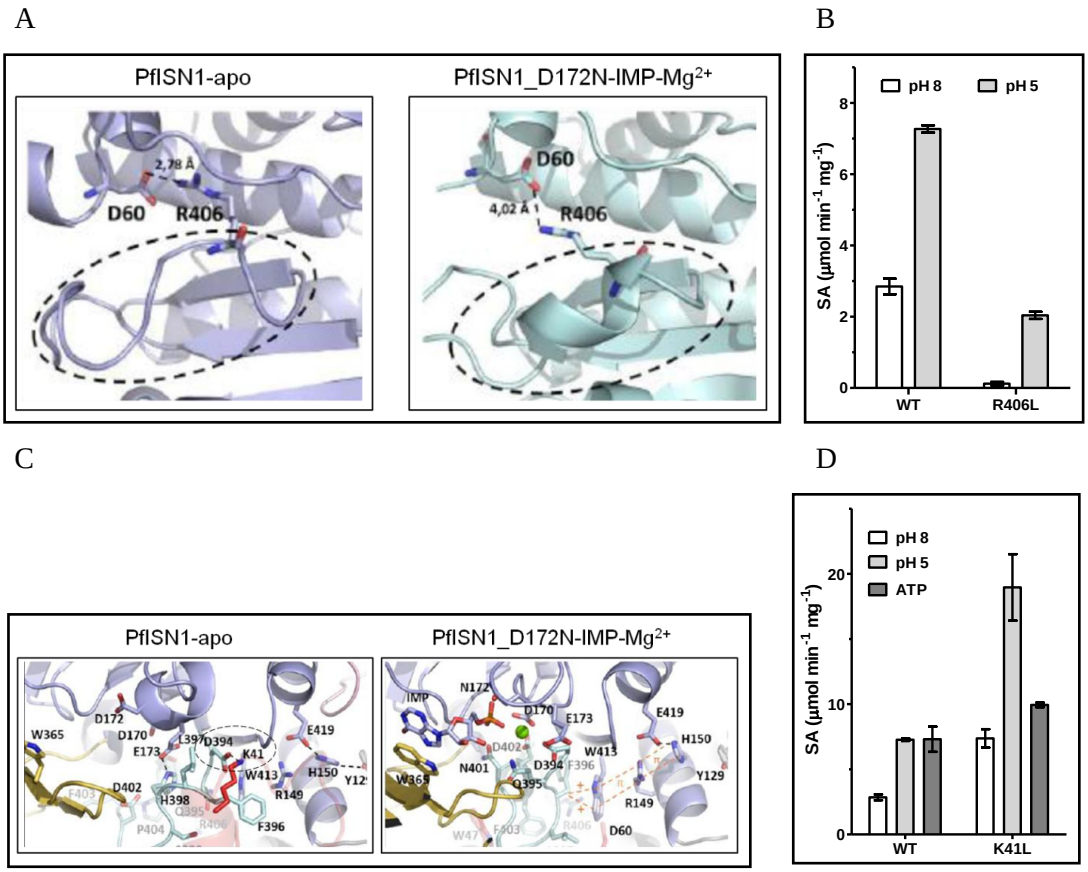

Figure 4.16. (A) Salt-bridge between D60 and R406 in the PfISN1-apo structure (left). In the PfISN1_D172N-IMP-Mg^{2+} structure, the salt-bridge is weakened. Motif IV loop is encircled. (B) IMP-hydrolyzing activity of PfISN1_R406L at pH 8.0 and pH 5.0 with 10 mM and 0.5 mM IMP, respectively. (C) Salt-bridge between D394 one subunit and K41 from another subunit (encircled) in the PfISN1-apo structure (left). In the PfISN1_D172N-IMP-Mg^{2+} structure (right), the salt bridge is absent as D394 flips towards the active site. (D) IMP-hydrolyzing activity of PfISN1_K41L at pH 8.0 in the presence and absence of ATP and at pH 5.0. 10 mM at pH 8.0 and 0.5 mM IMP at pH 5.0 were used in the assay.

Detailed kinetic characterization of PfISN1_K41L revealed that at pH 8.0, the enzyme had no significant change in V_{max} but a 4-fold lower K_m value than the wild-type enzyme, increasing its catalytic efficiency 5-fold higher than the wild-type enzyme. At pH 5.0, it had a 2-fold increase in V_{max} and a 10-fold increase in K_m value, decreasing its catalytic efficiency 4-fold lower than the wild-type enzyme (Fig. 4.17) Substrate titration plots under all the above conditions for PfISN1_K41L were hyperbolic in nature (see appendix C).

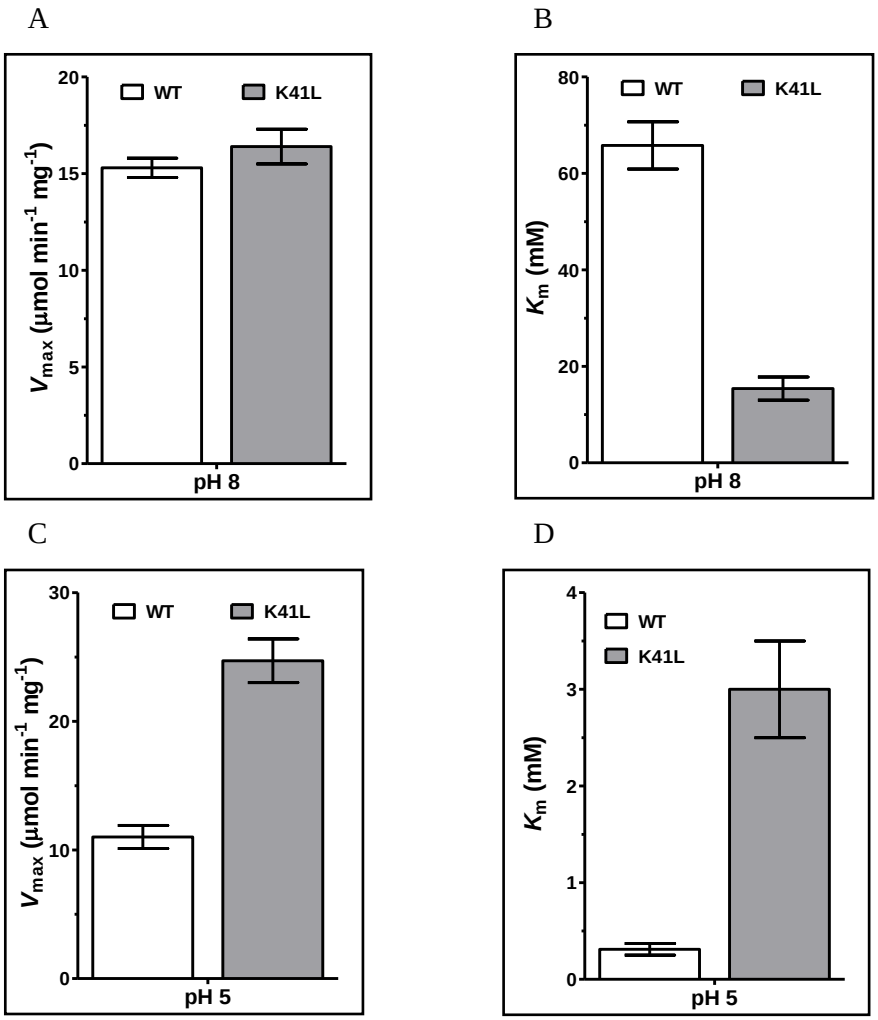

Figure 4.17. Kinetic parameters (V_{max} and K_m) of PfISN1_K41L at (A-B) pH 8.0 and (C-D) pH 5.0. See appendix C for kinetic parameter values.

Two other residues, F396 and H398 from motif IV loop do not interact directly with the ligand. However, during re-organization of the motif IV loop, F396 flips away from the catalytic site and forms a long-distance π-stack with H150, a residue whose significance is discussed in section 4.3.5. H398 which interacts with E173 from motif I loop in the PfISN1-apo structure (Fig. 16C) now adopts a different conformation upon ligand binding. While mutant PfISN1_F396L was inactive with IMP, PfISN1_H398V showed IMP-hydrolyzing activity comparable to the wild-type enzyme at pH 8.0 and pH 5.0 but showed 3-fold increased activation with ATP as compared to the wild-type enzyme (Fig. 4.18).

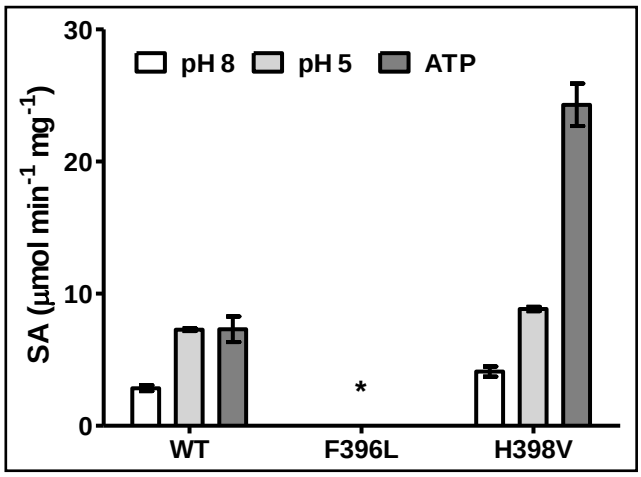

Figure 4.18. IMP-hydrolyzing activity of mutants PfISN1_F396L and H398V at pH 8.0 in the presence and absence of ATP and at pH 5.0. 10 mM IMP at pH 8.0, 0.5 mM IMP at pH 5.0 and 2 mM ATP were used in the assay. *No detectable activity.

Moreover, a detailed kinetic characterization of the PfISN1_H398V mutant revealed that it had no significant change in V_{max} but a 6-fold lower K_m than the wild-type enzyme, increasing its catalytic efficiency 7-fold higher than the wild-type enzyme. At pH 5.0, the enzyme had a 3-fold increase in V_{max} and a 5-fold increase in K_m, having no significant change in catalytic efficiency as compared to the wild-type enzyme (Fig. 4.19). Substrate titration plots under the above conditions for PfISN1_H398V were hyperbolic in nature (see appendix C). Thus, both PfISN1_K41L and H398V show increased affinity (low K_m value) for IMP at pH 8.0 suggesting that the conformation adopted by these residues in the PfISN1-apo structure could possibly restrict the accessibility of the substrate to the active site.

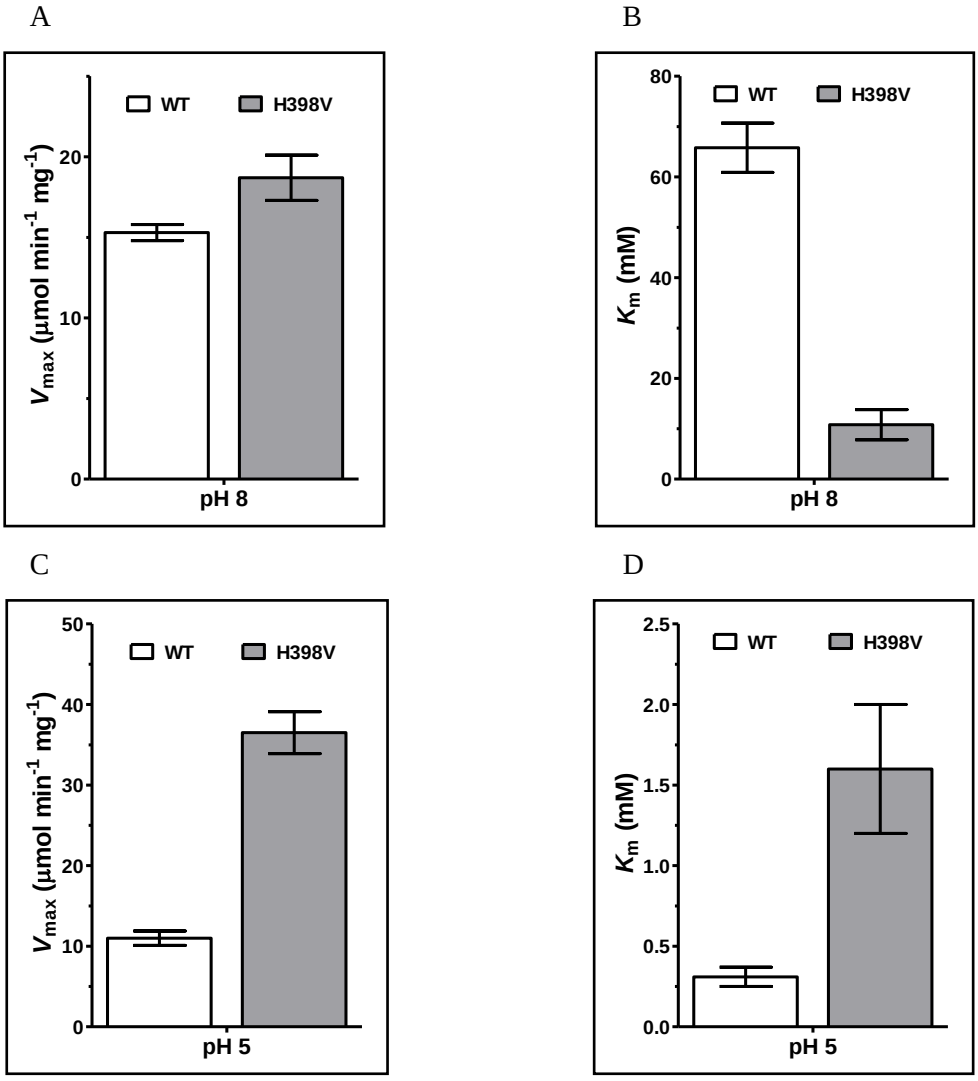

Figure 4.19. Kinetic parameters (V_{max} and K_m) of PfISN1_H398V at (A, B) pH 8.0 and (C, D) pH 5.0. See appendix C for kinetic parameter values.

Stoichiometry of IMP binding – In the PfISN1_D172N-IMP-Mg^{2+} structure, all four active sites in the tetramer are occupied by the ligand. This has also been confirmed in solution by isothermal titration calorimetry (ITC) wherein the PfISN1-D172N mutant was titrated against IMP, yielding a stoichiometry of 1:1 (Fig. 4.20).

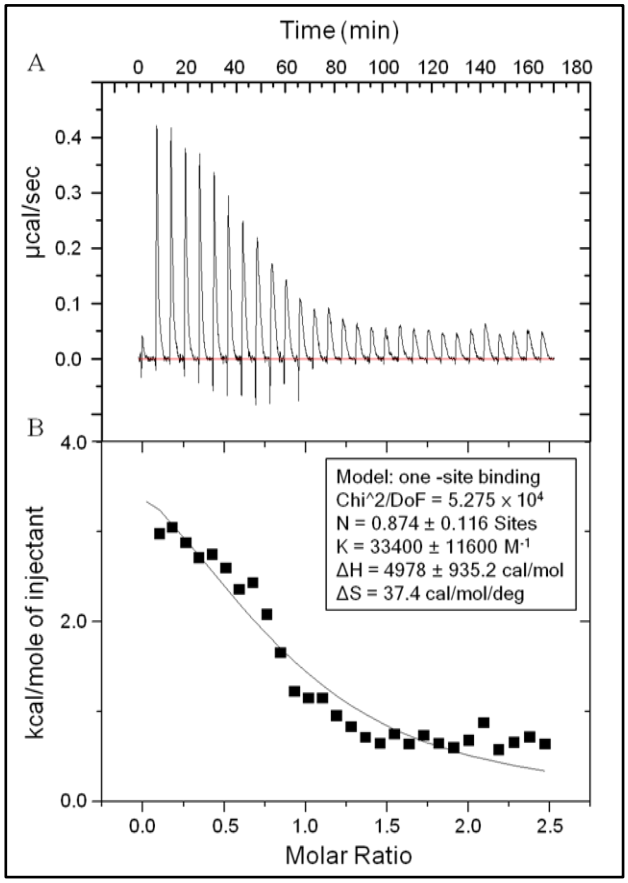

Figure 4.20. ITC data of IMP titration with PfISN1_D172N mutant protein. (A) Thermogram representing magnitude of heat change per unit time during each injection of IMP, corrected for heat of dilution of IMP. (B) Integrated normalized heat change of each injection plotted against molar ratio of IMP/protein. Solid line shows fit to one-site binding model with best-fit parameters shown in inset. Value of N represents number of IMP binding sites per monomer of protein. For more details refer to 'materials and methods' section.

4.3.5 Allosteric site in PfISN1

The presence of an ATP binding site supports from the allosteric modulation of the enzyme's activity by ATP as described in Chapter 2. The structure of ATP-bound wild-type enzyme (PfISN1-ATP) reveals four ATP binding sites per tetramer. However, in the structure, only two ATP molecules are bound at a time and only in the two subunits having unstructured NTDs. In the PfISN1-ATP structure, the allosteric site lies in a cleft formed by helix 6 from the OD and helices 7 and 17 from the catalytic domain wherein H150 from the core domain interacts with ATP by forming a π-stacking interaction with the adenine moiety of ATP. Interestingly, ATP binds at the very place where the C10 loop (L430-Q444) is situated in the PfISN1-Apo structure, forcing the latter to leave the cleft (Fig. 4.21). In presence of ATP, no electron density was seen for the C10 loop, suggesting it to be destabilized.

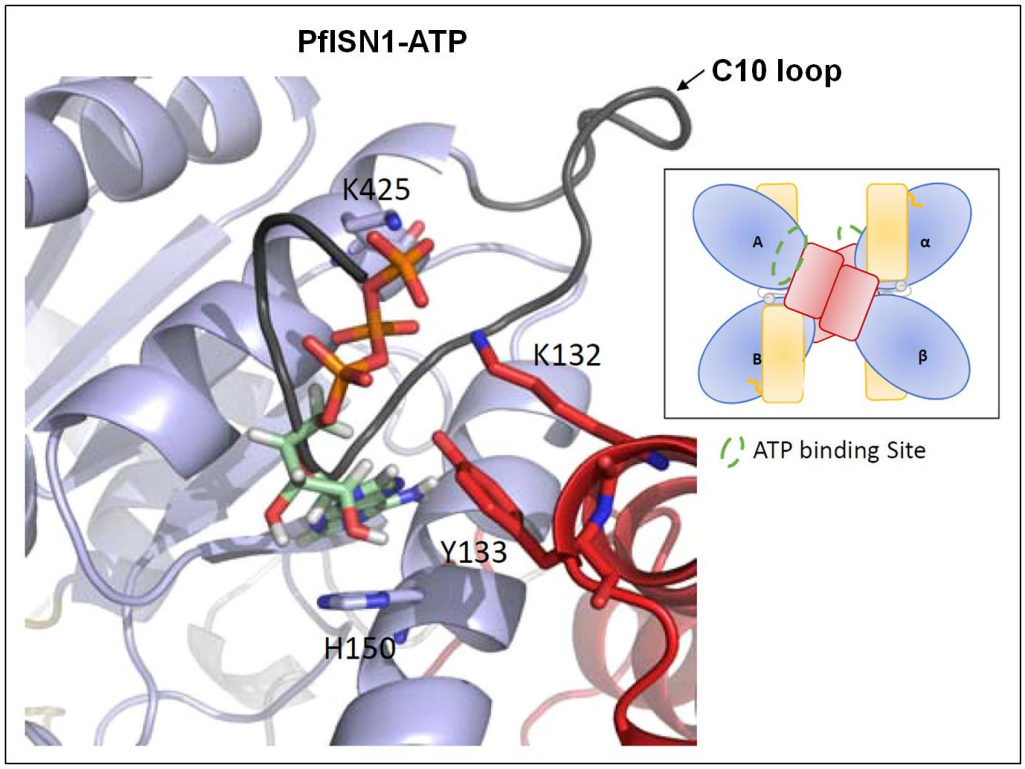

Figure 4.21. Allosteric site in PfISN1-ATP structure with the C10 loop from PfISN1-apo structure superposed. Residue H150 interacts with ATP. Inset shows location of the allosteric site in the tetrameric structure (top view). C10 loop from the apo structure is shown to be present in the allosteric site in the absence of ATP.

The PfISN1_H150V mutant showed 5-fold and 7-fold increase in IMP hydrolyzing activity at pH 8.0 and 5.0 as compared to wild-type enzyme, respectively but showed no activation by ATP (Fig. 4.22). This behavior was similar to that of the PfISN1_ΔC10 mutant (Fig. 4.3B). However, unlike the PfISN1_ΔC10 mutant, PfISN1_H150V was not inhibited by ATP. In both cases, absence of the C10 loop or its inability to bind to the allosteric site could be attributed to its increased activity. Moreover, the mutant PfISN1_H150V_ΔC10 also behaved similar to PfISN1_H150V (Fig. 4.22).

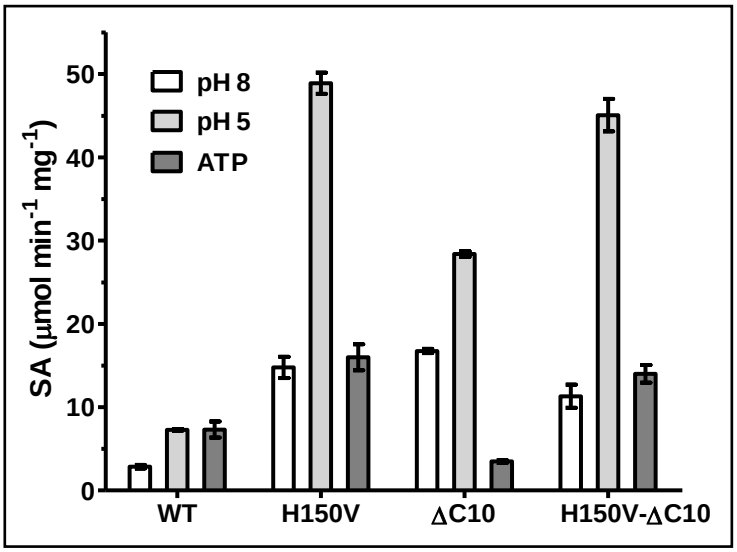

Figure 4.22. IMP-hydrolyzing activity of mutants PfISN1_H150V, ΔC10 and H150V-ΔC10 at pH 8.0 in the presence and absence of ATP and at pH 5.0. 10 mM IMP at pH 8.0, 0.5 mM IMP at pH 5.0 and 2 mM ATP were used in the assay.

The above observations lead to three important conclusions.

1. H150V is the residue that interacts with ATP and the C10 loop, but not simultaneously.

2. In the C10 mutant, inhibition of IMP-hydrolyzing activity by ATP is due to ATP binding exclusively to the allosteric site.

3. The C10 loop, through its interaction at the allosteric site, plays a regulatory role in enzyme function.

The third observation was further confirmed by a detailed kinetic characterization of the PfISN1_ΔC10 mutant which revealed that at pH 8.0, the enzyme had a 3-fold higher V_{max} and 3-fold lower K_m than the wild-type enzyme, increasing its catalytic efficiency 9-fold higher than the wild-type enzyme. At pH 5.0, the enzyme had a 6-fold increase in V_{max} and a 5-fold increase in K_m, having no significant change in catalytic efficiency as compared to the wild-type enzyme (Fig. 4.23). Substrate titration plots under the above conditions for PfISN1_ΔC10 were hyperbolic in nature (see appendix C).

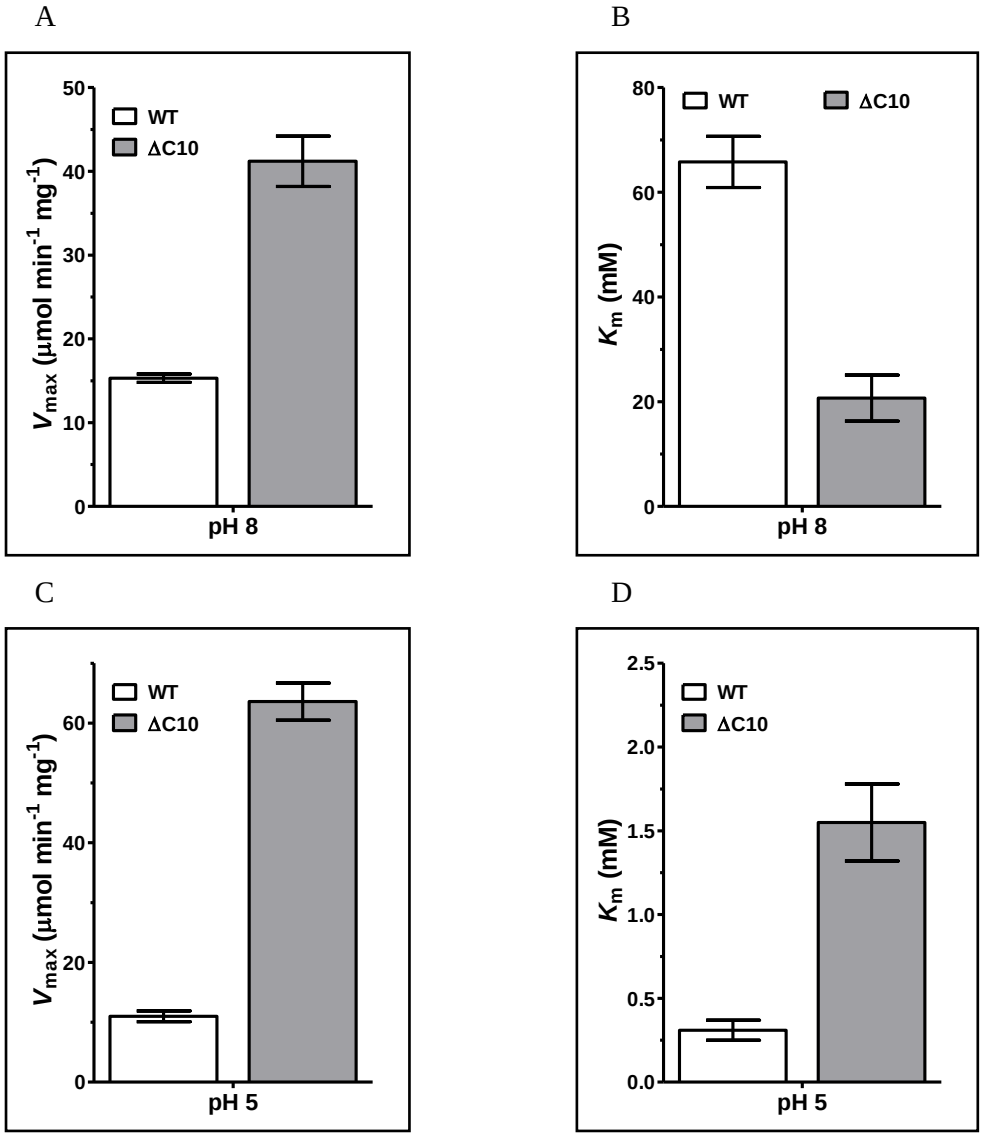

Figure 4.23. Kinetic parameters (V_{max} and K_m) of PfISN1_ΔC10 at (A, B) pH 8.0 and (C, D) pH 5.0.

4.3.6 Conformational changes induced upon ATP binding in PfISN1

Upon ATP binding, the enzyme undergoes a conformational change where the core and cap domains bend, thereby adopting a conformation that is more closed than that of the PfISN1-apo structure. Moreover, due to the interactions at interface 1, the ATP induced closure of two of the subunits force the other two subunits to open slightly. Active site architecture does not change significantly even in the presence of ATP (Fig. 4.24A) except for residue D178 which interacts with D172 in the presence of IMP-Mg^{2+}. In the PfISN1-ATP structure, it is closer to D172 than in the PfISN1-apo structure (Fig. 4.24B). Moreover, ATP molecules were not observed in the PfISN1_D172N-IMP-Mg^{2+} structure despite addition of ATP prior to crystallization, possibly due to the flip of F396 residue which occurs due to reorganization of motif IV

loop during IMP-Mg^{2+} binding. Upon flipping, F396 forms a long distance π-stacking interaction involving W413, R149 and H150 (Fig. 4.24C). Upon interacting with F396, H150 can no longer form a π-stack with the adenine base of ATP, forcing it out of the allosteric site. The importance of W413 is supported by the fact that the mutant PfISN1_W413L was inactive with IMP (Fig. 24D). To summarize, ATP activates the enzyme by preparing it for an induced-fit conformation by triggering the departure of the C10 Loop which in turn induces partial cap domain closure and bending of the subunit both of which are seen during IMP-Mg^{2+} binding.

4.3.7 Proposed catalytic mechanism in PfISN1

Based on the interaction of key residues with the ligands and the conformational changes induced during ligand binding, a mechanism of function in PfISN1 enzyme at physiological pH has been proposed. Upon IMP-Mg^{2+} binding, residues of motif I and IV are reoriented towards the active site in order to interact with the substrate. This is favored by the breaking of two salt-bridges (D60-R406 and K41-D394) which not only allow motif IV loop to reorganize but also contribute to reorganization of the NTD. The reorganization of NTD is a critical for enzyme function, as supported by the highly compromised activity of PfISN1_ΔN60 mutant. Reorientation of F396 from motif IV and its subsequent interaction with H150 forces destabilization of the C10 loop. Alternatively, presence of ATP at the allosteric stie also forces destabilization of the C10 loop. In either case, this destabilization triggers the bending of the subunit that increases the affinity for IMP. This observation is supported by the increased catalytic efficiency of PfISN1_ΔC10 mutant.

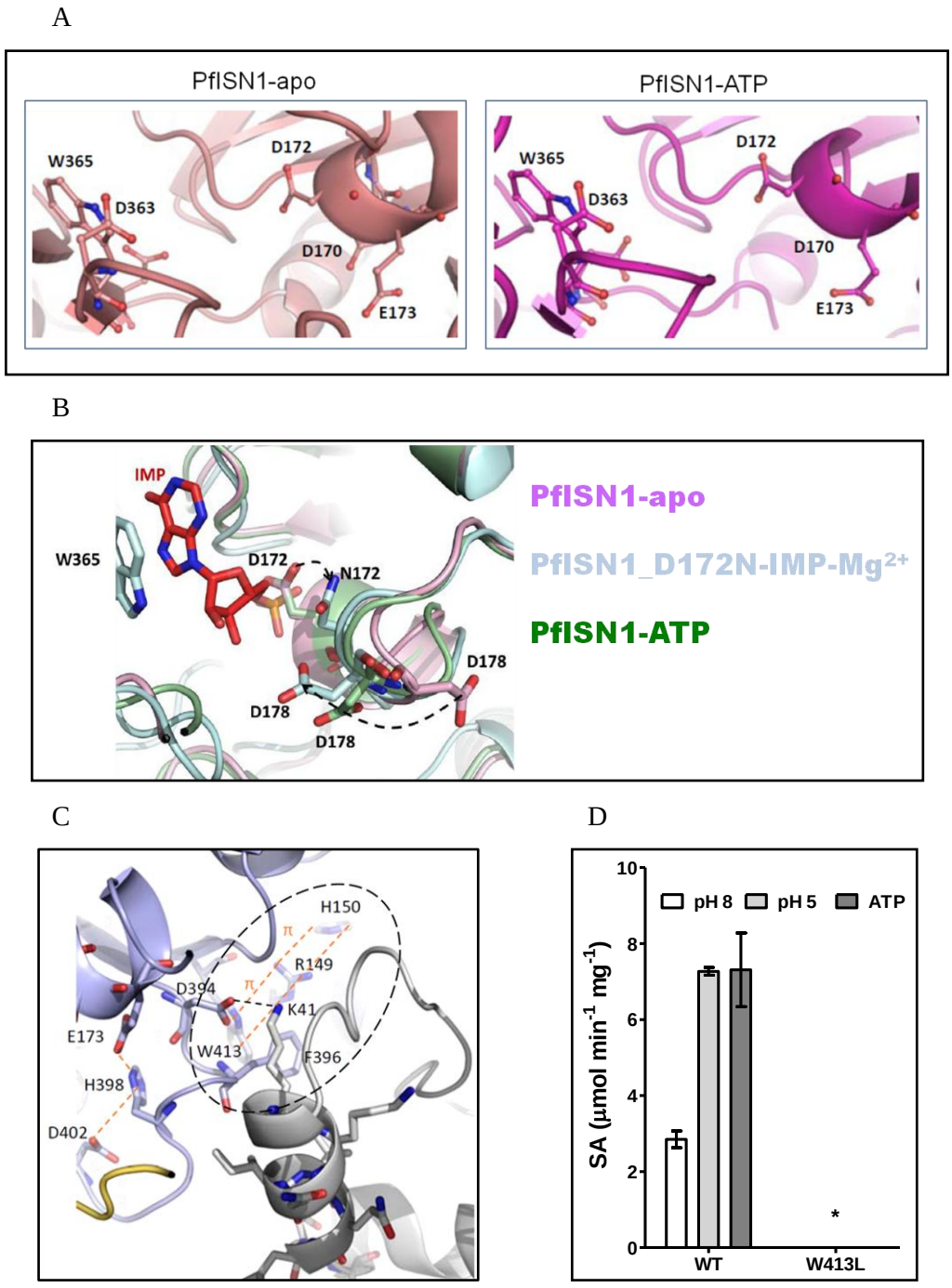

Figure 4.24. Conformational changes induced upon ATP binding. (A) Comparison of active site architecture between PfISN1-apo (left) and PfISN1-ATP structures (right). (B) Position of residue D178 in the PfISN1-apo, PfISN1-ATP and PfISN1_D172N-IMP-Mg^{2+} structures. (C) Long distance π-stack between F396 and H150. This interaction can also be seen in Fig. 4.16A (right panel). (D) IMP-hydrolyzing activity of PfISN1_W413L compared to wild-type enzyme at pH 8.0 in the presence and absence of ATP, and at pH 5.0. 10 mM IMP and 2mM ATP were used in the assay. SA indicates specific activity.

Further, hydrolysis of IMP-Mg^{2+} requires reopening of the enzyme to be able to release the newly formed inosine. In this conformation, the salt bridge between D60 and R406 is formed, while the formation of the phosphoaspartyl-enzyme intermediate allows the motif IV loop to reorganize and the NTD to return to its initial conformation. The return to PfISN1-apo conformation allows the release of the inosine to the medium, replaced by water molecules that will hydrolyze the phosphoaspartyl-enzyme intermediate. Finally, the conformation is stabilized by the return of the C10 loop into the allosteric site.

4.5 Conclusion

The crystal structures of PfISN1 protein under various conditions are the first structures to be reported for an ISN1 family protein. The domain organization and tetrameric assembly of the protein show several features that are different from mammalian 5'-nucleotidases. The core domain architecture however remains conserved, as found in other HAD members. The cap domain represents a C2-type structure. Two other domains NTD and OD are unique to this structure amongst 5'-nucleotidases. The active site in the PfISN1_D172N-IMP-Mg^{2+} is composed of the conserved motif residues as well as several other conserved and non-conserved residues that interact with IMP or Mg^{2+} and play a role in enzyme function. The features of the PfISN1-ATP structure have enabled the understanding of the mechanism of allosteric activation of PfISN1 enzyme by ATP. The regulatory role of NTD and C10 loop in enzyme function is a unique feature of PfISN1 enzyme, not reported previously in 5'-nucleotidases. Significant conformational changes including cap domain closure, destabilization of NTD and reorganization of motif IV loop (D394-R406) are observed upon ligand binding, which have provided a great deal of information regarding the mechanism of catalysis and allosteric regulation in PfISN1. This study has provided insight into the catalytic mechanism, allosteric regulation and structure-function relationship of PfISN1 enzyme.

4.6 Acknowledgement

We thank Prof. Raghavan Varadarajan (Dept. of MBU, IISc, Bangalore) for allowing us to use the VP-isothermal titration calorimeter for ITC experiment and their lab members Aparna and Deva for their assistance.

Chapter Five

Localization of PfISN1 in the intraerythrocytic stages of Plasmodium falciparum

Table of Contents

5.1 Abstract

Probing the *in vivo* physiological role of PfISN1 protein is critical in understanding the importance of the protein in *P. falciparum* metabolism. The localization of the protein in various asexual and sexual intraerythrocytic stages of the parasite was probed by indirect immunofluorescence using polyclonal antibodies raised in rabbit against the purified recombinant PfISN1 protein and visualized by confocal microscopy. In all the stages, the protein was found to be localized in the cytosol.

5.2 Introduction

Life cycle of *P. falciparum* involves two hosts. *P. falciparum* sporozoites are injected from an infected female *Anopheles* mosquito into the human host during a blood meal, where they migrate to the liver to initiate the hepatic stage. During this stage, they multiply and mature into schizonts which eventually rupture, with each schizont releasing several merozoites. These merozoites enter the bloodstream and invade erythrocytes to begin their intraerythrocytic life cycle (Fig. 5.1). During this cycle, the intraerythrocytic merozoites develop into the ring form, thereafter maturing into trophozoites and finally multiplying within the erythrocytes to form a schizont that upon rupturing releases several merozoites in the bloodstream. The merozoites invade fresh erythrocytes. Some merozoites escape this asexual cycle to form sexual stage gametocytes.

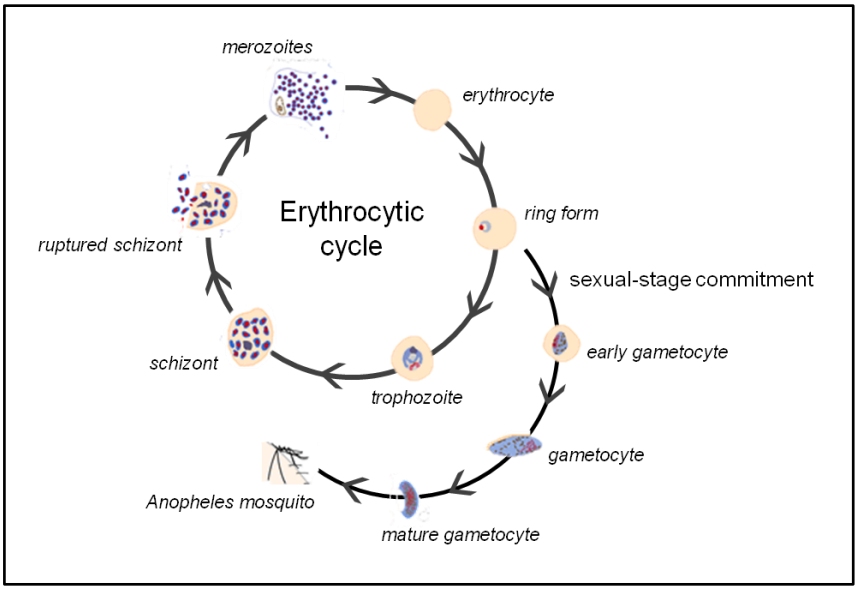

Figure 5.1. An illustration of the intraerythrocytic stages of life cycle of *P. falciparum* in the human host. Figure adapted from Centre for Disease Control and Prevention (Cdc, 2010) – Malaria at www.cdc.gov/malaria/about/biology.

Morphology of the various stages, as observed in Giemsa-stained smears of the parasite culture, is illustrated in Figure 5.2.

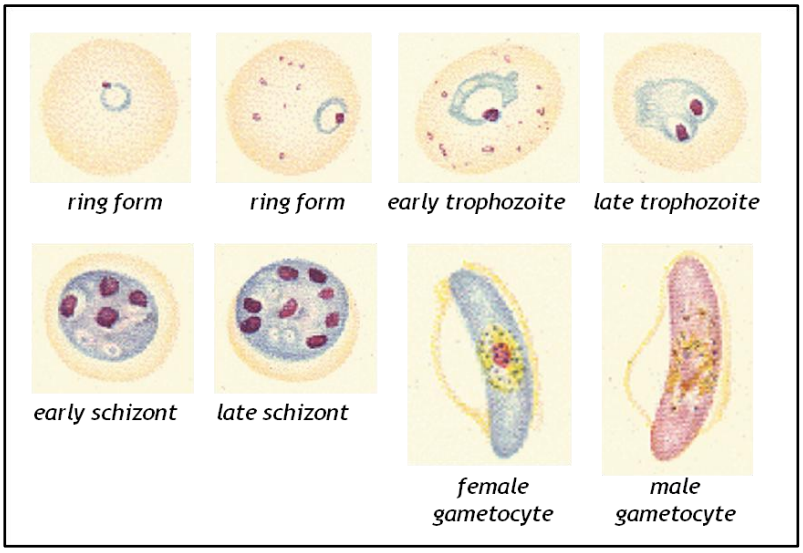

Figure 5.2. An illustration describing the morphology of various intraerythrocytic stages of *P. falciparum* life cycle, as seen under a light microscope after staining the blood smear with Giemsa stain [Hanssen 2010, Bannister 2000].

With the advancement of culturing techniques, *in vitro* culturing of the intraerythrocytic stages of *P. falciparum* has become a routine task and has been widely used for various *in vivo* studies like genomic, transcriptomic, proteomic and metabolomic profiling, immunocytochemical assays and genetic manipulation. Functional analysis of a gene can be conducted by manipulating gene function at the transcriptional, translational or protein level and studying the phenotypic changes associated with it.

5.3 Materials and methods

5.3.1 *In vitro* maintenance and synchronization of *Plasmodium falciparum* culture

Culture maintenance - The *in vitro* culture of the erythrocytic stages of the 3D7 strain of *P. falciparum* was maintained at 37 C in a candle jar (Trager and Jensen, 1976). The parasites were maintained on human erythrocytes at 5 % hematocrit, isolated from O+ blood collected from healthy volunteers in a culture medium containing RPMI-1640 (10.4 g/L), HEPES (5.94 g/L), sodium bicarbonate (0.2%), Albumax-I (0.5%), hypoxanthine (0.1 mM), glucose (0.45%) and gentamycin (40 mg/L). The parasitaemia of the culture was monitored every alternate day by making Giemsa-stained smears.

Culture synchronization – The culture was synchronized using 5% D-sorbitol. Ring-stage parasite culture at 5 % parasitemia was washed with 1X PBS to remove the culture medium. Five volumes of 5% sorbitol was added to volume of the culture pellet and incubated at room temperature for 5 minutes. The pellet was washed with complete medium to remove sorbitol and resuspended in the medium. This procedure lyses trophozoite and schizont-stage parasites while ring-stage parasites are resistant to sorbitol (Lambros and Vanderberg, 1979).

5.3.2 Production and enrichment of sexual stage gametocytes

For obtaining higher levels of gametocytes in the culture, the 3D7A cell line (MRA-151; MR4—Malaria Research and Reference Reagent Resource Centre, Manassas, USA was used since it has a higher sexual conversion rate. Gametocyte production and enrichment was done as described by Fivelman et al. (Fivelman et al., 2007). Briefly, at day 0, the synchronized ring-stage culture was stressed by the addition of fresh medium with a certain percentage of spent (parasite-conditioned) medium left behind, which may contain factors stimulating sexual stage development (Williams, 1999). The ratio of conditioned/fresh medium was decided based on the parasitaemia, with a higher ratio for lesser parasitaemia. At day 1, stressed schizonts were split by increasing the hematocrit from 3% to 4%. From day 0, 50 mM N-acetylglucosamine (NAG) was added to the medium, which eliminates the asexual stage parasites by preventing erythrocyte reinvasion (Ponnudurai et al., 1982). From day 6 to day 12, mid to late-stage gametocytes were observed in the Giemsa-stained smears.

5.3.2 Generation and purification of polyclonal anti-PfISN1 antibody

Purified recombinant PfISN1 (200 μg) was emulsified with equal volume of incomplete Freund's adjuvant and injected subcutaneously into a New Zealand white rabbit, followed by two booster doses, each 15 days apart. A small volume of blood was collected from the rabbit 15 days post second booster to check for antibody titer by a dot blot assay, followed by a major bleed. The serum was separated by centrifugation after coagulation of blood and stored in multiple aliquots at -20 °C. The polyclonal antibodies from the serum were purified by affinity chromatography using Sepharose beads conjugated to purified recombinant PfISN1. PfISN1-conjugated Sepharose beads were generated using purified ISN1 and CNBr-activated Sepharose. PfISN1-specific antibodies were isolated by overnight incubation of the serum with PfISN1-conjugated beads followed by elution of the bound antibody with 50 mM glycine, pH 2.8. The eluates were collected into tubes containing 50mM Tris HCl, pH 8.0. The positive

fractions were pooled, concentrated and stored in separate aliquots at -20 °C. These were used as anti-PfISN1 antibodies. Institutional animal ethics committee clearance for all animal-related experiments and procedures was obtained.

5.3.3 Immunobinding assays to determine the titer and specificity of PfISN1 antibody

Immunobinding assays involve estimation of the titer and specificity of antigen-antibody interaction through immunoblotting. Western blot analysis is widely used to determine the specificity of the antibody (Towbin et al., 1979; Burnette, 1981).

Western blot - The recombinant PfISN1 protein was run on a 12% SDS-PAGE gel alongside a pre-stained molecular weight marker ladder and transferred to a PVDF membrane using a Hoefer™ wet transfer apparatus (Hoefer® Inc. USA). The PVDF membrane was activated with methanol for 10 min prior to use. The membrane was then blocked with 2.5 % skimmed milk powder-containing PBS solution for 8 hours at 4 °C. The membrane was then incubated with the affinity-purified antibody at a dilution of 1:2000. The membrane was then washed with PBS solution containing 0.1 % Tween 20 and further incubated with anti-rabbit antibody conjugated with horseradish peroxidase (HRP) enzyme (1:1000 dilution) for 3 hrs at 4 °C. Following adequate washes, a chromogenic substrate, 3-amino-9-ethylcarbazole (AEC) was added to the membrane, which is oxidized by HRP in the presence of hydrogen peroxide to form a red insoluble precipitate, appearing as a red stain on the membrane.

Dot blot - The dot blot analysis is a simplified form of the western blot, used to estimate the antibody titer, which is the maximum antibody dilution at which a positive signal is obtained (Hawkes et al., 1982). 2 µg of the antigen was spotted on nitrocellulose membrane. The membrane was then blocked with 5 % skimmed milk powder containing phosphate-buffered saline (PBS) solution. The membrane was then washed with 0.1 % Tween 20 containing PBS solution. The membrane was then incubated with various dilutions of the purified antibody. After an adequate number of washing steps, the membrane was incubated with horseradish peroxidase (HRP) conjugated anti-rabbit antibody (1:1000 dilution) for 1 hr at room temperature. Following adequate number of washes, a chromogenic substrate, 3-amino-9-ethylcarbazole (AEC) was added to the membrane, which is oxidized by HRP in the presence of hydrogen peroxide to form a red insoluble precipitate, appearing as a red stain on the membrane.

5.3.4 Indirect immunofluorescence confocal microscopy

To check the *in vivo* localization of PfISN1 in the intraerythrocytic stages of *P. falciparum*, indirect immunofluorescence microscopy was used. The protocol used was as described in Tonkin et al. (Tonkin et al., 2004). Briefly, the parasite culture was fixed with 4% paraformaldehyde, permeabilized with 0.08% Triton X-100 and incubated with anti-PfISN1 primary antibody (1:400), followed by Alexa®-Fluor-488-conjugated goat anti-rabbit-IgG (Thermo Fisher Scientific Inc., USA) secondary antibody (1:1000). Hoechst® 33342 (Thermo Fisher Scientific Inc. USA) dye (1:2000 in PBS solution) was used to stain the nucleus. Thereafter, the culture was smeared on polylysine-coated slides and sealed with thinner. The images were acquired using Zeiss® LSM META 510™ laser-scanning confocal microscope and analyzed with Zeiss® LSM Image Examiner software.

5.3.5. Probing the physiological function of PfISN1 *in vivo*

Generation of pISN1GDB plasmid - The Pf3D7_1206100 gene fragment corresponding to a length of 1473 base pairs upstream of the 3' end of the coding strand (Pf3D7_1206100') was amplified using the following primers, containing *Xho*I (highlighted bold in forward primer) and *Avr*II (highlighted in bold in reverse primer) restriction sites at the 5' and 3' ends respectively.

Forward primer - 5' GAATAT**CTCGAG**GAACATTGCCATAGTGACAGCAGC 3'

Reverse primer - 5' CTGCTA**CCTAGG**TTGATTTTCATATAAAACTTCCGGAATAAATG 3'

The amplicon and pGDB plasmid were digested with *Avr*II and *Xho*I, and ligated to form the pISN1GDB plasmid and transformed into *E. coli*. The sequence of the cloned insert was confirmed by DNA sequencing. It contained the 3'-end of the coding sequence of PfISN1_1206100 gene in frame with the regulatable fluorescent affinity (RFA) tag.

Transfection in P. falciparum parasites by pre-loading of DNA into erythrocytes – For transfection, endotoxin-free pISN1GDB plasmid DNA was isolated using the Qiagen Endofree Plasmid Maxi kit (Qiagen, Netherlends). *P. falciparum* parasites have been shown to spontaneously uptake DNA from the cytoplasm of host erythrocytes, pre-loaded with the plasmid DNA through electroporation (Deitsch, 2001). This method has advantages over direct transfection into parasite-infected erythrocytes. The transfection procedure is described with a flow-chart in Figure 5.3. On day 0, 100 µg of pISN1GDB plasmid was resuspended in 400 µl of chilled cytomix buffer (120 mM KCl, 0.15 mM $CaCl_2$, 2 mM EGTA, 5 mM $MgCl_2$, 10 mM K_2HPO_4/KH_2PO_4 and 25 mM HEPES, pH

7.6). 1 ml of fresh chilled erythrocytes at 50% hematocrit were washed with 5 ml of chilled incomplete cytomix buffer, resuspended in the pISN1GDB-cytomix solution, and added to a pre-chilled electroporation cuvette (0.2 cm gap Gene Pulser®/MicroPulser™ cuvette (Bio-Rad Laboratories, Inc.)). Electroporation was carried out for two batches of the suspension, by applying a square wave pulse to batch I and an exponential decay wave pulse to batch II, using a Gene Pulser Xcell™ electroporator (Bio-Rad Laboratories, Inc.). Details of the electroporation program and critical evaluation parameters are given in flow-chart (Fig. 5.3). After the pulse, the suspensions was transferred to a sterile tube, washed and resuspended with warm (37 °C) culture medium. To both the batches, 1 ml of healthy schizont-stage *P. falciparum* PM1KO parasites at 5-6 % parasitemia were added. The culture was maintained as described in section 5.3.1. From day 1 onwards, 5 µM TMP was added to the culture medium for both the batches and Giemsa-stained smears were prepared every alternate day to monitor parasitemia. The pISN1GDB plasmid also contained a blasticidin (BSD) resistance cassette that allowed for positive selection of plasmid integration using the drug. Once the cultures attained a minimum of 4-6 % parasitemia, 2.5 µg/ml of BSD was added to the culture medium (batch I – day 3, batch II – day 7) for positive selection of the transfectants. Further on, both TMP and blasticidin were added to the culture medium and Geimsa-stained smears were prepared every alternate day to monitor parasitemia. However, parasites failed to appear in either of the batches after 30 days post drug pressure.

The pGDB plasmid and the PM1KO strain were kind gifts from Prof. Daniel Goldberg (School of Medicine, Washington University, St. Loius, MO, USA).

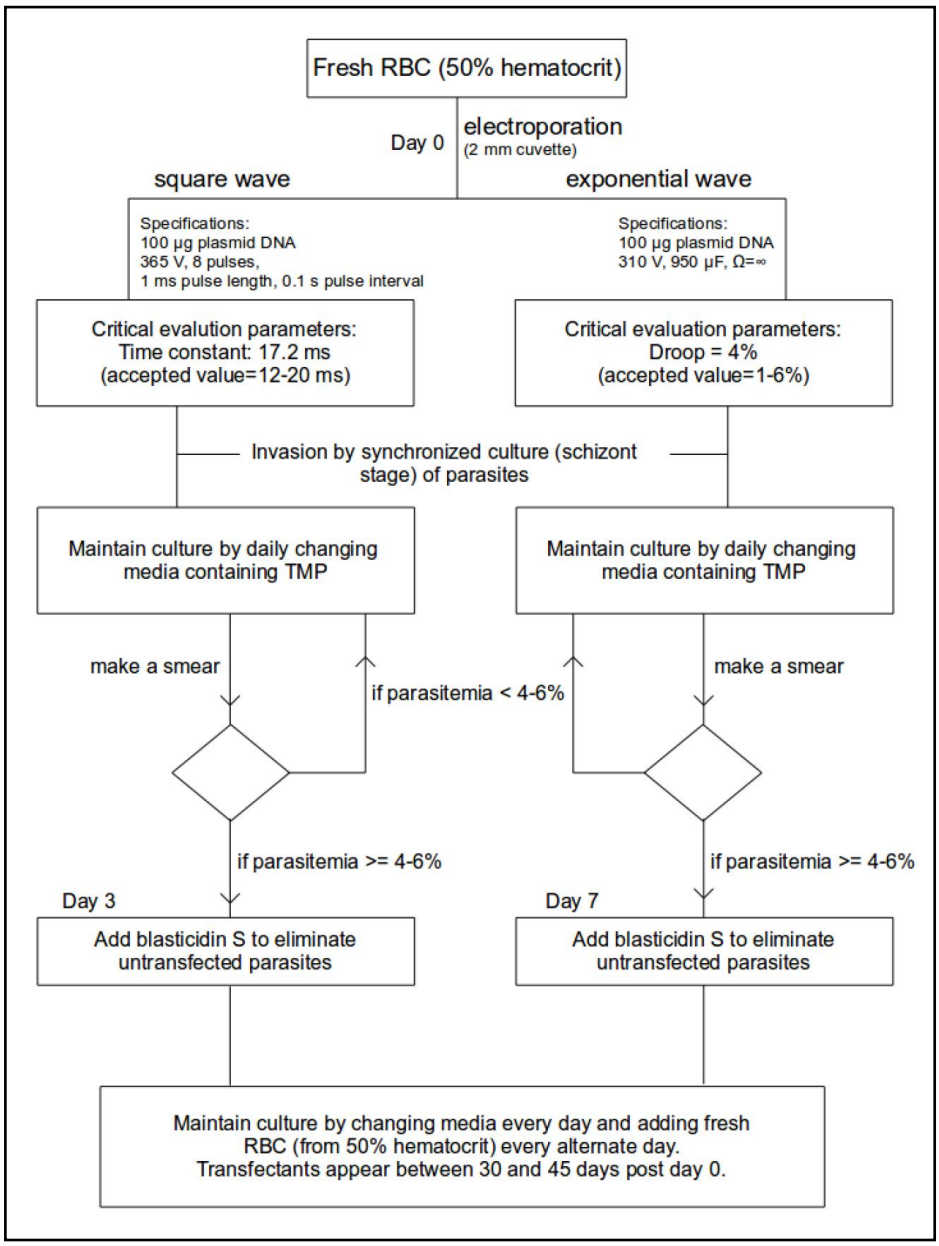

Figure 5.3. Flow-chart describing the procedure of transfection of *P. falciparum* PM1KO parasites by pre-loading of uninfected erythrocytes.

5.4 Results

5.4.1 Generation of polyclonal anti-PfISN1 antibodies in rabbit.

For immunocytochemical studies, antibodies against recombinant PfISN1 protein were raised in rabbit and affinity-purified by antigen interaction. Anti-PfISN1 antibodies in the purified fraction were detected up to a dilution of 1:10000 (Fig. 5.4).

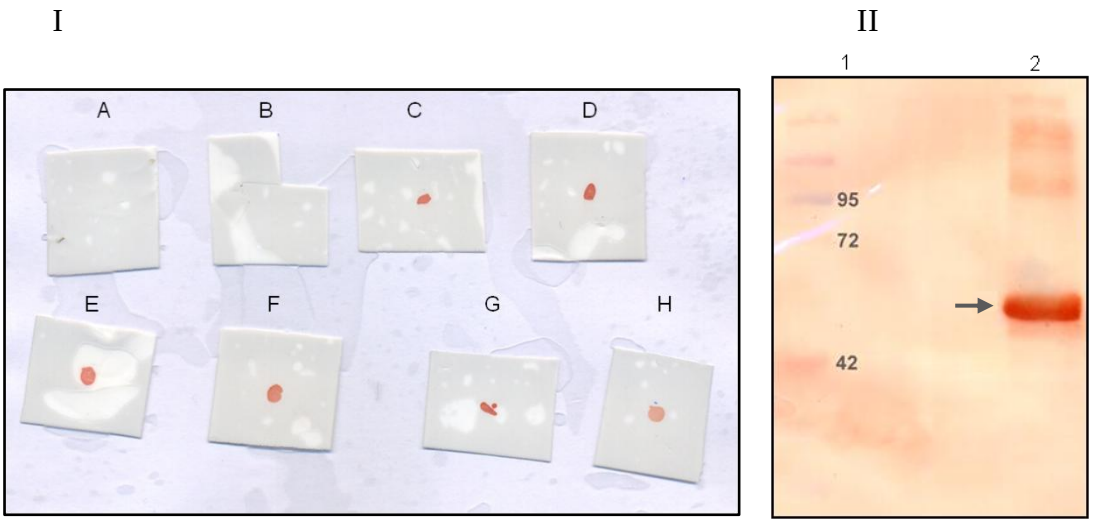

Figure 5.4. (I) Dot blot for detection of anti-PfISN1 antibody purified by affinity chromatography. Pre-immune serum 1:500 dilution (A). Blot without antigen (B). Purified anti-PfISN1 antibody at 1:500 (D), 1:1000 (G), 1:2000 (C), 1:4000 (E), 1:5000 (F) and 1:10000 (H) dilutions. (II) Western blot for detection of purified anti-PfISN1 antibody (1:1000 dilution). Lane 1 contains molecular weight (kDa) markers, lane 2 contains rabbit anti-PfISN1 antibody. A single band highlighted by a solid black arrow in lane 2 matches the molecular weight of recombinant PfISN1 protein, indicating the presence of specific anti-PfISN1 antibodies.

5.4.2 Localization of PfISN1 protein in *Plasmodium falciparum*

Indirect immunofluorescence was carried out to probe localization of PfISN1 protein using purified rabbit anti-PfISN1 antibodies as the primary antibodies. In order to rule out non-specific signal, a primary antibody (Fig. 5.4A) and pre-immune serum controls (Fig. 5.4B) were performed, which showed no significant fluorescence signal. The protein was found to be localized in the cytosol in all the intraterythrocytic stages of the protein (Fig. 5.5). The nucleus was stained using Hoechst® 33342 dye which binds to double-stranded DNA and emits a blue fluorescent signal.

A. No primary antibody control

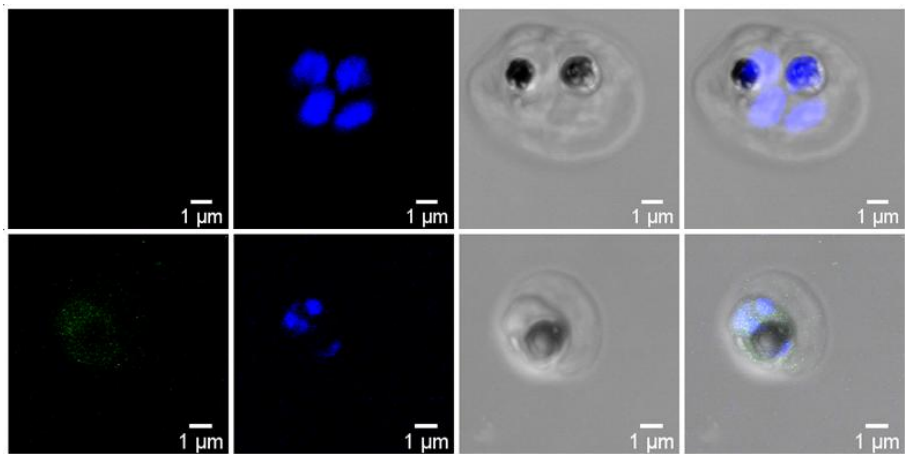

B. Pre-immune serum control

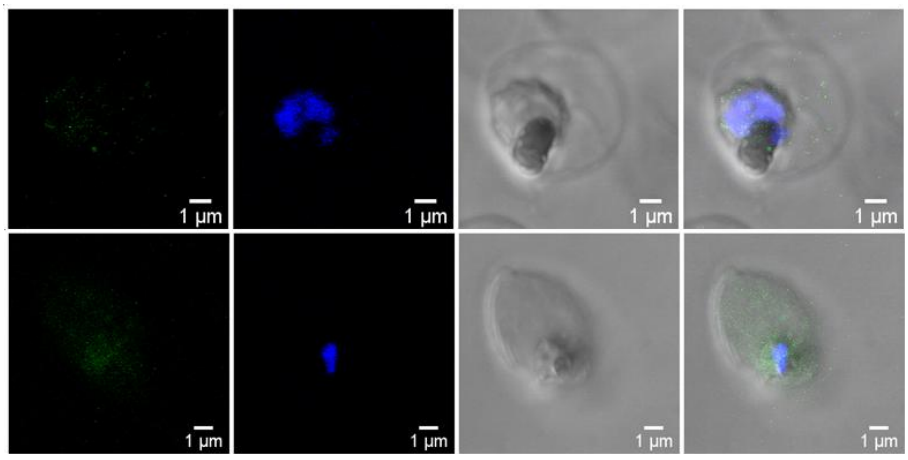

C. Ring form

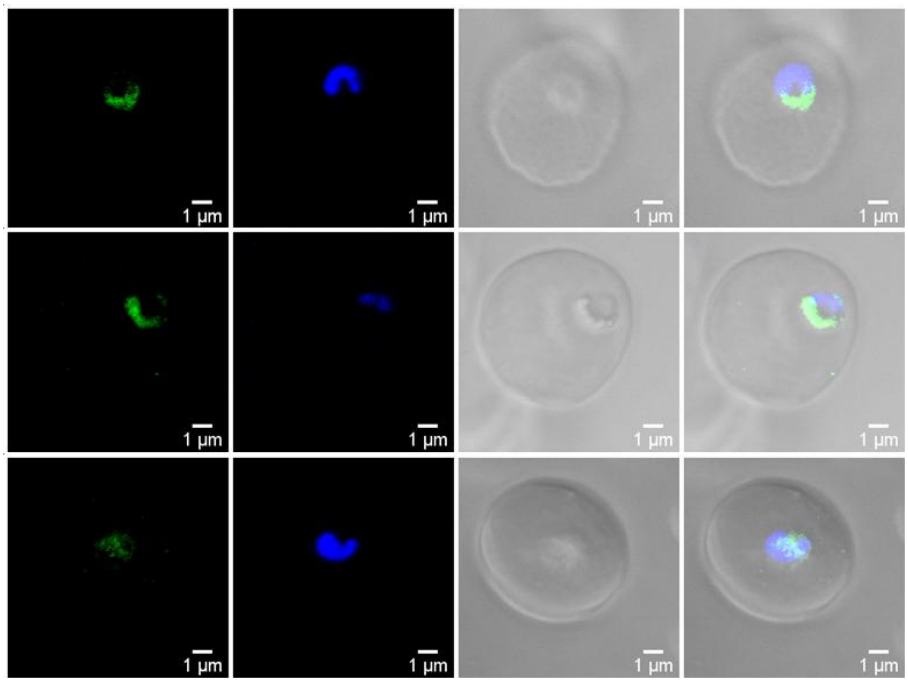

(figure continued on next page)

D. Schizont

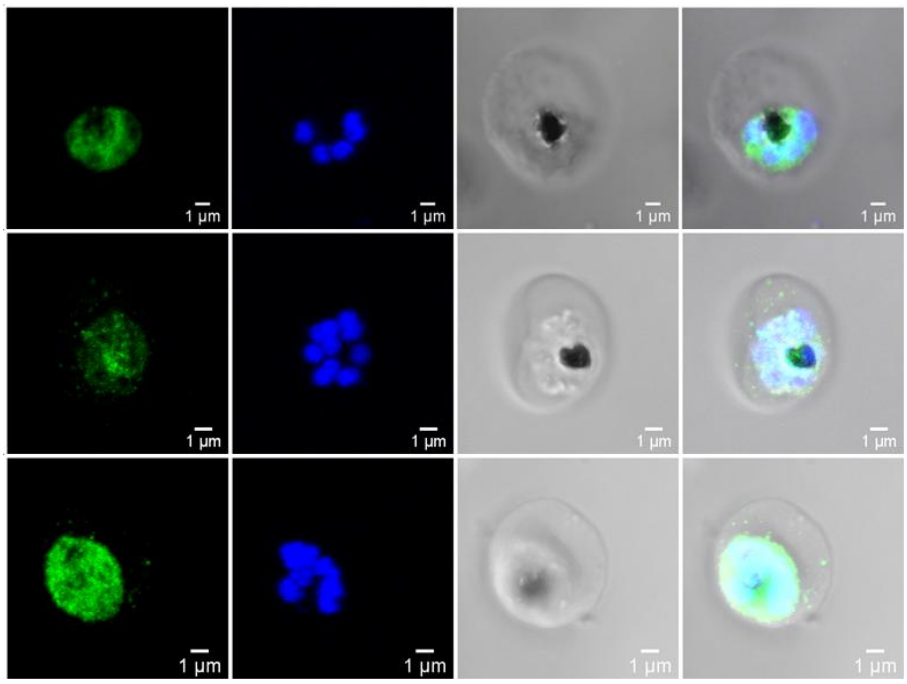

E. Trophozoite

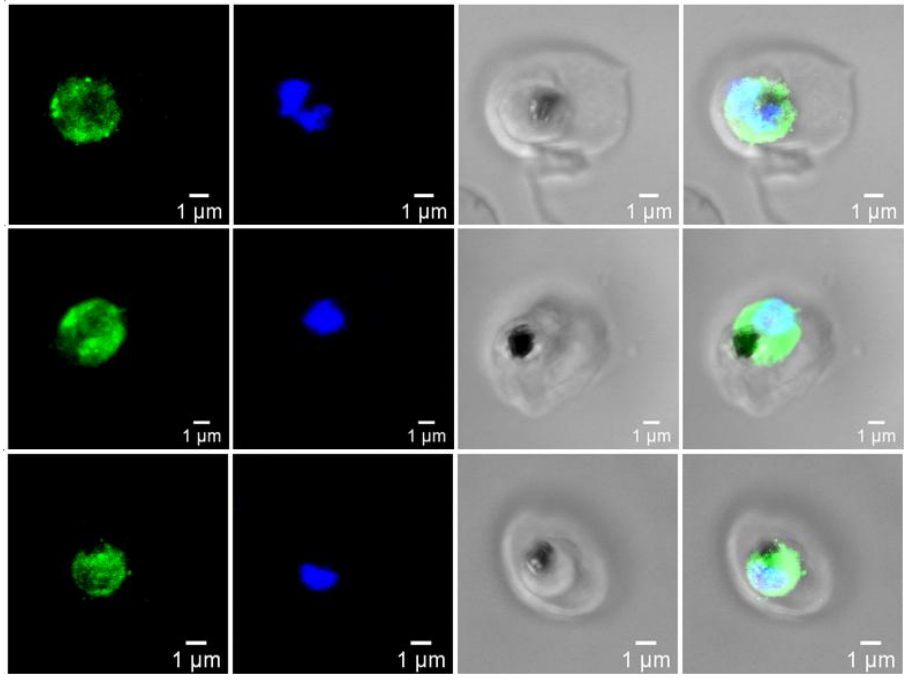

(figure continued on next page)

F. Gametocyte

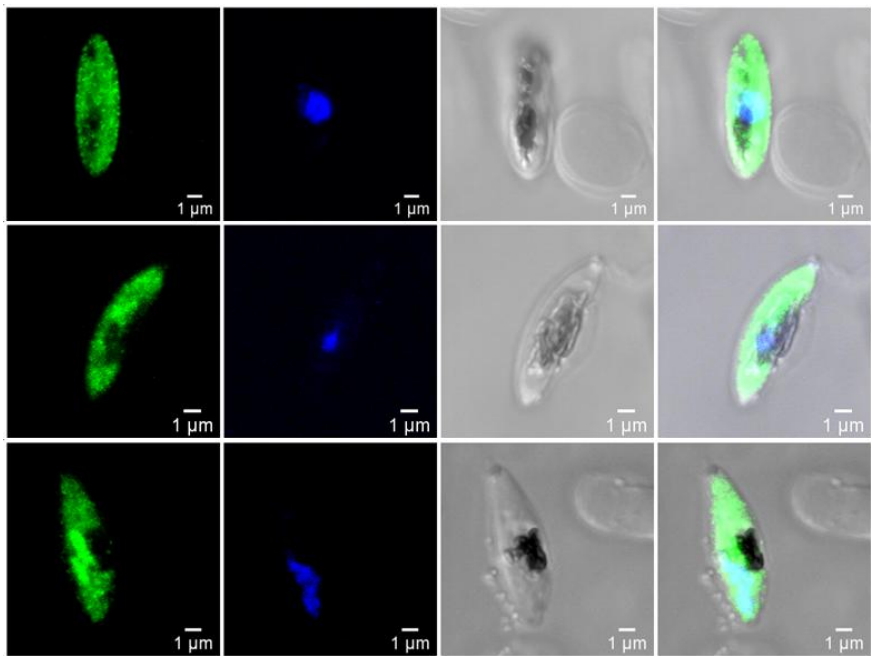

Figure 5.5. Localization of PfISN1 in asexual and sexual intraerythrocytic stages of *P. falciparum*. (A) Control with no primary (anti-PfISN1) antibody. (B) Control with pre-immune serum as primary antibody. (C) Ring form, (D) schizont, (E) trophozoite and (F) gametocyte stages with affinity-purified rabbit anti-PfISN1 antibody. In each image, panel 1 shows fluorescence from Alexa® 488, panel 2 from Hoechst® and panel 3 shows differential intereference contrast (DIC) image. Panels 1, 2 and 3 are merged in panel 4. Scale bar has been inserted at the right-bottom corner of each panel. For details see 'Materials and Methods' section.

5.4.3 Probing the physiological role of PfISN1 protein *in vivo*

The *in vitro* kinetic studies done on recombinant PfISN1 show that IMP is its most preferred physiological substrate (chapter 2), suggesting its important role in the purine salvage pathway. The enzyme has a pH-dependent kinetic profile. At high pH, the enzyme has a K_m for IMP much higher than intracellular IMP levels, causing the enzyme to be in an "off" state. However, it is activated in the presence of ATP and the K_m for IMP drops down to a much lower value, switching it to an "on" state. At low pH, the enzyme has only one state. It has a very low K_m value for IMP and the enzyme is in an "on" state with no modulatory effect of ATP. The low K_m state at low pH is the most efficient catalytic state of the enzyme, suggesting that the protein could be localized to an acidic intracellular compartment such as the food vacuole (Fig. 5.6). The intracellular location and physiological function of a protein are closely related. Immunofluorescence colocalization with pH-sensitive fluorescent dyes or food vacuole marker proteins can help in identifying organelle-specific localization of PfISN1 within the parasite. Acidotropic dyes like acridine orange, LysoTracker® and quinacrine are

low molecular weight fluorescent probes that localize specifically in acidic organelles (Pierzyńska-Mach et al., 2014). In *Plasmodium falciparum*, the chloroquine resistance transporter (CRT) protein is a widely used marker for the food vacuole membrane (Fidock et al., 2000; Cooper et al., 2002) while the merozoite surface protein 8 (msp8) is another marker protein localized in the food vacuole (Drew et al., 2005). Several studies pertaining to the localization of proteins in the food vacuole have been done in the recent past. Using transgenic parasites expressing GFP-tagged protein construct, Falcipain-2 (FP-2), a cysteine protease has been shown to be trafficked via the endoplasmic reticulum (ER) to the food vacuole (Dasaradhi et al., 2007). Using a similar approach, another protein called Plasmepsin-II, belonging to the family of aspartic proteases has also been shown to be trafficked to the food vacuole via cytoplasmic vacuoles and the ER (Klemba et al., 2004). Another important report is the localization of an M1-family aminopeptidase in the food vacuole, trafficked via the parasitophorous vacuole (Azimzadeh et al., 2010). The kinetic parameters of this enzyme also suggest that the enzyme maintains high catalytic efficiency at low pH (Ragheb et al., 2011), a case similar to PfISN1.

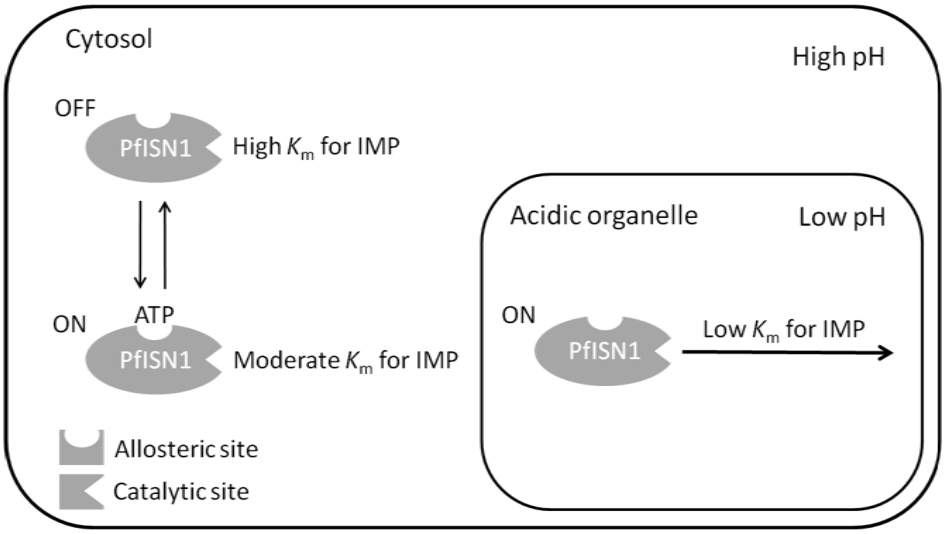

Figure 5.6. A schematic of the physiological implications of pH-dependent dual kinetic profile of PfISN1.

In order to understand the physiological role of PfISN1 in the parasite, its gene function must be probed *in vivo*. Despite the easy availability of *P. falciparum* culture, genetic manipulation has not been widely successful, partly due to the low transfection efficiency of the parasite. In spite of the low rate of functional analysis of *P. falciparum* genes, recent advances in molecular genetics have allowed successful targeted disruption of several genes (Webster and McFadden, 2014; de Koning-Ward et al.,

2015). Since knockout of essential genes is not feasible due to the haploid nature of the parasite genome, conditional systems that can regulate gene expression at the genome, transcriptional or protein level are being adopted (Armstrong and Goldberg, 2007). In a recent study, the function of a 28-residue asparagine repeat in Rpn6, a proteasome lid subunit protein, was probed using a regulatable fluorescent affinity (RFA) fusion tag which allowed protein regulation, probing live cell localization through fluorescence microcopy and affinity purification of the Rpn6 protein in *P. falciparum* (Muralidharan et al., 2011). This strategy was adopted for probing the function of PfISN1 *in vivo*. Briefly, a single-crossover homologous recombination strategy was used to fuse the RFA tag to the endogenous PfISN1 gene, PF3D7_1206100. A fragment from the 3'-end of PF3D7_1206100 gene coding for PfISN1 (Pf3D7_1206100') was cloned into pGDB plasmid (Fig. 5.7), in frame with the RFA tag. Details of the cloning procedure are described in the Materials and methods section.

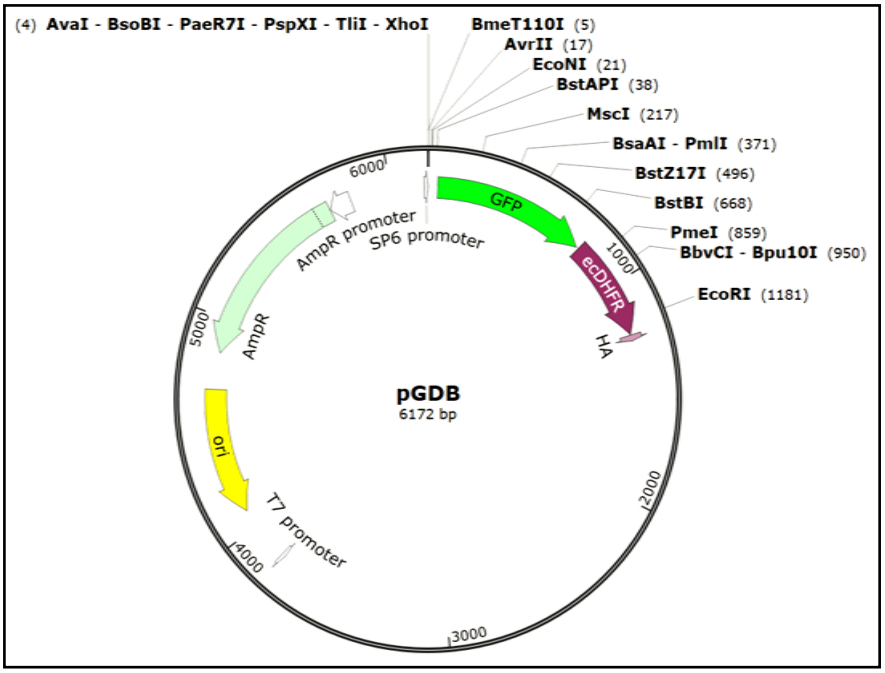

Figure 5.7. Map of pGDB plasmid with important features highlighted. The figure was generated using SnapGene® Viewer 4.1.2 (SnapGene software, GSL Biotech; available at www.snapgene.com).

Upon successful integration at the gene locus by a single site-specific homologous recombination, the fused construct would lead to the expressed fusion protein PfISN1-GFP-ecDHFR-HA, with green fluorescent protein (GFP), *E. coli* dihydrofolate reductase (ecDHFR) degradation domain and human influenza hemagglutinin (HA) tag at the C-terminal end of PfISN1. The ecDHFR degradation domain is destabilized in the absence of trimethoprim (TMP), leading to proteasomal degradation of the fusion

protein. Thus, addition of TMP to the culture medium stabilizes the degradation domain to prevent protein degradation. Localization of the protein can be observed in live cells by monitoring GFP fluorescence while the HA tag can be used to purify the fusion protein by affinity chromatography. A schematic diagram of this strategy is shown in Fig. 5.8.

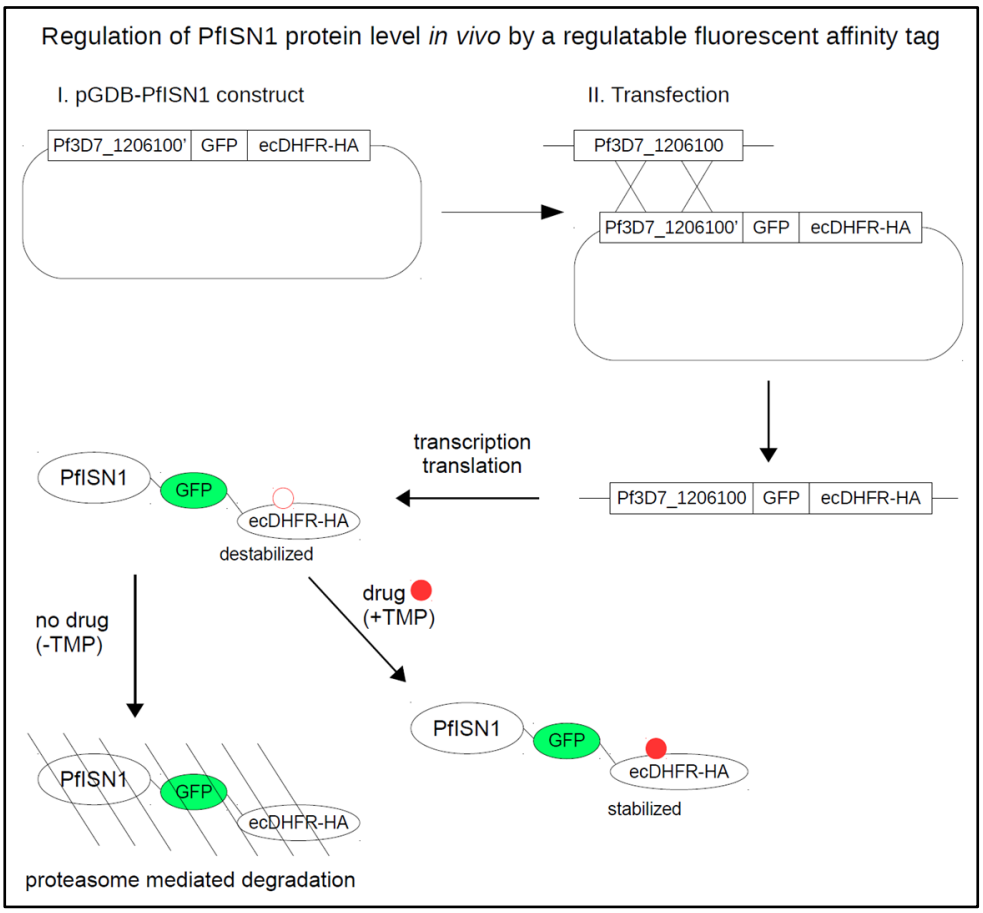

Figure 5.8. Schematic showing the pGDB-PFISN1 plasmid design and its application in context to monitoring and manipulating PfISN1 protein levels in *P. falciparum*. GFP, green fluorescent protein; ecDHFR, *E. coli* DHFR degradation domain; TMP, Trimethoprim.

The pISN1GDB plasmid was isolated and transfected into uninfected erythrocytes by electroporation. These erythrocytes pre-loaded with the plasmid were then invaded by a synchronized schizont-stage culture of the parasite. Details of the transfection procedure are provided in the Materials and methods section. Since TMP is toxic to the parasites, *P. falciparum* PM1KO strain was used, which contains a human DHFR (hDHFR) marker gene integrated via double crossover recombination into Plasmepsin I, a non-essential gene (Liu et al., 2005). The presence of the hDHFR marker renders the parasites resistant to TMP. A blasticidin (BSD) marker cassette in the pGDB plasmid allows for positive selection of transfectants. Parasites usually appear with 15-25 days

of applying drug pressure. However, parasites failed to appear even after 30 days of applying drug pressure (Fig. 5.9).

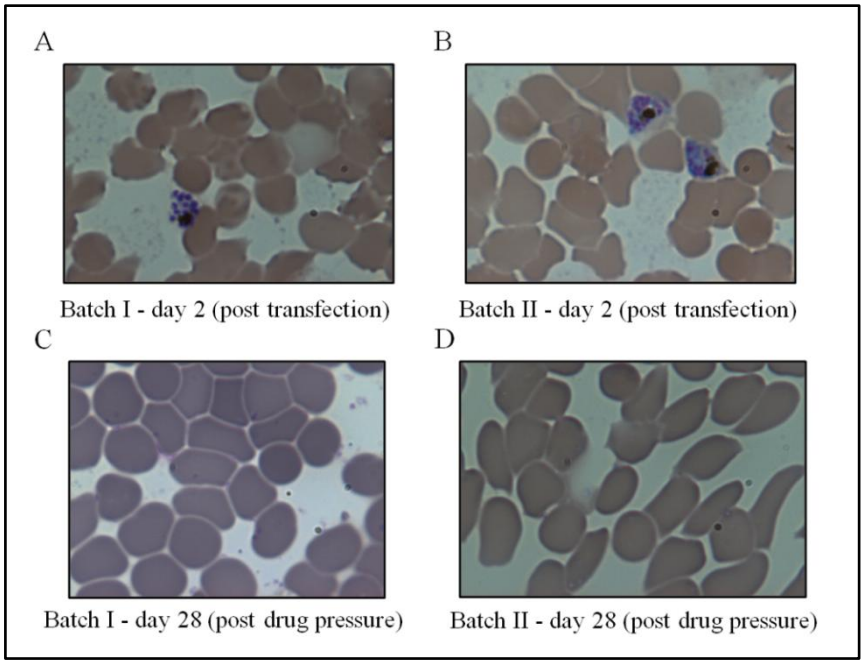

Figure 5.9. Giemsa-stained smears of *P. falciparum* PM1KO parasite cultures after transfection.

5.5 Conclusion

Using polyclonal anti-PfISN1 antibodies generated and indirect immunofluorescence, localization of the protein was probed in the intraerythrocytic stages of the parasite. To eliminate non-specific signal, a control without primary antibody and a pre-immune serum control were also performed, which showed no significant fluorescent signal. The protein was found to be localized in the cytosol in the asexual and gametocyte stages.

(This page is intentionally left blank)

Chapter Six

Conclusions and future directions

Table of Contents

A brief summary of the significant conclusions derived from this study on an IMP-specific 5'-nucleotidase from *P. falciparum* (PfISN1), and its future directions is given below. The summary includes biochemical characterization of the recombinant protein performed *in vitro*, including kinetic characterization, crystal structure and the structure-function relationship of several residues, as well as localization of the protein probed *in vivo* using indirect immunofluorescence microscopy and attempts using molecular genetics tools to probe the *in vivo* function of the protein.

6.1 The significance of 5'-nucleotidases and nucleotide metabolism in *Plasmodium*.

5'-nucleotidases play an important role in cellular metabolism. In the past seven decades, several mammalian 5'-nucleotidases have been biochemically characterized, revealing information about their substrate specificity, optimum conditions for activity, modulators and their physiological role. 5'-nucleotidases belong to the HAD superfamily of proteins, which is one of the largest superfamily containing over 70,000 proteins. However, only a little over 20,000 proteins have been functionally annotated. The vast sequence diversity amongst its members has made prediction of structure-function relationship a difficult task. Biochemical studies on various HAD members have revealed important information about their biochemical properties. Structural analysis of several HAD members have revealed conserved folds and motifs that are crucial for structure and function of these proteins.

Malaria is an infectious disease caused by *Plasmodium* species of parasite, with high mortality rates in developing countries. Efforts to prevent and eradicate malaria have been prevailing worldwide. The need for extensive research in areas of plasmodium biochemistry and anti-malarial drugs continues as the parasite has developed resistance against commonly used anti-malarial drugs (Socheat et al., 2003; Roberts, 2017). While anti-malarial drugs target the asexual stages of *Plasmodium* parasite in the human host, it is the sexual gametocytes that are responsible for transmission from the human host to the mosquito, stressing on the need to develop transmission-blocking agents that have a potent gametocytocidal activity (Maron et al., 2016; Sun et al., 2017). Of all the plasmodial species, *Plasmodium falciparum* is the most lethal as it causes cerebral malaria, a severe complication responsible for high mortality rate amongst infected patients. Purine nucleotide metabolism in *Plasmodium falciparum* has been considered as an effective target for anti-malarial drugs (Hyde, 2007; Cassera et al., 2011; Ducati et al., 2013) since enzymes of *de novo* purine

biosynthetic pathway are absent in the parasite, causing it to depend solely on the purine salvage enzymes to fulfill its purine nucleotide requirements (Chaudhary et al., 2004). While 5'-nucleotidases form an important part of the purine salvage pathway, homologs of mammalian 5'-nucleotidases were absent in plasmodium species. However, a new class of IMP-specific 5'-nucleotidases (ISN1) was discovered in yeast, with its homologs present in plasmodium, other apicomplexans and lower plants (Itoh et al., 2003). An *in silico* study showed that ISN1s belong to the HAD superfamily of proteins (Srinivasan and Balaram, 2007). Up till now, only ISN1 from *S. cerevisiae* has been biochemically characterized. Structural information on ISN1s is not yet available.

With the above information set in the background, a detailed structural and functional characterization of PfISN1 would provide valuable information, not only about nucleotide metabolism in *P. falciparum,* but also about the yet unknown structural and functional features in the ISN1 family of proteins.

6.2. Biochemical characterization of PfISN1 *in vitro*

PfISN1 protein was recombinantly expressed in *E. coli* for biochemical characterization. Kinetic characterization of the enzyme revealed that it hydrolyzed the nucleoside 5'-monophosphates IMP and AMP, with higher catalytic efficiency towards IMP. It preferred the divalent metal ion Mg^{2+} as its cofactor and had optimum activity at pH 4.0-5.0. It also hydrolyzed pNPP, a non-physiological substrate with catalytic efficiency 1000-fold lower than IMP. It was also activated by ATP at pH 5.0. No phosphotransferase activity was detected in the enzyme.

6.3. Structure-function relationship in PfISN1

HAD members contain four invariant motifs that are critical for catalysis. Of these, motif I (DXDXT/V) is the most important. It contains two aspartates, of which the first aspartate is a nucleophile attacking the phosphate group of the substrate while the second coordinates with the metal ion cofactor. While *in silico* studies done earlier had suggested that ISN1s belong to the HAD superfamily of proteins, it was biochemically validated in this study. Mutation of both the asparates D170 and D172 in PfISN1 led to a complete loss of IMP-hydrolyzing activity in the enzyme. Interestingly, mutants PfISN1_D172N and PfISN1_D172A showed significantly higher pNPP-hydrolyzing activity compared to the wild-type enzyme, and a strong affinity for the substrate IMP, indicating a significant role of D172 in hydrolysis of pNPP as well as binding of IMP.

Crystal structures of the PfISN1 protein under various conditions were solved by our collaborative group in France, lead by Prof. Nushin Aghajari (CNRS-University of Lyon, France). These are the first crystal structures obtained for an ISN1 protein till date. The domain organization and tetrameric assembly of the protein showed several features distinct from mammalian 5'-nucleotidases. The core domain architecture remained conserved while the cap domain represented a C2-type architecture. The N-terminal domain (NTD) and the oligomerization domain (OD) are unique to this structure. The NTD was found to play an important role in catalysis as its deletion resulted in significantly compromised enzyme activity.

The active site in the PfISN1_D172N-IMP-Mg^{2+} structure was composed of several conserved and non-conserved residues interacting with IMP-Mg^{2+}. Amongst these, W365 interacted with the purine moiety of IMP through a π-stacking interaction. Upon mutating W365 to leucine, enzyme activity was totally compromised. However, upon mutating it to phenylalanine or tyrosine, the activity was not compromised, suggesting that the aromatic nature of the residue is critical for substrate binding.

In the PfISN1-ATP structure, ATP was found to interact with a non-conserved residue H150 at the allosteric site. The importance of this residue in ATP binding and allosteric activation of PfISN1 was confirmed by the mutant PfISN1_H150V which showed no activation by ATP. In the absence of ATP, the C10 loop interacted with H150. The mutant PfISN1_ΔC10 showed higher activity compared to the wild-type enzyme, but inhibition in the presence of ATP, suggesting its regulatory role in enzyme function. Significant conformational changes including cap domain closure, destabilization of NTD and reorganization of motif IV loop, were observed upon ligand binding. Overall, 15 non-conservative mutations for 15 residues, 2 conservative mutations for 1 residue, and 4 deletion mutations were generated, which have provided valuable information regarding the mechanism of catalysis, allosteric activation by ATP, and ligand-induced conformational changes in the PfISN1 protein.

6.4. Probing the physiological role of PfISN1 through *in vivo* studies

Through indirect immunofluoresence microscopy using anti-PfISN1 antibodies raised in rabbit, the PfISN1 protein was found to be localized in the cytosol of the parasite, in the asexual and sexual intraerythrocytic stages. Since knockout of essential genes is not feasible due to the haploid nature of the parasite genome, conditional systems that can regulate gene expression at the genome, transcriptional or protein level are being adopted (Armstrong and Goldberg, 2007). In a recent study, the function of a

a proteasome lid subunit protein, Rpn6, was probed using a regulatable fluorescent affinity (RFA) fusion tag which allowed protein regulation, probing live cell localization through fluorescence microcopy and affinity purification of the Rpn6 protein in *P. falciparum* (Muralidharan et al., 2011). A short 3'-end of the coding sequence of the PfISN1 gene Pf3D7_1206100 was cloned in frame with the RFA tag into pGDB plasmid and was transfected into *P. falciparum* parasites. The tag contained GFP for fluorescence microscopy, ecDHFR degradation domain for protein stabilization and HA tag for affinity purification. Upon successful integration at the gene locus by a single-crossover homologous recombination, the levels of the expressed fusion protein can be regulated *in vivo* by the drug trimethoprim (TMP), which stabilizes the ecDHFR degradation domain. Uninfected erythrocytes were transfected with the plasmid, followed by the addition of schizont-stage parasites of *P. falciparum* PMIKO strain, which is resistant to TMP. Parasites transfected with the plasmid were positively selected with the drug blasticidin (BSD). Parasites usually appear within 15-25 days of applying drug selection pressure. However, after adding BSD, no parasites were found in the Giemsa-stained smears of the culture even after 30 days.

6.5. Future directions

HAD members exhibit an extensive substrate space. In keeping up with the current knowledge of this substrate space, a significant number of compounds are yet to be screened as putative substrates for PfISN1. A similar approach can also be considered for extending the modulator screen, as the modulator space amongst HAD members has not been explored extensively. The asymmetry in the quaternary structure of PfISN1 in the apo-form, global conformational changes observed in the IMP-bound structure, and asymmetry in ATP-binding at the allosteric site suggest inter-domain as well as inter-subunit communication in the functional enzyme. The kinetics and mechanism of ligand binding as well as their stoichiometry can be elucidated through the continuous measurement of enzyme activity under pre-steady state conditions using a couple-enzyme assay involving the purine nucleoside phosphorylase-xanthine oxidase (PNP-XO) system, which has been used for continuous measurement of 5'-nucleotidase hydrolysis activity (Groot et al., 1985; Zerez and Tanaka, 1985; Webb, 1992). Preliminary assays performed in the laboratory under steady state conditions have reported the detection of IMP-hydrolyzing activity specific to PfISN1. The assay needs further standardization before it can be used for pre-steady state measurements.

The intracellular location and physiological function of a protein are closely related. The optimum activity of PfISN1 at low pH *in vitro* suggests that the protein is probably localized in an acidic organelle like food vacuole in the parasite. Colocalization studies using pH-sensitive fluorescent dyes or food vacuole marker proteins can help in identifying organelle-specific localization of PfISN1 within the parasite. With recent advances made in plasmodium genetics, better molecular tools such as conditional expression systems and CRISPR/Cas9 technology are available (Ghorbal et al., 2014; Lee and Fidock, 2014; Crawford et al., 2017). These alternate approaches will be adopted to probe PfISN1 gene function *in vivo*. Amongst other apicomplexans, ISN1 from *Toxoplasma gondii* is closely related to PfISN1. Biochemical characterization of TgISN1 and other ISN1s can provide valuable information about the diverse and conserved features amongst ISN1 members.

(This page is intentionally left blank)

REFERENCES

1. Allegrini, S.; Scaloni, A.; Careddu, M. G.; Cuccu, G.; D'Ambrosio, C.; Pesi, R.; Camici, M.; Ferrara, L.; Tozzi, M. G. Mechanistic Studies on Bovine Cytosolic 5'-nucleotidase II, an Enzyme Belonging to the HAD Superfamily. *Eur J Biochem* **2004**, *271*, 4881–4891.

2. Allegrini, S.; Scaloni, A.; Ferrara, L.; Pesi, R.; Pinna, P.; Sgarrella, F.; Camici, M.; Eriksson, S.; Tozzi, M. G. Bovine Cytosolic 5′-Nucleotidase Acts through the Formation of an Aspartate 52-Phosphoenzyme Intermediate. *J. Biol. Chem.* **2001**, *276*, 33526–33532.

3. Allen, K. N.; Dunaway-Mariano, D. Phosphoryl Group Transfer: Evolution of a Catalytic Scaffold. *Trends Biochem Sci* **2004**, *29*, 495–503.

4. Altschul, S. F.; Madden, T. L.; Schäffer, A. A.; Zhang, J.; Zhang, Z.; Miller, W.; Lipman, D. J. Gapped BLAST and PSI-BLAST: A New Generation of Protein Database Search Programs. *Nucleic Acids Res.* **1997**, *25*, 3389–3402.

5. Amici, A.; Emanuelli, M.; Magni, G.; Raffaelli, N.; Ruggieri, S. Pyrimidine Nucleotidases from Human Erythrocyte Possess Phosphotransferase Activities Specific for Pyrimidine Nucleotides. *FEBS Lett.* **1997**, *419*, 263–267.

6. Aravind, L.; Galperin, M. Y.; Koonin, E. V. The Catalytic Domain of the P-Type ATPase Has the Haloacid Dehalogenase Fold. *Trends Biochem. Sci.* **1998**, *23*, 127–129.

7. Armstrong, C. M.; Goldberg, D. E. An FKBP Destabilization Domain Modulates Protein Levels in Plasmodium Falciparum. *Nat. Methods* **2007**, *4*, 1007–1009.

8. Aurrecoechea, C.; Brestelli, J.; Brunk, B. P.; Dommer, J.; Fischer, S.; Gajria, B.; Gao, X.; Gingle, A.; Grant, G.; Harb, O. S.; et al. PlasmoDB: A Functional Genomic Database for Malaria Parasites. *Nucleic Acids Res.* **2009**, *37*, D539-43.

9. Azimzadeh, O.; Sow, C.; Gèze, M.; Nyalwidhe, J.; Florent, I. Plasmodium Falciparum PfA-M1 Aminopeptidase Is Trafficked via the Parasitophorous Vacuole and Marginally Delivered to the Food Vacuole. *Malar J* **2010**, *9*, 189.

10. Baiocchi, C.; Pesi, R.; Camici, M.; Itoh, R.; Grazi Tozzi, M. Mechanism of the Reaction Catalysed by Cytosolic 5'-nucleotidase/phosphotransferase: Formation of a Phosphorylated Intermediate. *Biochem J* **1996**, *317*, 797–801.

11. Bardsley, W. G.; Wyman, J. Concerning the Thermodynamic Definition and Graphical Manifestation of Positive and Negative Cooperativity. *J. Theor. Biol.* **1978**, *72*, 373–376.

12. Barsotti, C.; Pesi, R.; Felice, F.; Ipata, P. L. The Purine Nucleoside Cycle in Cell-Free Extracts of Rat Brain: Evidence for the Occurrence of an Inosine and a Guanosine Cycle with Distinct Metabolic Roles. *Cell. Mol. Life Sci.* **2003**, *60*, 786–793.

13. Barsotti, C.; Pesi, R.; Giannecchini, M.; Ipata, P. L. Evidence for the Involvement of Cytosolic 5'-nucleotidase (cN-II) in the Synthesis of Guanine Nucleotides from Xanthosine. *J Biol Chem* **2005**, *280*, 13465–13469.

14. Becker, M. A.; Kim, M. Regulation of Purine Synthesis de Novo in Human Fibroblasts by Purine Nucleotides and Phosphoribosylpyrophosphate. *J. Biol. Chem.* **1987**, *262*, 14531–14537.

15. Bessey, O. A.; Lowry, O. H.; Brock, M. J. One Point Colorimetric Method of Determining Alkaline Phosphatase in Serum or Plasma. *J Biol Chem* **1946**, *164*.

16. Beyer, H. M.; Gonschorek, P.; Samodelov, S. L.; Meier, M.; Weber, W.; Zurbriggen, M. D. AQUA Cloning: A Versatile and Simple Enzyme-Free Cloning Approach. *PLoS One* **2015**, *10*, e0137652.

17. Bianchi, V.; Spychala, J. Mammalian 5'-nucleotidases. *J Biol Chem* **2003**, *278*, 46195–46198.

18. Bogan, K. L.; Evans, C.; Belenky, P.; Song, P.; Burant, C. F.; Kennedy, R.; Brenner, C. Identification of Isn1 and Sdt1 as Glucose- and Vitamin-Regulated Nicotinamide Mononucleotide and Nicotinic Acid Mononucleotide 5'-nucleotidases Responsible for Production of Nicotinamide Riboside and Nicotinic Acid Riboside. *J. Biol. Chem.* **2009**, *284*, 34861–34869.

19. Bontemps, F.; Van den Berghe, G.; Hers, H. G. 5'-Nucleotidase Activities in Human Erythrocytes. Identification of a Purine 5'-nucleotidase Stimulated by ATP and Glycerate 2,3-Bisphosphate. *Biochem J* **1988**, *250*, 687–696.

20. Bontemps, F.; Vincent, M. F.; Van den Bergh, F.; van Waeg, G.; Van den Berghe, G. Stimulation by Glycerate 2,3-Bisphosphate: A Common Property of Cytosolic IMP-GMP 5'-nucleotidase in Rat and Human Tissues. *Biochim Biophys Acta* **1989**, *997*, 131–134.

21. Bradford, M. M. A Rapid and Sensitive Method for the Quantitation of

Microgram Quantities of Protein Utilizing the Principle of Protein-Dye Binding. *Anal Biochem* **1976**, *72*, 248–254.

22. Brancucci, N. M. B.; Gerdt, J. P.; Wang, C.; De Niz, M.; Philip, N.; Adapa, S. R.; Zhang, M.; Hitz, E.; Niederwieser, I.; Boltryk, S. D.; et al. Lysophosphatidylcholine Regulates Sexual Stage Differentiation in the Human Malaria Parasite Plasmodium Falciparum. *Cell* **2017**, *171*, 1532–1544.

23. Braude, I. A.; De Clercq, E. Purification of Mouse Interferon by Sequential Chromatography. *J. Chromatogr.* **1979**, *172*, 207–219.

24. Bretonnet, A. S.; Jordheim, L. P.; Dumontet, C.; Lancelin, J. M. Regulation and Activity of Cytosolic 5'-nucleotidase II. A Bifunctional Allosteric Enzyme of the Haloacid Dehalogenase Superfamily Involved in Cellular Metabolism. *FEBS Lett* **2005**, *579*, 3363–3368.

25. Burnette, W. N. "Western Blotting": Electrophoretic Transfer of Proteins from Sodium Dodecyl Sulfate--Polyacrylamide Gels to Unmodified Nitrocellulose and Radiographic Detection with Antibody and Radioiodinated Protein A. *Anal. Biochem.* **1981**, *112*, 195–203.

26. Burnstock, G. Purinergic Signalling. *Br. J. Pharmacol.* **2006**, *147*, S172-81.

27. Burroughs, A. M.; Allen, K. N.; Dunaway-Mariano, D.; Aravind, L. Evolutionary Genomics of the HAD Superfamily: Understanding the Structural Adaptations and Catalytic Diversity in a Superfamily of Phosphoesterases and Allied Enzymes. *J Mol Biol* **2006**, *361*, 1003–1034.

28. Buschmann, J.; Moritz, B.; Jeske, M.; Lilie, H.; Schierhorn, A.; Wahle, E. Identification of Drosophila and Human 7-Methyl GMP-Specific Nucleotidases. *J Biol Chem* **2013**, *288*, 2441–2451.

29. Cappiello, M.; Mascia, L.; Scolozzi, C.; Giorgelli, F.; Ipata, P. L. In Vitro Assessment of Salvage Pathways for Pyrimidine Bases in Rat Liver and Brain. *Biochim. Biophys. Acta* **1998**, *1425*, 273–281.

30. Cassera, M. B.; Zhang, Y.; Hazleton, K. Z.; Schramm, V. L. Purine and Pyrimidine Pathways as Targets in Plasmodium Falciparum. *Curr. Top. Med. Chem.* **2011**, *11*, 2103–2115.

31. Cdc. CDC - Malaria http://www.cdc.gov/malaria/index.html.

32. Chaudhary, K.; Darling, J. A.; Fohl, L. M.; Sullivan, W. J.; Donald, R. G. K.; Pfefferkorn, E. R.; Ullman, B.; Roost, D. S. Purine Salvage Pathways in the

Apicomplexan Parasite Toxoplasma Gondii. *J. Biol. Chem.* **2004**, *279*, 31221–31227.

33. Chen, G. Q.; Sun, Y.; Jin, R.; Gouaux, E. Probing the Ligand Binding Domain of the GluR2 Receptor by Proteolysis and Deletion Mutagenesis Defines Domain Boundaries and Yields a Crystallizable Construct. *Protein Sci.* **1998**, *7*, 2623–2630.

34. Chen, P. S. J.; Toribara, T. Y.; Warner, H. Microdetermination of Phosphorus. *Anal. Chem.* **1956**, *28*, 1756–1758.

35. Cirri, P.; Chiarugi, P.; Camici, G.; Manao, G.; Raugei, G.; Cappugi, G.; Ramponi, G. The Role of Cys12, Cys17 and Arg18 in the Catalytic Mechanism of Low-M(r) Cytosolic Phosphotyrosine Protein Phosphatase. *Eur. J. Biochem.* **1993**, *214*, 647–657.

36. Clarke, D. M.; Loo, T. W.; MacLennan, D. H. Functional Consequences of Alterations to Amino Acids Located in the Nucleotide Binding Domain of the Ca2(+)-ATPase of Sarcoplasmic Reticulum. *J. Biol. Chem.* **1990**, *265*, 22223–22227.

37. Collet, J. F.; Stroobant, V.; Pirard, M.; Delpierre, G.; Van Schaftingen, E. A New Class of Phosphotransferases Phosphorylated on an Aspartate Residue in an Amino-Terminal DXDX(T/V) Motif. *J. Biol. Chem.* **1998**, *273*, 14107–14112.

38. Collet, J. F.; Stroobant, V.; Van Schaftingen, E. Mechanistic Studies of Phosphoserine Phosphatase, an Enzyme Related to P-Type ATPases. *J. Biol. Chem.* **1999**, *274*, 33985–33990.

39. Cooper, R. A.; Ferdig, M. T.; Su, X.-Z.; Ursos, L. M. B.; Mu, J.; Nomura, T.; Fujioka, H.; Fidock, D. A.; Roepe, P. D.; Wellems, T. E. Alternative Mutations at Position 76 of the Vacuolar Transmembrane Protein PfCRT Are Associated with Chloroquine Resistance and Unique Stereospecific Quinine and Quinidine Responses in Plasmodium Falciparum. *Mol. Pharmacol.* **2002**, *61*, 35–42.

40. Crawford, E. D.; Quan, J.; Horst, J. A.; Ebert, D.; Wu, W.; DeRisi, J. L. Plasmid-Free CRISPR/Cas9 Genome Editing in Plasmodium Falciparum Confirms Mutations Conferring Resistance to the Dihydroisoquinolone Clinical Candidate SJ733. *PLoS One* **2017**, *12*, e0178163.

41. Dasaradhi, P. V; Korde, R.; Thompson, J. K.; Tanwar, C.; Nag, T. C.; Chauhan,

V. S.; Cowman, A. F.; Mohmmed, A.; Malhotra, P. Food Vacuole Targeting and Trafficking of Falcipain-2, an Important Cysteine Protease of Human Malaria Parasite Plasmodium Falciparum. *Mol Biochem Parasitol* **2007**, *156*, 12–23.

42. Daughtry, K. D.; Huang, H.; Malashkevich, V.; Patskovsky, Y.; Liu, W.; Ramagopal, U.; Sauder, J. M.; Burley, S. K.; Almo, S. C.; Dunaway-Mariano, D.; et al. Structural Basis for the Divergence of Substrate Specificity and Biological Function within HAD Phosphatases in Lipopolysaccharide and Sialic Acid Biosynthesis. *Biochemistry* **2013**, *52*.

43. de Koning-Ward, T. F.; Gilson, P. R.; Crabb, B. S. Advances in Molecular Genetic Systems in Malaria. *Nat. Rev. Microbiol.* **2015**, *13*, 373–387.

44. Deitsch, K. W. Transformation of Malaria Parasites by the Spontaneous Uptake and Expression of DNA from Human Erythrocytes. *Nucleic Acids Res.* **2001**, *29*, 850–853.

45. DIECKHOFF, J.; KNEBEL, H.; HEIDEMANN, M.; MANNHERZ, H. G. An Improved Procedure for Purifying 5'-nucleotidase from Various Sources. Evidence for Tissue and Species Differences in Their Molecular Mass and Affinity for F-Actin. *Eur. J. Biochem.* **1985**, *151*, 377–383.

46. Drew, D. R.; Sanders, P. R.; Crabb, B. S. Plasmodium Falciparum Merozoite Surface Protein 8 Is a Ring-Stage Membrane Protein That Localizes to the Parasitophorous Vacuole of Infected Erythrocytes. *Infect. Immun.* **2005**, *73*, 3912–3922.

47. Ducati, R. G.; Namanja-Magliano, H. A.; Schramm, V. L. Transition-State Inhibitors of Purine Salvage and Other Prospective Enzyme Targets in Malaria. *Future Med. Chem.* **2013**, *5*, 1341–1360.

48. Dumora, C.; Lacoste, A. M.; Cassaigne, A.; Mazat, J. P. Allosteric Regulation of Phosphonoacetaldehyde Hydrolase by N-Butylphosphonic Acid. *Biochem. J.* **1991**, *280*, 557–559.

49. Edgar, R. C. MUSCLE: Multiple Sequence Alignment with High Accuracy and High Throughput. *Nucleic Acids Res.* **2004**, *32*, 1792–1797.

50. Felsenstein, J. CONFIDENCE LIMITS ON PHYLOGENIES: AN APPROACH USING THE BOOTSTRAP. *Evolution (N. Y).* **1985**, *39*, 783–791.

51. Fersht, A. *Enzyme Structure and Mechanism*, 2nd ed.; W. H. Freeman, 1985.

52. Fidock, D. A.; Nomura, T.; Talley, A. K.; Cooper, R. A.; Dzekunov, S. M.; Ferdig, M. T.; Ursos, L. M.; Sidhu, A. B.; Naudé, B.; Deitsch, K. W.; et al. Mutations in the P. Falciparum Digestive Vacuole Transmembrane Protein PfCRT and Evidence for Their Role in Chloroquine Resistance. *Mol. Cell* **2000**, *6*, 861–871.

53. Fini, C.; Minelli, A.; Camici, M.; Floridi, A. Effects of Dithiothreitol, Dithioerythritol and Chelating Agents on 5'-nucleotidase from Bull Seminal Plasma. *Biochim. Biophys. Acta* **1985**, *827*, 403–409.

54. Fini, C.; Palmerini, C. A.; Damiani, P.; Stochaj, U.; Mannherz, H. G.; Floridi, A. 5'-nucleotidase from Bull Seminal Plasma, Chicken Gizzard and Snake Venom Is a Zinc Metalloprotein. *Biochim. Biophys. Acta* **1990**, *1038*, 18–22.

55. Fivelman, Q. L.; McRobert, L.; Sharp, S.; Taylor, C. J.; Saeed, M.; Swales, C. A.; Sutherland, C. J.; Baker, D. A. Improved Synchronous Production of Plasmodium Falciparum Gametocytes in Vitro. *Mol Biochem Parasitol* **2007**, *154*, 119–123.

56. Frame, I. J.; Merino, E. F.; Schramm, V. L.; Cassera, M. B.; Akabas, M. H. Malaria Parasite Type 4 Equilibrative Nucleoside Transporters (ENT4) Are Purine Transporters with Distinct Substrate Specificity. *Biochem. J.* **2012**, *446*, 179–190.

57. Frech, C.; Chen, N. Genome Comparison of Human and Non-Human Malaria Parasites Reveals Species Subset-Specific Genes Potentially Linked to Human Disease. *PLoS Comput Biol* **2011**, *7*, e1002320.

58. Fritzson, P. Regulation of Nucleotidase Activities in Animal Tissues. *Adv. Enzyme Regul.* **1977**, *16*, 43–61.

59. Fuhrmann, J.; Subramanian, V.; Thompson, P. R. Targeting the Arginine Phosphatase YwlE with a Catalytic Redox-Based Inhibitor. *ACS Chem. Biol.* **2013**, *8*, 2024–2032.

60. Galtier, N.; Gouy, M.; Gautier, C. SEAVIEW and PHYLO_WIN: Two Graphic Tools for Sequence Alignment and Molecular Phylogeny. *Comput. Appl. Biosci.* **1996**, *12*, 543–548.

61. Gardiner, D. L.; Skinner-Adams, T. S.; Brown, C. L.; Andrews, K. T.; Stack, C. M.; McCarthy, J. S.; Dalton, J. P.; Trenholme, K. R. Plasmodium Falciparum:

New Molecular Targets with Potential for Antimalarial Drug Development. *Expert Rev Anti Infect Ther* **2009**, *7*, 1087–1098.

62. Garvey, E. P.; Lowen, G. T.; Almond, M. R. Nucleotide and Nucleoside Analogues as Inhibitors of Cytosolic 5'-nucleotidase I from Heart. *Biochemistry* **1998**, *37*, 9043–9051.

63. Garvey, E. P.; Prus, K. L. A Specific Inhibitor of Heart Cytosolic 5′-Nucleotidase I Attenuates Hydrolysis of Adenosine 5′-Monophosphate in Primary Rat Myocytes. *Arch. Biochem. Biophys.* **1999**, *364*, 235–240.

64. Gazziola, C.; Ferraro, P.; Moras, M.; Reichard, P.; Bianchi, V. Cytosolic High K(m) 5'-nucleotidase and 5'(3')-Deoxyribonucleotidase in Substrate Cycles Involved in Nucleotide Metabolism. *J. Biol. Chem.* **2001**, *276*, 6185–6190.

65. Ghorbal, M.; Gorman, M.; Macpherson, C. R.; Martins, R. M.; Scherf, A.; Lopez-Rubio, J.-J. Genome Editing in the Human Malaria Parasite Plasmodium Falciparum Using the CRISPR-Cas9 System. *Nat. Biotechnol.* **2014**, *32*, 819–821.

66. Giorgelli, F.; Bottai, C.; Mascia, L.; Scolozzi, C.; Camici, M.; Ipata, P. L. Recycling of Alpha-D-Ribose 1-Phosphate for Nucleoside Interconversion. *Biochim. Biophys. Acta* **1997**, *1335*, 6–22.

67. Godinho, L. M.; de Sá-Nogueira, I. Characterization and Regulation of a Bacterial Sugar Phosphatase of the Haloalkanoate Dehalogenase Superfamily, AraL, from Bacillus Subtilis. *FEBS J.* **2011**, *278*, 2511–2524.

68. Gouet, P.; Courcelle, E.; Stuart, D. I.; Métoz, F. ESPript: Analysis of Multiple Sequence Alignments in PostScript. *Bioinformatics* **1999**, *15*, 305–308.

69. Grondal, E. J.; Zimmermann, H. Purification, Characterization and Cellular Localization of 5'-nucleotidase from Torpedo Electric Organ. *Biochem. J.* **1987**, *245*, 805–810.

70. Groot, H. D. E.; Groot, H. D. E.; Noll, T. Enzymic Determination of Inorganic Phosphates, Organic Phosphates and Phosphate-Liberating Enzymes by Use of Nucleoside Phosphorylase-Xanthine Oxidase (Dehydrogenase)-Coupled Reactions. *Biochem J* **1985**, *229*, 255–260.

71. Hawkes, R.; Niday, E.; Gordon, J. A Dot-Immunobinding Assay for Monoclonal and Other Antibodies. *Anal. Biochem.* **1982**, *119*, 142–147.

72. Heckman, K. L.; Pease, L. R. Gene Splicing and Mutagenesis by PCR-Driven

Overlap Extension. *Nat. Protoc.* **2007**, *2*, 924–932.

73. Hill, A. V. The Possible Effects of the Aggregation of the Molecules of Hæmoglobin on Its Dissociation Curves. *J. Physiol.* **1910**, *40*, iv–vii.

74. Hinder, R. A.; Bremner, C. G. Relative Role of Pyloroplasty Size, Truncal Vagotomy, and Milk Meal Volume in Canine Gastric Emptying. *Am. J. Dig. Dis.* **1978**, *23*, 210–216.

75. Höglund, L.; Reichard, P. Cytoplasmic 5'(3')-Nucleotidase from Human Placenta. *J. Biol. Chem.* **1990**, *265*, 6589–6595.

76. Honrubia, F. M.; Grijalbo, M. P.; Gomez, M. L.; Lopez, A. Surgical Treatment of Neovascular Glaucoma. *Trans. Ophthalmol. Soc. U. K.* **1979**, *99*, 89–91.

77. Huang, H.; Pandya, C.; Liu, C.; Al-Obaidi, N. F.; Wang, M.; Zheng, L.; Toews Keating, S.; Aono, M.; Love, J. D.; Evans, B.; et al. Panoramic View of a Superfamily of Phosphatases through Substrate Profiling. *Proc. Natl. Acad. Sci. U. S. A.* **2015**, *112*, E1974-83.

78. Hunsucker, S. A.; Mitchell, B. S.; Spychala, J. The 5'-nucleotidases as Regulators of Nucleotide and Drug Metabolism. *Pharmacol Ther* **2005**, *107*, 1–30.

79. Hyde, J. E. Targeting Purine and Pyrimidine Metabolism in Human Apicomplexan Parasites. *Curr. Drug Targets* **2007**, *8*, 31–47.

80. Ishida, T.; Kinoshita, K. PrDOS: Prediction of Disordered Protein Regions from Amino Acid Sequence. *Nucleic Acids Res.* **2007**, *35*, W460-4.

81. Itoh, R. IMP-GMP 5'-nucleotidase. *Comp. Biochem. Physiol. B.* **1993**, *105*, 13–19.

82. Itoh, R. Purification and Some Properties of an IMP-Specific 5'-nucleotidase from Yeast. *Biochem J* **1994**, *298*, 593–598.

83. Itoh, R.; Saint-Marc, C.; Chaignepain, S.; Katahira, R.; Schmitter, J.-M.; Daignan-Fornier, B. The Yeast ISN1 (YOR155c) Gene Encodes a New Type of IMP-Specific 5'-nucleotidase. *BMC Biochem.* **2003**, *4*, 1–7.

84. Joshi, J. G.; Handler, P. Phosphoglucomutase. VI. Purification and Properties of Phosphoglucomutases from Human Muscle. *J. Biol. Chem.* **1969**, *244*, 3343–3351.

85. Kicska, G. A.; Tyler, P. C.; Evans, G. B.; Furneaux, R. H.; Kim, K.; Schramm,

V. L. Transition State Analogue Inhibitors of Purine Nucleoside Phosphorylase from *Plasmodium Falciparum*. *J. Biol. Chem.* **2002**, *277*, 3219–3225.

86. Klemba, M.; Beatty, W.; Gluzman, I.; Goldberg, D. E. Trafficking of Plasmepsin II to the Food Vacuole of the Malaria Parasite Plasmodium Falciparum. *J Cell Biol* **2004**, *164*, 47–56.

87. Koshland, D. E.; Jr. Application of a Theory of Enzyme Specificity to Protein Synthesis. *Proc. Natl. Acad. Sci. U. S. A.* **1958**, *44*, 98–104.

88. Krug, U.; Patzschke, R.; Zebisch, M.; Balbach, J.; Sträter, N. Contribution of the Two Domains of E. Coli 5'-nucleotidase to Substrate Specificity and Catalysis. *FEBS Lett.* **2013**, *587*, 460–466.

89. Kuang, R.; Chan, K.-H.; Yeung, E.; Lim, B. L. Molecular and Biochemical Characterization of AtPAP15, a Purple Acid Phosphatase with Phytase Activity, in Arabidopsis. *Plant Physiol.* **2009**, *151*, 199–209.

90. Kumar, S.; Stecher, G.; Tamura, K. MEGA7: Molecular Evolutionary Genetics Analysis Version 7.0 for Bigger Datasets. *Mol. Biol. Evol.* **2016**, *33*, 1870–1874.

91. Lahiri, S. D.; Zhang, G.; Dai, J.; Dunaway-Mariano, D.; Allen, K. N. Analysis of the Substrate Specificity Loop of the HAD Superfamily Cap Domain. *Biochemistry* **2004**, *43*, 2812–2820.

92. Lahiri, S. D.; Zhang, G.; Dunaway-Mariano, D.; Allen, K. N. The Pentacovalent Phosphorus Intermediate of a Phosphoryl Transfer Reaction. *Science* **2003**, *299*, 2067–2071.

93. Lakowicz, J. R. *Principles of Fluorescence Spectroscopy*; Kluwer Academic/Plenum, 1999.

94. Lambros, C.; Vanderberg, J. P. Synchronization of Plasmodium Falciparum Erythrocytic Stages in Culture. *J. Parasitol.* **1979**, *65*, 418–420.

95. Larrouy-Maumus, G.; Biswas, T.; Hunt, D. M.; Kelly, G.; Tsodikov, O. V; de Carvalho, L. P. Discovery of a Glycerol 3-Phosphate Phosphatase Reveals Glycerophospholipid Polar Head Recycling in Mycobacterium Tuberculosis. *Proc Natl Acad Sci U S A* **2013**, *110*, 11320–11325.

96. Lasonder, E.; Rijpma, S. R.; van Schaijk, B. C. L.; Hoeijmakers, W. A. M.; Kensche, P. R.; Gresnigt, M. S.; Italiaander, A.; Vos, M. W.; Woestenenk, R.; Bousema, T.; et al. Integrated Transcriptomic and Proteomic Analyses of P.

Falciparum Gametocytes: Molecular Insight into Sex-Specific Processes and Translational Repression. *Nucleic Acids Res.* **2016**, *44*, 6087–6101.

97. Le, S. Q.; Gascuel, O. An Improved General Amino Acid Replacement Matrix. *Mol. Biol. Evol.* **2008**, *25*, 1307–1320.

98. Lee, M. C.; Fidock, D. A. CRISPR-Mediated Genome Editing of Plasmodium Falciparum Malaria Parasites. *Genome Med.* **2014**, *6*, 63.

99. Lee, R. S.; Ford, H. C. 5'-Nucleotidase of Human Placental Trophoblastic Microvilli Possesses Cobalt-Stimulated FAD Pyrophosphatase Activity. *J. Biol. Chem.* **1988**, *263*, 14878–14883.

100. Liu, J.; Gluzman, I. Y.; Drew, M. E.; Goldberg, D. E. The Role of *Plasmodium Falciparum* Food Vacuole Plasmepsins. *J. Biol. Chem.* **2005**, *280*, 1432–1437.

101. Loret, M. O.; Pedersen, L.; François, J. Revised Procedures for Yeast Metabolites Extraction: Application to a Glucose Pulse to Carbon-Limited Yeast Cultures, Which Reveals a Transient Activation of the Purine Salvage Pathway. *Yeast* **2007**, *24*, 47–60.

102. Luo, M.; Guo, Y.-C.; Deng, J.-Y.; Wei, H.-P.; Zhang, Z.-P.; Leng, Y.; Men, D.; Song, L.-R.; Zhang, X.-E.; Zhou, Y.-F. Characterization of a Monomeric Heat-Labile Classical Alkaline Phosphatase from Anabaena Sp. PCC7120. *Biochem.* **2010**, *75*, 655–664.

103. Maron, M. I.; Magle, C. T.; Czesny, B.; Turturice, B. A.; Huang, R.; Zheng, W.; Vaidya, A. B.; Williamson, K. C. Maduramicin Rapidly Eliminates Malaria Parasites and Potentiates the Gametocytocidal Activity of the Pyrazoleamide PA21A050. *Antimicrob. Agents Chemother.* **2016**, *60*, 1492–1499.

104. Martin, G.; Keller, W.; Doublié, S. Crystal Structure of Mammalian poly(A) Polymerase in Complex with an Analog of ATP. *EMBO J.* **2000**, *19*, 4193–4203.

105. Maruyama, K.; Clarke, D. M.; Fujii, J.; Inesi, G.; Loo, T. W.; MacLennan, D. H. Functional Consequences of Alterations to Amino Acids Located in the Catalytic Center (Isoleucine 348 to Threonine 357) and Nucleotide-Binding Domain of the Ca2+-ATPase of Sarcoplasmic Reticulum. *J. Biol. Chem.* **1989**, *264*, 13038–13042.

106. Maruyama, K.; MacLennan, D. H. Mutation of Aspartic Acid-351, Lysine-352, and Lysine-515 Alters the Ca2+ Transport Activity of the Ca2+-ATPase

Expressed in COS-1 Cells. *Proc. Natl. Acad. Sci. U. S. A.* **1988**, *85*, 3314–3318.

107. Mazzon, C.; Rampazzo, C.; Scaini, M. C.; Gallinaro, L.; Karlsson, A.; Meier, C.; Balzarini, J.; Reichard, P.; Bianchi, V. Cytosolic and Mitochondrial Deoxyribonucleotidases: Activity with Substrate Analogs, Inhibitors and Implications for Therapy. *Biochem Pharmacol* **2003**, *66*, 471–479.

108. Michaelis, L.; Menten, M. L. Kinetic Der Invertinwirkung. *Biochem. Z.* **1913**, *49*, 333–369.

109. MONOD, J.; CHANGEUX, J. P.; JACOB, F. Allosteric Proteins and Cellular Control Systems. *J. Mol. Biol.* **1963**, *6*, 306–329.

110. MONOD, J.; JACOB, F. Teleonomic Mechanisms in Cellular Metabolism, Growth, and Differentiation. *Cold Spring Harb. Symp. Quant. Biol.* **1961**, *26*, 389–401.

111. Muralidharan, V.; Oksman, A.; Iwamoto, M.; Wandless, T. J.; Goldberg, D. E. Asparagine Repeat Function in a Plasmodium Falciparum Protein Assessed via a Regulatable Fluorescent Affinity Tag. *Proc. Natl. Acad. Sci. U. S. A.* **2011**, *108*, 4411–4416.

112. Nagappa, L. K.; Balaram, H. Biochemical and Physiological Characterization of HADs from Plasmodium Spp. (unpublished results).

113. Neet, K. E. Cooperativity in Enzyme Function: Equilibrium and Kinetic Aspects. *Methods Enzymol.* **1995**, *249*, 519–567.

114. Ngo, T. D.; Van Le, B.; Subramani, V. K.; Thi Nguyen, C. M.; Lee, H. S.; Cho, Y.; Kim, K. K.; Hwang, H. Y. Structural Basis for the Substrate Selectivity of a HAD Phosphatase from Thermococcus Onnurineus NA1. *Biochem. Biophys. Res. Commun.* **2015**, *461*, 122–127.

115. Numa, N.; Ishida, Y.; Nasu, M.; Sohda, M.; Misumi, Y.; Noda, T.; Oda, K. Molecular Basis of Perinatal Hypophosphatasia with Tissue-Nonspecific Alkaline Phosphatase Bearing a Conservative Replacement of Valine by Alanine at Position 406. *FEBS J.* **2008**, *275*, 2727–2737.

116. O'Brien, P. J.; Lassila, J. K.; Fenn, T. D.; Zalatan, J. G.; Herschlag, D. Arginine Coordination in Enzymatic Phosphoryl Transfer: Evaluation of the Effect of Arg166 Mutations in Escherichia Coli Alkaline Phosphatase. *Biochemistry* **2008**, *47*, 7663–7672.

117. O'Sullivan, W. J.; Smithers, G. W. Stability Constants for Biologically

Important Metal-Ligand Complexes. *Methods Enzym.* **1979**, *63*, 294–336.

118. Ong, C. N.; Kong, Y. M.; Ong, H. Y.; Teramoto, K. The *in Vitro* and *in Vivo* Effects of Lead on δ-Aminolevulinic Acid Dehydratase and Pyrimidine 5′-Nucleotidase. *Pharmacol. Toxicol.* **1990**, *66*, 23–26.

119. Paglia, D. E.; Valentine, W. N. Characteristics of a Pyrimidine-Specific 5'-nucleotidase in Human Erythrocytes. *J. Biol. Chem.* **1975**, *250*, 7973–7979.

120. Park, J.; Guggisberg, A. M.; Odom, A. R.; Tolia, N. H. Cap-Domain Closure Enables Diverse Substrate Recognition by the C2-Type Haloacid Dehalogenase-like Sugar Phosphatase Plasmodium Falciparum HAD1. *Acta Crystallogr. Sect. D Biol. Crystallogr.* **2015**, *71*, 1824–1834.

121. Parker, M. D.; Hyde, R. J.; Yao, S. Y.; McRobert, L.; Cass, C. E.; Young, J. D.; McConkey, G. A.; Baldwin, S. A. Identification of a Nucleoside/nucleobase Transporter from Plasmodium Falciparum, a Novel Target for Anti-Malarial Chemotherapy. *Biochem. J.* **2000**, *349*, 67–75.

122. Pauling, L. Molecular Architecture and Biological Reactions. *Chem. Eng. News* **1946**, *24*, 1375–1377.

123. Pesi, R.; Turriani, M.; Allegrini, S.; Scolozzi, C.; Camici, M.; Ipata, P. L.; Tozzi, M. G. The Bifunctional Cytosolic 5'-nucleotidase: Regulation of the Phosphotransferase and Nucleotidase Activities. *Arch Biochem Biophys* **1994**, *312*, 75–80.

124. Piec, G.; Le Hir, M. The Soluble "Low-Km" 5'-nucleotidase of Rat Kidney Represents Solubilized Ecto-5'-nucleotidase. *Biochem J* **1991**, *273*, 409–413.

125. Pierzyńska-Mach, A.; Janowski, P. A.; Dobrucki, J. W. Evaluation of Acridine Orange, LysoTracker Red, and Quinacrine as Fluorescent Probes for Long-Term Tracking of Acidic Vesicles. *Cytom. Part A* **2014**, *85*, 729–737.

126. Ponnudurai, T.; Lensen, A. H. W.; Leeuwenberg, A. D. E. M.; Meuwissen, J. H. E. T. Cultivation of Fertile Plasmodium Falciparum Gametocytes in Semi-Automated Systems. 1. Static Cultures. *Trans. R. Soc. Trop. Med. Hyg.* **1982**, *76*, 812–818.

127. Price, R. N.; Uhlemann, A.-C.; Brockman, A.; McGready, R.; Ashley, E.; Phaipun, L.; Patel, R.; Laing, K.; Looareesuwan, S.; White, N. J.; et al. Mefloquine Resistance in Plasmodium Falciparum and Increased pfmdr1 Gene Copy Number. *Lancet* **2004**, *364*, 438–447.

128. Proudfoot, M.; Kuznetsova, E.; Brown, G.; Rao, N. N.; Kitagawa, M.; Mori, H.; Savchenko, A.; Yakunin, A. F. General Enzymatic Screens Identify Three New Nucleotidases in Escherichia Coli. Biochemical Characterization of SurE, YfbR, and YjjG. *J Biol Chem* **2004**, *279*, 54687–54694.

129. Ragheb, D.; Dalal, S.; Bompiani, K. M.; Ray, W. K.; Klemba, M. Distribution and Biochemical Properties of an M1-Family Aminopeptidase in Plasmodium Falciparum Indicate a Role in Vacuolar Hemoglobin Catabolism. *J Biol Chem* **2011**, *286*, 27255–27265.

130. Rampazzo, C.; Gallinaro, L.; Milanesi, E.; Frigimelica, E.; Reichard, P.; Bianchi, V. A Deoxyribonucleotidase in Mitochondria: Involvement in Regulation of dNTP Pools and Possible Link to Genetic Disease. *Proc. Natl. Acad. Sci. U. S. A.* **2000a**, *97*, 8239–8244.

131. Rampazzo, C.; Johansson, M.; Gallinaro, L.; Ferraro, P.; Hellman, U.; Karlsson, A.; Reichard, P.; Bianchi, V. Mammalian 5'(3')-Deoxyribonucleotidase, cDNA Cloning,and Overexpression of the Enzyme in Escherichia Coli and Mammalian Cells *. *J. Biol. Chem.* **2000b**, *275*, 5409–5415.

132. Rebora, K.; Desmoucelles, C.; Borne, F.; Pinson, B.; Daignan-Fornier, B. Yeast AMP Pathway Genes Respond to Adenine through Regulated Synthesis of a Metabolic Intermediate. *Mol. Cell. Biol.* **2001**, *21*, 7901–7912.

133. Rees, D. C.; Duley, J. A.; Marinaki, A. M. Pyrimidine 5' Nucleotidase Deficiency. *Br. J. Haematol.* **2003**, *120*, 375–383.

134. Reichard, P. Interactions Between Deoxyribonucleotide and DNA Synthesis. *Annu. Rev. Biochem.* **1988**, *57*, 349–374.

135. Reis, J. L. Nucleotidase and Its Relation to the Deamination of Nucleotides in the Heart and the Muscles. *Bull. Soc. Chim. Biol.* **1934**, *16*, 385–399.

136. Reis, J. L. Studies on 5-Nucleotidase and Its Distribution in Human Tissues. *Biochem J* **1950a**, *46*.

137. Reis, J. L. Sur La Presence de La 5-Nucleotidase Dans Les Tissus Animaux. *Bull. Soc. Chim. Biol.* **1940**.

138. Reis, J. L. The Specificity of Phosphomonoesterases in Human Tissues. *Biochem J* **1950b**, *48*, 548–551.

139. Reis, J. L. Über Die Aktivität Der 5-Nukleotidase in Den Tierischen Und Menschlichen Geweben. *Enzymologia* **1937a**, *2*, 185-.

140. Reis, J. L. Über Die Spezifische Phosphatase Der Nervengewebe. *Enzymologia* **1937b**, *2*, 110–116.

141. Rinaldo-Matthis, A.; Rampazzo, C.; Reichard, P.; Bianchi, V.; Nordlund, P. Crystal Structure of a Human Mitochondrial Deoxyribonucleotidase. *Nat. Struct. Biol.* **2002**, *9*, 779–787.

142. Roberts, L. Drug-Resistant Malaria Advances in Mekong. *Science.* **2017**, *358*, 155–156.

143. Roy, A.; Kucukural, A.; Zhang, Y. I-TASSER: A Unified Platform for Automated Protein Structure and Function Prediction. *Nat. Protoc.* **2010**, *5*, 725–738.

144. Roy, S.; Nagappa, L. K.; Prahladarao, V. S.; Balaram, H. Kinetic Mechanism of Plasmodium Falciparum Hypoxanthine-Guanine-Xanthine Phosphoribosyltransferase. *Mol. Biochem. Parasitol.* **2015**, *204*, 111–120.

145. Sala-Newby, G. B.; Freeman, N. V. E.; Curto, M. A.; Newby, A. C. Metabolic and Functional Consequences of Cytosolic 5′-Nucleotidase-IA Overexpression in Neonatal Rat Cardiomyocytes. *Am. J. Physiol. Circ. Physiol.* **2003**, *285*, H991–H998.

146. Sala-Newby, G. B.; Freeman, N. V; Skladanowski, A. C.; Newby, A. C. Distinct Roles for Recombinant Cytosolic 5'-nucleotidase-I and -II in AMP and IMP Catabolism in COS-7 and H9c2 Rat Myoblast Cell Lines. *J. Biol. Chem.* **2000**, *275*, 11666–11671.

147. Sala-Newby, G. B.; Newby, A. C. Cloning of a Mouse Cytosolic 5'-nucleotidase-I Identifies a New Gene Related to Human Autoimmune Infertility-Related Protein. *Biochim. Biophys. Acta* **2001**, *1521*, 12–18.

148. Sala-Newby, G. B.; Skladanowski, A. C.; Newby, A. C. The Mechanism of Adenosine Formation in Cells. Cloning of Cytosolic 5'-nucleotidase-I. *J. Biol. Chem.* **1999**, *274*, 17789–17793.

149. Santos, C. A.; Saraiva, A. M.; Toledo, M. A. S.; Beloti, L. L.; Crucello, A.; Favaro, M. T. P.; Horta, M. A. C.; Santiago, A. S.; Mendes, J. S.; Souza, A. A.; et al. Initial Biochemical and Functional Characterization of a 5'-nucleotidase from Xylella Fastidiosa Related to the Human Cytosolic 5'-nucleotidase I. *Microb. Pathog.* **2013**, *59*, 1–6.

150. Schnick, C.; Robien, M. A.; Brzozowski, A. M.; Dodson, E. J.; Murshudov, G.

N.; Anderson, L.; Luft, J. R.; Mehlin, C.; Hol, W. G. J.; Brannigan, J. A.; et al. Structures of *Plasmodium Falciparum* Purine Nucleoside Phosphorylase Complexed with Sulfate and Its Natural Substrate Inosine. *Acta Crystallogr. Sect. D Biol. Crystallogr.* **2005**, *61*, 1245–1254.

151. Seegmiller, J. E.; Rosenbloom, F. M.; Kelley, W. N. Enzyme Defect Associated with a Sex-Linked Human Neurological Disorder and Excessive Purine Synthesis. *Science* **1967**, *155*, 1682–1684.

152. Serina, L.; Blondin, C.; Krin, E.; Sismeiro, O.; Danchin, A.; Sakamoto, H.; Gilles, A. M.; Bârzu, O. Escherichia Coli UMP-Kinase, a Member of the Aspartokinase Family, Is a Hexamer Regulated by Guanine Nucleotides and UTP. *Biochemistry* **1995**, *34*, 5066–5074.

153. Shenoy, A. R.; Visweswariah, S. S. Site-Directed Mutagenesis Using a Single Mutagenic Oligonucleotide and DpnI Digestion of Template DNA. *Anal Biochem* **2003**, *319*, 335–336.

154. Silvestrini, F.; Lasonder, E.; Olivieri, A.; Camarda, G.; van Schaijk, B.; Sanchez, M.; Younis Younis, S.; Sauerwein, R.; Alano, P. Protein Export Marks the Early Phase of Gametocytogenesis of the Human Malaria Parasite Plasmodium Falciparum. *Mol. Cell. Proteomics* **2010**, *9*, 1437–1448.

155. Singh, B.; Sung, L. K.; Matusop, A.; Radhakrishnan, A.; Shamsul, S. S.; Cox-Singh, J.; Thomas, A.; Conway, D. J. A Large Focus of Naturally Acquired Plasmodium Knowlesi Infections in Human Beings. *Lancet* **2004**, *363*, 1017–1024.

156. Smith, R. H.; Muren, O.; Scott, R. B.; Frable, W. J. Transbronchial Brush Biopsy: Anti-Mortem Diagnosis of Pulmonary Infiltrates in Non-Hodgkin's Lymphoma. *Va. Med.* **1978**, *105*, 359–362.

157. Socheat, D.; Denis, M. B.; Fandeur, T.; Zhang, Z.; Yang, H.; Xu, J.; Zhou, X.; Phompida, S.; Phetsouvanh, R.; Lwin, S.; et al. Mekong Malaria. II. Update of Malaria, Multi-Drug Resistance and Economic Development in the Mekong Region of Southeast Asia. *Southeast Asian J. Trop. Med. Public Health* **2003**, *34*, 1–102.

158. Srinivasan, B. Structure-Function Studies on Three Members of the Haloacid Dehalogenase (HAD) Superfamiy of Enzymes, Jawaharlal Nehru Centre for Advanced Scientific Research, 2011.

159. Srinivasan, B.; Balaram, H. ISN1 Nucleotidases and HAD Superfamily Protein Fold: In Silico Sequence and Structure Analysis. *Silico Biol* **2007**, *7*, 187–193.

160. Srinivasan, B.; Forouhar, F.; Shukla, A.; Sampangi, C.; Kulkarni, S.; Abashidze, M.; Seetharaman, J.; Lew, S.; Mao, L.; Acton, T. B.; et al. Allosteric Regulation and Substrate Activation in Cytosolic Nucleotidase II from Legionella Pneumophila. *FEBS J.* **2014**, *281*, 1613–1628.

161. Srinivasan, B.; Nagappa, L. K.; Shukla, A.; Balaram, H.; Balaram, H. Prediction of Substrate Specificity and Preliminary Kinetic Characterization of the Hypothetical Protein PVX_123945 from Plasmodium Vivax. *Exp. Parasitol.* **2015**, *151*, 56–63.

162. Stadtman, E. R.; Earl, J. M.; Brown, E. B. Nucleotidases of Clostridium Propionicum II. ROLE OF ELECTRON TRANSPORT SYSTEMS IN ACTIVATION OF A DIPHOSPHOPYRIDINE PYROPHOSPHATASE. *J. BIOLOQICAL CHEAWSTRY* **1960**, *235*.

163. Stinson, R. A.; McPhee, J. L.; Collier, H. B. Phosphotransferase Activity of Human Alkaline Phosphatases and the Role of Enzyme Zn2+. *Biochim. Biophys. Acta* **1987**, *913*, 272–278.

164. Stocchi, V.; Cucchiarini, L.; Canestrari, F.; Piacentini, M. P.; Fornaini, G. A Very Fast Ion-Pair Reversed-Phase HPLC Method for the Separation of the Most Significant Nucleotides and Their Degradation Products in Human Red Blood Cells. *Anal. Biochem.* **1987**, *167*, 181–190.

165. Sun, W.; Huang, X.; Li, H.; Tawa, G.; Fisher, E.; Tanaka, T. Q.; Shinn, P.; Huang, W.; Williamson, K. C.; Zheng, W. Novel Lead Structures with Both Plasmodium Falciparum Gametocytocidal and Asexual Blood Stage Activity Identified from High Throughput Compound Screening. *Malar. J.* **2017**, *16*, 147.

166. Sylvestre, J.; Chahlaoui, J.; Ethier, S. [Contribution of Axial Tomography to the Study of the Mediastinum]. *Union. Med. Can.* **1978**, *107*, 1091–1094.

167. Tao, D.; Ubaida-Mohien, C.; Mathias, D. K.; King, J. G.; Pastrana-Mena, R.; Tripathi, A.; Goldowitz, I.; Graham, D. R.; Moss, E.; Marti, M.; et al. Sex-Partitioning of the Plasmodium Falciparum Stage V Gametocyte Proteome Provides Insight into Falciparum-Specific Cell Biology. *Mol. Cell. Proteomics* **2014**, *13*, 2705–2724.

168. Thaithong, S. Clones of Different Sensitivities in Drug-Resistant Isolates of Plasmodium Falciparum. *Bull. World Health Organ.* **1983**, *61*, 709–712.

169. Tonkin, C. J.; van Dooren, G. G.; Spurck, T. P.; Struck, N. S.; Good, R. T.; Handman, E.; Cowman, A. F.; McFadden, G. I. Localization of Organellar Proteins in Plasmodium Falciparum Using a Novel Set of Transfection Vectors and a New Immunofluorescence Fixation Method. *Mol Biochem Parasitol* **2004**, *137*, 13–21.

170. Towbin, H.; Staehelin, T.; Gordon, J. Electrophoretic Transfer of Proteins from Polyacrylamide Gels to Nitrocellulose Sheets: Procedure and Some Applications. *Proc. Natl. Acad. Sci. U. S. A.* **1979**, *76*, 4350–4354.

171. Tozzi, M. G.; Camici, M.; Pesi, R.; Allegrini, S.; Sgarrella, F.; Ipata, P. L. Nucleoside Phosphotransferase Activity of Human Colon Carcinoma Cytosolic 5'-nucleotidase. *Arch Biochem Biophys* **1991**, *291*, 212–217.

172. Trager, W.; Jensen, J. B. Human Malaria Parasites in Continuous Culture. *Science.* **1976**, *193*, 673–675.

173. Van Den Berghe, G.; Vincent, M. F.; Bontemps, F. Pathways and Control of Adenine Nucleotide Catabolism in Anoxic Rat Hepatocytes. *Biomed Biochim Acta* **1989**, *48*, S5-10.

174. VOLKNANDT, W.; VOGEL, M.; PEVSNER, J.; MISUME, Y.; IKEHARA, Y.; ZIMMERMANN, H. 5'-Nucleotidase from the Electric Ray Electric Lobe. Primary Structure and Relation to Mammalian and Procaryotic Enzymes. *Eur. J. Biochem.* **1991**, *202*, 855–861.

175. Wallden, K.; Nordlund, P. Structural Basis for the Allosteric Regulation and Substrate Recognition of Human Cytosolic 5'-nucleotidase II. *J Mol Biol* **2011**, *408*, 684–696.

176. Walther, T.; Novo, M.; Rossger, K.; Letisse, F.; Loret, M. O.; Portais, J. C.; Francois, J. M. Control of ATP Homeostasis during the Respiro-Fermentative Transition in Yeast. *Mol Syst Biol* **2010**, *6*, 344.

177. Webb, M. R. A Continuous Spectrophotometric Assay for Inorganic Phosphate and for Measuring Phosphate Release Kinetics in Biological Systems. **1992**, *89*, 4884–4887.

178. Webster, W. A. J.; McFadden, G. I. From the Genome to the Phenome: Tools to Understand the Basic Biology of Plasmodium Falciparum. *J. Eukaryot.*

Microbiol. **2014**, *61*, 655–671.

179. Wilkinson, A. J.; Fersht, A. R.; Blow, D. M.; Winter, G. Site-Directed Mutagenesis as a Probe of Enzyme Structure and Catalysis: Tyrosyl-tRNA Synthetase Cysteine-35 to Glycine-35 Mutation. *Biochemistry* **1983**, *22*, 3581–3586.

180. Williams, J. L. Stimulation of Plasmodium Falciparum Gametocytogenesis by Conditioned Medium from Parasite Cultures. *Am. J. Trop. Med. Hyg.* **1999**, *60*, 7–13.

181. Winter, G.; Fersht, A. R.; Wilkinson, A. J.; Zoller, M.; Smith, M. Redesigning Enzyme Structure by Site-Directed Mutagenesis: Tyrosyl tRNA Synthetase and ATP Binding. *Nature* **1982**, *299*, 756–758.

182. Wolfenden, R. Analog Approaches to the Structure of the Transition State in Enzyme Reactions. *Acc. Chem. Res.* **1972**, *5*, 10–18.

183. Wolfenden, R. Transition State Analog Inhibitors and Enzyme Catalysis. *Annu. Rev. Biophys. Bioeng.* **1976**, *5*, 271–306.

184. Wolfenden, R.; Snider, M. J. The Depth of Chemical Time and the Power of Enzymes as Catalysts. *Acc. Chem. Res.* **2001**, *34*, 938–945.

185. Worku, Y.; Paul Luzio, J.; Newby, A. C. Identification of Histidyl and Cysteinyl Residues Essential for Catalysis by 5′-Nucleotidase. *FEBS Lett.* **1984**, *167*, 235–240.

186. Yamaoka, T.; Yano, M.; Kondo, M.; Sasaki, H.; Hino, S.; Katashima, R.; Moritani, M.; Itakura, M. Feedback Inhibition of Amidophosphoribosyltransferase Regulates the Rate of Cell Growth via Purine Nucleotide, DNA, and Protein Syntheses. *J. Biol. Chem.* **2001**, *276*, 21285–21291.

187. Yegutkin, G. G.; Henttinen, T.; Samburski, S. S.; Spychala, J.; Jalkanen, S. The Evidence for Two Opposite, ATP-Generating and ATP-Consuming, Extracellular Pathways on Endothelial and Lymphoid Cells. *Biochem. J.* **2002**, *367*, 121–128.

188. Yeh, J. I.; Biemann, H.-P.; Privé, G. G.; Pandit, J.; Koshland Jr, D. E.; Kim, S.-H. High-Resolution Structures of the Ligand Binding Domain of the Wild-Type Bacterial Aspartate Receptor. *J. Mol. Biol.* **1996**, *262*, 186–201.

189. Zerez, C. R.; Tanaka, K. R. A Continuous Spectrophotometric Assay for

Pyrimidine-5 ’ -Nucleotidase. *Anal. Biochem.* **1985**, *151*, 282–285.

190. Zhong, S.; Hsu, F.; Stefan, C. J.; Wu, X.; Patel, A.; Cosgrove, M. S.; Mao, Y. Allosteric Activation of the Phosphoinositide Phosphatase Sac1 by Anionic Phospholipids. *Biochemistry* **2012**, *51*, 3170–3177.

191. Zimmermann, H. 5’-Nucleotidase: Molecular Structure and Functional Aspects. *Biochem J* **1992**, *285*, 345–365.

(This page is intentionally left blank)

APPENDIX A

ELSEVIER LICENSE
TERMS AND CONDITIONS

Feb 19, 2018

This Agreement between ARPIT P SHUKLA ("You") and Elsevier ("Elsevier") consists of your license details and the terms and conditions provided by Elsevier and Copyright Clearance Center.

License Number	4292390538614
License date	Feb 19, 2018
Licensed Content Publisher	Elsevier
Licensed Content Publication	Journal of Molecular Biology
Licensed Content Title	Evolutionary Genomics of the HAD Superfamily: Understanding the Structural Adaptations and Catalytic Diversity in a Superfamily of Phosphoesterases and Allied Enzymes
Licensed Content Author	A. Maxwell Burroughs,Karen N. Allen,Debra Dunaway-Mariano,L. Aravind
Licensed Content Date	Sep 1, 2006
Licensed Content Volume	361
Licensed Content Issue	5
Licensed Content Pages	32
Start Page	1003
End Page	1034
Type of Use	reuse in a thesis/dissertation
Intended publisher of new work	other
Portion	figures/tables/illustrations
Number of figures/tables/illustrations	1
Format	both print and electronic
Are you the author of this Elsevier article?	No
Will you be translating?	No
Original figure numbers	figure 3
Title of your thesis/dissertation	Structure-function study of an IMP-specific 5'-nucleotidase from Plasmodium falciparum
Expected completion date	Jan 2018
Estimated size (number of pages)	200
Requestor Location	ARPIT P SHUKLA JAWAHARLAL NEHRU CENTRE FOR ADVANCED SCIENTIFIC RESEARCH, JAKKUR BANGALORE, KARNATAKA 560064 India Attn: ARPIT SHUKLA
Publisher Tax ID	GB 494 6272 12
Total	0.00 USD
Terms and Conditions	

ELSEVIER LICENSE
TERMS AND CONDITIONS

Jan 24, 2018

This Agreement between ARPIT P SHUKLA ("You") and Elsevier ("Elsevier") consists of your license details and the terms and conditions provided by Elsevier and Copyright Clearance Center.

License Number	4275240854005
License date	Jan 24, 2018
Licensed Content Publisher	Elsevier
Licensed Content Publication	Trends in Biochemical Sciences
Licensed Content Title	Phosphoryl group transfer: evolution of a catalytic scaffold
Licensed Content Author	Karen N. Allen,Debra Dunaway-Mariano
Licensed Content Date	Sep 1, 2004
Licensed Content Volume	29
Licensed Content Issue	9
Licensed Content Pages	9
Start Page	495
End Page	503
Type of Use	reuse in a thesis/dissertation
Intended publisher of new work	other
Portion	figures/tables/illustrations
Number of figures/tables/illustrations	1
Format	both print and electronic
Are you the author of this Elsevier article?	No
Will you be translating?	No
Original figure numbers	Figure 3
Title of your thesis/dissertation	Structure-function study of an IMP-specific 5'-nucleotidase from Plasmodium falciparum
Expected completion date	Jan 2018
Estimated size (number of pages)	200
Requestor Location	ARPIT P SHUKLA JAWAHARLAL NEHRU CENTRE FOR ADVANCED SCIENTIFIC RESEARCH, JAKKUR BANGALORE, KARNATAKA 560064 India Attn: ARPIT SHUKLA
Total	0.00 USD
Terms and Conditions	

APPENDIX B

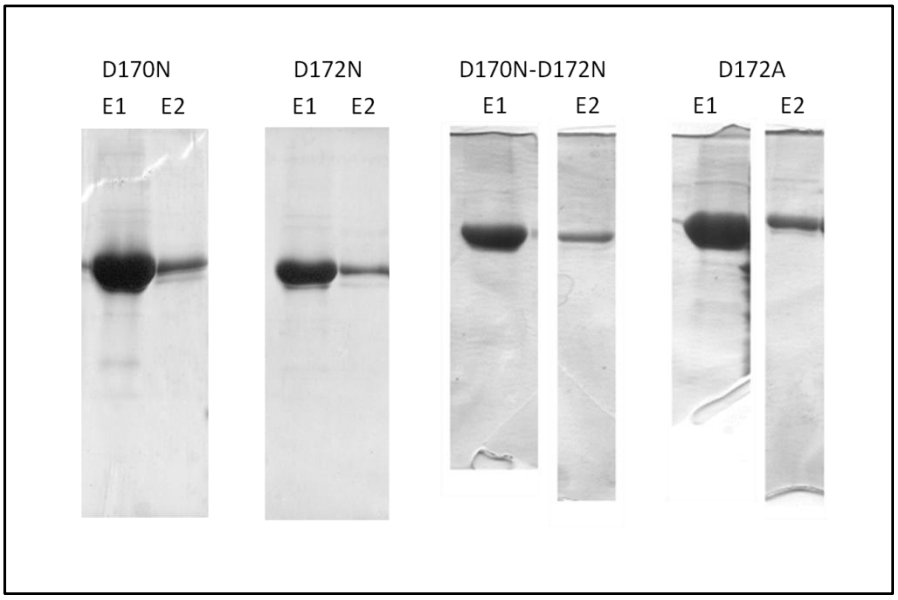

Figure B1. SDS-PAGE of eluted fractions of PfISN1 mutants D170N, D172N, D170N-D172N and D172A.

Table B1. Kinetic parameters of PfISN1 wild-type enzyme and mutants D172N and D172A with substrate pNPP.

Protein	V_{max} (nmol min^{-1} mg^{-1})	K_m (mM)	k_{cat} (sec^{-1}) x 10^{-2}	k_{cat}/K_m (sec^{-1} mM^{-1}) x 10^{-2}
Wild-type	3.01 ± 0.07	5.94 ± 0.22	0.3 ± 0.0062	0.045 ± 0.0019
D172N	319 ± 14	1.5 ± 0.2	28.2 ± 1.2	18.8 ± 2.64
D172A	22.2 ± 2.0	4.7 ± 1.1	1.96 ± 0.18	0.42 ± 0.104

APPENDIX C

Table C1. Kinetic parameters of PfISN1 wild-type enzyme and mutants ΔN30, ΔC10, K41L and H398V with substrate IMP at pH 8.0 and 5.0*.

Protein	V_{max} (µmol min^{-1} mg^{-1})	K_m (mM)	k_{cat} (sec^{-1})	k_{cat}/K_m (sec^{-1} mM^{-1})
pH 8.0				
Wild-type	15.3 ± 0.5	65.8 ± 4.9	13.5 ± 0.4	0.2 ± 0.02
ΔN30	34.3 ± 2.4	29.9 ± 5.5	30.3 ± 2.1	1.01 ± 0.20
ΔC10	41.2 ± 3.0	20.7 ± 4.4	36.4 ± 2.6	1.76 ± 0.39
K41L	16.4 ± 0.9	15.4 ± 2.4	14.5 ± 0.8	0.94 ± 0.15
H398V	18.7 ± 1.4	10.8 ± 3.0	16.5 ± 1.2	1.53 ± 0.44
pH 5.0				
Wild-type	11.0 ± 0.9	0.31 ± 0.06	9.72 ± 0.79	31.4 ± 6.6
ΔN30	65.9 ± 2.6	2.7 ± 0.3	58.2 ± 2.3	21.3 ± 2.7
ΔC10	63.6 ± 3.1	1.6 ± 0.2	56.2 ± 2.7	36.2 ± 5.6
K41L	24.7 ± 1.7	3.0 ± 0.5	21.8 ± 1.5	7.28 ± 1.31
H398V	36.5 ±2.6	1.6 ± 0.4	32.2 ± 2.3	20.2 ± 5.2

*FOOTNOTE: Values represent mean ± SD of 3 independent measurements.

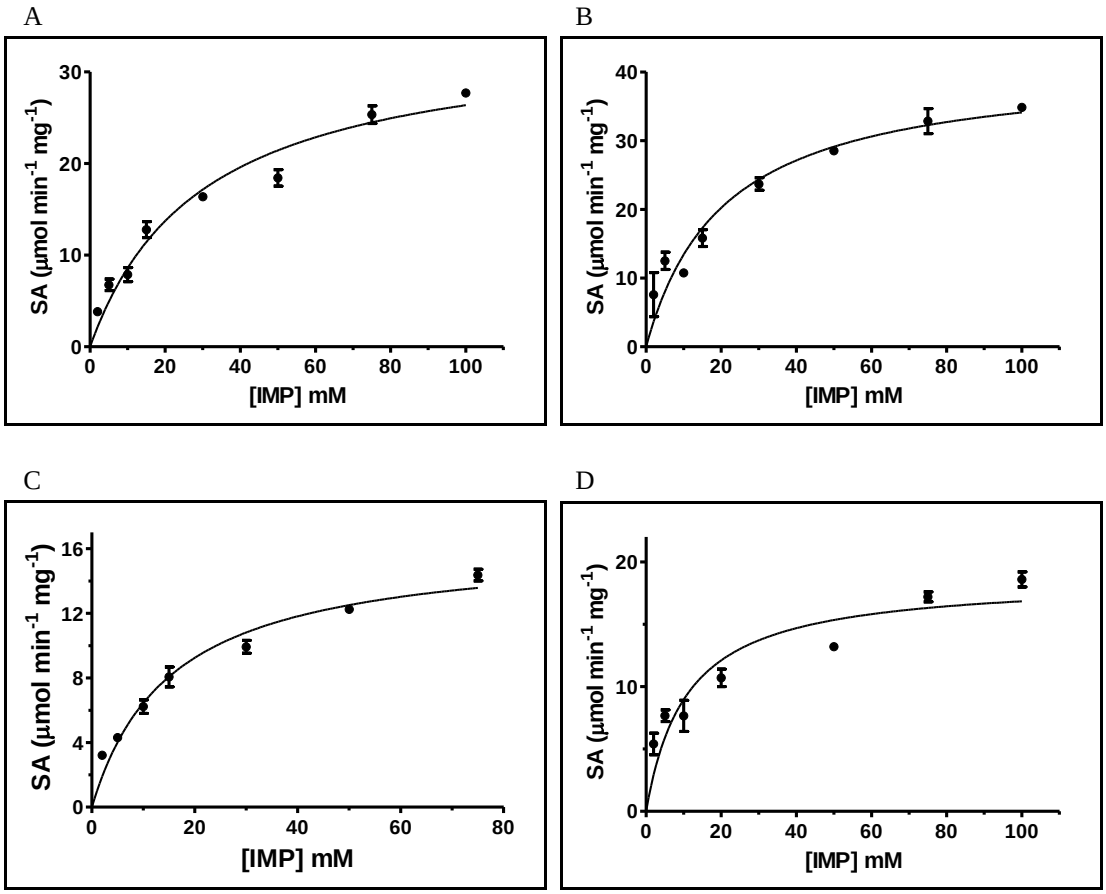

Figure C1. Initial velocity *vs* IMP concentration plots for PfISN1 mutants (A) ΔN30, (B) ΔC10, (C) K41L and (D) H398V at pH 8.0. Values represent mean ± SD of three independent measurements.

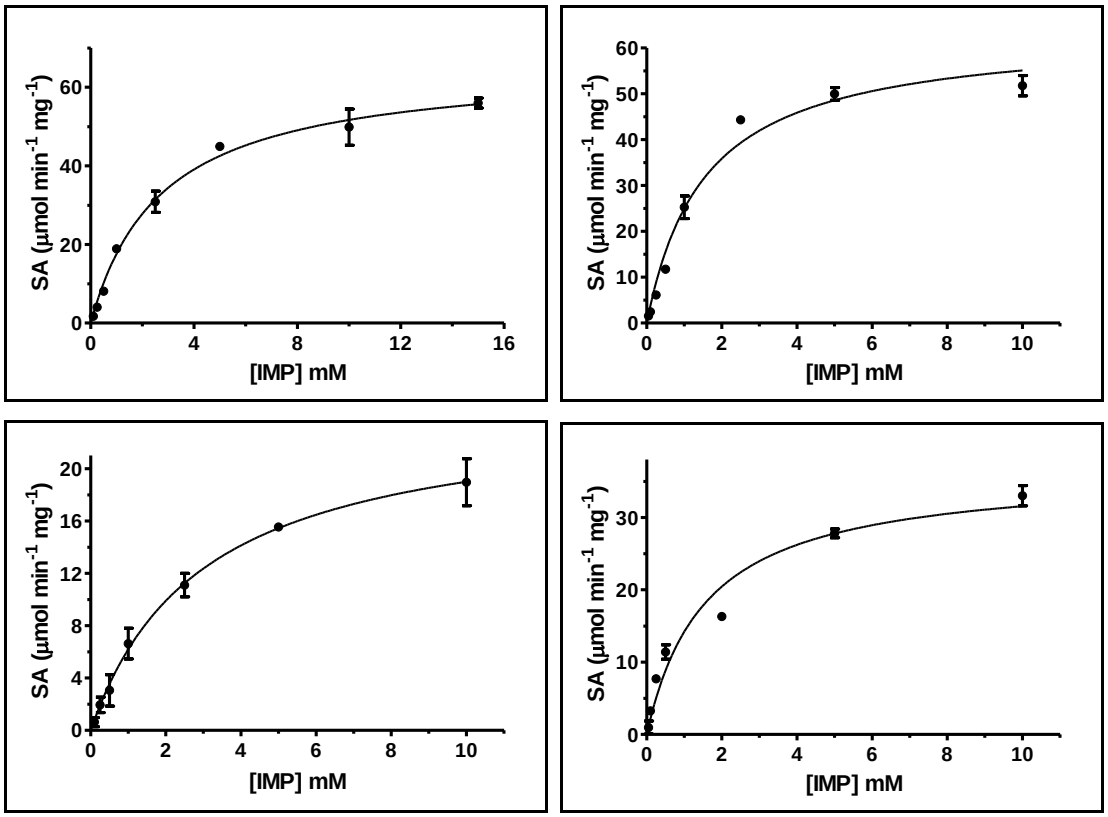

Figure C2. Initial velocity *vs* IMP concentration plots for PfISN1 mutants (A) ΔN30, (B) ΔC10, (C) K41L and (D) H398V at pH 5.0. Values represent mean ± SD of three independent measurements.